

MOLECULAR DYNAMICS SIMULATIONS OF LIPID-BASED DRUG DELIVERY SYSTEMS

A thesis submitted for the degree of

DOCTOR OF PHILOSOPHY

From

Monash Institute of Pharmaceutical Sciences

Monash University (Parkville Campus)

By

Woldeamanuel Anteneh Birru

B. Sc. Chem., B. Sc. Comp. Science, M. Sc. Bioinformatics

June 2015

Drug Delivery, Disposition and Dynamics

Monash Institute of Pharmaceutical Sciences

Monash University (Parkville Campus)

381 Royal Parade, Parkville

Victoria 3052, Australia

© The author (2015). Except as provided in the Copyright Act 1968, this thesis may not be reproduced in any form without the written permission of the author.

Dedicated to:

Those who are suffering from modern slavery, systematic abuse and subtle racism.

TABLE OF CONTENTS

TABLE OF CONTENTS.....	IV
ABSTRACT.....	VIII
ACKNOWLEDGMENTS.....	XI
PUBLICATIONS	XV
ABSTRACTS AND PRESENTATIONS	XVI
LIST OF ABBREVIATIONS.....	XVII
1 GENERAL INTRODUCTION.....	2
1.1 BACKGROUND.....	2
1.2 STATEMENT OF THE PROBLEM.....	3
1.3 SCOPE AND ORGANISATION OF THE THESIS	4
1.4 LIPID-BASED DRUG FORMULATION	5
1.5 TYPES OF LIPID FORMULATIONS.....	7
1.6 EQUILIBRIUM PHASE BEHAVIOUR AS FORMULATION TOOL	8
1.7 GASTROINTESTINAL FLUIDS.....	11
1.7.1 <i>Bile Salts</i>	12
1.7.2 <i>Endogenous, Exogenous Lipids and Lipid Digestion</i>	13
1.7.3 <i>Impact of Lipid Digestion on Adsorption of Poorly-Water Soluble Drugs</i>	17
1.7.4 <i>Experimental Methods for Studying the Structural Properties of Colloidal Phases</i> .	18
1.8 MOLECULAR DYNAMICS (MD) SIMULATION	19
1.8.1 <i>Molecular Dynamics Analysis Methods</i>	20
1.8.2 <i>Limitations of Molecular Dynamics Simulation</i>	21
1.8.3 <i>Molecular Mechanics Force Fields</i>	22
1.9 MOLECULAR DYNAMICS SIMULATION AND THE STUDY OF MOLECULAR SELF-ASSEMBLY ..	23
1.9.1 <i>Water/Lipids Systems</i>	24
1.9.2 <i>Water/Bile Salts Systems</i>	27
1.9.3 <i>Water/Bile Salts/Lipids Systems</i>	28
1.9.4 <i>Water/Fatty Acid Systems</i>	29
1.9.5 <i>SUMMARY: MD simulations of self-Assembling systems</i>	31

2 IMPROVING FORCE FIELD PARAMETERS FOR ALCOHOL AND ETHYLENE GLYCOL FUNCTIONAL GROUPS.....	34
2.1 INTRODUCTION.....	34
2.2 LOGP AND GIBBS FREE ENERGY.....	36
2.3 GIBBS FREE ENERGY CALCULATION FROM MOLECULAR DYNAMICS	38
2.3.1 <i>Thermodynamic Integration Method</i>	39
2.3.2 <i>The Bennett Acceptance Ratio (BAR) Method</i>	40
2.3.3 <i>logP from Gibbs Energy</i>	41
2.4 METHODS	42
2.5 DIHEDRAL ANGLE POTENTIAL.....	43
2.6 LATENT HEAT OF VAPORISATION.....	46
2.7 GIBBS FREE ENERGY.....	46
2.8 THERMODYNAMIC INTEGRATION VERSUS BENNETT'S ACCEPTANCE RATIO	47
2.9 INFLUENCE OF SIMULATION CELL SIZE ON FREE ENERGIES	50
2.10 WET VERSUS DRY OCTANOL	52
2.11 RESULTS.....	54
2.11.1 <i>Gibbs Free Energy of Hydration</i>	54
2.11.2 <i>Re-Parameterisation of GROMOS 53A6</i>	59
2.11.3 <i>Calculation of logP of the n-Alkanes</i>	63
2.11.4 <i>Calculation of logP of Alcohols</i>	65
2.11.5 <i>Calculation of logP of Ethylene Glycols</i>	67
2.11.6 <i>Calculation of logP of Amino Acid Analogues</i>	69
2.12 DISCUSSION.....	73
2.13 CONCLUSIONS	75
3 DIGESTION OF PHOSPHOLIPIDS AFTER SECRETION OF BILE INTO THE DUODENUM CHANGES THE PHASE BEHAVIOUR OF BILE COMPONENTS	78
3.1. ABSTRACT	78
3.2. INTRODUCTION.....	79
3.3 MATERIALS AND METHODS.....	84
3.3.1 <i>Materials</i>	84
3.3.2 <i>Fasted State Simulated Intestinal Fluid Buffer</i>	84
3.3.3 <i>Lipid Stock Solutions Preparation</i>	84

3.3.4	<i>Bile Salt Stock Solutions Preparation</i>	85
3.3.5	<i>Turbidity</i>	85
3.3.5	<i>Dynamic light scattering</i>	86
3.4	RESULTS	87
3.4.1	<i>Selection of a Representative Bile Salt and Lipid</i>	88
3.4.2	<i>Phase Behaviour of Bile Salt: Lipid Mixtures</i>	91
3.4.3	<i>Particle Size Measurement of GDX/POPC and GDX/(LPC+OA) Mixtures</i>	95
3.5	DISCUSSION.....	99
3.6	CONCLUSIONS	102
3.7	ACKNOWLEDGMENT	102
4	THE PHASE BEHAVIOUR OF MODEL INTESTINAL FLUIDS STUDIED USING MOLECULAR DYNAMICS SIMULATIONS; THE IMPACT OF LIPID DIGESTION.....	105
4.1.	ABSTRACT	105
4.2.	INTRODUCTION.....	105
4.3.	MATERIALS AND METHODS	109
4.3.1	<i>NMR Methods</i>	109
4.3.2	<i>Molecular Dynamics Simulations</i>	110
4.4.	RESULTS AND DISCUSSION	112
4.4.1	<i>The Effects of Phospholipid Digestion</i>	112
4.4.2	<i>The Impact of Fatty Acid Ionisation on Mixed Micelle Formation</i>	122
4.4.3	<i>The Interaction of Bile Salt with Digested and Undigested Lipids</i>	126
4.4.4	<i>Micelle Diffusion</i>	133
4.5.	CONCLUSIONS	135
4.6.	ACKNOWLEDGEMENT.....	135
5	MODELLING THE PHASE BEHAVIOUR AND DRUG SOLUBILISATION CAPACITY OF A TYPE I LIPID-BASED DRUG FORMULATION AFTER DIGESTION IN THE INTESTINE: AN EXPERIMENTAL AND MOLECULAR DYNAMICS STUDY	138
5.1	ABSTRACT	138
5.2	INTRODUCTION.....	139
5.3	MATERIALS AND METHODS	142
5.3.1	<i>Materials</i>	142
5.3.2	<i>Fasted Simulated Intestinal Fluids Buffer</i>	142

5.3.3	<i>Preparation of Lipid Stock Solutions</i>	142
5.3.4	<i>Preparation of Mixture of Bile Salt and Digested Triglyceride</i>	143
5.3.5	<i>Turbidity</i>	143
5.3.6	<i>Dynamic Light Scattering</i>	144
5.3.7	<i>LC-MS assays</i>	144
5.3.8	<i>Microscopy</i>	146
5.3.9	<i>Molecular Dynamics Simulation</i>	146
5.4	RESULTS	147
5.4.1.	<i>Experimental Studies</i>	147
5.4.2.	<i>Turbidity Measurement of LPC+OA/GDX/dTGL/H₂O</i>	149
5.4.3.	<i>Modelling Studies</i>	154
5.5	DISCUSSION	166
5.6	CONCLUSION	169
5.7	ACKNOWLEDGMENT	169
6	SUMMARY	171
7	EPILOGUE	179
8	REFERENCES	180
9	APPENDICES	196
9.1	APPENDIX 1	196
9.2	APPENDIX 2	198
9.3	APPENDIX 3	200
9.4	APPENDIX 4	212
9.5	APPENDIX 5	218

ABSTRACT

Molecular dynamics (MD) simulation is a powerful technique to investigate molecular self-assembly. It can be used to model and understand the interactions of biological membranes, proteins, and lipids. Above their critical micelle concentration (CMC), molecules that are composed of hydrophilic head group and hydrophobic tail group aggregate spontaneously to form a wide variety of assemblies ranging from micelles, rodlike structures, and bilayers to more complex phases such as hexagonal and cubic phases. These self-assembly processes are of fundamental importance in drug discovery and development. In the area of drug discovery and development, it is vital to have an effective means of improving the bioavailability of poorly water-soluble drugs (PWSD). Lipid-based delivery systems (LBDDS) are one of the important approaches of improving the bioavailability of PWSD.

The nature of gastrointestinal (GI) fluids strongly influences the absorption of PWSDs. The dissolution rate and the amount of drugs dissolved is determined by the nature of the GI fluids and their solubilisation capacity. Within the GI tract there are endogenous as well as exogenous solubilising components. The endogenous components are secreted from the gall bladder, whereas the exogenous components are those which are administered in the drug formulation as well as resulting from meals. After oral administration, drugs must remain dissolved within the GI tract before partitioning into and then across the enterocyte. Although the self-assembly process of lipids and lipophilic excipients within the GI tract are thought to have a significant influence on drug solubilisation and the degree of drug supersaturation, the molecular understanding of these structures is limited.

The first section of this work describes the modification of the GROMOS 53A6 united atom force field particularly for polyethylene glycol (PEG). Then, using MD simulations and experimental methods such as turbidity, particle size measurement, cross-polarized light microscopy and NMR, the current study explores the phase behaviour of (i) the 1-palmitoyl-2-oleoyl-sn-glycero-3-

phosphocholine (POPC), sodium glycochenodeoxycholate (GDX), and water system, and (ii) the 1-palmitoyl-2-hydroxy-sn-glycerol-3-phosphocoline (Lyso PC), GDX and water system and constructs ternary phase diagrams of these mixtures. It also investigates part of the quaternary phase diagram of Lyso PC, glycerol 1-monooleate (GMO), GDX and water, which was used to investigate the structures formed in the intestine after digestion of triglycerides. The solubilisation capacity of the lipidic microenvironment on PWSD has also been investigated using LC-MS and MD simulation. The association structures of these various systems have been modelled and compared to the experimental phase behaviour of the analogous systems. It is indicated in these studies that digestion and digested products have a significant impact on the phase behaviour of the contents of the small intestine and on solubilisation and bioavailability of PWSDs.

In summary, this thesis contributes to a better understanding of the performance of lipid-based formulations (LBF) and shines a light on the use of MD simulations as a prediction tool to model LBDDS.

Monash University

Monash Institute of Graduate Research

Declaration for thesis based or partially based on conjointly published or unpublished work.

General Declaration

In accordance with Monash University Doctorate Regulation 17.2 Doctor of Philosophy and Research Master's regulations the following declarations are made:

I hereby declare that this thesis contains no material which has been accepted for the award of any other degree or diploma at any university or equivalent institution and that, to the best of my knowledge and belief, this thesis contains no material previously published or written by another person, except where due reference is made in the text of the thesis.

This thesis includes one original paper accepted in peer reviewed journals, two submitted publications and one unpublished chapter. The core theme of the thesis is to explore the benefit of atomistic molecular dynamics (MD) simulation to gain insight into the behaviour of lipid-based drug delivery systems (LBBDS). The ideas, development and writing up of all the papers in the thesis were the principal responsibility of myself, the candidate, working within the Drug delivery, Disposition and Dynamics Theme of the Monash Institute of Pharmaceutical Sciences under the supervision of Professor Colin W. Pouton, co-supervisor Dr David K. Chalmers and co-supervisor Professor Christopher J. H. Porter.

The inclusion of co-authors reflects the fact that the work came from active collaboration between researchers and acknowledges input into team-based research.

In the case of Chapter three, four and five my contribution to the work included the majority of the experimental work, data analysis and interpretation, the concept and design of all studies, the preparation of the initial drafts of all manuscripts and the subsequent revision and formulation of conclusions and hypotheses resulting from the relevant studies.

Thesis chapter	Publication title	Publication status*	Nature and extent of candidate's contribution
3	Digestion of phospholipids after secretion of bile into the duodenum changes the phase behaviour of bile components	Published	Planning and conducting experimental work, data evaluation and drafting and revision of manuscript
4	The phase behaviour of model intestinal fluids studied using molecular dynamics simulations; the impact of lipid digestion	To be submitted	Planning and conducting the modelling work, data evaluation and drafting and revision of manuscript
5	Modelling the phase behaviour and drug solubilisation capacity of a type I lipid-based drug formulation after digestion in the intestine: an experimental and molecular dynamics study	To be submitted	Planning and conducting the experimental and modelling work, data evaluation and drafting and revision of manuscript

I have not renumbered sections of submitted or published papers in order to generate a consistent presentation within the thesis.

Signed: 

Date: 12/06/2015

ACKNOWLEDGMENTS

I would like to start my acknowledgements by borrowing a statement from a popular soccer player: "I don't want to be hard and I don't want to be negative, but I want to be honest." I don't want this acknowledgment to be a repetition of all the acknowledgements that I have read so far. I want it to be honest and exemplary. As Dr Martin Luther King Jr. said "Nothing in the world is more dangerous than sincere ignorance and conscientious stupidity." When I say this I don't mean that my acknowledgements are full of harsh words, rather I want them to be inspiring.

This PhD has been a major part of my life since I settled in Australia. After a very comfortable life in my own country, as a new settler in a new country I faced challenges at the beginning of my Australian life. I tasted these challenges on a small scale when I was studying in Germany but living as a student and settling for good in another country is quite different. In the first years of my life in Melbourne, I found a person who helped me to focus on the positives rather than being frustrated by the challenges that I was facing. He was too humble to have coffee with me, and too understanding to go with me to introduce me to new people. He discussed with me all the hard-core sciences, and told me that I can be what I want to be. In all these, I never sensed the slightest underestimation or discrimination. Instead, I felt that I was valued. He is the man who made me love Australia. Now it is so easy for me to forgive those who are bad to me when I remember that there are people like Professor David A. Winkler who love others like themselves. Just knowing this by itself has given me the power to forgive the worst things that have happened to me in the journey of life. I don't have enough words to express my gratefulness to you for what you have done for me. You count as one of the few truly influential people in my life.

I learned that in my PhD studies I met two kinds of people. Those who inspired me and those who drained me. I grew up inspired by people whom I never met, only reading and listening about them inspired me. The most inspiring person for me that I have worked closely with is one of my supervisors, Professor Colin W. Pouton. Your genuineness, transparency and understanding gave me courage to love research and the area of drug delivery science. In all aspects of life,

whether it is about my PhD project or any other thing, I always find some substance in your conversation. I learned many things from you more than you can imagine by simply talking to you and observing you. I sensed that you are considerate and you don't want me to feel bad in any situation. I am glad that I worked in your group.

When I started my PhD I was very naive about all the academic processes. I have worked in other areas but never in an academic environment until my brief work at Monash Clayton, which ended up in tragedy. That experience gave me a bad feeling about research and academia. The good thing is Dr. David K. Chalmers, one of my supervisors, turned this around, giving me good academic guidance during the early days of my PhD. In this project, you helped me to learn a lot about computational chemistry in a way that I have never learnt before. It might not be visible, as I am not too flamboyant in the way that I explain what I have learnt, but I know it is in me and I will use all of what I have learnt in this PhD when the need arises. Thank you for your guidance that helped me to start my PhD in a positive spirit.

Dr. Dallas B. Warren is the one who literally taught me all, about drug delivery systems and all sort of lab work and analysis methods from scratch. You are generous enough to answer all my silly questions and correct all my worst analysis methods. Not only that, you also challenged me, in the middle of my PhD project, to walk by myself. I am always impressed by your mathematics knowledge and carefulness in drawing a conclusion from the analysis that we have done. Thank you for being patient with me and showing me all that I needed to know, without any hesitation.

Professor Chris H. J. Porter, also one of my supervisors, helped me to gain insight by explaining, during the lipid group meeting and in all other meetings, all the odds that we are facing in the drug delivery systems. Dr Hassen Benamure is always uplifting my spirits by encouraging me and appreciating the work that I have done in this PhD project; it means a lot to me. Thanks for all that both of you have done for me.

I would like to thank Victorian Life Science Computation Initiative (VLSCI) for their generous support throughout my PhD by providing me a number of travel grants and a top up scholarship. Special thanks to Dr. Christina Hall for her great support and understanding.

Everything in my PhD project did not go smoothly. Things were not looking great particularly, at the end of my PhD. I had many frustrating moments, as I had encouraging moments. I was drained, as I was inspired, I was underestimated as I was uplifted. I experienced partiality, as I was given a privilege. I was snooped, as I was given freedom. I was considered as a liar, as I was appreciated for my honesty. In all that, I am grateful not only for how the good and safe part of the process shaped me, but also for all those hard times, sleepless nights, feeling of loneliness and conversations to myself which moulded me better and faster than I expected. I realize that what Dr Martin Luther King, Jr. said is true. “The ultimate measure of a man is not where he stands in a moment of comfort and convenience, but where he stands at times of challenge and controversy.” In those times, I got a chance to decide to be calm and positive in the middle of thunder, even if I had moments of mourning. In all this, I have learnt to expect the unexpected in situations that I will face in the future. In those experiences, I also learnt that there is always a light behind every shadow, which makes a way, so that I will not be afraid of my future shadows, as I know that they don’t come without light.

I would like to thank all my family members who have been patient with me in all of this process; especially, my mother Senait Zelek and my brother Seyoum A. Birru for their continued support and understanding. Solomon, Seble, Tigist, Tutu and Messeret thanks for your concerns about me as loving brother and sisters. Aman, Barni, Kalebo, Beth, Nati and Blen thanks for being a reason for me to fight the good fight in life to be a good example for you. You are my energy to embrace life. My friends who were with me in all this PhD; especially, Davide, Bindu, Azi and Betse, I am so grateful to have you as a friend. My office mates and fellow PhD students, who have been with me for the last four years, thank you for your friendship and company, in the mountains as well as in the valleys. Special thanks to Luke, Tony, Jeff, San, Sam, Tramir and Steven Yap.

Finally I would like to thank my father Anteneh Birru, even if you departed from me at a very crucial time, and still I don't understand the reason why, thank you for putting those qualities in me while I was still a very small kid that no one could give me right now like you have done it, and for allowing me to feel your spirit every single moment.

My message to those who read this thesis by any chance is, let us all embrace a love and compassion-based formulation of life instead of greed and abuse, to cure the main diseases of human kind: poverty and recession.

PUBLICATIONS

This thesis is a compilation of the following manuscripts:

Chapter 3

Woldeamanuel A. Birru, Dallas B. Warren, Ahmed Ibrahim, Hywel D. Williams, Hassan Benameur, Christopher J.H Porter, David K. Chalmers and Colin W. Pouton. Digestion of phospholipids after secretion of bile into the duodenum changes the phase behaviour of bile components. (Published in *Molecular Pharmaceutics*, July 2014)

Chapter 4

Woldeamanuel A. Birru, Dallas B. Warren, Stephen J. Headey, Hassan Benameur, Christopher J. H. Porter, Colin W. Pouton and David K. Chalmers. The phase behaviour of model intestinal fluids studied using molecular dynamics simulations; the impact of lipid digestion. (*Manuscript to be submitted*)

Chapter 5

Woldeamanuel A. Birru, Dallas B. Warren, Sifei Han, Hassan Benameur, Christopher J. H. Porter, Colin W. Pouton and David K. Chalmers. Modelling the phase behaviour and drug solubilisation capacity of a Type I lipid-based drug formulation after digestion in the intestine: an experimental and molecular dynamics study. (*Manuscript to be submitted*)

ABSTRACTS AND PRESENTATIONS

Woldeamanuel Birru, Dallas Warren, Christopher Porter, Colin Pouton, David: Molecular Dynamics Simulations of Lipid Drug Delivery Systems.

Poster: ASB 2013, 37th Annual meeting of Australian Society for Biophysics, RMIT University Melbourne 24 – 27 November 2013. Abstract P71.

Woldeamanuel Birru, Dallas Warren, Christopher Porter, Colin Pouton, David: Molecular Dynamics Simulations of Lipid Drug Delivery Systems.

Oral: Association of Molecular Modellers of Australasia 2012, MM2012, August 30 – September 1, 2012, Queenstown New Zealand. Abstract 29.

Woldeamanuel Birru, Dallas Warren, Christopher Porter, Colin Pouton, David: Molecular Modelling of Lipid Drug Formulations.

Abstract: Journal of Cheminformatics 2012, 4(Suppl 1)

Woldeamanuel Birru, Dallas Warren, Christopher Porter, Colin Pouton, David: Molecular Modelling of Lipid Drug Formulations.

Oral: GCC 2011, 7th German Conference on Chemoinformatics, November 6 – 8, 2011, Goslar Germany.

Woldeamanuel Birru, Dallas Warren, Christopher Porter, Colin Pouton, David Chalmers: Modelling of Lipid Drug Formulations.

Poster: 2010 Super Computing Conference, New Orleans, Louisiana 12 – 19 November 2010.

LIST OF ABBREVIATIONS

BCS:	Biopharmaceutical classification system
BD:	Bile salt
CH:	Cholesterol
CMC:	Critical micellar concentration
CpHMD:	Constant pH molecular dynamics
DEG:	Diethylene glycol
DGL:	Diglyceride
D _h :	Hydrodynamics diameter
DMPEG6:	Dimethoxy polyethylene glycol with six units
EPR:	Electron Paramagnetic Resonance
dTGL:	Digested triglyceride
FA:	Fatty acid
FaSSIF:	Fasted State Simulated Intestinal Fluid
FeSSIF:	Fed State Simulated Intestinal Fluid
GDX:	glycodeoxycholic acid, sodium salt
GI:	Gastrointestinal
GALT:	Gut associated lymphoid tissue
GMO:	Glycerol monooleoyl
HLB:	Hydrophile-lipophile balance

LBDDS:	Lipid-based drug delivery system
LBF:	Lipid-based formulation
L-BFGS:	Broyden-Fletcher-Goldfarb-Shanno
LC-MS:	Liquid chromatography and mass spectroscopy
LFCS:	Lipid formulation classification system
LINCS:	Linear Constraint Solver
LJ:	Lenard Jones
logP:	Logarithm of the octanol/water partition coefficient
LPC:	1-palmitoyl-2-hydroxy-sn-glycerol-3-phosphocoline
Lyso	PC: Lyso phospholipid
MD :	Molecular Dynamics
MEG:	Monoethylene glycol
MGL:	Monoglyceride
NMR:	Nuclear Magnetic Resonance
NPT:	Constant number of molecules at constant Pressure and Temperature
NTU:	Nephelometry turbidity unit
NVT:	Constant number of molecules at constant Volume and Temperature
OA:	Oleic acid
PC:	Phosphatidylcholine
PDI:	Polydispersity index
PEG:	Polyethylene glycol

PEG-11:	Polyethylene glycol with eleven units
PENTEG:	Pentaethylene glycol
PL:	Phospholipid
PME:	Particle-mesh Ewald
POPC:	1-palmitoyl-2-oleoyl-sn-glycerol-3-phosphocholine
PWSD:	Poorly water-soluble drug
SEDDS:	Self-emulsifying drug delivery system
SMEDDS:	Self-emulsifying drug delivery system
SPC:	Simple Point Charge
TEG:	Triethylen glycol
TTEG:	Tetraethylene glycol
VLSCI:	Victorian life science computation initiative
^w / _w :	Weight in weight

“Computing is not about computers any more. It is about living.”

Nicholas Negroponte

CHAPTER ONE

GENERAL INTRODUCTION

1 GENERAL INTRODUCTION

1.1 BACKGROUND

Lipid-based delivery systems are one of the important approaches for improving the bioavailability of poorly water-soluble drugs (PWSD)¹. Lipid-based delivery systems (LBDDS) can range from simple oil to complex, oil, surfactant and co-solvent mixtures. There are four formulation types outlined by the Lipid Formulation Classification System (LFCS)². Generally, non-ionic surfactants which are considered to be non-toxic for oral ingestion are present in all the formulation types. Above their critical micellar concentration (CMC), non-ionic surfactants that are composed of hydrophilic head group and hydrophobic tail group aggregate spontaneously in the presence of water to form a wide variety of assemblies ranging from micelles, rodlike structures, and bilayers to more complex phases such as hexagonal and cubic phases. This self-assembly process is of fundamental importance in the area of drug discovery and development. In this area, it is vital to have an effective means of improving the bioavailability of PWSD. Structures formed by lipid systems can enhance bioavailability by providing sites for drug solubilisation, both in the lipid-based product itself and in the intestine after administering of the product. The internal structure of formulations is not adequately understood at the molecular level and even less is known about the structures that form when formulations interact with bile and pancreatic enzymes in the intestine.

Molecular dynamics (MD) is one of the disciplines of molecular modelling in which successive configurations of the system are generated by solving Newton's laws of motion. Molecular dynamics simulation can be defined as a computational technique that provides insight into the behaviour of molecules and molecular systems. It can be used to model and understand molecular level interactions of biological membranes, proteins, and lipids and it is now possible to simulate the interactions of small solutes with complex biological membranes by explicit simulation of lipid-bilayers³. Understanding of molecular systems at microscopic level is the main

attribute of molecular dynamics techniques. Hence, this work focuses on the molecular level understanding of excipients, which are involved in formulation, and intestinal digestion of lipid based drug delivery systems.

1.2 STATEMENT OF THE PROBLEM

The absorption and bioavailability of drugs can be limited by their solubility, dissolution rate and permeability. Drugs with poor solubility are called poorly water soluble drugs (PWSD). The poor solubility of new chemical entities is the biggest challenge of formulation scientists in the process of developing orally bioavailable drugs. Gastrointestinal (GI) fluids have an important influence on the process of absorption of PWSD. The dissolution rate and the mass of drug dissolved can be determined by the nature of the GI fluids and their solubilisation capacity⁴. Within the GI tract there are endogenous as well as exogenous solubilizing components. The endogenous components are secreted from the gall bladder, whereas, the exogenous components are those which are administered from the lipid formulation as well as derived from meals⁵. After oral administration, drugs must primarily dissolve within the GI tract before partitioning into and then across the enterocyte⁶. Although, the self-assembling processes of different molecules especially lipids and lipophilic excipients, within the GI tract have a significant influence on drug solubilisation and the degree of drug supersaturation, the molecular understanding of these structures is limited. This is primarily due to the fact that it occurs on a very fast time scale (nanosecond), and on a very short length scale (nanometre), making experimental investigation difficult. However, nowadays, due to the increase in computer power and due to algorithmic advances it is possible to simulate the self-aggregation of surfactants using atomistic MD simulations.

The aim of this work is to develop an *in silico* formulation method by investigating the interaction of lipids, surfactants and digestion products within the gastrointestinal contents to efficiently improve the solubilisation capacity and increase the bioavailability of poorly water-soluble drugs after oral administration. One of the important aspects of the work was to improve the current molecular dynamics force fields for molecules often used in LBDDS. Many of the excipients used,

such as polyethylene glycols and polyethoxylated non-ionic surfactants do not have a well-defined molecular dynamics force field. Therefore, *in silico* work included running different phase behaviour simulations (formulation and non-formulation) and comparing simulations with the results of laboratory experiments, such as Nephelometry, Dynamics Light Scattering (DLS), Liquid Chromatography and Mass Spectrometry (LCMS) and Nuclear Magnetic Resonance (NMR), to improve the reliability of the modelling methods as a prediction tool.

1.3 SCOPE AND ORGANISATION OF THE THESIS

The principal hypothesis of this project is that the digestion products produced by the action of pancreatic enzymes on lipid formulations have the potential to change the phase behaviour of the GI tract. This in turn may have a considerable impact on the capacity for solubilisation and subsequent absorption of poorly water-soluble drugs.

This project therefore aims to develop an *in silico* formulation method by investigating the difference in association structures formed by undigested and digested biliary lipids, and the interaction of digestion products and poorly water-soluble drugs with the gastrointestinal contents. The work aims to provide resolution at atomistic level, by conducting a series of phase behaviour simulations and comparing these simulations with the results of laboratory experiments to improve the reliability of the modelling methods as a prediction tool.

Additionally, the project endeavours to improve the current molecular dynamics force fields for molecules often used in lipid based drug delivery systems. In particular, the project focuses mainly on poly ethylene glycols (PEG), which are used as cosolvents in lipid formulations and are also present in many non-ionic surfactants. The current GROMACS united atom force field GROMOS 56A6 was parameterised to develop a well-defined molecular dynamics force field.

This thesis begins with a literature survey (Chapter one). The experimental work is presented as a compilation of one traditional thesis chapter and three manuscripts. Chapter two is written as a traditional thesis chapter and describes the parameterisation techniques of the force field.

Chapter three is a manuscript describing an experimental study of the phase behaviour of undigested and digested bile components. This paper was recently published in *Molecular Pharmaceutics*. Chapters four and five are manuscripts in submission. Chapter four is focused on molecular dynamics studies of the materials described in Chapter three. Chapter five integrates knowledge of digestion of triglycerides with the structures formed by digestion of bile, and also investigates the solubilisation of drugs in these complex mixtures. The thesis is concluded in Chapter 6 with a short discussion chapter. Epilogue and Appendices that comprise additional supporting information, which are not included in the main chapters of the thesis follow.

1.4 LIPID-BASED DRUG FORMULATION

The biopharmaceutical classification system (BCS) is a system that differentiates drugs on the basis of their solubility and permeability, guided by the intestinal drug absorption provided by the U.S. Food and Drug Administration. BCS assigns drugs with high lipid permeability and low water solubility to BSC class II. Poor drug solubility is a significant and frequently encountered problem in drug discovery as many new drug candidates that emerge from drug discovery program are BCS class II⁷. The current estimation of insufficiently soluble drug candidates as percentage of all new chemical entities is between 40% and 70%⁸. The bioavailability of PWSD candidates in BCS class II can be markedly improved by formulation. To achieve optimum biosolubility of these drugs, their solubilisation state throughout the gastrointestinal tract should be maintained^{4b}.

Lipid-based delivery systems are an important option for the oral formulation of drugs that are poorly soluble in water. Lipid formulations have often proven to be effective in enhancing the oral bioavailability of poorly water-soluble drugs but the development of lipid-based formulations has so far been limited. Although the relationship between formulation and drug absorption is well understood, performance *in-vivo* cannot be predicted with confidence at present due, in part, to a lack of basic quantitative knowledge and understanding of drug trafficking between lipid, digested lipid components, and the epithelial boundary where absorption occurs.

A variety of excipients can be included in lipid formulations and the diversity makes a comparison of lipid-based formulations difficult¹. The solubilisation of drugs is highly dependent on the proportion of the chemical components of the formulation. The main advantage of lipid formulation is that potentially the drug remains in solution throughout its period in the gastrointestinal tract^{4b} thus avoiding the slow dissolution of hydrophobic drugs from crystalline form. Many pharmaceutical excipients are sourced from natural triglyceride oils, and contain a variety of fatty acid esters. In addition, they may contain semi-synthetic products such as surfactants. This heterogeneity complicates the study of the internal structure of lipid formulations by spectroscopic techniques. Increasing the molecular level understanding of these events will greatly enhance our knowledge of the *in vivo* dispersion and solubilisation patterns of lipid-based formulations.

1.5 TYPES OF LIPID FORMULATIONS

A wide range of excipients, can be used in formulations including triglycerides, partial glycerides, semi-synthetic oily esters, and semi-synthetic non-ionic surfactant esters. Four types of lipid formulations were characterized in The Lipid Formulation Classification System (LFCS) in 2000 with additional formulations being added in 2006^{2, 4b}. *“The main purpose of the LFCS is to enable in vivo studies to be interpreted more readily and subsequently to facilitate the identification of the most appropriate formulations for specific drugs, i.e. with reference to their physicochemical properties.”-Pouton C. W and Porter, C.J.H¹.*

Most types of formulations contain either oil or water insoluble surfactants that promote self-emulsification and play a role in providing solubilizing the formulated drugs. Balancing the hydrophilicity and hydrophobicity of the surfactant helps to maintain the drug in its solubilized state throughout the gastrointestinal tract and allows it to reach the lumen of the small intestine without precipitation. Although there is much to be learned about the environment of the small intestine, what is clear is that the presence of lipids and other water insoluble non-ionic surfactants may increase the bioavailability of the PWSD⁶. It is believed that a significant factor that increases bioavailability is that the secretion of bile salts (BS) and endogenous biliary lipids including phospholipid (PL) and cholesterol (CH) is enhanced by the presence of lipids and digested lipid products⁹. The secretion of BS, PL and CH lead to the formation of mixed micelles of these compounds. Additionally the presence of exogenous lipids, either from the formulation or those provided in food, will influence the mixed micelles of endogenous components to form different aggregation states. This leads to the need to understand of the equilibrium phase behaviour of the small intestine in more detail.

Table 1.1 The Lipid Formulation Classification System: characteristic features, advantages and disadvantages of the four essential types of 'lipid' formulations^a.

Formulation Type	Materials	Characteristics	Advantage	Disadvantage
Type I	Oils without surfactants (e.g. tri-, di- and monoglycerides)	Non-dispersing, requires digestion	GRAS status; simple; excellent capsule compatibility	Formulation has poor solvent capacity unless drug is highly lipophilic
Type II	Oils and water-insoluble surfactants	SEDDS formed without water-soluble components	Unlikely to lose solvent capacity on dispersion	Turbid oil/water dispersion (particle size 0.25–2 µm)
Type III	Oils, surfactants, cosolvents (both water-insoluble and water-soluble excipients)	SEDDS/SMEDDS formed with water-soluble components	Clear or almost clear dispersion; drug absorption without digestion	Possible loss of solvent capacity on dispersion; less easily digested
Type IV	Water-soluble surfactants and cosolvents (no oils)	Formulation disperses typically to form a micellar solution	Formulation has good solvent capacity for many drugs	Likely loss of solvent capacity on dispersion; may not be digestible

^a Adapted from Pouton, C.W. and Porter, C.J.H.¹

1.6 EQUILIBRIUM PHASE BEHAVIOUR AS FORMULATION TOOL

Lipid-based delivery systems are typically self-dispersing systems and are often referred to as self-emulsifying drug delivery systems (SEDDS)^{2, 4b, 10}. Systems with such properties are found in type II, III and IV formulations. When an emulsion is formed by the mechanical force provided by gentle mixing oil and water, it is called self-emulsification. Self-emulsification can be achieved *in vivo* by the digestive motility of the stomach and intestine¹¹. Self-emulsifying systems can be produced by blending hydrophilic surfactants with or without water-soluble cosolvents with oils². The presence of surfactants facilitates the self-emulsification process, leading to the formation of different phases depending on the concentration of surfactants and temperature of the system¹². Different phases are formed depending on the hydrophile-lipophile balance (HLB) of the

surfactant. These phases can be normal micellar phase, reverse micellar phase, discontinuous micellar cubic phase, lamellar phase, normal hexagonal phase, reverse hexagonal phase, bicontinuous cubic phase, and discontinuous reverse cubic phase¹³ as shown in Figure 1.1.

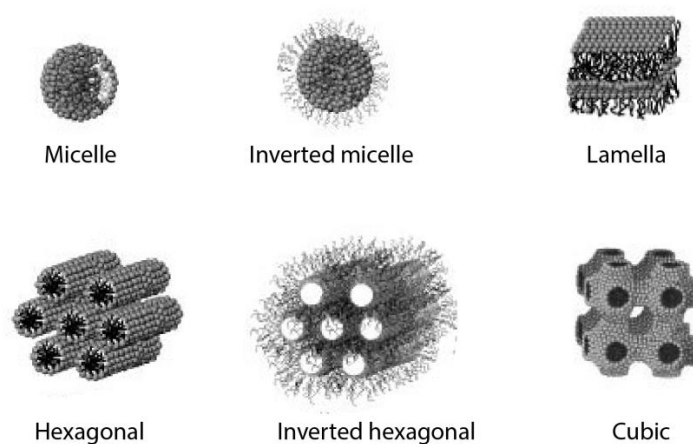


Figure 1.1 Structures formed by self-assembled surfactants in aqueous solutions, depending their hydrophile-lipophile balance (HLB).

Surfactants are amphiphiles that contain both hydrophobic groups (water insoluble or oil soluble component) and hydrophilic groups (water soluble component). In an oil/water mixture, the hydrophobic group will dissolve in oil phase, while the water-soluble head group remains in the water phase. Surfactants are generally classified into three categories, anionic (negatively charged), non-ionic (neutral) and cationic (positively charged). Anionic surfactants include alkylbenzene sulphonates (detergents), sulphates, (fatty acid) soaps, lauryl sulfate (foaming agent), di-alkyl sulposuccinate (wetting agent) and lignosulphonates (dispersants)¹⁴. Surfactants that do not ionize in aqueous solution are called non-ionic surfactants and their hydrophilic group is of a non-dissociable type, such as an alcohol, phenol, ether, ester, or amide. A large proportion of non-ionic surfactants are made hydrophilic by the presence of a polyethylene glycol chain, obtained by the polycondensation of alcohols with ethylene oxide or an esterification reaction between fatty acids and polyoxyethylene¹⁵. Cationic surfactants are dissociated in water into an amphiphilic cation and an anion, mostly of the halogen type. A large proportion of this class

contains a nitrogen of the alkyl type, often derived from natural fatty acids compounds such as fatty amine salts and quaternary ammoniums, with one or several long chain¹⁶. Additionally, there are amphoteric surfactants that act as anionic surfactant in basic solution or as cationic surfactant in an acidic solution, whereby the charge of the hydrophilic part is controlled by the pH of the solution.

Lipids, fatty acids and different kinds of surfactants are all used in LBDDS. A number of publications have investigated the phase behaviour of lipids as they are part of many important biological processes. Lipids in an aqueous environment readily form bilayers under physiological conditions¹⁷. Triglycerides are assumed to form cubic microstructures before their digestion into mono and di glycerides¹⁸. Single-chain fatty acids, which are the result of digestion of triglycerides, are amphiphiles that can form micelles, lamella, vesicles and liquid crystals at different pH, temperature, composition, and concentrations¹⁹. Non-ionic surfactants, like ethoxylated oleic acid²⁰ polyethylene glycols^{13a} and silicon surfactants²¹, have also been studied. Above their critical micellar concentration (CMC), and depending on pH, temperature, concentration and especially on the chain length of their hydrophobic and hydrophilic components, they form different types of phases such as micelles, hexagonal phase, cubic phase, lamella and liquid crystals.

Orally administered formulation excipients can therefore affect drug absorption by enhancing drug solubilisation in the GI tract through alterations to the composition and character of the phase behaviour of GI components⁶. Understanding of the changes made and stimulated by the presence of formulation excipients in the GI tract is therefore vital. To understanding these changes and the degree of influence of formulation excipients on the GI tract, it is therefore important to consider the endogenous components and the characteristics of gastrointestinal fluids.

1.7 GASTROINTESTINAL FLUIDS

The gastrointestinal (GI) tract is a long tube having muscular walls and lined with epithelium that begins at the oral cavity passes through the body and ends at the rectum, see Figure 1.2. In humans, the GI tract is typically 450 cm long of which 395 cm consists of the large and small intestine. Although it varies in each section, the GI tract wall consists of four layers namely; inner *mucosa*, *submucosa*, *muscularis externa* (collection of smooth muscles) and *serosa* (a covering of connective tissues). The total surface area of the GI tract is about the size of a tennis court. The main function of the GI tract is to transfer nutrients, water and electrolytes from the external environment to the internal environment of the body. The lumen of the digestion system is the contact between the internal and external environment. It is estimated that nearly seven litres of fluids are secreted by the digestive system every day. These fluids are secreted by the GI epithelial cells and the salivary glands, pancreas and liver, which comprise the accessory organs and glands of the digestive system. Ions, digestive enzymes, mucus, and bile are the primary components of these fluids. The largest collection of lymphocytes, 80% of all lymphocyte in the body, are found in the small intestine, in the gut-associated lymphoid tissue (GALT)²².

Ions and water, which are first secreted and then reabsorbed along the tract, are the largest component of secreted fluids. The ions secreted primarily consist of H^+ , K^+ , Cl^- , HCO_3^- and Na^+ . Water follows the movement of these ions. H^+ and Cl^- are also secreted by the parietal cells into the lumen, which are responsible for creating acidic conditions in the stomach, which has a pH that reaches as low as 1 as H^+ is pumped into the stomach by exchange with K^+ . Lower in the GI tract, HCO_3^- is secreted to neutralize the acid secretions that are emptied into the duodenum by the small intestine. Pancreatic acinar cells produce the HCO_3^- in the form of $NaHCO_3$ in an aqueous solution. Due to the high concentration of both HCO_3^- and Na^+ present in the duct, an osmotic gradient is created, which the water follows. Digestive enzymes are the second largest secretion products of the GI tract. These are secreted in the mouth, stomach and intestines. Some of these enzymes are secreted by accessory digestive organs and the epithelial cells of the

stomach and intestine. Mucus produced by the Mucus cells in the stomach and goblet cells in the intestine, which serves to lubricate and protect the inner mucosa of the tract is composed of a family of glycoproteins termed mucins and is generally very viscous. Bile is a fluid secreted from hepatocytes in the liver, which is stored in the gall bladder before release into the small intestine. The primary constituents of bile are water, bile salt, cholesterol, phospholipid, bicarbonate, bile pigments and organic wastes²²⁻²³.

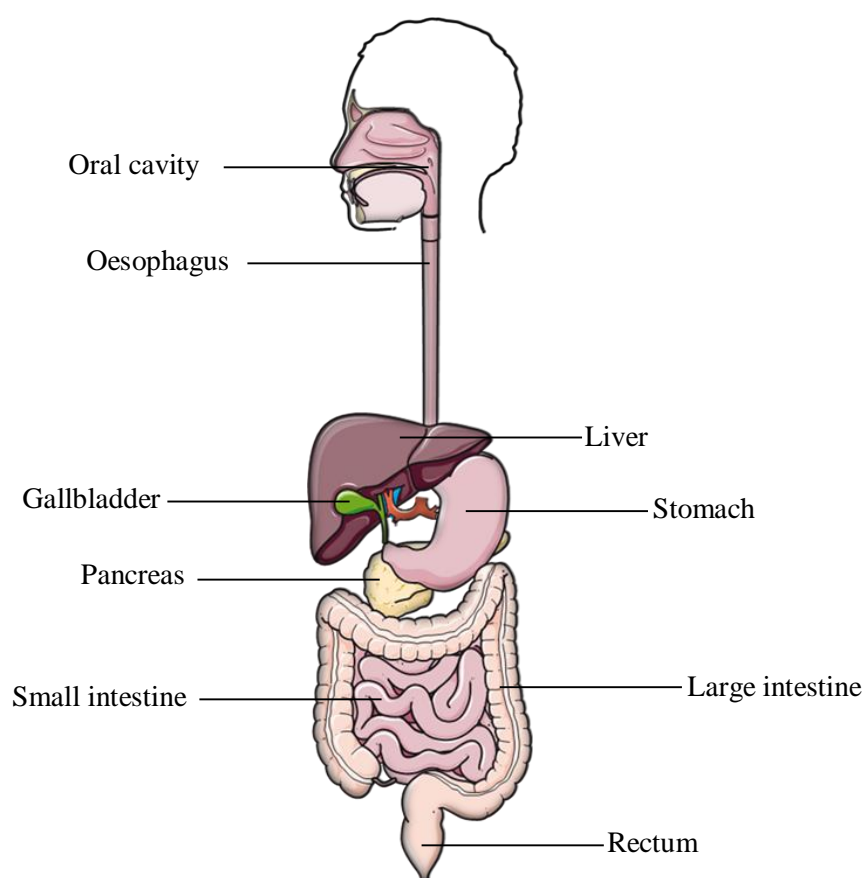


Figure 1.2 Diagram of gastrointestinal tract

1.7.1 Bile Salts

Bile salts are co-secreted in the form of mixed micellar complexes with cholesterol and phospholipid in bile. They are produced in a molar ratio of approximately 16:4:1 bile salt, cholesterol and phospholipid²⁴. These salts are synthesised in hepatocytes from steroidal bile acids conjugated to an amino acid. There is no well-defined tail and head groups in the structure of the bile salt. They have hydroxyl groups on one face and methyl groups on the other face they exhibit planar polarity. They act as detergents to solubilize lipids during digestion²⁵. Due to their

amphoteric nature, bile salts are active non-enzymatic substances that promote digestion and absorption of fat-soluble vitamins and lipid by forming an emulsion in aqueous environment. There are a number of bile salts species found within bile, with different composition namely; glycocholate, taurocholate, glycochenodeoxycholate, taurochenodeoxycholate, glycodeoxycholate, taurodeoxycholate, glycolithocholate, tauroolithocholate, glyoursodeoxycholate, taoursodeoxycholate, sulfoglycolithocholate, sulfotauroolithocholate²²⁻²³,²⁶. The critical micelle concentration (CMC) of the most abundant bile salts are 4-20 μM for cholates (NaC), 2-5 μM for deoxycholates (NaDC), 6-9 μM for chenodeoxycholate (NaCDC) and 2-19 μM for ursodeoxycholate (NaUDC)²⁵. Other compounds such as the waste products of drug degradation are also present in the bile. The critical micelle temperatures of common di- and trihydroxy bile salts are below 0° C. Therefore, most bile salts form micelles at all ambient temperatures. In aqueous solution, all monocarboxylated micellar concentrations of bile salts have an intrinsic thermodynamic pK_a value between -4.8 and 5.0, similar to propanoic acid. In general, the pK_a values of glycine-conjugated and unconjugated bile acids are 3.9 and 5.0 respectively, but their pK_a values are influenced by the nuclear substituents, the state of conjugation and bile salt concentration²⁷.

1.7.2 Endogenous, Exogenous Lipids and Lipid Digestion

Endogenous lipids are biliary-derived lipids that are stored in the gall bladder and are released into the duodenum in the presence of ingested food products. The main components of lipid present in the gall bladder are phosphatidylcholine (PC) and cholesterol. Exogenous lipids are provided by food and formulation related lipids typically triglycerides, diglycerides, monoglycerides, cholesterol, phospholipids, long-chain fatty acids and the fat-soluble vitamins. Triglycerides are the primary form of lipids in plants and animals and almost 90% of fat calories come from them²².

Lipid digestion is the mechanical and chemical breakdown of lipids into micro molecules so that they can be absorbed across the intestinal epithelium into the body²⁸. Since lipids are water

insoluble, they are partly processed in the stomach and enter the small intestine in the form of a coarse emulsion with reduced surface area. In order to increase the surface area and facilitate enzymatic digestion, bile salts are secreted from liver to the small intestine. Bile salts, together with lipases are involved in breaking down of the coarse emulsion into smaller and stable particles²⁵. Digestion of lipids in food is initiated in the stomach by gastric lipase, allowing a degree of emulsification to take place. As shown in Figure 1.3, lipases carry out the digestion process of lipids by removing two fatty acids from triglyceride molecule, producing one monoglyceride and two free fatty acids. In the case of phospholipids, pancreatic phospholipase A₂ carries out the digestion and one free fatty acid and one lyso phospholipid are produced^{22, 28a}.

Colipase is required to help gastric lipase to adsorb to the surface of an oil droplet in order to carry out the digestion of triglycerides. Colipase is a protein cofactor secreted by the pancreas that anchors lipase to triglyceride, providing that the degradation products have been removed by the action of bile salts. As digestion of lipids progresses, bile salts, fatty acids, phospholipids, monoglycerides and cholesterol form small mixed micelles and enter into the unstirred aqueous layer close to the enterocyte lining to the small intestine lumen. As lipids are lipophilic, they move out from the micelles and are absorbed into the epithelial cell by simple diffusion into and across the membrane. After entering to the enterocytes, the free fatty acids and monoglyceride are reassembled to form triglyceride. The triglyceride, together with cholesterol and proteins, form lipid-rich droplets called chylomicrons, which leave the cell at the basolateral surface by exocytosis. The chylomicrons are then absorbed into the lymphatic system and drain into the blood via the thoracic duct. Medium chain triglycerides and shorter free fatty acids do not always aggregate with chylomicrons and are absorbed by crossing the capillary membrane and directly entering the blood^{22, 28-29}. Figure 1.4, illustrates the above explanation in a schematic format.

When food is present in the stomach, gastric lipase activity becomes high and digestion of dietary lipids commences. However, in the fasted state, as the gastric lipase activity is low, the digestion

of formulation lipids in the fasted stomach is limited. Hence, in the fasted state digestion of formulation lipids is expected to occur after entry into the intestine²³. After digestion, formulation lipids follow the same path of absorption as dietary lipids. It is estimated that 10% of lipolysis is taken place in stomach which is referred to as gastric lipolysis and 56 % occurs in the small intestinal^{28b}.

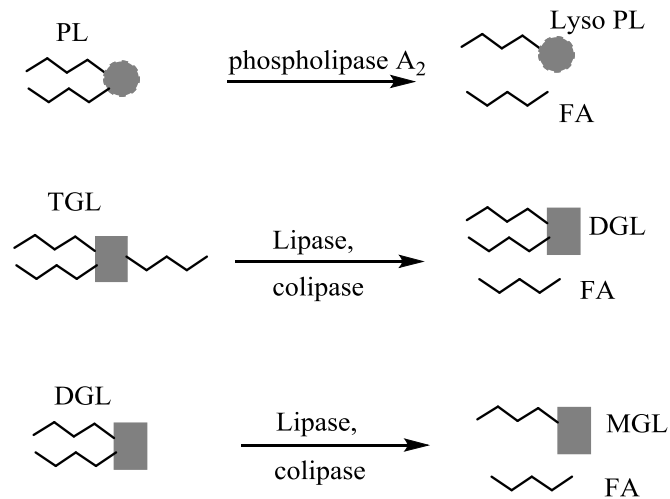


Figure 1.3 Lipolysis of phospholipids (PL) into lyso phospholipid (Lyso PL) and fatty acid (FA) and two-step hydrolysis of triglyceride (TGL) into monoglyceride (MGL) and two fatty acids.

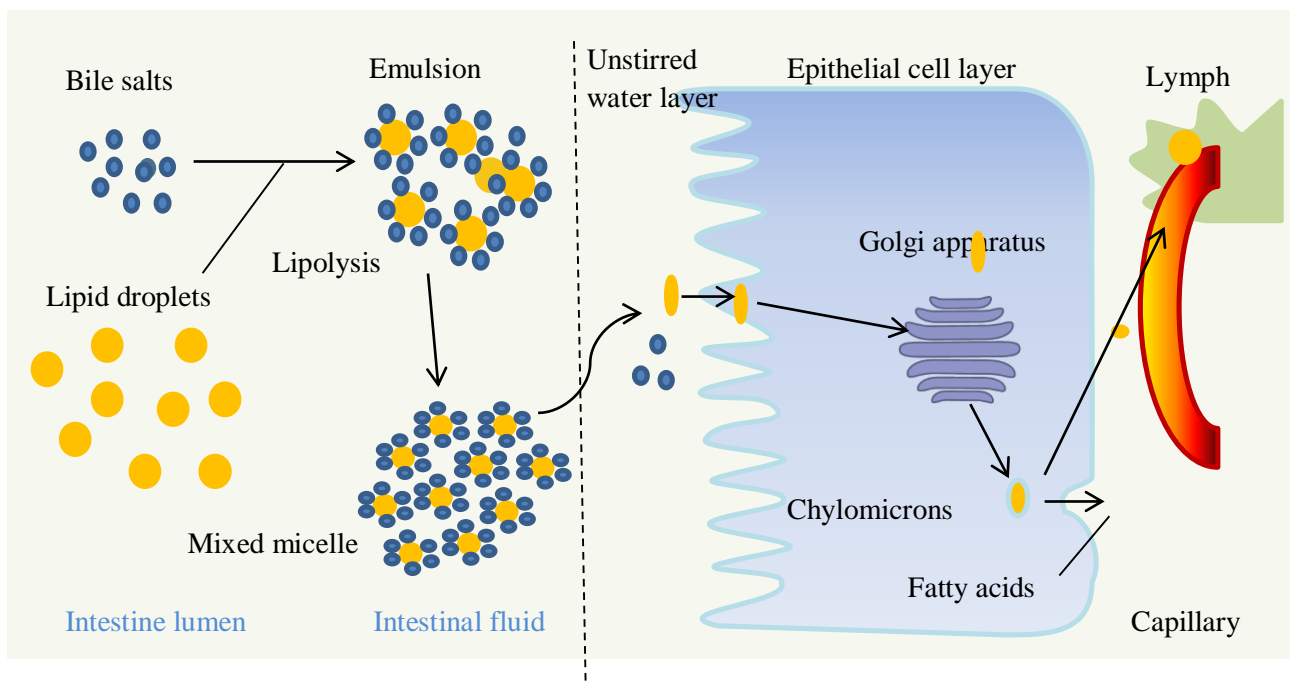


Figure 1.4 Schematic illustration of lipid digestion and absorption.

1.7.3 Impact of Lipid Digestion on Adsorption of Poorly-Water Soluble Drugs

It is important to understand the significance of the lipid digestion and absorption processes to predict the biopharmaceutical properties of lipid-based formulations of PWSDs. It is suggested that digestion products, together with bile components gradually release a PWSD that is partitioned in the lipid phase into the GI fluid³⁰. Digested products of lipids (endogenous and exogenous) are more water-soluble than the parent triglyceride; hence their nature of interaction of lipid digestion products with the aqueous contents of the GI tract changes as a function of digestion and solubility. They are delivered to the adsorptive cells of the gastrointestinal tract in solubilised form from within the mixed micelles of bile salt^{2, 11}, see Figure 1.5. Although the specific mechanisms of absorption of the lipid digestion products are not fully understood at molecular level, it is believed that the common role of the intestinal mixed micellar phase is to solubilise poorly-water soluble compounds and provide a concentration absorption gradient of lipids^{28a}. It is believed that lipids are absorbed as single molecules from aqueous solution rather than collectively as micelles. Hence, the situation becomes rather complicated when considering the fate of drugs, which are dissolved, in the co-administered lipid^{29, 31}.

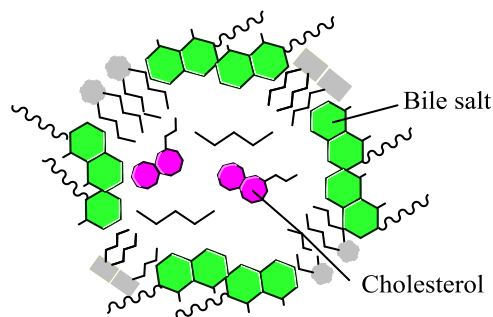


Figure 1.5 Schematic illustration of structure of mixed micelles by bile salt during lipolysis.

It has been observed that the bioavailability of PWSD can be improved by administering them with lipids³². Hence, digestion of exogenous lipids such as tri or di glycerides can generate free fatty acids that can be solubilised by biliary components. This leads to the formation of colloidal phases including vesicles and micelles, which represent different forms of dispersed lipidic microenvironments, offering a higher surface area available for drug diffusion and release, which increases the solubilisation of co-administered PWSD in the small intestine when compared to

the fasted state³³. This explains the positive effect of food, and indeed the presence of ingested lipid compounds as part of the formulation as well as a meal can improve absorption of the drug³⁴. Another means of improving absorption of PWSD in the small intestine is by generating drug supersaturation in the intestinal unstirred water layer^{33a}. Several processes may generate this drug supersaturation and the digestion of triglycerides and/or surfactants within the formulation is among them³⁵.

To investigate the thermodynamic and structural properties of colloidal phases, different instrumental and theoretical methods can be applied. These methods help us to understand and improve the absorption of PWSD in the small intestine.

1.7.4 Experimental Methods for Studying the Structural Properties of Colloidal Phases

Different instrumental methods such as Nephelometry, Dynamic Light Scattering (DLS) and Nuclear Magnetic Resonance (NMR) have been applied to investigate thermodynamic and structural properties of different phase systems. Nephelometry is a method that determines the turbidity of a given phase system based upon light scattered by the sample. The higher the intensity of scattered light, the higher the turbidity, and the bigger the particle size. DLS is a non-invasive technique that measures the speed of particles that are undergoing Brownian motion. The speed of these particles is influenced by the size of the particle, the viscosity and the temperature of the sample. The velocity of Brownian motion is defined by the translational diffusion coefficient, and this diffusion coefficient is converted into particle size by using the Stokes-Einstein equation³⁶;

$$D = \frac{kT}{6\pi\eta r_s}$$

where k is the Boltzmann constant, T the temperature, η the viscosity of the liquid and r_s the (hydrodynamic) radius of the molecule. The NMR method used in this study is DOSY or diffusion ordered NMR. This method allows the determination of atomic diffusion coefficients³⁷.

1.8 MOLECULAR DYNAMICS (MD) SIMULATION

Another fundamental theoretical technique to investigate the thermodynamic and structural properties of colloidal phases at atomistic level is molecular dynamics (MD) simulation. Newton's laws of motion states that the acceleration (a) of a particle depends on the mass (m) of the particle and the force (F) applied to the particle.

$$F = ma$$

We can use this evaluation to calculate the dynamics of a molecular system (a molecular dynamics simulation), generating a set of successive atomic configurations (a trajectory). The first molecular dynamics simulation was performed in the late 1950s by Alder and Wainwright using a condensed hard-sphere model system where the spheres move at constant velocity in a straight line between collisions³⁸. In more realistic models of intermolecular interactions, the force on each particle will change whenever the particle changes its position, or whenever any of the other interacting particles change their position. The first more realistic simulation was performed in 1964 by Rahman on argon using a continuous potential, and Rahman also performed the first simulation of molecular water with Stillinger in 1971³⁸.

To set up a molecular dynamics simulation, a starting model must be constructed, for example using a protein model from an X-ray crystal structure. The force on each atom must be calculated at each step by differentiating the potential function. The potential function is a combination of various terms such as bonds, angles, torsional terms and non-bonded interactions, which are described in the force field.

In case of the study of phase behaviour using MD simulation, the same procedure mentioned above has applied. In this study, all the systems under investigation have been started from random configuration and then equilibrated at body temperature of 310 K and reference pressure of 1 bar after energy minimization step. Since the systems have to be relaxed slowly to the target pressure Berendsen isotropic pressure coupling has been used. Velocity rescaling temperature

coupling method has been applied in both equilibration and production simulations. This thermostat ensures that a proper canonical ensemble is generated in all the systems under study. Before the final production run, preproduction simulations have been performed for all the systems using velocity rescaling temperature coupling and Parrinello-Rahman pressure coupling. The purpose of the preproduction run is to make sure the system has reached the target pressure and temperature and is equilibrated well before running prolonged production simulations. Berendsen pressure coupling has the advantage of reaching the target pressure smoothly and was used at first in the initial pre-production runs. Parrinello-Rahman pressure coupling more accurately reproduces the canonical ensemble and was used in the production simulations³⁹.

Throughout the study, a 15 nm cubic periodic box has been used as it gives an appropriate trade-off between periodic cell artefacts and CPU time. This issue was investigated by our group by comparing 5, 10 and 20 nm cubic periodic boxes⁴⁰. It is clear that using even larger periodic boxes in this project could further reduce the risk of artefacts and enable the modelling of larger colloidal structures but the simulations would become more computationally expensive. Doubling the cell dimensions results in an 8-fold increase in the number of atoms and makes the simulation computationally very expensive.

The three site SPC/E water model has been extensively validated for simulations of biological systems and we have used it for all the systems studied in this project⁴¹. The SPC/E water model is parameterized to reproduce the experimental value of the liquid density at room temperature and pressure as well as the enthalpy of vaporization of water by using self-polarization correction⁴².

1.8.1 Molecular Dynamics Analysis Methods

It is possible to calculate various thermodynamic properties from MD simulations. It is also important to compare the calculated results with experimentally obtained values to analyse the accuracy of the simulation. A number of analytical methods are implemented in this study other than calculating the basic thermodynamic properties such as the internal energy, heat capacity,

pressure and temperature of the system. Radial distribution functions (RDF), spatial distribution functions (SDF), radii of gyration, diffusion coefficients, solvent accessible surface areas (SASA) and molecular aggregation numbers are used throughout this study. Since our system is liquid, these analyses are useful to describe the system structure and to analyse the differences between various phase systems.

To define these analytical methods in simple words, the RDF describes how the density of a system varies as a function of distance from a reference particle⁴³. In a similar way, the SDF describes the three-dimensional density distribution of atoms in the local coordinate system linked to a reference molecule or a part of it⁴⁴. The radius of gyration describes the distribution of the components of the system around a reference axis. The diffusion coefficient describes the mean square displacement of a particle as a function of observation time. The SASA describes the atomic surface area of the solute exposed to the solvent⁴³. Molecular aggregation is calculated by comparing distances between carbon atoms of molecules, and when two molecules are separated by less to equal to 0.4 nm they are considered to be one aggregate⁴⁵.

1.8.2 Limitations of Molecular Dynamics Simulation

Molecular dynamics studies are very useful, but there are a number of limitations that need to be considered. Firstly, the molecular dynamics simulations performed in this work use a classical mechanics approximation to the Schrödinger equation. This means that there is no explicit representation of electrons and many phenomena that depend on movement of electrons are not replicated by the force field (for example, creation or breaking of bonds). Therefore, one of the major limitations to MD simulations is the accuracy of the force fields used to model the molecular components. Force field parameters are under constant and continuous revision and Chapter 2 describes efforts to improve the GROMOS 53A6 force field for the simulation of polyethylene glycol surfactants. Additionally, computational restrictions limit the number of atoms that can be included in the simulation, leading to restrictions on the size of the MD computational cell. Similarly, the total time that can be modelled in this work is restricted to 100-200 ns. Another

important limitation is the use of rigid non-polarizable water models. These models describe the interaction of water molecules in an approximate way.

1.8.3 Molecular Mechanics Force Fields

A molecular mechanics force field can be simply defined as a set of classical mechanics mathematical functions that encapsulate the intra- and inter- molecular interactions within a molecular system. A simple molecular mechanics force field contains four components. The first describes the interaction between pairs of bonded atoms; this is often modelled by a harmonic potential that increases in energy when the bond is stretched from the reference position. The second component describes the change in potential energy as bond angles deviate from their ideal values, again often modelled using harmonic potential. The third term is a torsional potential, which represents the potential due to rotation of a bond. The fourth component is the energy of the non-bonded interactions that are calculated between all pairs of atoms that are at least three bonds apart. This non-bonded component is composed of an electrostatic interaction, which is modelled by Coulomb potential term, and a van der Waals interaction, which is modelled by a Lennard–Jones potential term or similar potential terms. More complicated force fields may contain extra factors in addition to these four basic components. The main purpose of any force field in molecular dynamics is to reproduce the structural properties and energies of the simulated system⁴⁶. A crucial feature of any force field is transferability of the functional form and parameters. This means being able to use the same set of parameters with different, related models without developing a new set of parameters for each individual molecule. It is important to remember that as force fields are *empirical*, there is no ‘correct’ form of a force field³⁸.

Molecular mechanics force fields may omit some atoms from the model system in order to speed up the calculations. Simulations which explicitly represent all atoms in the system including nonpolar hydrogen atoms are known as ‘all atom’ force fields. ‘United atom’ force fields implicitly include nonpolar hydrogen atoms within carbon parameters. ‘Coarse-grained’ force fields represent molecules in a more abstract way by grouping subsets of atoms together to form ‘super

atoms'. Atomistic-level simulations require much greater processing power than united atom or coarse-grain simulations to model large-scale systems. Alternatively coarse-grain simulations are much faster but neglect many important details of the molecular interactions, leading to a much greater approximation of the system.

In this study we have used the GROMOS 53A6 united atom force field, which is the product of successive re-parameterizations with respect to the previous GROMOS 43A3 and 43A4 force fields. These force fields have been used to model a variety of chemical and physical systems ranging from glasses and liquid crystals, to polymers and crystals and solutions of biomolecules. The GROMOS 53A6 parameters were developed by Oostenbrink *et. al*⁴⁷. in 2004 by fitting the parameters to the experimental data to reproduce thermodynamic properties such as, densities and heat of vaporization of pure liquids in a range of small polar molecules and adjusting the partial charges to reproduce the hydration free enthalpies in water.

1.9 MOLECULAR DYNAMICS SIMULATION AND THE STUDY OF MOLECULAR SELF-ASSEMBLY

Molecular dynamics simulations have been used to study the spontaneous aggregation of molecules in a large variety of systems. The main focus of this literature review is to describe the molecular systems that have been investigated, the simulation initial conditions, how long simulations were run, what type of force fields and software packages were used, and the analysis methods that have been implemented to analyse the final structures.

Since the focus of this work is on the molecular self-assembly of water, bile salts, lipids and fatty acids, the studies that have been conducted by other researches on these systems will be assessed in the following sections.

1.9.1 Water/Lipids Systems

This review describes water/lipid systems that have been investigated to date in order to understand where the study of water/lipid systems is at this time.

To develop a more detailed description of phospholipid structures by comparing the simulation results with experimental data Wendoloski *et al.*⁴⁸ reported a 125 ps MD simulation of lysophosphatidylethanolamine (LPE) micelles incorporating 85 LPE and 1591 water molecules in 1989. This work is a very simple and a very short simulation which only evaluated the difference between pre-equilibrated and equilibrated LPE micelles.

Ten years later, Wymore *et al.*⁴⁹ ran a 1.2 ns, constant pressure MD simulation of a dodecylphosphocholine (DPC) micelle/water system using TIP3P water model with an all atom force field. The simulation, which was started from a well-structured spherical micelle of DPC containing 60 monomers, was analysed to investigate micelle structure, shape fluctuation, water head group interaction, conformation of hydrocarbon chain and *trans-gauche* transition rate. Using radius of gyration and radial distribution functions (RDF), the micelle radius and the average distance between different groups of atoms and the neighbouring DPC monomers were calculated. This work is considerably more advanced and better explained than all the previous MD simulation work on micelles. This gives us a better understanding of the interactions of lipids with water molecules, especially with the TIP3P water model. The detailed analysis method and the comparison of the simulation results with experimental data make this paper a good guide for the work that we have conducted.

In the following year, to observe the effect of aggregate size on the micelle structure, to compare the relaxation behaviour of lipids with NMR relaxation data and to build a starting model for future work, Tieleman *et al.*⁵⁰ modelled solutions of dodecylphosphocholine (DPC) at three different concentrations using 40, 54 and 65 molecules of DPC using the SPC water model. Each simulation was started from a well-structured micelle of DPC using united-atom force field. Additionally, Marrink *et al.*⁵¹ used a united atom force field to observe the self-assembly of

dodecylphosphocholine (DPC) surfactant molecules in SPC water molecules starting from random structures. The spontaneous aggregation of 54 DPC molecules into micelles, rod-like micelles and spheres was observed during this study but was dependent on the DPC concentration. The longest simulation time was 16 ns in a 9 nm box. The results showed that the rod-like micelle was formed within 1 ns of the simulation and it took 6 ns before spherical micellar aggregation was observed. The kinetic analysis of the simulation results indicated that the spontaneous aggregation of DPC is much faster than expected from theoretical models.

Another interesting study is that of Marrink *et. al.*⁵² on self-assembly of phospholipids into bilayers. They claim that this work is the first to demonstrate aggregation of lipids into bilayers with atomic detail. Studying bilayers is more complicated than micelle aggregation due to the balance between hydrophobicity and solvation, and the aggregation involves collective mesoscopic dynamics. Several simulations were run using dipalmitoylphosphatidylcholine (DPPC), palmitoyloleoylphosphatidylcholine (POPC), dioleoylphosphatidylcholine (DOPC) and dioleoylphosphatidylethanolamine (DOPE) using the GROMACS software package. The total simulation time was 0.5 μ s, which is the longest to date in the area of molecular self-assembly. The systems were initiated from randomly distributed lipid molecules and these lipids gradually formed bilayers with the same characteristic time scales. Several simulations using different system sizes were run and observed very similar aggregation behaviour regardless of the number of molecules in the systems. In almost all systems the monolayers contained almost equal numbers of lipids. The existence of hydrophilic pores in the bilayers, which is a biologically important phenomenon in equilibrium membranes, was also briefly explained.

In the same year, a simulation study of lipid diamond cubic phase using glycerolmonoolein (GMO) was performed by Marrink and Tieleman⁵³. Using different water/GMO ratios (0.260, 0.269, 0.276 and 0.279), four systems were simulated by constructing different GMO molecules in one unit cell of the diamond cubic phase. The GROMACS software package was used with an all atom force field for GMO. The SPC water model was used and each system was run for 7.5 ns. The starting

structure was constructed from general assumptions based on some examples. The overall organization of the surfactant and water phase within the system and with the local arrangement of the individual molecules were analysed.

Starting from a random solution, the phase behaviour of a DPPC/PA/water 1:2:20 mixture as a function of temperature was studied by Marrink and *et. al.*⁵⁴ in the year 2006. Three sets of molecular dynamics simulations with the aim of investigating the transition of lipids from lamellar to non-lamellar phases were performed. The system adopted either a gel phase at temperatures below ~ 330 K or an inverted hexagonal phase above ~ 330 K. The possibility of direct transformation from a gel to an inverted hexagonal phase at elevated temperature (~ 390 K) was also suggested. The spontaneous aggregation of stalks, which are inter-lamellar connections, took place within a nanosecond time scale and their subsequent elongation leads to the formation of an inverted hexagonal phase. GROMACS simulation suite for all simulations with the GROMOS-87 force field was used.

Using GROMACS software suite with the GROMOS 42a6 united atom force field, Warren *et.al.*⁵⁵ performed a 40 ns molecular dynamics simulation on glyceride lipid formulations, with propylene glycol and water in late 2000. The simulation was started from randomly distributed glyceride molecules within a cubic simulation box, which were then solvated with the propylene glycol and/or water molecules. The force field was parameterized for propylene glycol and new partial charges were derived before they ran the simulation. Some physical properties of polyethylene glycol were calculated and compared with the experimental results to check reliability. Several independent simulation such as propylene glycol by itself for the parameterization and calculations of different physical properties, polyethylene glycol with increasing water content, all the three glycerol independently with increasing water content, mixtures of mono and di glycerol and mono, di in 1:1 molar ratio and tri glycerol in 1:1:1 molar ratio with increasing water content were simulated. Finally, the mixture of mono and di glycerol and polyethylene glycol with increasing water content were simulated. The effects of water content on the structures were

analysed. Diffusion coefficients of propylene glycol and water at different water content, and also the percentage hydration of MGL, DGL and water molecules were calculated. In 2010, Janosi and Gorfe⁵⁶ also performed constant temperature and pressure MD simulations of a 2-oleoyl-1-palmitoyl-sn-glycero-3-phosphocholine (POPC) bilayer containing 23% 2-oleoyl-1-palmitoyl-sn-glycero-3-glycerol (POPG) using the CHARMM force field but they started their simulation from a well-structured bilayer.

These water/lipids studies have helped us to understand the spontaneous aggregation of lipids into micelles, rod-like micelles, spheres and bilayers. Specifically, the work of Warren *et. al.* provides an insight into the structural changes that occur on dispersion of a formulation in an aqueous phase and suggests that MD modelling has a significant potential to be used as a predictive tool for the structure of lipid formulations.

1.9.2 Water/Bile Salts Systems

The following two studies have been conducted to investigate the self-assembly of bile salts in water. In these studies, MD simulation methods were used to propose different models of bile salt micelles and their assembly process was investigated.

Warren *et. al.*^{26c} investigated the spontaneous self-aggregation of six different types of bile salts starting from a random distribution. The main aim of the work was to investigate the micellar structures formed by bile salts at atomistic level. In this study, bile salts exhibited unusual properties. This includes the shape and size of the micelles of the bile salts due to their planar hydrophobic and hydrophilic faces. The GROMACS simulation package with an ffgmx united atom force field, which is based on the GROMOS-87 force field was used. Different shapes were formed by the self-assembling process of the bile salts, which varied from oblate to spherical or prolate micelles. The intermolecular hydrogen bonding within the micelles was found to be an important factor in determining the micelle size, structure and dynamics. Models of the bile salt micelles were proposed and compared to three previously proposed models⁵⁷. From the

comparison the model of bile salt micelles of Warren *et. al.* exhibited more disordered and dynamic behaviour than the earlier models.

The aggregation behaviour and physicochemical properties of bile salt and bile salt/fatty acid mixtures was examined by Turner *et. al.*⁵⁸. The GROMACS software package and the GROMOS 98 united atom force field were used to investigate trihydroxy bile salt, glycocholate and oleic acid. The self-assembly of glycocholate in water from an initial randomly distributed system of 31 glycocholate molecules was investigated with the quick assembly of the bile salt into small micellar aggregates such as dimers and trimers before stabilizing as larger micelles observed. The local atom density profile and critical micelle concentration of glycocholate were calculated.

The results of these simulation studies were in a good agreement with previously published experimental results. Furthermore, they enhance our understanding of the colloidal species formed by bile salts and highlight the unique properties of bile salts that come from their planar hydrophobic and hydrophilic faces.

1.9.3 Water/Bile Salts/Lipids Systems

The self-assembly of bile salts and lipids in aqueous environment is a major aspect of this study. Hence, the following review lists the works that have been done by other researches on water/bile salts/lipids system to date.

Marrink and Mark⁵⁹ have reported more complicated simulations using phospholipids (PC), bile salts (BS) and cholesterol (CH). 0.15 M NaCl was inserted in the system to mimic the physiological contents of the gall bladder. Three different systems, composed of different numbers of phospholipids, bile salts and cholesterol were simulated. From the results of the time evolution of the principal radii of the micelles, the authors concluded that the micelles are very flexible, especially those that had high bile salt content.

The structure and dynamics of cholic acid (CA) and dodecylphosphocholine (DPC) aggregates were investigated using NAMD software with all atom CHARMM general force field by Sayyed-

Ahmad *et. al.*⁶⁰. Starting from a solvated DPC micelle they investigated seven independent simulations with different molar ratios of CA and DPC and different water contents. The main aim of this work was to investigate the thermodynamic and structural properties of CA and DPC mixed micelles. The sizes and aggregation numbers of the DPC-CA mixed micelles were linearly dependent on CA molarity, which is in agreement with the radial shell model reported by Nichols and Ozarowski⁶¹.

Prakash *et. al.*⁶² reported all-atom MD simulations of cholic acid (CA), ibuprofen (IBU) and dodecylphosphocholine (DPC) mixtures to study their spontaneous aggregation as well as their adsorption on a DPC micelle. They reported that the size of CA–IBU mixed micelles varied with their molar ratio in a non-linear manner, and that micelles of different sizes adopted similar shapes but differed in composition and internal interactions. These observations were supported by NMR chemical shift changes, NMR Rotating frame Overhauser Effect Spectroscopy (ROESY), and dynamic light scattering experiments. The main aim of their study was to investigate the aggregation behaviour of CA and IBU in the presence and absence of a pre-formed PC micelle at atomistic level.

These studies revealed the thermodynamic and structural properties of bile salts and lipids in aqueous environment. It is shown that the size of the mixed micelles formed by bile salts and lipids are highly dependent on the molar ratio of the bile salts. Additionally, it is notable that the previous works do not consider the significance of the lipid digestion on the thermodynamic and structural properties of bile salts and lipids mixed micelles.

1.9.4 Water/Fatty Acid Systems

Another aspect of this study is to investigate the impact of digestion products of lipids. As discussed previously, digestion of phospholipids produces one fatty acid and one lyso phospholipid. Also, digestion of triglyceride molecule produces two fatty acids and one monoglyceride. Therefore, in this section different MD simulations studies of water/fatty acid

systems have been reviewed in order to understand the spontaneous self-assembly process of fatty acids in an aqueous environment.

Watanabe *et al.*⁶³ undertook MD simulations of the water/sodium octanoate system and analysed the structure of the micelle of sodium octanoate in 1998. The simulation was started from a well-structured micelle of sodium octanoate and the simulation, which was composed of 15 monomers, was run for 0.2 ns. The micelle was stable throughout the whole simulation period. In their analyses the radius of micelle was measured and they provided density profiles of carbon, solvent water, counter ion and the head group carbon atom with respect to the micelle centre of mass. The mean radius of the micelle was in a good agreement with the value obtained from neutron scattering data. Additionally, this result is similar to results obtained using NMR and Raman spectroscopy.

An intensive MD simulation study of the phase behaviour of the binary sodium laurate/water and sodium oleate/water, ternary sodium laurate/sodium oleate/water systems was performed by King *et al.*⁴⁰. The simulation results were compared to published phase diagrams. The GROMACS software suite with the GROMOS 53A6 united atom force field was used. The results were analysed using radial distribution functions, average fraction of trans C-C bonds of the surfactants, and Gibbs energies of atom pair association as a function of surfactant concentration. By performing multiple MD simulations the phase of a system at a given point on the phase diagram was predicted. Their simulations accurately model the experimentally observed phase behaviour of this system. This work compared the MD and experimental phase behaviours at identical concentrations and indicated that MD simulation can be used as a prediction tool for different water/surfactant systems.

Recently, MD simulations were reported to investigate the microstructure of type I lipid formulation using GROMACS software suite and the GROMOS 43A2 force field by Warren *et al.*⁶⁴. The aim was to study type-I formulations at the molecular level as they interact with water during dispersion. The investigation was done on a simple lipid formulation, by itself and in the presence

of five poorly-water soluble drugs (acyclovir, danazol, hydrocortisone, ketoprofen (protonated and un-protonated) and progesterone). The formulation contained mono- and di-lauroyl glycerides (MGL and DGL). Different analysis tools were implemented to evaluate the final simulation results such as calculating the water coordination number of the first hydration shells of atoms of each system, self-diffusion of water and glyceride, spatial distribution functions of water and glycerol atoms around drugs in the formulations and water and glycerol coordination numbers for selected drug atoms as a function of water concentration.

These works provide a good basis to extend this work into more complex lipid formulations using MD simulation. Specifically, the study of Warren *et. al.* provides important information about the dynamic behaviour of the excipients in formulation, such as aggregation, that will result in poor solubilisation properties. They also shed light on our understanding of partitioning of PWSD in lipid formulations.

1.9.5 SUMMARY: MD simulations of self-Assembling systems

To date, a variety of self-assembling systems have been studied using MD simulations. Since work undertaken in this study work focuses on the self-assembly of excipients and the intestinal digestion of lipid based drug delivery systems, understanding the different types of self-assembly systems is vital to the design of our studies. Although most studies reviewed deal with simple micellar structures, the analytical methods implemented provide guidance with how we can proceed on our analysis methods.

Most of the simulations reported in the literature have been started from randomly distributed surfactant molecules in water using the SPC/E and TIP3P water models. Most atomistic simulations use a united atom force fields with a few using an all atom force field. The most commonly used MD software package was GROMACS; there was limited use of NAMD. The common analytical methods were: radial distribution function, radius of gyration, diffusion coefficient, solvent accessible area and time correlation functions.

Comparisons of simulation and experimental data are vital to test the accuracy of the calculated results and to provide standards for improving the methodology. In all the studies reviewed above, the results of the computed values were compared with published experimental results. In most cases, the results were in good agreement. Since it is impossible to model a complete experimental system, the comparison between experimental and modelled systems is generally limited. As mentioned above, this is a limitations of MD simulation.

"The real danger is not that computers will begin to think like men, but that men will begin to think like computers."

Sydney J. Harris

CHAPTER TWO

IMPROVING FORCE FIELD PARAMETERS FOR ALCOHOL AND ETHYLENE GLYCOL FUNCTIONAL GROUPS

2 IMPROVING FORCE FIELD PARAMETERS FOR ALCOHOL AND ETHYLENE GLYCOL FUNCTIONAL GROUPS

2.1 INTRODUCTION

This project focuses on the molecular level understanding of excipients, which are involved in the formulation of lipid-based drug delivery systems (LBDD). Lipid formulations for the oral administration of drugs generally consist of a drug dissolved in a mixture of excipients, which can include combinations of pure triglyceride oils, glycerides, lipophilic surfactants, hydrophilic surfactants and water-soluble cosolvents². A molecular dynamics (MD) simulation approach has been used to understand the phase behaviour and molecular interactions within the phases formed by bile salts and phospholipids (a model of the intestinal lumen) and LBDD system components. Before investigating the phase behaviour of the intestinal lumen and LBDD systems, the force field used in the modelling requires validation, mainly for non-ionic surfactants. Because the focus of biological force fields is mostly on protein structures, i.e. amino acid chains, lipids and nucleotides (RNA and DNA), modifications are typically required for use of the force field for molecules outside of that scope.

Ultimately, we want to understand the behaviour of LBDD systems with the intestinal lumen. One component of LBDD systems that is of particular interest are the non-ionic surfactants containing polyethylene oxide chains. Some examples are pentaethylene glycol monododecyl ether ($C_{12}E_5$), hexaethylene glycol monododecyl ether ($C_{12}E_6$), heptaethylene glycol monododecyl ether ($C_{12}E_7$), and octaethylene glycol monododecyl ($C_{12}E_8$) (structures available in Appendix 1) which are derived from hydrolysed vegetable oils¹. These compounds have been studied experimentally, but the understanding of their behaviour at the molecular level is currently limited. A current limitation to research into these molecules using molecular dynamics simulations is that the ethylene glycol portion of these non-ionic surfactants is not well parameterized in the GROMOS 53A6 united atom force field⁶⁵. Force fields are parameterized to reproduce a selection of

experimentally measured molecular properties that can be calculated from simulations. Typically these molecular properties include; density of the liquid, dipole moment, and latent heats of vaporisation and solvation. The simulation result of the underlying physicochemical properties that are involved in those molecular property values should be a good approximation to the experimental values. However, when a property of interest is not encompassed by those molecular properties used to parameterise the force field, then reproduction of experimental results is not guaranteed.

The aim of this part of the project is to develop improved parameters of polyethylene glycol (PEG) surfactants. It is important that we have a well parameterized force field if we wish to model lipid formulation containing PEG surfactants. A new parameter set (53A6OXY) is developed by Horta et. al.⁷³ for the GROMOS force field, that combines reoptimized parameters for the oxygen-containing chemical functions (alcohols, ethers, aldehydes, ketones, carboxylic acids, and esters) with the current biomolecular force field version (53A6) for all other functions. But they use cyclohexane as a solvent in their reoptimization process, which makes it difficult for us to find the experimental log P values of PEGs to compare it with the calculated value using free energy method. Hence, we decided to reparametrize the original GROMOS 53A6 using octanol as a solvent.

To begin with, we explored the applicability of the GROMOS 53A6 force field for a selection of molecules and determined that further refinement of the parameters for alcohols was required to reproduce the correct free energies. Optimisation of the alcohol functional group was performed to best reproduce the logP for octanol. Then the partial atomic charges of the ethylene glycol functional group were optimised to best reproduce the logP of penta-ethylene glycol. The improved atomic charges, denoted 53A6_{PEG}, were then tested with a series of alkanes, alcohols, ethylene glycols and amino acid analogues.

2.2 LOGP AND GIBBS FREE ENERGY

The partition coefficient ($\log P$) of active pharmaceutical ingredients (APIs) is probably the most important input parameter used within the pharmaceutical industry. The partition coefficient is the ratio of equilibrium concentrations of a molecule when partitioned between two immiscible phases; in this case it is between 1-octanol and water (see Equation 1). The prediction of drug partitioning, hydrophobicity and even pharmacokinetic characteristics within biological systems can be quantified by expressions based on the octanol/water partition coefficient⁶⁶.

$$\log P(\text{octanol/water}) = \frac{[\text{Solute}]_{\text{octanol}}}{[\text{Solute}]_{\text{water}}} \quad 1$$

Gibbs energy is always expressed as the relative energy between two states; it is never an absolute value. A process with a negative Gibbs free energy change will undergo the process spontaneously, whereas a positive value requires work to be added to the system for the process to occur (see Equation 2). It is possible to calculate the partition coefficient of a solute from the Gibbs free energy of the solute in octanol and water, which can be calculated using molecular dynamics simulations.

$$\Delta G(T, P) = \Delta H - T\Delta S \quad 2$$

where T is temperature and P is pressure.

In order to calculate the Gibbs energy of a system using molecular dynamics simulations, a molecular model is required that describes the thermodynamic behaviour of the system correctly. That is, the Hamiltonian (\hat{H} , operator describing to the total internal energy of the system) used to calculate the interatomic forces must be chosen such that all configurations have the correct relative probability. In the case of molecular dynamics, the Hamiltonian is the sum of all the equations representing the interactions within the simulated system i.e. bonded, electrostatic and van der Waals interactions and kinetic energy. In practice, the choice of Hamiltonian is a compromise between accuracy and computational efficiency; with the evaluation of the energy

and forces needing to be computationally inexpensive enough to permit sufficient sampling, yet of sufficient accuracy to estimate the Gibbs free energy reliably⁶⁷.

The Gibbs free energy is a state function that can be calculated by molecular simulation based on the construction of a thermodynamic cycle that may include non-physical transformations. Thus, the Gibbs energy of hydration at temperature T and pressure P , $\Delta G_{\text{hydration}}(P, T)$, can be calculated using the thermodynamic cycle^{38, 68} presented in Figure 2.1.

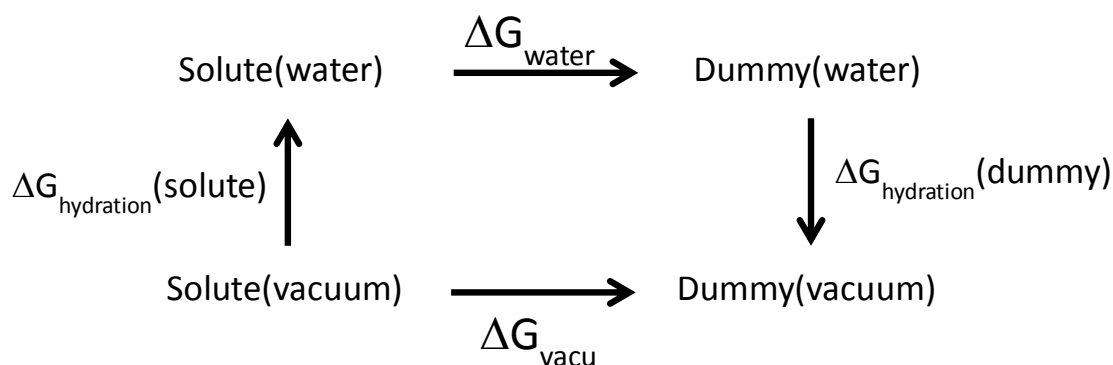


Figure 2.1 Thermodynamic cycle for the calculation of the Gibbs energy change of hydration of a solute ($\Delta G_{\text{hydration}}(\text{solute})$); the transfer of a solute from a vacuum to water.

Where $\Delta G_{\text{hydration}}$ is the Gibbs free energy change associated with the mutation of the solute molecule into a dummy (non-interacting) molecule in water, ΔG_{vacuum} is the Gibbs free energy associated with the mutation process in a vacuum and $\Delta G_{\text{hydration}}(\text{dummy})$ is the solvation Gibbs free energy of the dummy molecule. Since dummy molecules do not interact with their environment, there are no electrostatic or van der Waals interactions and $\Delta G_{\text{hydration}}(\text{dummy})$ is equal to zero. Note that the intramolecular bonded interactions for a dummy molecule are identical to those with the fully interacting solute molecules. Therefore, the thermodynamic cycle for hydration of a solute molecule based on Figure 2.1, can be written as shown in Equation 3.

$$\begin{aligned}\Delta G_{\text{hydration}}(\text{solute}) &= \Delta G_{\text{vacuum}} - \Delta G_{\text{hydration}}(\text{dummy}) - \Delta G_{\text{water}} \\ &= \Delta G_{\text{vacuum}} - \Delta G_{\text{water}}\end{aligned}\quad 3$$

Likewise, the octanol solvation Gibbs free energy at temperature T and pressure P , $\Delta G_{\text{solv}}(P, T)$, can be calculated in a similar way using thermodynamic cycle shown in Figure 2.2.

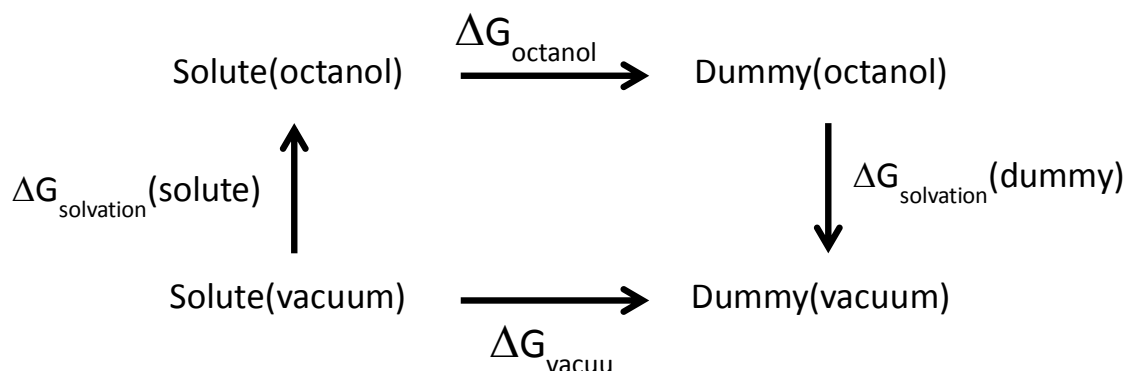


Figure 2.2 Thermodynamic cycle for calculation of the Gibbs energy change of solvation of a solute ($\Delta G_{\text{solvation}}(\text{solute})$), the transfer of a solute from a vacuum to octanol.

Therefore, the thermodynamic cycle for solvation of a solute molecule into octanol based on Figure 2.2, can be written as shown in Equation 4.

$$\begin{aligned}\Delta G_{\text{solvation}}(\text{solute}) &= \Delta G_{\text{vacuum}} - \Delta G_{\text{solvation}}(\text{dummy}) - \Delta G_{\text{octanol}} \\ &= \Delta G_{\text{vacuum}} - \Delta G_{\text{octanol}}\end{aligned}\quad 4$$

2.3 GIBBS FREE ENERGY CALCULATION FROM MOLECULAR DYNAMICS

The calculation method for the Gibbs free energy change using molecular dynamics requires the simulation to be carried out in the isothermal-isobaric (NPT) ensemble, where N is the number of molecules, P is pressure and T is temperature and all are constant. It is estimate by considering two well defined states; an initial state (state 0, the reference state) and a final target state (state 1)⁶⁹. These have the Hamiltonians \hat{H}_0 and \hat{H}_1 respectively. A coupling parameter, λ , is added to the Hamiltonian, $\hat{H}(p, q; \lambda)$, where p is the linear momentum and q is the atomic position, and is used to describe the transition between the two states. There are a number of methods that can be used to calculate the transformation from state 0 to state 1, with thermodynamic integration (TI) and Bennett acceptance ratio (BAR) being the two considered here.

2.3.1 Thermodynamic Integration Method

The thermodynamic integration method is one of the methods used to calculate the free energy difference between two states. It is implemented in the GROMACS^{43, 70} molecular dynamics software suite. The solvation process is the transfer of solutes from a (gas/vacuum) in to solution, and the solvation free energy may be defined as the free energy difference given by the total reversible work associated with changing the Hamiltonian of the system from the gas to the liquid state⁶⁹.

The algorithm of thermodynamic integration method for calculations of solvent and vacuum free energies, is estimated by considering two generic well-defined states, an initial state (state 0) which is a reference state and a final target state (state 1) with Hamiltonians \hat{H}_0 and \hat{H}_1 respectively. A coupling parameter, λ , can be added to the Hamiltonian, $\hat{H}(p, q; \lambda)$, where p is the linear momentum and q is the atomic position, and used to describe the transition between the two states:

$$\hat{H}(p, q; 0) \longrightarrow \hat{H}(p, q; 1) \quad 5$$

Considering several discrete and independent λ values between 0 and 1, equilibrium averages can be used to evaluate derivatives of the free energy with respect to λ . In order to get the energy difference between them the derivatives of the free energy along a continuous path connecting the initial and final states can be integrated, see Equation 6. The choice of number of λ values have to be sufficient to ensure that a smooth $\partial \hat{H} / \partial \lambda$ curve is obtained and minimise the integration errors.

$$\Delta G = \int_0^1 \left\langle \frac{\partial \hat{H}(p, q, \lambda)}{\partial \lambda} \right\rangle_{\lambda} d\lambda \quad 6$$

The Gibbs energy of hydration (Equation 3) can be calculated from two sets of simulations, between state 0 and state 1, in water and vacuum, as shown in Equation 7. The same calculation

can also be performed to calculate the Gibbs energy change of solvation in octanol, with two sets of simulations in octanol and vacuum.

$$\Delta G_{\text{hydration}} = \int_0^1 \left\langle \frac{\partial \hat{H}}{\partial \lambda} \right\rangle_{\text{vacuum}} d\lambda - \int_0^1 \left\langle \frac{\partial \hat{H}}{\partial \lambda} \right\rangle_{\text{water}} d\lambda \quad 7$$

2.3.2 The Bennett Acceptance Ratio (BAR) Method

The Bennett's acceptance ratio (BAR) algorithm estimates the difference in Gibbs energy between two states⁷¹ using the configuration information for the two adjoining states. It is different to the thermodynamic integration method, which only requires the derivative at a given state to estimate the Gibbs energy change with adjoining states. The BAR method automatically adds series of individual free energies into a combined free energy estimate. Individual free energy difference relies of two simulations at different states; the Gibbs energy difference between state i and state j is given by Equation 8 and controlled by a λ . Bennett then showed that the value of ΔG which satisfied Equation 9 minimised the estimate of the Gibbs energy change between the two states. This equation is solved numerically to obtain the value of the Gibbs energy change.

$$\Delta G = -kT \log \frac{E_j}{E_i} \quad 8$$

where k is the Boltzmann constant, and E_i and E_j are the potential energies (J mol^{-1}) of the system in state i and j , respectively.

$$\sum_{i=1}^{n_i} \frac{1}{1 + e^{(\ln(\frac{n_i}{n_j}) + \beta \Delta E_{ij} + \beta \Delta G)}} - \sum_{j=1}^{n_j} \frac{1}{1 + e^{(\ln(\frac{n_j}{n_i}) + \beta \Delta E_{ji} + \beta \Delta G)}} = 0 \quad 9$$

where n_i and n_j are the number of values from energy distributions for state i and j , and β is $1/kT$.

Error estimation in this method is done by splitting the data into blocks, then determining the free energy differences over those blocks and assuming that blocks are independent. The final error estimates are determined from the average variance of five blocks by default⁴³.

2.3.3 logP from Gibbs Energy

The octanol/water partition coefficient (logP) can be calculated using a thermodynamic cycle that is similar to those shown previously⁶⁸.

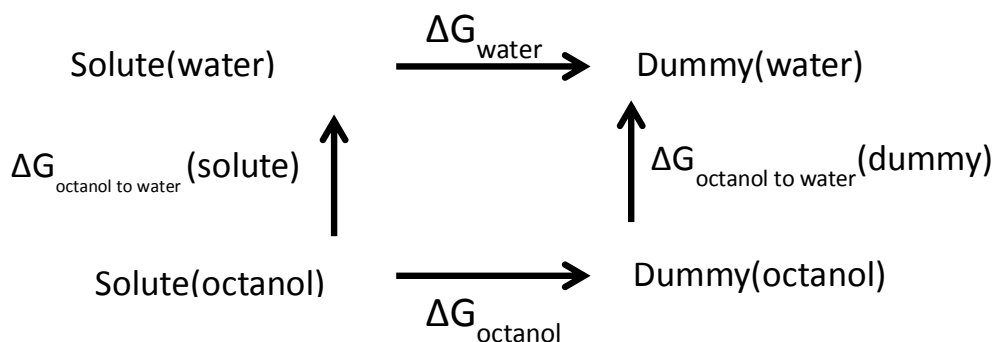


Figure 2.3 Thermodynamic cycle for calculation of the Gibbs energy change of transfer of a solute from octanol to water ($\Delta G_{\text{octanol to water}}(\text{solute})$).

The thermodynamic cycle for movement of a solute molecule from octanol to water can therefore be written as shown in Equation 5:

$$\begin{aligned}\Delta G_{\text{octanol to water}}(\text{solute}) &= \Delta G_{\text{octanol}} + \Delta G_{\text{octanol to water}}(\text{dummy}) - \Delta G_{\text{water}} \\ &= \Delta G_{\text{octanol}} - \Delta G_{\text{water}}\end{aligned}\quad 5$$

$\Delta G_{\text{octanol to water}}(\text{solute})$ is related to the partition coefficient between octanol and water (logP) by Equation 6⁶⁸, where T is temperature (K) and R is the gas constant ($8.314 \text{ J K}^{-1} \text{ mol}^{-1}$).

$$\Delta G_{\text{octanol to water}}(\text{solute}) = -2.303RT \log P \quad 6$$

Therefore, the partition coefficient of the solute between octanol and water can be calculated from the Gibbs energies of hydration and solvation in octanol, according to Equation 12.

$$\begin{aligned}\log P(\text{octanol/water}) &= \frac{\Delta G_{\text{octanol to water}}}{2.303RT} \\ &= \frac{\Delta G_{\text{water}} - \Delta G_{\text{octanol}}}{2.303RT}\end{aligned}\quad 7$$

2.4 METHODS

Molecular dynamics simulations were performed with the GROMACS simulation package⁷⁰ versions 4.0.7 and 4.5.4 using the GROMOS 53A6 united atom force field⁴⁷. Calculations were performed on the Victorian Life Sciences Computation Initiative (VLSCI) Linux cluster compute nodes. The integration of Newton's equations of motion was carried out by GROMACS using a leap-frog dynamic algorithm⁷² with a time step of 2 fs. Langevin (stochastic) dynamics were used to control the temperature with a frictional constant of 1 ps and 298 K reference temperature. The use of Stochastic dynamics eliminates problems that may arise with performing Gibbs energy calculations using conventional thermostats with molecular dynamics⁷³. Simulation boxes were cubic, with periodic boundary conditions and hydrated octanol systems contained 0.275 water mole fraction (3 % w/w)⁷⁴, which is experimentally calculated.

The initial coordinate files of solutes were built using Maestro⁷⁵ and topology files were built manually. The simple-point-charge (SPC) water model was used to describe the solvent water molecules⁷⁶. Initial molecular configurations were generated by random placement of the molecules within the simulation box using the *silico* script⁴⁵ *random_box*. The pre-production run procedure comprised of energy minimization, followed by the simulation in the isothermal-isobaric (NPT) ensemble, of 100 ps to equilibrate the system. The production runs were of 5 ns duration under NPT conditions as the calculated free energy values were observed to reach constant values well within the 5 ns simulation. Coulomb interaction was PME with 0.9 nm cut-off distance for coulomb as well as van der Waals and 4 interpolation order for PME. Two energy minimisation procedures were employed; the first was the limited-memory Broyden-Fletcher-Goldfarb-Shanno (L-BFGS) algorithm⁷⁷ for 5,000 steps, followed by a second procedure a steepest descents minimization for 500 steps. Two energy minimization steps are used to get a better minimized structure of the system. L-BFGS converges very quickly and premature minimization happens. Steepest descent also has a problem of finding the correct energy minimization, but when the two are used in conjunction the result becomes best. The λ dependence of the Lennard-Jones

potential was interpolated between neighbouring states using soft-core interactions; $\alpha = 0.5$, power = 1.0, and $\sigma = 0.3$ ^{73, 78}. The soft-core potential V_{sc} are shifted version of the regular potentials. This is fully described in GROMACS manual section 4.5.1. The equations are:

$$V_{sc}(r) = (1-\lambda)V^A(r_A) + \lambda V^B(r_B), \quad r_A = (\alpha\sigma_A^6\lambda^p + r^6)^{1/6} \text{ and } r_B = (\alpha\sigma_B^6(1-\lambda)^p + r^6)^{1/6}$$

where, V^A and V^B are the normal “hard core” Van der Waals or electrostatic potentials in state A ($\lambda=0$) and state B ($\lambda=1$) respectively, α is soft-core parameter, p is the soft-core λ power, σ is the radius of interaction, which is $(C_{12}/C_6)^{1/6}$ or an input parameter (sc_sigma) when C_6 or C_{12} is zero.

All bonds were constrained using the LINCS algorithm⁷⁹. The system density was directly obtained using g_energy^{44, 80} and dihedral distributions were obtained using g_angle^{44, 80}. Both scripts are part of GROMACS.

2.5 DIHEDRAL ANGLE POTENTIAL

The dihedral angle function used by the GROMOS 53A6 force field⁴⁷ is of the form shown in Equation 8:

$$V_{dihedral}(\phi) = k_\phi(1 + \cos(n\phi - \phi_r)) \quad 8$$

where $V_{dihedral}$ is the potential energy of the dihedral bond, ϕ is the dihedral angle between atoms i, j, k and l , n the periodicity, range of ϕ is 180 to -180, k_ϕ the force constant and ϕ_r the phase shift. In some situations, for example alkanes⁸¹, this potential is insufficient to correctly describe the dihedral bond distribution and dynamics and instead the Ryckaert-Bellemans dihedral bond potential is used, see equation 9.

$$V_{dihedral}(\phi) = C_0 + C_1 \cos \psi + C_2 \cos^2 \psi + C_3 \cos^3 \psi + C_4 \cos^4 \psi + C_5 \cos^5 \psi \quad 9$$

where $\psi = \phi - 180$.

A 10 ns simulation of PEG-11 (undecaethylene glycol, see Figure 2.4 for molecular structure) in SPC water model was performed to determine the dihedral distributions using the GROMOS 53A6 periodic dihedral potentials gd_3 and gd_23, corresponding to the O-CH₂-CH₂-O and CH₂-O-CH₂-

CH₂ dihedrals, respectively. The dihedral distributions obtained for these two dihedrals are shown in Figure 2.5 as the black solid lines. The distribution exhibited for the O-CH₂-CH₂-O appears too flat, with little preference for the gauche confirmation and the absence of the peak corresponding to the trans configuration at ± 180 . Therefore, the dihedrals were changed to a Ryckaert-Bellemans potential based on the *ab initio* calculations of Anderson and Wilson⁸². The dihedral bond parameters reported by Anderson and Wilson are in the form to be used by a Fourier dihedral function, as shown in Equation 15. These can be converted to the Ryckaert-Bellemans function using equation 16, with the parameters summarised in Table 2.1.

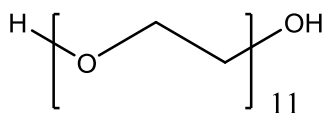


Figure 2.4 Structure of PEG-11, undecaethylene glycol.

Table 2.1 Dihedral bond potential parameters (kJ mol^{-1}) for the dihedrals within the ethylene glycol functional group from Anderson and Wilson⁸²; including parameters for use the Fourier (F_n) and Ryckaert-Belleman (C_n) functions.

Fourier Series		$F1$	$F2$	$F3$	$F4$
O-C-C-O		3.114	-12.206	11.688	18.785
C-O-C-C		-6.538	9.511	12.820	-5.300
Ryckaert-Belleman	$C0$	$C1$	$C2$	$C3$	$C4$
O-C-C-O	-4.804	15.974	87.348	-23.376	-75.143
C-O-C-C	12.652	22.499	-30.713	-25.640	21.202

$$V_{\text{dihedral}}(\phi) = \frac{1}{2} [F_1(1 + \cos \phi) + F_2(1 - \cos 2\phi) + F_3(1 + \cos 3\phi) + F_4(1 - \cos 4\phi)] \quad 10$$

$$C_0 = F_2 + \frac{1}{2}(F_1 + F_3)$$

$$C_1 = \frac{1}{2}(-F_1 + 3F_3)$$

$$C_2 = -F_2 + 4F_4$$

$$C_3 = -2F_3$$

$$C_4 = -4F_4$$

$$C_5 = 0$$

11

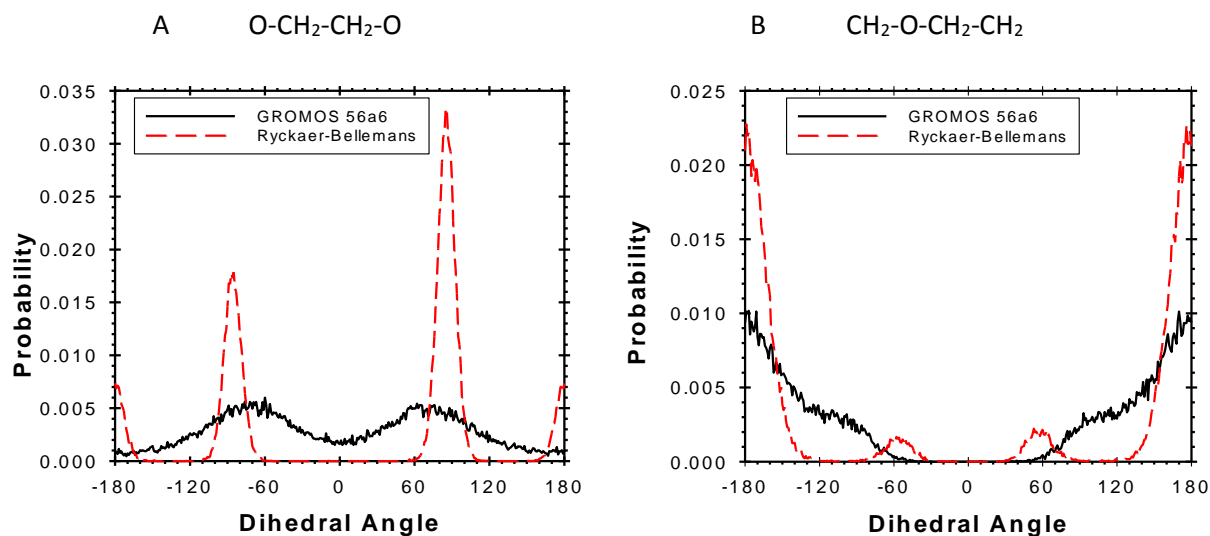


Figure 2.5 Dihedral distributions for PEG-11 in water the dihedrals A) O-CH₂-CH₂-O (gd_3 and Ryckaert-Belleman) and B) CH₂-O-CH₂-CH₂ (gd_23 and Ryckaert-Belleman).

The modification of the dihedral potentials produced a distribution of angles that more closely matches the distribution of angles reported by Anderson and Willison, see Figure 2.6b. Additionally, this allowed reproduction of the results obtained by Ying Xue *et al*⁸³ (using polyethylene glycol as a spacer on the conformational properties of small peptides). Ying Xue *et al* used the ethylene glycol parameters from Anderson and Wilson and observed polyethylene glycol molecules forming a helical structure in water. This confirmation of the polyethylene glycol molecule is predicted theoretically and observed experimentally^{82, 84}. A helical conformation of the PEG-11 molecule was observed, with the conformation shown in Figure 2.6.

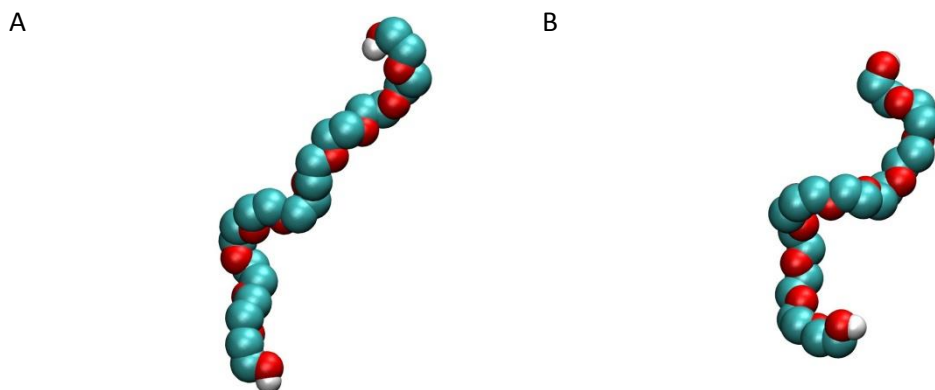


Figure 2.6 Helical conformation of PEG-11 in water using the A) GROMOS 53A6 dihedral potentials *gd_3* and *gd_23* and B) Ryckaert-Bellemans dihedral potential from Anderson and Wilson⁸² for the O-CH₂-CH₂-O and CH₂-O-CH₂-CH₂ dihedrals. Molecule representation only include polar hydrogens, with atom coloured cyan for carbon, red for oxygen and white for hydrogens.

2.6 LATENT HEAT OF VAPORISATION

The latent heat of vaporization was calculated from molecular dynamics simulations from the difference in the enthalpy between the vapour and liquid phases, see Equation 12⁸⁵.

$$\Delta H_{vap} = E_{potential}(gas) + RT - \left(\frac{E_{potential}(liquid)}{n(liquid)} \right) \quad 12$$

Where ΔH_{vap} is the latent heat of vapourisation (kJ mol⁻¹), $E_{potential}(gas)$ is the potential energy of a molecule in a vacuum (kJ mol⁻¹), R is the gas constant, T the temperature (K), $E_{potential}(liquid)$ the potential energy of a liquid simulation (kJ mol⁻¹), and $n(liquid)$ is the number of molecules in the liquid simulation.

2.7 GIBBS FREE ENERGY

Calculation of the Gibbs free energy change between states requires independent calculations to be performed at a sufficient number of λ values so that the derivative of the Hamiltonian is sufficiently smooth (for TI method) and there is sufficient overlap between adjacent states (for BAR method). Integrals for the TI method were calculated using the trapezoidal rule from the

$dH/d\lambda$ versus λ curve. Calculations of the Gibbs free energy using the BAR method used the GROMACS script `g_bar`^{80a}. The following values were used for the calculation of hydration (Gibbs free energy of molecules in water) and solvation (Gibbs free energy of molecules in octanol), where $\lambda = 0$ refers to a fully interacting solute, and $\lambda = 1$ to a non-interacting (dummy) solute. The $\log P$ value for each molecule was calculated using Equation 10.

- Hydration: 0.0, 0.01, 0.02, 0.05, 0.1, 0.12, 0.15, 0.2, 0.25, 0.3, 0.35, 0.4, 0.45, 0.5, 0.55, 0.6, 0.65, 0.7, 0.75, 0.8, 0.82, 0.85, 0.9, 0.95, 0.98, 1.0
- Solvation: 0.0, 0.01, 0.03, 0.05, 0.1, 0.2, 0.3, 0.4, 0.5, 0.6, 0.65, 0.7, 0.75, 0.8, 0.85, 0.9, 0.95, 1.0

2.8 THERMODYNAMIC INTEGRATION VERSUS BENNETT'S ACCEPTANCE RATIO

The more commonly utilised method of calculating the Gibbs energy change between two states is the thermodynamic integration method (TI), with the more thorough BAR method, though certainly not a new technique, now becoming the recommended method⁸⁶. A comparison was made of the Gibbs energy change of hydration and solvation in octanol for mono, di and penta ethylene glycol (MEG, DEG and PEG, respectively) between using the TI and BAR methods for unevenly (0.0, 0.01, 0.03, 0.05, 0.1, 0.2, 0.3, 0.4, 0.5, 0.6, 0.65, 0.7, 0.75, 0.8, 0.85, 0.9, 0.95, 1.0) and evenly (0.0, 0.1, 0.2, 0.3, 0.4, 0.5, 0.6, 0.7, 0.8, 0.9, 1.0) spaced λ values. The unevenly spaced λ values were selected to have more data points in the region where the $dH/d\lambda$ value changes rapidly with λ . The inclusion of more data points allows a better approximation of the area under the curve, as required by the TI method, and better overlap of the energies of neighbouring states, as required by the BAR method. A sample plot of $dH/d\lambda$ versus λ for mono-ethylene glycol (MEG) is shown in Figure 2.7, illustrating the characteristic rapid decrease in the derivative from $\lambda = 0$ to 0.1 and a more gradual change in the region of $\lambda = 0.6$ to 1.0. The results are presented in Table 2.2 and all comparisons for accuracy are made against the more efficient and robust BAR method⁸⁶.

The use of the TI method with a small number of λ values provides an estimate of the Gibbs energy change that is significantly lower than found with the BAR method. This under estimation is expected since there is an insufficient number of data points are present in the regions where $dH/d\lambda$ is change rapidly to provide an accurate estimation of the area under the curve. The use of the additional values in the regions of greatest change improves the values calculated; however they are still 1-2% lower. Using a smaller number of λ values does not make a huge statistical difference to the estimate of the Gibbs energy changes. These conclusions are consistent with the results obtained by de Ruiter *et al.*^{86b} and Shirts and Pande^{86a} for similar systems. Subsequently the BAR method was used to calculated the Gibbs energy change state using with the unevenly spaced values for λ . Even though it would be possible to reduce the number of calculation points from 18 to 11, the 64% increase in calculation time was deemed to be a tolerable cost to ensure an accurate estimate of the Gibbs free energy change for all molecules and conditions.

Table 2.2 Gibbs free energy of hydration ($\Delta G_{\text{hydration}}$, water) and solvation ($\Delta G_{\text{solvation}}$, octanol) for mono-ethylene glycol (MEG), di-ethylene glycol (DEG) and penta-ethylene glycol (PENTEG) using the Bennett's acceptance ratio (BAR) and thermodynamic integration (TI) methods. (Data provided by Dallas Warren).

Solute		$\Delta G_{\text{hydration}}$ (kJ mol ⁻¹)		$\Delta G_{\text{solvation}}$ (kJ mol ⁻¹)	
	λ Spacing\ Method	Even	Uneven	Even	Uneven
MEG					
	TI	-63.46	-101.30	-64.08	-104.30
	BAR	-103.70	-103.57	-105.55	-106.68
DEG					
	TI	-213.86	-263.20	-212.13	-267.81
	BAR	-267.91	-266.70	-267.62	-270.69
PENTEG					
	TI	-656.46	-750.20	-656.56	-755.25
	BAR	-755.23	-743.23	-756.72	-760.16

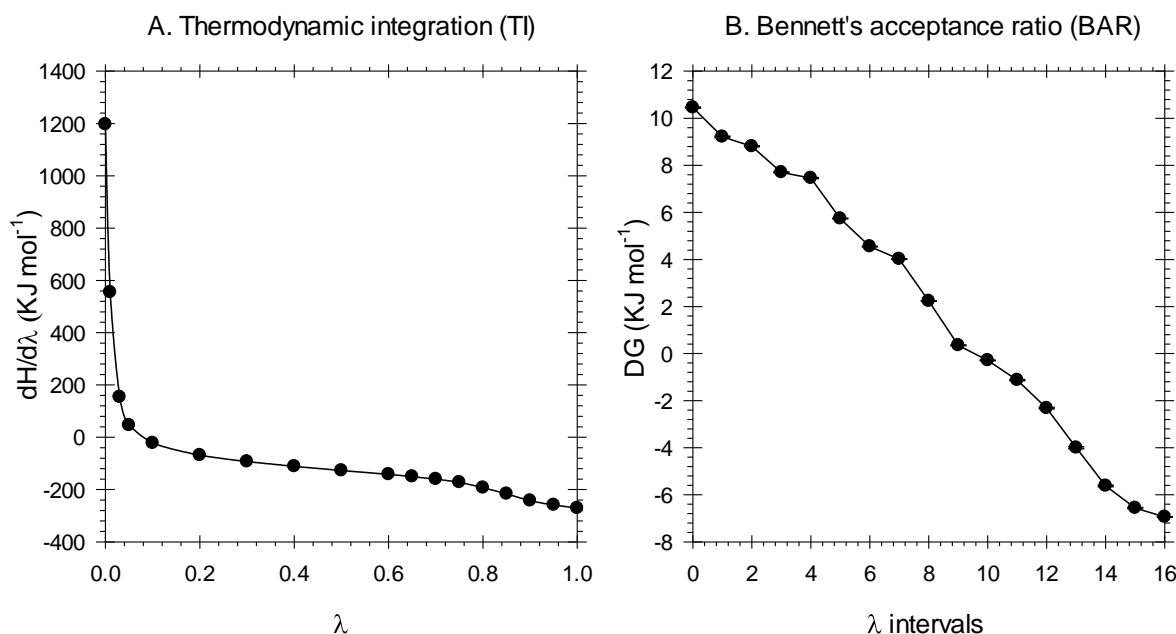


Figure 2.7 The differential of the Hamiltonian mono-ethylene glycol (MEG) in water, A. TI method, as a function of $dH/d\lambda$ versus λ for from fully interacting ($\lambda=0$) to non-interacting ($\lambda=1$), B. BAR method as a function of the free energy estimate (DG) versus intervals of lambda.

2.9 INFLUENCE OF SIMULATION CELL SIZE ON FREE ENERGIES

When calculating the logP of the series of alcohols from methanol to dodecanol, it was observed that there was a deviation in the results obtained for heptanol and nonanol from the alcohol series trend (see Table 2.3). This may be a result of the molecule length becoming comparable to the box dimensions, so heptanol to dodecanol were simulated in a variety of different box sizes to predict the influence of box size on the calculated logP. The results are summarised in Table 2.3 and plotted in Figure 2.8. The small box size of 3x3x3nm does not exhibit the expected linear increase in logP and instead showed fluctuation as the alcohol chain length increases, with significant deviation from the expected values. Increasing the dimensions to 5x5x5 nm reduces these fluctuations significantly, with increasing to 7x7x7 nm results in a linear relationship between alcohol chain length and the calculated logP. There is an obvious offset of approximately 1 unit

in the calculated logP values compared with the experimental values. This is discussed later in this chapter.

Considering these effects, simulations using a bigger box for heptanol, octanol, nonanol, decanol and dodecanol were performed. It indicated that the increment in the box size from 3 nm to 5 nm and even more to 7 nm gives more consistent logP values but, deviate more from the experimental result, shown on Table 2.3 and Figure 2.8.

Table2.3 Comparison of calculated logP for alcohols for different simulation box dimensions using the original GROMOS 53A6 united atom force field. Values reported are the average of two runs, the error estimate is \pm the difference between the two estimates.

Solute	Cubic Box Dimension (nm ³)			Experimental
	3nm	5nm	7nm	
Hexanol	2.78 \pm 0.01	3.23 \pm 0.02	3.30 \pm 0.02	2.03
Heptanol	2.19 \pm 0.01	3.55 \pm 0.02	3.68 \pm 0.01	2.62
Octanol	4.63 \pm 0.04	4.65 \pm 0.02	4.17 \pm 0.02	3.07
Nonanol	3.82 \pm 0.01	5.39 \pm 0.04	4.88 \pm 0.04	4.02
Decanol	4.71 \pm 0.02	5.69 \pm 0.01	5.73 \pm 0.02	4.57
Dodecanol	6.10 \pm 0.04	6.12 \pm 0.07	7.63 \pm 0.02	5.13

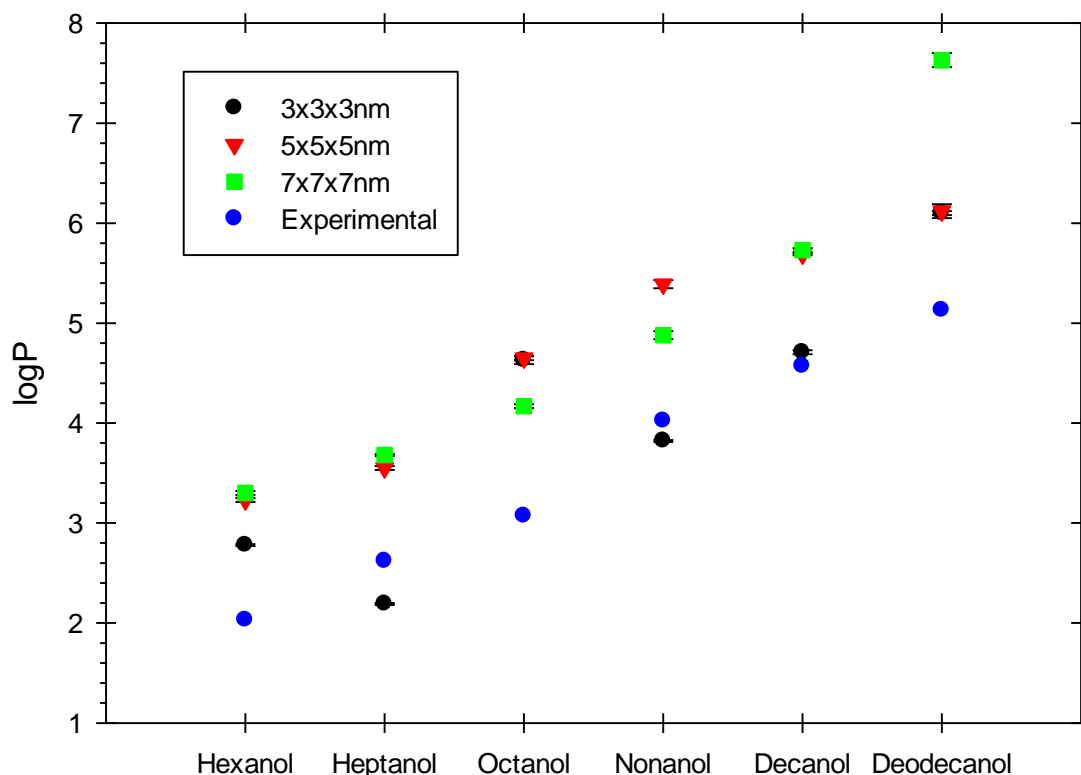


Figure 2.8 Influence of simulation box dimension on the calculated $\log P$ for a series of alcohols.

2.10 WET VERSUS DRY OCTANOL

The experimental measurement of the octanol-water partition coefficients involves the mixing of octanol and water, along with the solute of interest, which is then allowed to reach thermodynamic equilibrium. The octanol and water are largely immiscible in each other, as shown by the $\log P$ values of octanol (3.07)⁸⁷ and water (-1.38)⁸⁸. In the case of octanol, the amount of octanol that partitions into the water phase is sufficiently small that it is not a concern from the view of molecular dynamics simulations of the system. However, water has a high enough octanol solubility that there is an amount of water present that can be easily represented within a molecular dynamics simulation; 0.275 mole fraction or ~3% w/w ⁷⁴. This water present in the octanol phase might be expected to influence the calculated $\log P$ values. To determine what influence that the inclusion of water within the octanol phase has on the calculated $\log P$, a series of linear alcohols ranging in size from hexanol to dodecanol were simulated in an octanol phases

consisting of both octanol alone and octanol containing 3% w/w water. The water/octanol systems were constructed by placing water molecules randomly in the simulation box followed by the addition of octanol molecules. The systems were then equilibrated for 10,000 steps at room temperature of 298 K using velocity rescaling temperature and for 10,000 steps using Berendsen isotropic pressure coupling at a reference pressure of 1 bar after 5,000 steps of steepest decent energy minimization step. The results of these calculations are presented in Table 2.4 and plotted in Figure 2.9. The presence of water does not have a significant effect on the calculated logP that is outside of the variability obtained for independent simulations. These results are consistent with the previously reported difference in Gibbs free energy between pure and water saturated octanol of 0.2 to 0.4 kJ mol⁻¹⁸⁹. The one exception to this is dodecanol, with the addition of water decreasing the logP to a value that is more consistent with the linear relationship exhibited by the other, shorter chain alcohols. The inclusion of water in the octanol phase incurs an insignificant increase in the time required for a calculation and is a more realistic representation of the real system, therefore all subsequent octanol phase simulations included 3% w/w water.

Table 2.4 Calculated octanol-water partition coefficient (logP) for a series of alcohols with the octanol consisting of neat octanol(dry) or containing 3% w/w water(wet). Values reported are the average of two runs, the error estimate is \pm the difference between the two estimates.

Solute	Dry	Wet	Experimental ⁸⁷
Hexanol	3.30 \pm 0.02	3.21 \pm 0.02	2.03
Heptanol	3.68 \pm 0.01	3.91 \pm 0.02	2.62
Octanol	4.17 \pm 0.02	4.64 \pm 0.02	3.07
Nonanol	4.88 \pm 0.04	5.09 \pm 0.01	4.02
Decanol	5.73 \pm 0.02	5.62 \pm 0.04	4.57
Dodecanol	7.63 \pm 0.02	6.97 \pm 0.01	5.13

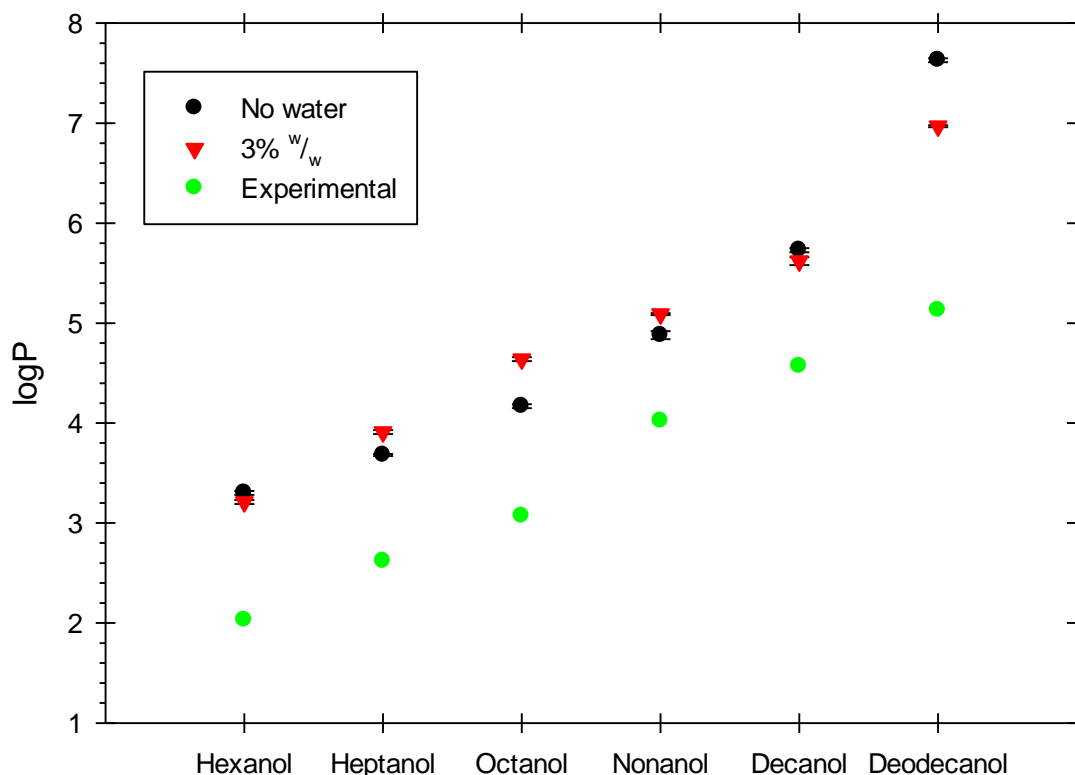


Figure 2.9 Influence of the presence of 3% w/w of water in the octanol phase on the calculated $\log P$ for a series of alcohols.

2.11 RESULTS

2.11.1 Gibbs Free Energy of Hydration

The Gibbs free energies of hydration were calculated for a selection of solute molecules using GROMOS 53A6 force field. The results summarised in Table 2.5 and compared to a number of other theoretical methods. The GROMOS 53A6 force field reproduces the experimental values well with a graphical comparison made in Figure 2.10. The differences between experimental and calculated values for alkanes (methane, pentane and octane) and toluene have an absolute deviation of 3.3 to 6.3 kJ mol⁻¹, which is within the range reported for Shirts and Pande⁹⁰. However, once a polar oxygen is added to the molecule, then the value obtained is no longer as accurate. Of particular concern is ethoxyethane, with the correct magnitude but of the wrong sign. From this

it can be concluded that the GROMOS 53A6 is parameterised well in terms of being able to reproduce the Gibbs energy of hydration for simple hydrocarbons. However, improvements need to be made to enable better fitting of functional groups containing oxygen i.e. alcohol and ether.

A more thorough investigation of the Gibbs free energy of hydration of the alcohols was then performed using a 5 nm box and a larger number of lambda values, with the results presented in Table 2.6. The solubility of the alcohols in water decreases with increasing alkane chain length, as indicated by the increase in the Gibbs free energy change. However, the values obtained are not sufficiently close to the experimental values, with the variation up to 9 kJ mol⁻¹. Subsequently, re-parameterisation of the alcohol functional group was performed to improve the reproduction of these values, as detailed in the following section.

Table 2.5 Comparison of the computed Gibbs energy of hydration ($\Delta G_{\text{hydration}}$ kJ mol⁻¹) using different force fields, # denotes results from this study.

Solute	GROMOS	RESP/	ChelpG/	AM1/	RESP/	ChelpG/	AM1/	Experimental ⁹¹
	53A6 #	GAFF ⁹¹	GAFF ⁹¹	GAFF ⁹¹	MSI ⁹¹	GAFF ⁹¹	MSI ⁹¹	
Methane	8.61	10.89	12.95	12.11	10.27	10.39	10.47	8.29
Pentane	8.92	11.18	7.71	12.74	16.76	13.74	14.10	9.88
Octane	9.98	11.65	14.25	13.91	13.87	16.29	17.01	12.27
Methanol	-22.6	-18.97	-16.24	-12.39	-14.19	-12.64	-9.84	-21.39
Ethoxyethane	11.05	0.04	-3.06	-5.99	1.38	-3.22	-1.42	-11.05
Toluene	-2.24	-1.09	5.78	1.09	3.35	7.83	2.93	-3.7
Mono ethylene glycol	-50.00	-53.97	-53.97	-42.54	-32.87	-26.8	-27.93	-38.94

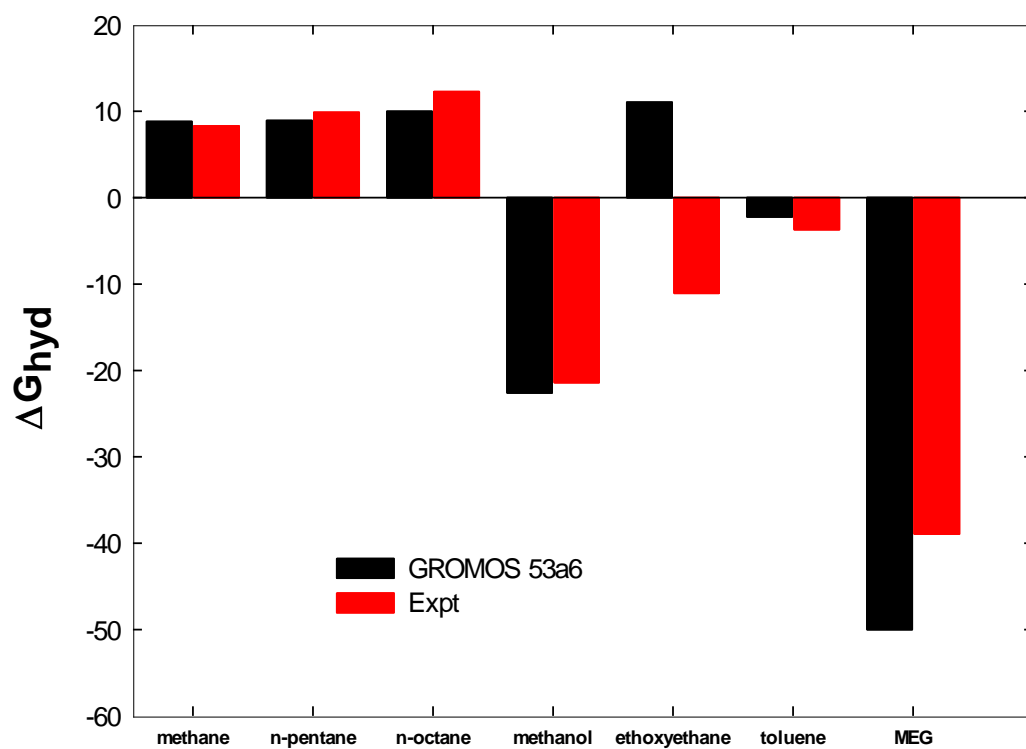


Figure 2.10 Comparison of simulation results with experimental data for ΔG_{hyd} .

Table 2.6 Gibbs free energy change (kJ mol^{-1}) for vacuum, water and hydration calculated using the GROMOS 53A6 forcefield and experimental value. Values reported are the average of two runs, the error estimate is \pm the difference between the two estimates.

Solute	ΔG_{vacuum}	ΔG_{water}	$\Delta G_{\text{hydration}}$	Experimental $\Delta G_{\text{hydration}}^{87}$
Methanol	0.07 \pm 0.01	27.01 \pm 0.01	-26.94 \pm 0.01	-21.38
Ethanol	0.06 \pm 0.01	23.88 \pm 0.01	-23.27 \pm 0.01	-20.96
Propanol	-0.027 \pm 0.01	17.49 \pm 0.01	-17.52 \pm 0.01	-19.34
Butanol	0.09 \pm 0.01	19.19 \pm 0.02	-19.10 \pm 0.01	-19.74
Pentanol	-0.13 \pm 0.01	14.77 \pm 0.02	-14.91 \pm 0.01	-18.70
Hexanol	-0.05 \pm 0.02	18.57 \pm 0.01	-18.62 \pm 0.01	-18.24
Heptanol	-0.47 \pm 0.02	22.51 \pm 0.01	-15.60 \pm 0.01	-18.49
Octanol	0.44 \pm 0.01	26.36 \pm 0.01	-26.02 \pm 0.01	-17.11
Nonanol	0.27 \pm 0.01	19.49 \pm 0.02	-19.23 \pm 0.01	-
Decanol	0.17 \pm 0.02	19.87 \pm 0.02	-19.70 \pm 0.02	-
Dodecanol	0.43 \pm 0.01	18.48 \pm 0.02	-18.05 \pm 0.01	-

2.11.2 Re-Parameterisation of GROMOS 53A6

As discussed previously, the Gibbs free energy of hydration of the alcohol and ethylene oxide (ether) functional groups calculated using the GROMOS 53A6 force field parameters do not accurately reproduce the experimental values. Horta *et.al.*⁹² modified the GROMOS 53A6 parameter set to produce GROMOS 53A6_{oxy}, with the goal of improving the MD simulation to generate results closer to experimental data on aqueous and non-aqueous solvation of pure organic liquids. Horta *et. al.* focused on the oxygen containing functional groups; alcohols, ethers, aldehydes, ketones, carboxylic acids, and esters. Adjustment of the partial charges of the atoms within each functional group was one of the methods used to obtain a better fit to the experimental data. Experimental data used by the authors included density of the liquid, latent heat of vaporisation, and Gibbs energy change of hydration and solvation in cyclohexane.

To improve the ability of the GROMOS 53A6 force field to reproduce experimentally observed partitioning of small molecules between organic and aqueous phases, we performed a study where we scaled the atomic charges of all atoms of the functional group, maintaining a group total charge of 0, and then calculating the logP of a molecule containing that functional group. The atomic partial charges for the alcohol and ether functional groups from the GROMOS 53A6 force field and the modified force field (denoted 53A6_{PEG}) are presented in Table 2.

Table 2.7 Atomic partial charges of atoms for the alcohol and ethylene oxide (ether) functional groups for the GROMOS 53A6 forcefield; original and modified partial charges.

	53A6	53A6 _{PEG}
Alcohol		
H	0.407	0.361
O	-0.563	-0.650
CH ₂	0.156	0.289
Ethylene Oxide (Ether)		
CH ₂	0.210	0.357
O	-0.420	-0.714
CH ₂	0.210	0.357

2.11.2.1 The influence of Alcohol Partial Charges on logP

To investigate the influence of the alcohol partial charge on the partition coefficient of alcohols, the charges of the three atoms of the alcohol functional group 1-octanol were scaled over the range from -0.500 to -0.845 for the oxygen, and the logP was then calculated for octanol. As octanol was used as a solvent for the logP calculation, it was used as a model compound for the modification process of the alcohol. The calibration of the partial atomic charges on oxygen was performed systematically, guided by chemical perception and a roughly incremental approach, followed by scaling the partial atomic charges of hydrogen and methyl to make up the difference. The definition of charged groups, all van der Waals interaction parameters, bond-stretching and bond-angle bending parameters were kept unchanged with respect to the 53a6 force field. The results for the partial charges for GROMOS 53A6 and 53A6_{oxy} are indicated for comparison. The relationship between the partial charge and logP went through a minimum at approximately -0.650. At this point, the logP value was 3.77, the closest value obtained to the experimental value of 3.07⁸⁷. This value was used to define the improved partial charges for the alcohol functional group (H 0.361, O -0.650, CH₂ 0.289) as shown in Table 2.7.

The influence that changing the alcohol partial charges has on the liquid density and latent heat of vaporisation of octanol was checked. Liquid simulations of 479 octanol molecules (1 bar, 298 K) and a single molecule in vacuum (298K) were carried out using GROMOS 53A6 or with the modified alcohol partial charges. The values calculated are summarised in Table 2.8, which also showed the experimentally measured literature values. Adjusting the partial charges made little difference to the calculated density and improved the latent heat of vaporisation when compared to the estimate from the 53A6 force fields.

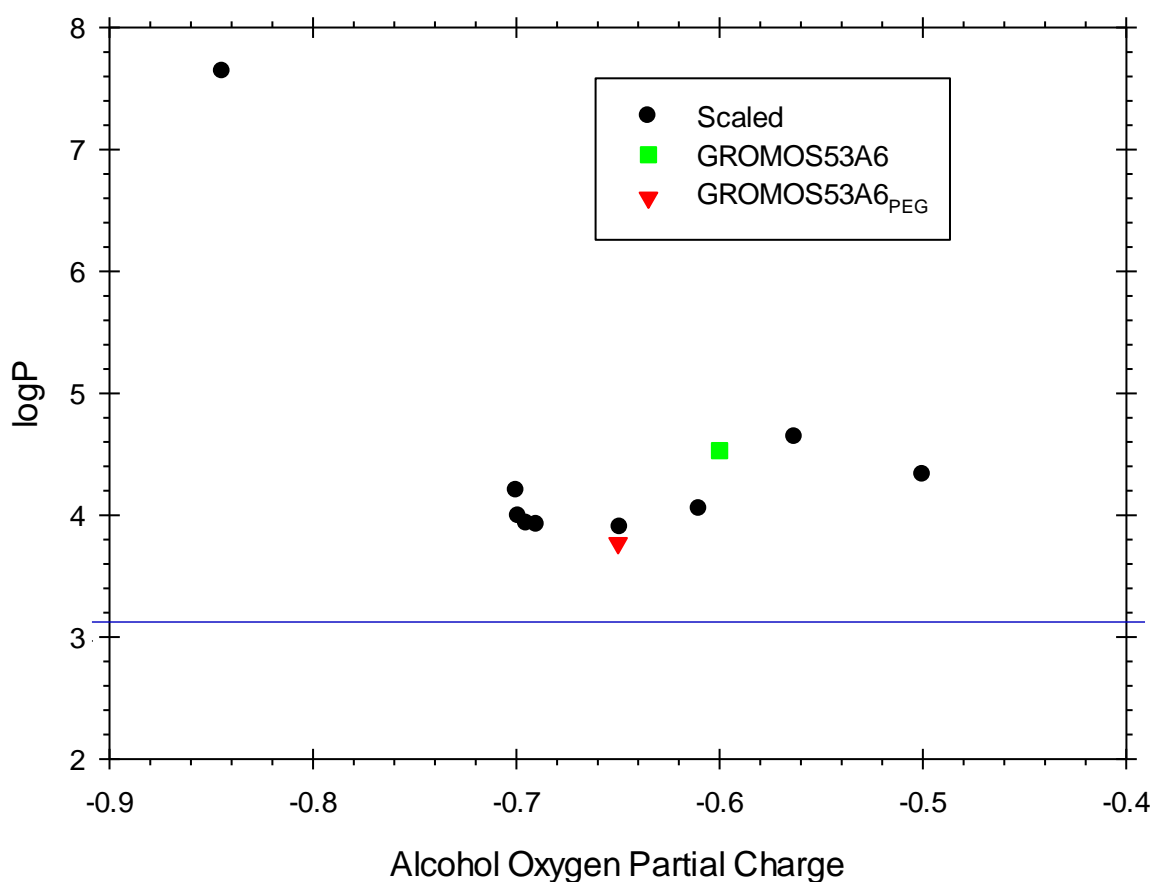


Figure 2.11 A comparison of simulation results of logP values for different partial charges. 1-Octanol was used as a model compound. The blue line represents the experimental logP value. ($n=1$)

Table 2.8 Experimental and calculated density and latent heat of vapourisation (ΔH_{vap}) of octanol at 298K.

	GROMOS 53A6	GROMOS 53A6 _{PEG}	Experimental
ρ (kg m ⁻³)	827.8	828.0	826.2 ⁹³
ΔH_{vap} (kJ mol ⁻¹)	76.9	72.2	70.98 ⁹⁴

2.11.2.2 The Influence of Partial Charges on Ethylene Glycol Partitioning

It is evident that the partitioning of ethylene glycol is very poorly predicted using current force fields. The logP of penta ethylene glycol (experimental logP = -2.30⁹⁵) was calculated while the charges of the three atoms, (with the two methyls being equivalent) of the ethylene glycol (ether) functional group, were scaled over the range -0.420 to -0.840 for the oxygen. Considering that PENTEG is hydrophilic the partial charge of oxygen was increased step by step in order to increase the PENTEG hydrophilicity. While the partial charges of these atoms were optimised, the terminal alcohol groups were maintained at the GROMOS 53A6 partial charge values. The definitions of charged groups, all van der Waals interaction parameters, bond-stretching and bond-angle bending parameters were kept unchanged with respect to 53A6 force field. The results of these simulations are presented in Figure 2.12, with the logP plotted against the partial charge of the oxygen atom. The results for the partial charges for GROMOS 53A6 and 53A6_{PEG} are also shown for comparison. The calculated logP value goes through a minimum centered on an oxygen charge of -0.714 (CH₂ = 0.357), with a logP of -0.11. The terminal alcohols were then altered to the 53A6_{PEG} partial charges, resulting in the penta ethylene glycol logP model with a predicted logP value of -2.64. This compares more favourably with the experimental value of -2.30. These improved partial charges were used for subsequent molecules containing the ethylene glycol functional group, as shown in Table 2.7.

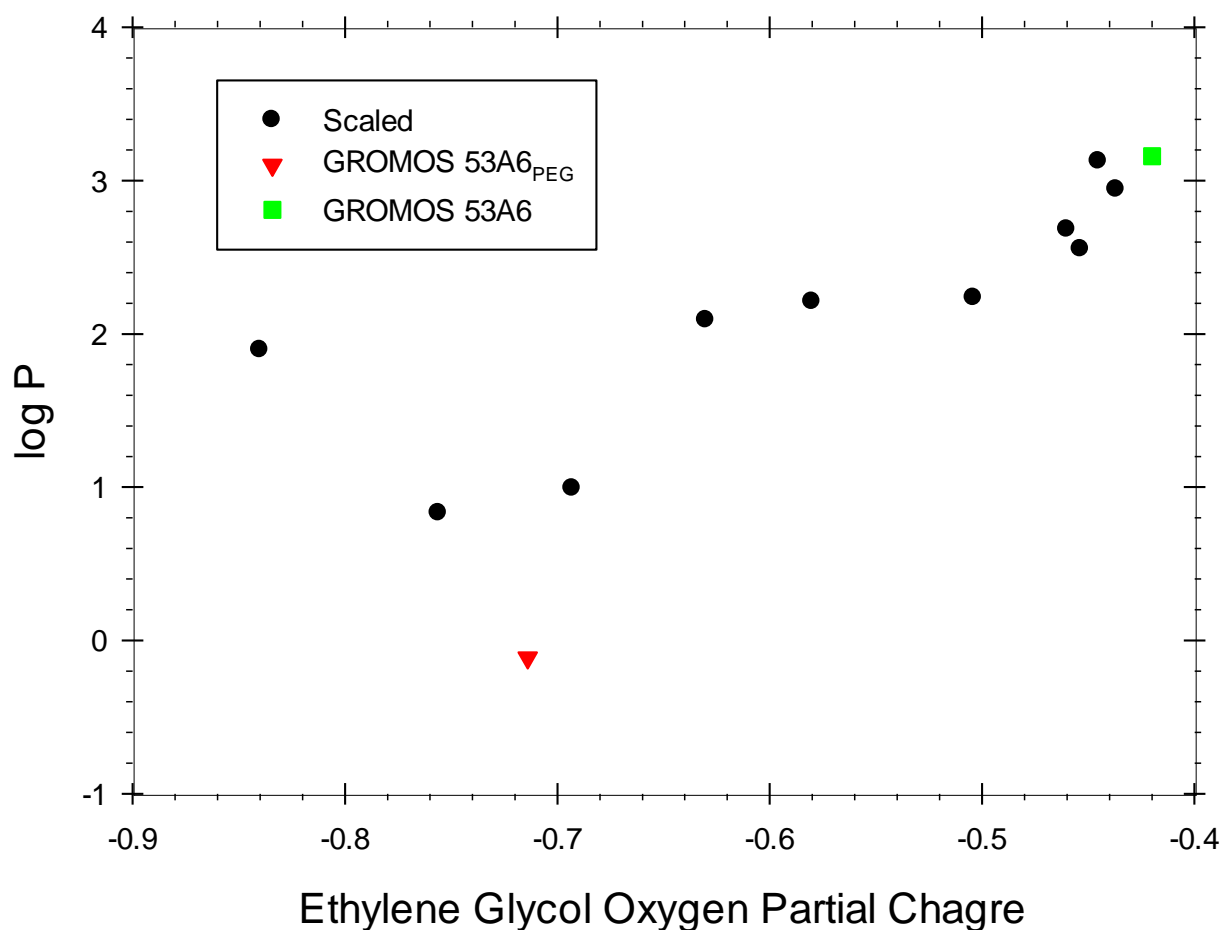


Figure 2.12. The calculated $\log P$ of penta ethylene glycol (PEG) as a function of the ether oxygen partial charge. ($n=1$)

2.11.3 Calculation of $\log P$ of the n-Alkanes

The $\log P$ values of the series of the n-alkanes from methane to dodecane (excluding undecane since no experimental value has been reported) were calculated using both the GROMOS 53A6 and 53A6_{PEG} partial charges. The $\log P$ calculated results are presented in Table 2.9 and plotted in Figure 2.13, along with the experimental values. This data clearly shows that altering the partial charges of the octanol made no difference to the accuracy of the $\log P$ value obtained. The RMSDs (root mean square deviations) between the calculated and the experimental value was 0.84 and 0.90 for 53A6 and 53A6_{PEG}, respectively. This result was expected since the alkane molecules are located almost exclusively within the region of the octanol alkane chain in the wet octanol

simulations, not in or near the reverse micellar like region of the alcohol functional groups with water.

Table 2.9 $\log P$ of a series of *n*-alkanes, calculated using the 53A6 and 53A6_{PEG} octanol model. Values reported are the average of two runs, the error estimate is \pm the difference between the two estimates.

Solute	Octanol Model		Experimental	Difference (Experimental – Force Field)	
	53A6	53A6 _{PEG}		53A6	53A6 _{PEG}
Methane	1.14 \pm 0.02	1.16 \pm 0.01	1.09 ⁹⁶	-0.05	-0.07
Ethane	1.76 \pm 0.02	1.76 \pm 0.03	1.81 ⁹⁶	0.05	0.05
Propane	2.51 \pm 0.05	2.53 \pm 0.04	2.36 ⁹⁶	-0.15	-0.17
Butane	3.27 \pm 0.04	3.30 \pm 0.04	2.80 ⁹⁶	-0.47	-0.50
Pentane	3.62 \pm 0.04	3.72 \pm 0.03	3.45 ⁹⁷	-0.17	-0.27
Hexane	4.06 \pm 0.04	4.09 \pm 0.06	4.00 ⁹⁷	-0.06	-0.09
Heptane	5.41 \pm 0.04	5.44 \pm 0.05	4.50 ⁹⁷	-0.91	-0.94
Octane	5.87 \pm 0.05	5.96 \pm 0.05	5.15 ⁹⁷	-0.72	-0.81
Nonane	6.67 \pm 0.08	6.83 \pm 0.07	5.65 ⁹⁷	-1.02	-1.18
Decane	6.80 \pm 0.07	6.86 \pm 0.09	6.25 ⁹⁷	-0.55	-0.61
Dodecane	9.01 \pm 0.06	9.10 \pm 0.05	6.80 ⁹⁷	-2.21	-2.30

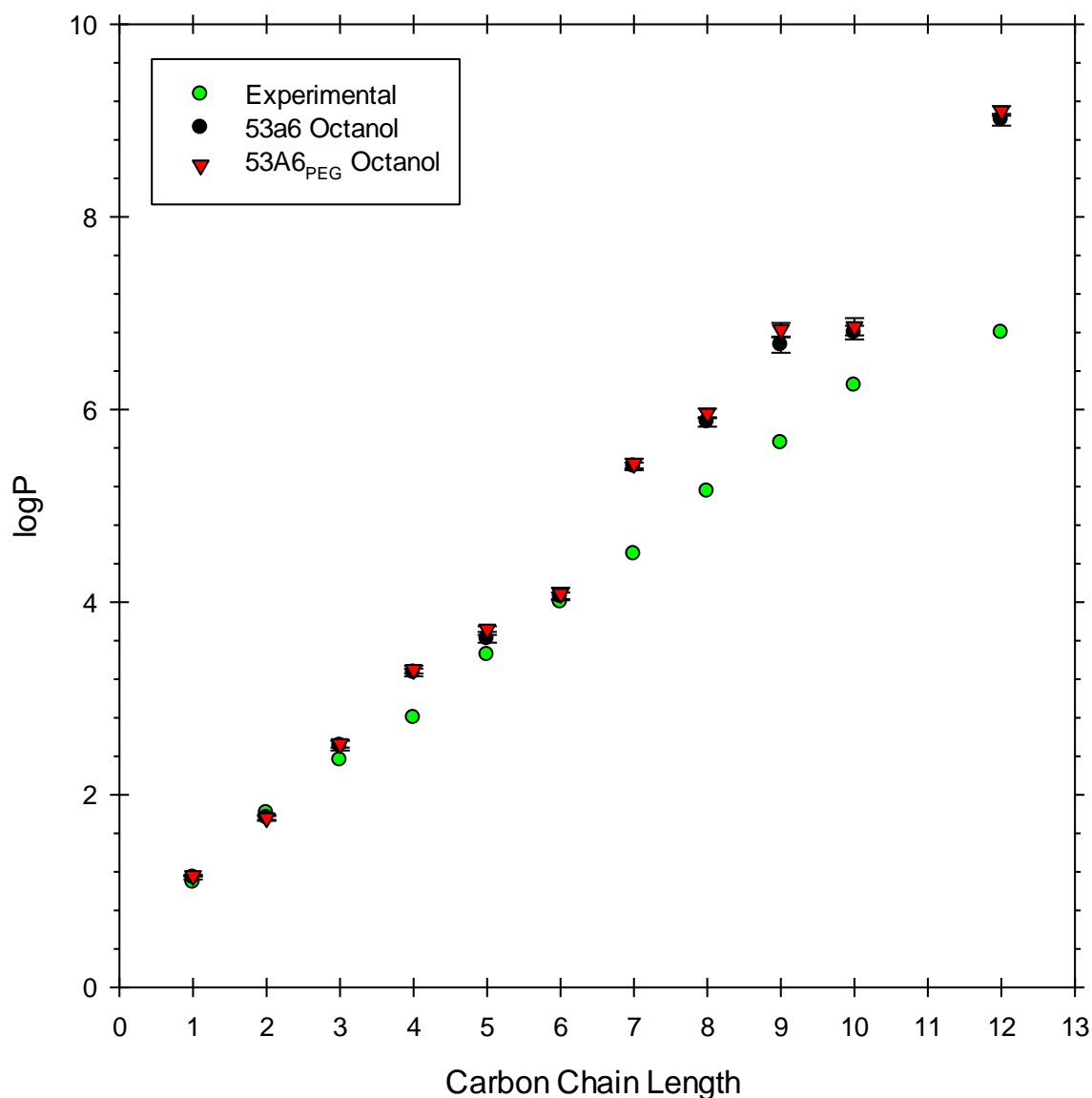


Figure 2.13 $\log P$ values of the n -alkane series from methane to dodecane; calculated (using both 53A6 and 53A6_{PEG} parameterised octanol) and experiment.

2.11.4 Calculation of $\log P$ of Alcohols

The $\log P$ values of the series of alcohols from methanol to dodecanol (excluding undecanol) were calculated using the GROMOS 53A6 and 53A6_{PEG} partial charges for the alcohol functional group. The results are presented in Table 2.10 and plotted in Figure 2.14. The change in the partial charges of the alcohol functional group improved the calculated $\log P$, with the RMSD decreasing from 1.18 to 0.76. However, there is still an offset of approximately 0.3 to 1 kJ mol⁻¹ between the

calculated and experimental values. This indicates that some further adjustment of the forcefield parameters will be required to better approximate the Gibbs free energy difference between dissolution in water and octanol. The over estimation of the logP indicates that either the interactions with water are being over estimated or those with octanol (specifically the alkane chain) under estimated, or a combination of both. The simple adjustment of the atomic partial charges is obviously insufficient, suggesting that the Lennard-Jones parameters of the atoms requires adjustment. Moving into this area increases the complexity of the problem and this will need to be looked into in future projects/studies.

Table 2.10 logP of the series of *n*-alcohols from methanol to dodecanol, including calculated using 53A6 and 53A6_{PEG} octanol and the experimental values.

	Octanol Model			Difference	
	53A6	53A6 _{PEG}	Experimental ⁸⁷	(Experimental – Force Field)	
				53A6	53A6 _{PEG}
Methanol	0.01 ± 0.09	-0.42 ± 0.05	-0.74	-0.75	-0.32
Ethanol	0.86 ± 0.09	0.32 ± 0.08	-0.30	-1.16	-0.62
Propanol	1.16 ± 0.10	0.67 ± 0.08	0.25	-0.91	-0.42
Butanol	2.02 ± 0.13	1.47 ± 0.07	0.84	-1.18	-0.63
Pentanol	2.48 ± 0.07	2.15 ± 0.07	1.51	-0.97	-0.64
Hexanol	3.11 ± 0.06	2.49 ± 0.07	2.03	-1.08	-0.46
Heptanol	3.83 ± 0.07	3.48 ± 0.12	2.62	-1.21	-0.86
Octanol	4.67 ± 0.10	4.21 ± 0.09	3.07	-1.60	-1.14
Nonanol	5.12 ± 0.13	4.67 ± 0.10	4.02	-1.10	-0.47
Decanol	5.86 ± 0.16	5.55 ± 0.10	4.57	-1.29	-0.98
Dodecanol	6.59 ± 0.14	6.23 ± 0.22	5.13	-1.46	-1.10

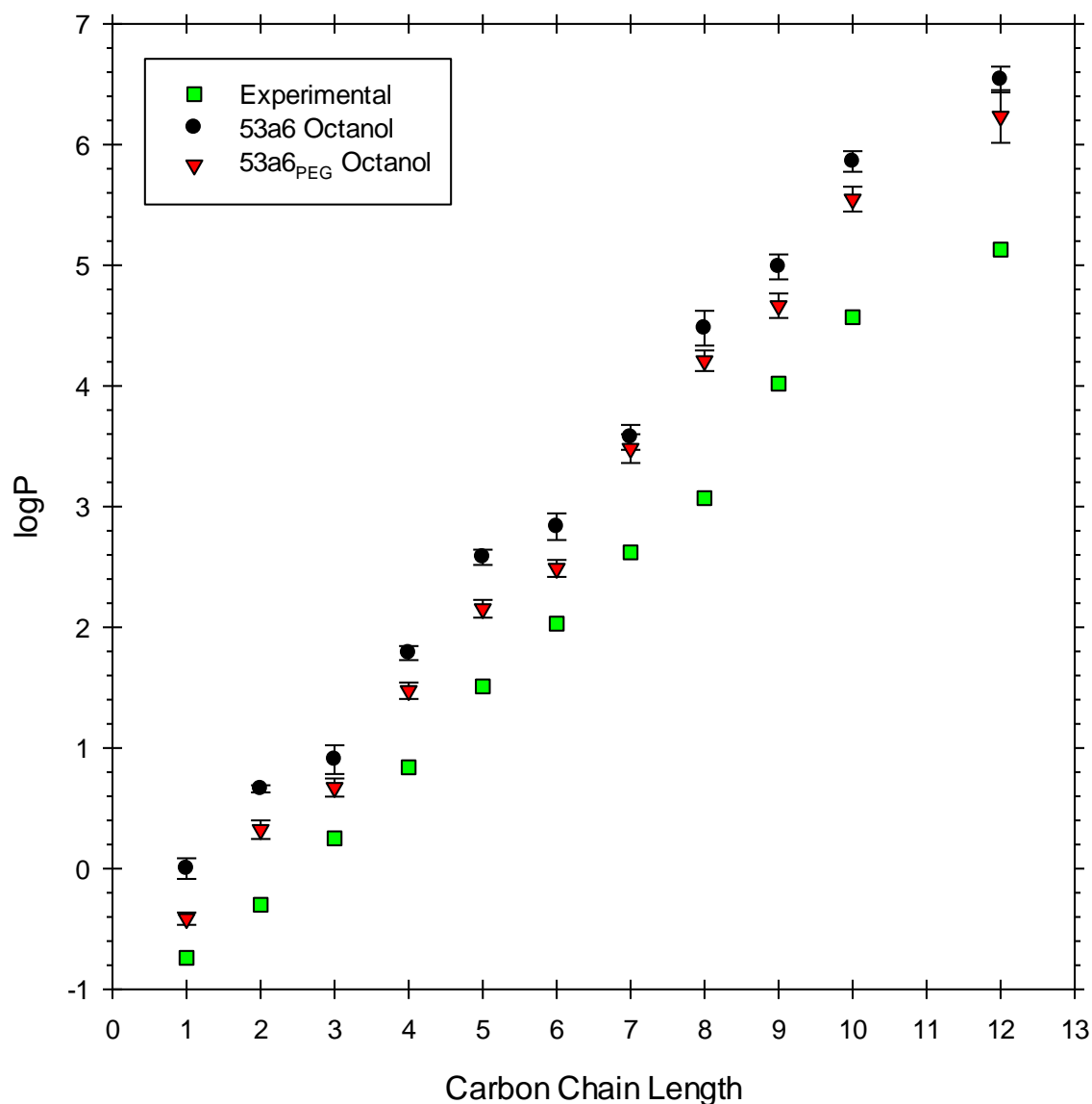


Figure 2.14 *logP* values of alcohols series from methanol to dodecanol; calculated (using both 53A6 and 53A6_{PEG} parameterised octanol) and experiment.

2.11.5 Calculation of logP of Ethylene Glycols

The logP of the first five members in the poly ethylene glycol series $[\text{HO}(\text{CH}_2\text{-CH}_2\text{-O})_n\text{-H}]$, $n = 1$ to 5] were calculated using the GROMOS 53A6 and 53A6_{PEG} force fields. The results are presented in Figure 2.15 and plotted in Table 2.11. The values calculated using the 53A6 partial charges are entirely wrong, with the poly ethylene glycols preferring to interact with octanol rather than water, while the experimental values indicate that they actually prefer water as shown by the

negative logP values. The improved 53A6_{PEG} partial charges changed this balance of interactions and reduced the RMSD between the predicted and experimental values from 2.30 to 0.89. However, at short chain lengths the logP value appeared to be dominated by the interactions of the terminal alcohol groups, and the addition of an ethylene glycol group from MEG to DEG and DEG to TEG failed to have a clear impact on the calculated logP. As found with the alcohol functional group, more involved parameterisation will be required to get a better estimate.

Table 2.11 Calculated logP values for a series of ethylene glycol molecules with GROMOS 53A6 and modified octanol models compared with the experimental values.(n=1)

Molecule	53A6	53A6 _{PEG}	Expt'l	Difference (Expt'l – Force Field)	
				53A6	53A6 _{PEG}
Mono-ethylene glycol(MEG)	-0.49	-0.52	-1.36 ⁸⁸	-0.87	-0.84
Di-ethylene glycol (DEG)	0.30	-0.49	-1.47 ⁹⁵	-1.77	-0.98
Tri-ethylene glycol(TEG)	0.29	-0.52	-1.75 ⁹⁵	-2.04	-1.23
Tetra-ethylene glycol(TTEG)	0.72	-1.23	-2.02 ⁹⁵	-2.74	-0.79
Penta-ethylene glycol(PENTEG)	1.01	-2.64	-2.30 ⁹⁵	-3.31	0.34

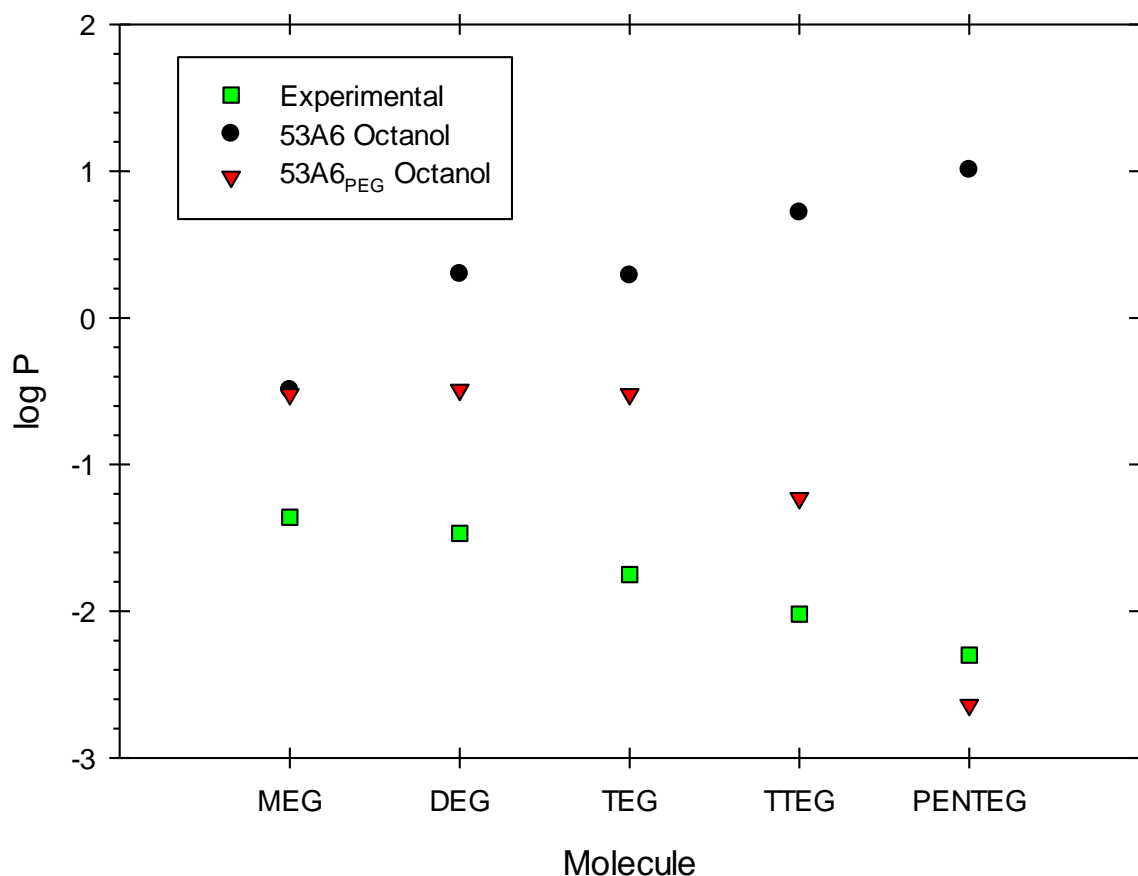


Figure 2.15 Comparison between the $\log P$ calculated for a series of ethylene glycol molecules using the GROMOS 53A6 and modified (53A6_{PEG}) forcefield parameters and the experimental values. For molecular table see Table 2.11.

2.11.6 Calculation of $\log P$ of Amino Acid Analogues

Oostenbrink *et. al.*⁴⁷ had parameterized the biomolecular force field GROMOS 53A6 to reproduce the free energies of solvation of amino acid side chain analogues in water and in cyclohexane. These amino acid side chain analogues were generated by replacing the amino acid – R group bond by a hydrogen, H – R. In this study, we calculated the $\log P$ of the same amino acid analogues in water and 1-octanol using GROMOS 53A6 and 53A6_{PEG} and compared the results.

The results and experimental values are presented in Table 2.12. The side chain analogues are grouped in a typical manner; hydrophobic, aromatic, polar neutral, polar positive, and polar negative (structures available in Appendix 1). The values for the hydrophobic and aromatic

members are plotted in Figure 2.16 and the polar side chain analogues are shown in Figure 2.17. As revealed by the overall RMSD values, the logP values calculated using the 53A6_{PEG} were not as good when using the improved octanol partial charges as the values calculated using 53A6. The non-polar amino acid analogues were good for both 53A6 and 53A6_{PEG}, although 53A6_{PEG} produced slightly worse estimates. But the value for polar amino acid analogues were poor for both force fields (although 53A6_{PEG} was better for the alcohols that we parameterized). The only overall improvement occurred with the hydrophobic group of analogues, which is consistent with the results reported earlier with the series of alkanes.

This indicates that altering a single functional group parameter will not change the entire force field set to reproduce better results across the other functional groups. The interactions are more complex and improvements will require parameterization and adjustment of all the functional groups.

Table 2.12 *logP* of the amino acid side chain analogues. # denotes software predicted values.

Amino Acid	Side Chain Analogue	Octanol Model		Experimental
		53A6	53A6 _{PEG}	
Hydrophobic				
Alanine	Methane	1.14 ± 0.02	1.16 ± 0.01	1.09 ⁹⁶
Isoleucine	Butane	3.27 ± 0.04	3.30 ± 0.04	2.80 ⁹⁶
Leucine	Isobutane	2.99 ± 0.05	2.93 ± 0.04	2.36 ⁹⁸
Methionine	Ethyl(methyl) sulfane	2.18 ± 0.08	2.03 ± 0.06	1.49 ⁹⁹ #
Valine	Propane	2.51 ± 0.05	2.53 ± 0.04	2.36 ⁹⁶
Aromatic				
Phenylalanine	Toluene	2.83 ± 0.15	3.02 ± 0.17	2.73 ⁹⁷
Tryptophane	3-methylindole	2.04 ± 0.08	3.88 ± 0.25	2.60 ¹⁰⁰
Tyrosine	<i>p</i> -cresol	2.52 ± 0.04	2.75 ± 0.07	2.62 ⁹⁷
Polar – “Neutral”				
Asparagine	Acetamide	0.07 ± 0.09	0.59 ± 0.11	-1.26 ⁹⁷
Cysteine	Methanethiol	0.60 ± 0.05	1.12 ± 0.02	0.93 ⁹⁹ #
Glutamine	Propanamide	0.19 ± 0.07	0.78 ± 0.12	-0.78 ⁹⁷
Serine	Methanol	0.00 ± 0.09	-0.42± 0.05	-0.74 ⁸⁷
Threonine	Ethanol	0.66 ± 0.09	0.32 ± 0.08	-0.30 ⁸⁷
Polar – “Positive”				
Arginine	1-propylguanidine	1.17 ± 0.20	2.33 ± 0.35	-0.59 ⁹⁹ #
Histidine	4-methylimidazole	1.37 ± 0.14	1.11 ± 0.07	0.31 ⁹⁹ #
Lysine	Butan-1-amine	1.06 ± 0.46	2.49 ± 0.43	0.86 ⁹⁷
Polar – “Negative”				
Aspartic acid	Acetic acid	1.02 ± 0.15	1.91 ± 0.08	-0.17 ⁹⁷
Glutamic acid	Propanoic acid	1.85 ± 0.04	2.53 ± 0.05	0.19 ⁹⁷

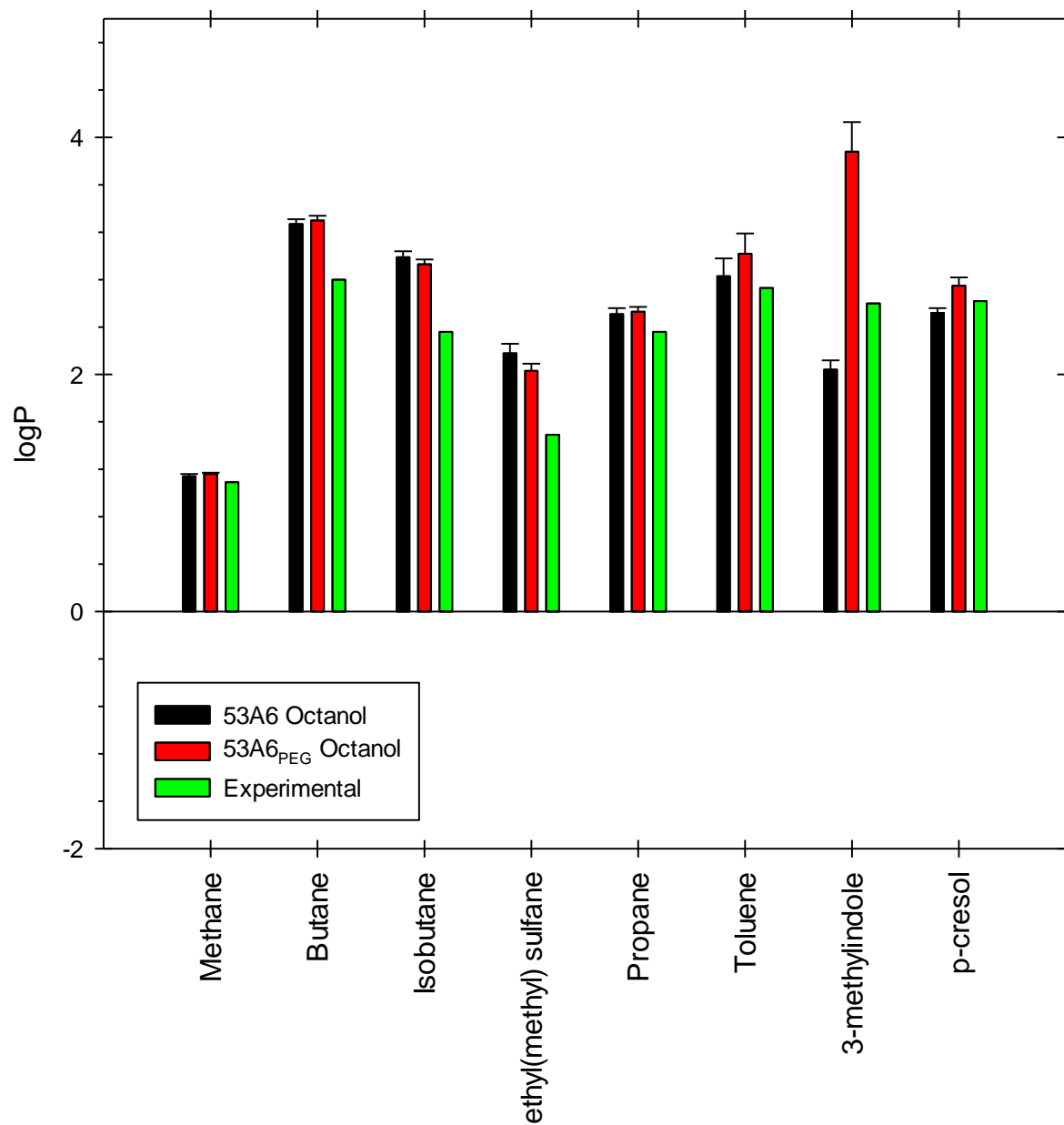


Figure 2.16 Comparison of the logP values (calculated using 53A6 and 53A6_{PEG} charges and experimental) of the analogues of the hydrophobic and aromatic amino acid side chains (R-amino acid bond replaced by R-H).

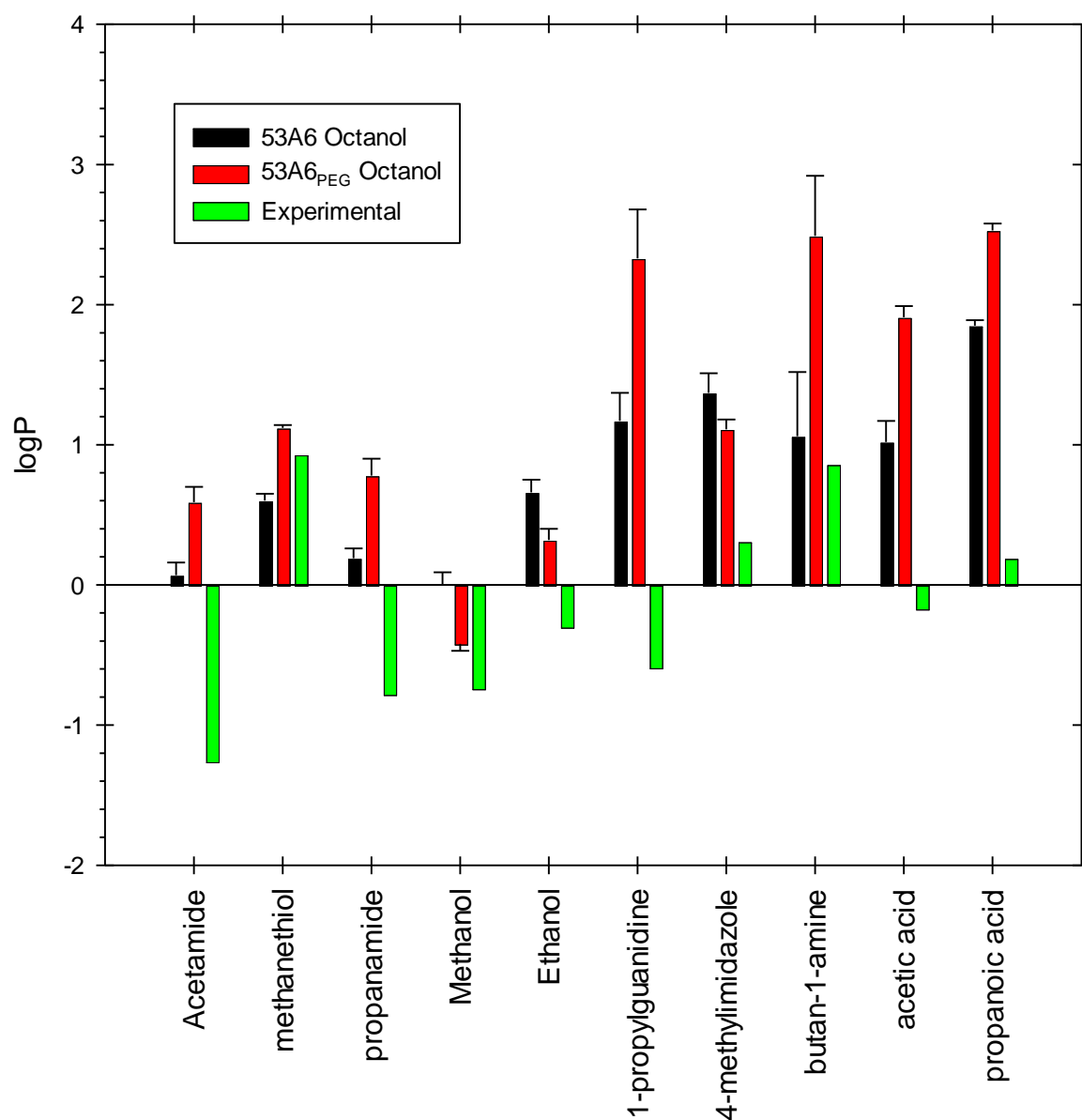


Figure 2.17 Comparison of the logP values (calculated using 53A6 and 53A6_{PEG} charges and experimental) of the analogues of the polar amino acid side chains (*R*-amino acid bond replaced by *R*-H).

2.12 DISCUSSION

To evaluate the ability of the GROMOS 53A6 united atom force field to correctly model the free energies of hydration and solvation of small molecules in octanol, the partition coefficients of a number of small molecules were calculated. Since experimental hydration free energies are

available for a significant number of molecules and the logP is typically available for nearly all, these are good molecular properties for parameterisation and validation of force fields and the computational treatments of solvation. It is known that achieving good estimates of the free energy of hydration or solvation does not necessarily lead to good estimates of structural properties. The use of logP is potentially a good property to model as it provides an insight into the interactions of a given molecule in both aqueous (hydrophilic) and lipid (lipophilic) media, which is a necessity in many biochemical processes and in the pharmaceutical industry. The free energy of solvation is also a highly desirable quantity to compute, being the factor that determines how a chemical process will proceed and a measure of the probability that a system will adopt a given state. A number of papers have been published on the hydration free energies computed for different compounds using different force fields^{73, 91, 101}. Adjusting the partial charges is relatively less complex when compared to adjusting van der Waals parameters. The parameterisation of the GROMOS 53A6 force field⁶⁵ in this study focused on adjustment of the atomic partial charges of functional groups to reproduce free energies of hydration and solvation in octanol of some small molecules; alkanes, alcohols and polar amino acid analogues. Dihedral bond modification was also employed in this work to reproduce the desired flexibility of PEG molecules. The method implemented here is more flexible and not limited to mutations between similar structures. However, the complete decoupling implemented in this study requires large changes in the Hamiltonian, and potentially larger errors are introduced in the calculations; hence, more intermediate states are required. Another advantage of this kind of methodology is that the experimental data is not required as an input in order to calculate the absolute free energies computationally.

The method for calculating the free energy of hydration implemented in this project was capable of predicting the free energies of a selection of solutes with good accuracy compared with experimental results. A comparison between different force fields allowed us to conclude that 53A6 produces the most accurate estimate of the free energy of hydration. Differences to experimental data are of the order of 0.42kJ mol^{-1} , which is approximately the precision of the

experimental methods used to measure the free energies of hydration. 53A6 atomic partial charges of the alcohol functional group (H 0.407, O -0.563, CH₂ 0.156) was found to poorly reproduce the logP of octanol, so these charges were optimised (H 0.361, O -0.650, CH₂ 0.289) to provide better reproduction of the logP of octanol. Further optimisation was then performed on the partial charges of the ethylene glycol functional group (from O -0.420, CH₂ 0.210 to O -0.714, CH₂ 0.357) to better reproduce the logP of penta-ethylene glycol. The improved alcohol model was then used to calculate the logP of a series of alkanes, alcohols, ethylene glycols and amino acid analogues. For the alkanes, the accuracy of the logP values was unchanged. In the case of the alcohols and ethylene glycols, the fit to the experimental logP values was improved, with a significant improvement obtained in the case of the ethylene glycols. However, there was no improvement for the amino acid analogues. This indicates that there is further optimisation of the forcefield is required in order to better reproduce the properties of a wider range of functional groups and molecules. Further modifications to the atomic partial charges and exploration of the influence of the Lennard Jones parameters on reproduction of logP values are required to decrease the deviation of the calculated from experimental values.

2.13 CONCLUSIONS

In this present work, we improved the biomolecular force-field version of the GROMOS 53A6 united atom force field by developing a new parameter set (53A6_{PEG}). The atomic partial charges of the alcohol and ethylene glycol functional groups in this parameter set were optimised to better reproduce the logP of a series of alcohols and ethylene glycols. Additionally, the dihedral bond of the ethylene glycol functional group was improved. The absolute free energies of hydration and solvation in octanol of a selection of small molecules were estimated by a process of fully decoupling the solute from the solvent. Previous studies have often performed the relative free energies by mutations between the two solutes¹⁰². At this stage the value of GROMOS 53A6_{PEG} is still under investigation and has not been used in Chapters 4 and 5.

Declaration for Thesis Chapter 3

Declaration by candidate

In the case of Chapter 3, the nature and extent of my contribution to the work was the following:

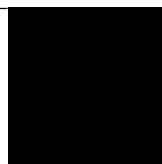
Nature of contribution	Extent of contribution
Planning and executing experimental work, data evaluation and drafting and revision of manuscript	65%

The following co-authors contributed to the work. If co-authors are students at Monash University, the extent of their contribution in percentage terms must be stated:

Name	Nature of contribution	Extent of contribution
C. W. Pouton*	Project supervisor, data and manuscript review	NA
D. K. Chalmers	Project supervisor, data and manuscript review	NA
C. J. H. Porter	Project co-supervisor, data and manuscript review	NA
D. B. Warren	Supervision of experimental works and manuscript review	NA
A. Ibrahim	Performing the initial selection of molecules using nephelometry	NA
H. D. Williams	Manuscript review	NA
H. Benameur	External supervision and manuscript review	NA

The undersigned hereby certify that the above declaration correctly reflects the nature and extent of the candidate's and co-authors' contributions to this work*.

**Candidate's
Signature**



Date:
12/06/2015

**Main
Supervisor's
Signature**



Date:
12/06/2015

“Science is a wonderful thing if one does not have to earn one’s living at it.”

Albert Einstein

CHAPTER THREE

DIGESTION OF PHOSPHOLIPIDS AFTER SECRETION OF BILE INTO THE DUODENUM CHANGES THE PHASE BEHAVIOUR OF BILE COMPONENTS

Woldeamanuel A. Birru,^{1,3} Dallas B. Warren^{2,3}, Ahmed Ibrahim³, Hywel D. Williams⁴, Hassan Benameur⁴, Christopher J.H Porter³, David K. Chalmers¹ and Colin W. Pouton^{2,3}

¹Medicinal Chemistry, Monash Institute of Pharmaceutical Sciences*

²Drug Discovery Biology, Monash Institute of Pharmaceutical Sciences

³Drug Delivery, Disposition and Dynamics, Monash Institute of Pharmaceutical Sciences

⁴Capsugel Research & Development, Pharmaceutical Sciences, Strasbourg France.

*Monash Institute of Pharmaceutical Sciences, Monash University (Parkville Campus), 381 Royal Parade, Parkville, Victoria 3052, Australia

3 DIGESTION OF PHOSPHOLIPIDS AFTER SECRETION OF BILE INTO THE DUODENUM CHANGES THE PHASE BEHAVIOUR OF BILE COMPONENTS

3.1. ABSTRACT

Bile components play a significant role in the absorption of dietary fat, by solubilizing the products of fat digestion. The absorption of poorly water-soluble drugs from the gastrointestinal tract is often enhanced by interaction with the pathways of fat digestion and absorption. These processes can enhance drug absorption. Thus the phase behaviour of bile components and digested lipids is of great interest to pharmaceutical scientists who seek to optimise drug solubilisation in the gut lumen. This can be achieved by dosing drugs after food or preferably by formulating the drug in a lipid-based delivery system. Phase diagrams of bile salts, lecithin and water have been available for many years but here we investigate the association structures that occur in dilute aqueous solution, in concentrations that are present in the gut lumen. More importantly, we have compared these structures with those that would be expected to be present in the intestine soon after secretion of bile. Phosphatidylcholines are rapidly hydrolysed by pancreatic enzymes to yield equimolar mixtures of their monoacyl equivalents and fatty acids. We constructed phase diagrams that model the association structures formed by the products of digestion of biliary phospholipids. The micelle-vesicle phase boundary was clearly identifiable by dynamic light scattering and nephelometry. The data indicate that a significantly higher molar ratio of lipid to bile salt is required to cause a transition to lamellar phase, i.e. liposomes in dilute solution. Mixed micelles of digested bile have a higher capacity for solubilisation of lipids and fat digestion products and can be expected to have a different capacity to solubilize lipophilic drugs. We suggest that mixtures of lysolecithin, fatty acid and bile salts are a better model of molecular associations in the gut lumen and such mixtures could be used to better understand the interaction of drugs with the fat digestion and absorption pathway.

3.2. INTRODUCTION

Oral delivery of poorly water-soluble drugs (PWSDs), which are predominant among candidate drugs emerging from contemporary drug discovery campaigns, presents significant technical challenges. Lipid-based formulations (LBFs) aim to present the PWSD to the gastrointestinal lumen as a colloidal solution, avoiding the slow dissolution process from solid dosage forms. LBFs are mixtures that can be encapsulated in soft or hard, gelatin or polymer capsules. The capsule contents may include oils, surfactants and cosolvents, and LBFs are often formulated to self-emulsify in the GI lumen. Upon dispersion of the LBF, oily ester components are subject to digestion in the small intestine, thus the solubilisation capacity of the formulation may change. This can lead to drug precipitation, at which point the advantage of the lipid formulation may be lost²³. Care is required in lipid formulation design, because if the formulator focuses on maximising the mass of drug dissolved in the capsule formulation, without consideration of the fate of the drug upon dispersion and digestion, then the performance of the product *in vivo* may be poor. To understand the mechanism of absorption of PWSDs, it is important to understand the digestive system of the small intestine¹. Additionally, in order to predict the fate of different drugs in LBFs, a good understanding of gastrointestinal digestion and the phase behaviour of the species present in the gut lumen is vital¹⁰³. Dietary lipids also play a significant role in the absorption process of poorly soluble drugs^{29b, 104}, and food often enhances the bioavailability of PWSDs. However pharmaceutical scientists are keen to avoid dependence on food, and it is desirable that the bioavailability of the drug from a delivery system should be similar whether the product is administered to fed or fasted subjects. Therefore, to rationalize proper design of lipid based drug formulations it is essential to investigate lipid digestion and the way bile components and formulation components contribute to the solubilisation and absorption of PWSDs^{35a, 35d, 40, 105}.

Although LBFs have generated considerable interest in recent years, surprisingly little is known about the molecular association structures that are formed in the intestinal lumen after the formulation is digested. Digestion of lipidic excipients leads to colloidal phases such as vesicles

and micelles, a dispersed lipidic microenvironment, that increases the solubilisation of co-administered PWSD in the small intestine when compared to the fasted state³³. A detailed understanding of how drugs are solubilized within such structures will be needed to allow formulators to optimize the performance of LBFs. This will require a full understanding of the contents of the GIT lumen, and how the environment changes during gastrointestinal transit and absorption of gut contents. In this study, as a starting point, we have investigated the influence of digestion on the association structures formed by bile components. Whilst there is adequate data available on the phase behaviour of bile components as they exist in the gall bladder, we hypothesized that phase behaviour is likely to be markedly affected by digestion, as soon as the bile is secreted into the intestine.

Figure 3.1 taken from previous work in our laboratory shows the *in vitro* digestion profile of lecithin conducted under standard lipolysis conditions as reported by Williams *et al*¹⁰⁶. This experiment clearly shows that the digestion of lecithin, is rapid in the presence of pancreatin with 60% of the sample being digested within five minutes. The hydrolysis of phosphatidylcholines to lysophosphatidylcholines takes place well before absorption of the phospholipid from the GIT, which suggests that the important colloidal species in relation to solubilization of lipids and PWSDs will be mixed micelles or vesicles containing bile salts, lysolecithin and fatty acids.

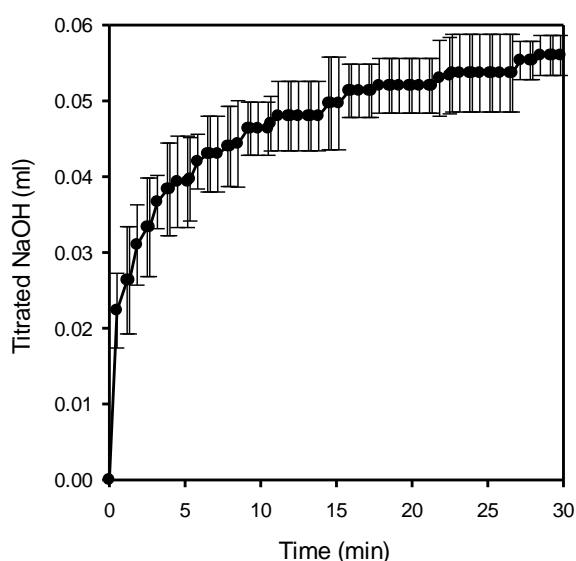


Figure 3.1 Titration of fatty acids (FA) produced upon the digestion of lecithin by pancreatic enzymes in a standard *in vitro* model^{35c}. Digestion tests were performed using 3 mM sodium taurodeoxycholate, 0.75 mM phosphatidylcholine, 2 mM tris-maleate, 150 mM NaCl and 1.4 mM CaCl₂ and 0.2 M NaOH was used as the titrant.

Bile salts, which are amphiphilic and aggregate to form micelles in aqueous environment are bio-surfactants in the GIT and play a vital role in digestion and absorption of lipids²⁵⁻²⁶. It is believed that bile salts facilitate the digestion of lipids by solubilisation of lipid digestion products into lamellar phase or mixed micelles. This removes digestion products from droplets of digested fat and accelerates further digestion and absorption of lipidic excipients^{27d}. Under physiological conditions bile salt mixed micelles swell through solubilisation of endogenous and dietary lipids digestion products. The phase transitions that occur in the intestine, from lamellar to mixed micellar, depend on the relative molar proportion of each component. These complex molecular interactions play a large part in the absorption of lipids from the small intestine^{11,12}.

The phase behaviour of the ternary system of bile salt, phospholipid and water was first reported over 45 years ago, with some significantly early work performed in the 1960s by Small *et. al.*^{17h}. Small and his group examined the ternary phase behaviour of bile salt-cholesterol-water; lecithin-cholesterol-water and bile salt-lecithin-water system using polarized microscopy and X-ray diffraction to investigate the effect of increasing the lecithin concentration on the phase behaviour^{17h}. Staggers *et. al.* studied ternary lipid systems composed of a physiological mixture of bile salts, mixed intestinal lipids, fatty acid, racemic monooleylglycerol, and cholesterol using quasi-elastic light scattering and electron photomicrography. This allowed the authors to develop an equilibrium phase diagram corresponding to aqueous lipid compositions of upper small intestinal contents during lipid digestion and absorption in adult human beings^{17d}. Bunge *et. al.* investigate a ternary lipid mixture of palmitoyl-oleoyl-phosphatidylcholine, palmitoyl-erythro-sphingosylphosphorylcholine and cholesterol to understand the non-homogenous distribution of lipids at high temperatures using fluorescence microscopy, NMR, and electron paramagnetic resonance spectroscopy¹⁰⁷. Furthermore, Mazer and Carey characterized the formation of

micellar aggregates of sodium taurocholate, egg lecithin, and cholesterol solutions using quasi-elastic light scattering¹⁰⁸.

Whilst these studies indicate the likely phase behaviour of bile when it is first secreted into the intestine, the above studies were not performed at physiological concentrations and did not consider the role of digestion on phase behaviour. The primary aim of the study reported here is to compare the structures formed by bile components and digested bile components at concentrations found within the intestine.

This paper presents phase studies of the phospholipid (2-didodecanoyl-sn-glycero-3-phosphocholine (POPC))-bile salt (Glycodeoxycholic acid, sodium salt (GDX))-water and digested phospholipid (1-palmitoyl-2-hydroxy-sn-glycerol-3-phosphocholine (LPC)+ oleic acid (OA))-bile salt (GDX)-water ternary systems at physiologically relevant concentrations, with the primary focus being on identification of the phase boundary between the micellar and vesicular phases. We investigate the solubilisation capacities of the bile salts (individually and as a mixture in proportions as found in human bile) which we select GDX as a representative bile salt for our study. Additionally, we compare the ability of GDX to solubilise POPC and dilauroyl phosphatidylcholine (DLPC) and egg lecithin which is a natural mixture of lipids.

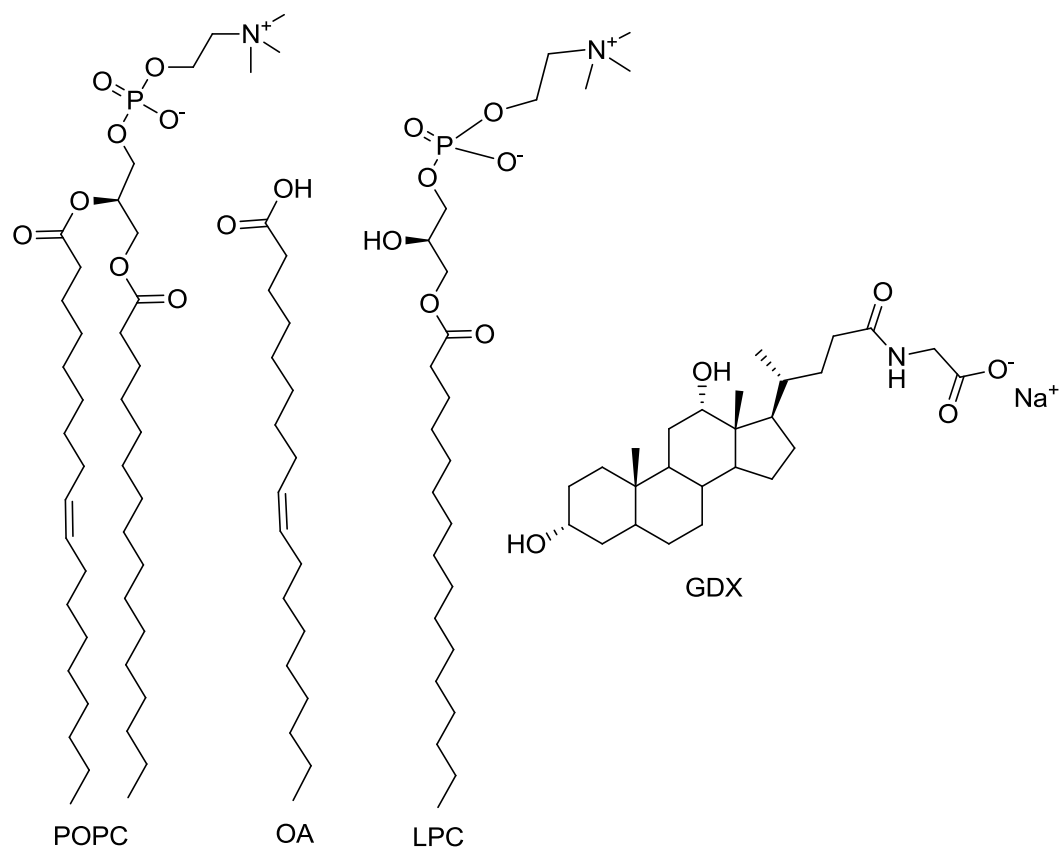


Figure 3.2. Structures of 1-palmitoyl-2-oleoyl-sn-glycerol-3-phosphocholine (POPC), 1-palmitoyl-2-hydroxy-sn-glycerol-3-phosphocoline (LPC), oleic acid (OA) and glycodeoxycholic acid, sodium salt (GDX).

3.3 MATERIALS AND METHODS

3.3.1 Materials

The phospholipids 1-palmitoyl-2-oleoyl-sn-glycerol-3-phosphocholine (POPC), 1-palmitoyl-2-hydroxy-sn-glycerol-3-phosphocoline (LPC) and 1, 2-didodecanoyl-sn-glycero-3-phosphocholine (DLPC) were obtained from Avanti Polar Lipids Inc. in powder form. Egg lecithin was from Lipoid GmbH, Germany. Glycodeoxycholic acid, sodium salt (GDX) was obtained from Calbiochem, oleic acid (OA) (> 99% pure), glycocholate (GCH), glycochenodeoxycholate (GCD), taurocholate (TCH), taurochenodeoxycholate (TCD), and taurodeoxycholate (TDX) were obtained from Sigma-Aldrich. Sodium hydroxide (pellets), sodium phosphate monohydrate and sodium chloride were analytical grade. All water used was obtained from a Milli-Q water purification system (Millipore).

3.3.2 Fasted State Simulated Intestinal Fluid Buffer

Fasted state simulated intestinal fluid buffer (FaSSIF buffer) was based on the published composition of complete FaSSIF¹⁰⁹, minus the phospholipid and bile salt components and thus was composed of: 0.174 g of NaOH, and 1.977 g of NaH₂PO₄·H₂O and 3.093 g of NaCl in a 500 ml of purified water. The pH was adjusted to 6.5 ± 0.02 using 1 M NaOH and 1 M HCl as required.

3.3.3 Lipid Stock Solutions Preparation

Lipid solutions were prepared using the evaporated film method; 0.175 g of lipid (POPC or LPC+OA) was dissolved in 10 ml of methanol and the methanol evaporated within a round bottom flask using a rotary evaporator. The resulting lipid film was then dispersed in 6.825g of the aqueous phase FaSSIF buffer, generating a 2.5% w/w stock solution. The lipids in the stock solution were solubilised and form a turbid solution indicating the presence of vesicular phase. This stock solution was diluted and vortex-mixed for 5 minutes to prepare 0.25, 0.5, 1.0 1.5, 2.0 and 2.25 % w/w solutions as required. The same method was used to prepare 1% w/w solutions of DLPC and egg-lecithin.

3.3.4 Bile Salt Stock Solutions Preparation

The aqueous stock solutions of 2.5% w/w GDX was prepared by dissolving of 0.175 g of GDX into 6.825 g of FaSSIF buffer. The stock was diluted to give 0.25, 0.5, 1.0, 1.5, 2.0 and 2.25 % w/w solutions as required.

Stock solutions of 1% w/w of GDX, GCH, GCD, TCH, TDX, TCD and a mixture of five most abundant bile salts in human bile^{26c} (30% GCH, 29% GCD, 12% TCH, 11% TCD and 9% GDX) dissolved in a FaSSIF buffer were also prepared.

3.3.5 Turbidity

The required volumes of the lipid and bile salt stock solutions were mixed *in situ* within the individual wells of a 96 microwell plate, with the plate and introduced into the nephelometer (see below). The delay between mixing of the solution and the first turbidity measurement was recorded (approximately 9 to 10 minutes). Turbidity measurements of each plate were repeated every 10 minutes until the signal value stabilised. All measurements were performed at 37°C and the mean of 3 data sets was determined for each solution.

The turbidity of the mixtures, measured in arbitrary nephelometry turbidity units (NTU), was monitored using a NEPHLOstar Galaxy microplate nephelometer (BMG Labtechnologies, Germany), which measures the turbidity as a function of back scattered light, (not light absorption). The nephelometer program settings used were: gain = 70, cycle time = 30 s, measurement time per well = 0.30 s, positioning delay = 0.5 s. The backscattered laser light (λ = 635 nm) was monitored at an angle of 80°. Polystyrene, flat-bottomed 96-microwell plates (NUNC, Thermo Scientific, USA) were used.

3.3.5 Dynamic light scattering

A Malvern Zetasizer Nano ZS ZEN3600 (Worcestershire, UK) was used to measure the hydrodynamic diameter of particles. Measurements were conducted at 37°C using low-volume disposable sizing cuvettes (cell type ZEN0112, Sarstedt, Germany). The backscattered laser light ($\lambda = 633\text{nm}$) was monitored at a measurement angle of 173°. The viscosity of the dispersant (water) was used as sample viscosity. The equipment was calibrated using 60 nm \pm 2.7 nm and 220 \pm 6nm diameter nanosphere size standards of polystyrene polymer latex (supplied by Duke scientific corporation, USA) in water. The polydispersity index (PDI) for the standards were < 0.2.

The required volumes of the lipid and bile salt stock solutions were mixed *in situ* within the individual cuvette and then introduced into the nanosizer. Solutions were prepared in the region of the phase boundary, previously identified using turbidity measurements. Measurements were carried out one day after sample preparation and the average of 6 data sets was taken for each solution.

Dilute solutions of GDX in buffer are transparent micellar solutions, the micellar structures being less than 10 nm in diameter resulting in weak scattering of visible light. In contrast, vesicular suspensions of POPC or (LPC+OA) in the absence of GDX are of dimensions typical of multilamellar liposomes, in the range 100-1000 nm (unless high energy homogenization is used to reduce their size). These are turbid suspensions that cause extensive scattering of visible wavelengths of light. The addition of bile salt to the vesicular phase of phospholipids produces a less turbid solution and, if sufficient bile salt is added, can completely solubilize the vesicles forming mixed micelles^{17h, 110}.

Particle size can be determined by measuring the random changes in the intensity of light scattered from a mixture or solution¹¹¹. Using the refractive index of lipid, the instrument generates the distribution of volume and numbers of particle sizes from the intensity distribution. In this study, since we were interested in determining the phase boundary, we used the intensity distribution to analyse our data. The reason the intensity distribution was preferred is that at the

phase boundary the volume or number of vesicles within the mixture was negligible compared to the volume or number of micellar particles. Hence, there was no visible peak for the volume or number distribution of the vesicular particles at the point at which the vesicles first appeared in the system (as the fraction of lipid increases).

3.4 RESULTS

To understand the phase behaviour of phospholipid/bile salt systems and investigate the effects of lipid digestion upon this phase behaviour, a simplified model system for undigested and digested phospholipids and bile was used. The systems contained of a single bile salt mixed with either a single phospholipid or an equimolar combination of lysophospholipid and fatty acid. The structures formed were initially investigated using nephelometry (turbidity measurements), a high-throughput method¹¹² that can readily be performed in 96-well plates and has the potential to distinguish between micellar and vesicle phases. The phase boundary experiments were carried out by mixing phospholipids and bile salt solutions to make sample sets having constant total lipid content, ranging from 0.25 to 2.5 % w/w. As the amount of POPC added to the GDX solutions increased, lamellar aggregation structures (i.e. multilamellar vesicles) were formed. The comparatively large size of vesicles caused a strong backscattering of the laser light and consequently a high value of turbidity was detected. The turbidity of each sample (in arbitrary turbidity units) was plotted against the mass fraction of phospholipid or lyso-phospholipid/fatty acid present in the sample. The nephelometry results were cross-validated by measuring the particle size using dynamic light scattering (DLS) measurements. The phase boundary between micelles and vesicles phases was subsequently located as the point of intersection of lines fitted to the two adjoining regions of the turbidity curve. An example of the turbidity curve is shown in Figure 3.3, indicating how the phase boundary was identified.

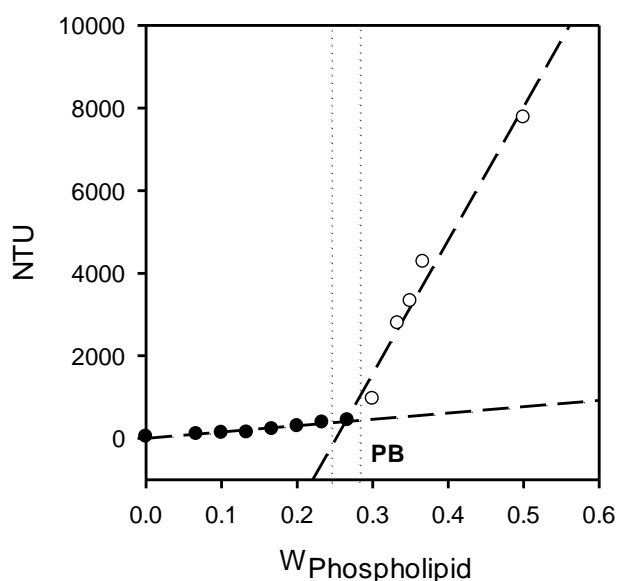


Figure 3.3. Determination of micelle/vesicle phase boundary by nephelometry. In a typical nephelometry experiment, turbidity is plotted as nephelometry turbidity units (NTU) versus mass fraction of total bile salt phospholipid content (as a fraction of bile salt plus phospholipid, $W_{\text{Phospholipid}}$). Filled and open circles represent micelles and vesicles respectively, the dashed lines represent best fit for the micellar and vesicular regions. The phase boundary, (PB), shown as dotted vertical lines, indicates the range of mass fraction of lipids around the intersection of the two slopes where it was considered to be the phase boundary between the mixed micellar and the ‘micelles plus vesicles’ phases.

3.4.1 Selection of a Representative Bile Salt and Lipid

One of the objectives of the study was to select a single pure bile salt and pure lipid that could be used in phase studies to represent the physiological mixtures found in the human GI tract. The use of single, representative compounds is important for parallel computational studies which we are undertaking using molecular dynamics which aims to improve our understanding of the atomistic behaviour of the system of the phase behaviour of digested and undigested phospholipids, bile salt and water. We first examined the solubilisation of phospholipids by different pure bile salts at physiologically relevant concentration.

The most abundant bile salts in human bile are; glycocholate (GCH 30 mol %), glycochenodeoxycholate (GCD 29 mol %), taurocholate (TCH 12 mol %),

taurochenodeoxycholate (TCD 11 mol %), glycodeoxycholate (GDX 9 mol %) and taurodeoxycholate (TDX 2 mol %)^{26c, 113}. It has been reported that 95% of the phospholipids (PLs) in bile are secreted as phosphatidylcholine (PC), principally as two molecular species 1-palmitoyl, 2-linoleyl (16:O-18:2) phosphatidylcholine or 1-palmitoyl, 2-oleoyl (16:O-18:1) phosphatidylcholine (POPC)^{26c, 114}. Given this knowledge we chose to model bile using pure POPC and GDX which we believe is representative of the mixture found in bile. The choice of GDX was validated by an initial series of experiments. To represent digested bile for the bulk of the work, we used mixtures of palmitoyl lysophosphatidylcholine, oleic acid and GDX.

Figure 3.4a shows turbidity plots for each of six bile salts mixed in different mass fractions with POPC. This illustrates marked differences in the ability of the individual bile salts to solubilise POPC into mixed micelle. The experiments were performed so that the total mass of bile salt plus POPC was maintained at a constant concentration of 1%^{w/w} in buffer. The mass fraction of POPC (as a fraction of bile salt plus POPC), W_{Lipid} , is plotted on the horizontal axis. Turbidity is low at low W_{Lipid} indicating that POPC is solubilised within a mixed micellar phase. As W_{Lipid} is increased, turbidity rises gradually until a critical point is reached above which the bile salt is unable to solubilise POPC in micelles. A phase boundary is crossed above which, micelles exist in equilibrium with lamellar phase vesicles. At the critical point, identified by the phase boundary, the turbidity increases sharply due to the increased scattering caused by the larger vesicular particles. As W_{Lipid} is further increased, the turbidity reaches a maximum value, after which it decreases due to the presence of larger multilamellar vesicles which tend to sediment during the timecourse of the turbidity measurement. The turbidly values in this region cannot be used to identify phase behaviour and for simplicity have been omitted from the plotted data. Some examples of the complete turbidity versus W_{Lipid} graphs are provided in Appendix 2 Figure 9.2.1.

The ability of each pure bile salt to solubilise POPC in micellar form is reflected in the value of W_{Lipid} at the phase boundary. The two conjugated trihydroxy bile salts, TCH and GCH were poor solublisers of POPC, with a substantial increase in the turbidity evident at $W_{\text{Lipid}} < 0.1$. Conversely,

the glycine-conjugated dihydroxyl compounds GCD and GDX were able to solubilise the two highest mass fractions of POPC. The taurine-conjugated equivalent compounds, TDC and TDX were poorer solubilisers than their glycine-conjugated analogues, but were much better solubilisers than the trihydroxyl bile salts. Thus the POPC solubilisation capacity of the bile salts ranked in the following order: TCH < GCH < TCD < TDX < GDX < GCD. This order corresponds directly with the hydrophobic indices of bile salts reported by Donovan *et. al.*¹¹⁵.

In order to determine which single bile salt best represented the phase behaviour of the natural mixture found in bile we tested a mixture of the five most abundant bile salts (GCH, GCD, TCH, TDX and GDX) combined in the same proportions as found in human bile (by weight: 30% GCH, 29% GCD, 12% TCH, 11% TDX and 9% GDX). This mixture was an effective POPC solubiliser with similar solubilisation capacity to the glycine-conjugated dihydroxyl bile salts, GDX and GCD. Either of these two bile salts on their own reproduces the solubilisation capacity of a physiologically representative mixture of the bile salts, and would both be suitable single component models. As GDX is significantly less expensive than GCD, we selected GDX as the model of choice for future studies. The ability of GDX to solubilise pure POPC, DLPC or PC from egg lecithin is shown in Figure 3.4b. The latter is a natural mixture of lipids and lipid fragments found in egg yolk, and is composed of phosphoric acid, choline, fatty acids, glycerol, glycolipids, triglycerides, and phospholipids. The main phospholipid components of egg lecithin are PC (80 %) and PE (11%)¹¹⁶. POPC is the most abundant PC and egg lecithin has been extensively used as a model compound for representation of natural PC mixtures¹¹⁷ and mixtures of phospholipids in different phase studies^{17h, 17i, 108, 115}. The turbidity curves for the three phospholipids showed that the phase behaviour of POPC and egg lecithin when mixed with GDX were very similar. However, the shorter chain-length, saturated lipid DLPC was significantly better solubilised by the bile salt. This indicated that POPC was a good choice as a model of mixed phospholipids. Therefore, we decided to focus future studies on the GDX: POPC system, and its digested equivalent, GDX:LPC:OA (Figure 3.2). It should be noted that *in vitro* digestion models used during lipid formulation performance evaluation typically utilize TDX as the model bile salt^{35b, 35c,}

¹¹⁸. Given that the results of the present study show that TDX and GDX show only marginal differences in PL solubilisation (Figure 3.4a), it is unlikely that formulation performance will change dramatically on using either of these two dihydroxyl bile salts. This statement and our decision to select a dihydroxyl bile salt is supported by previous work by Williams *et. al.*^{35c}, which report similar digestion rate and extent of lipid formulations in the presence of TDX or a bile mixture (mimicking the typical bile salt secretion in the bovine and human gall bladder), but not when using only a trihydroxyl bile salt (TCH).

3.4.2 Phase Behaviour of Bile Salt: Lipid Mixtures

In this study we were interested in identifying the point beyond which POPC can no longer be solubilised into a mixed micellar phase, i.e. the phase boundary between micellar solution and the region in which micelles exist in equilibrium with vesicular phases. In particular we were interested in comparing the ternary phase diagrams of the GDX/POPC/buffer system with the GDX/digested POPC (i.e. equimolar LPC+OA)/buffer system, within the concentration region relevant to physiological conditions. The latter digestion system contained equimolar concentrations of LPC and OA (to reflect the presence of fatty acid liberated from PC on digestion to LPC).

Figure 3.5 presents the turbidity data for these systems as a function of W_{Lipid} . Figure 3.5a shows the GDX/POPC/buffer system, at seven different total concentrations of POPC and GDX (0.25, 0.5, 1.0, 1.5, 2.0, 2.25, and 2.5 % w/w). This plot indicates that a significant increase in turbidity occurred with increased POPC mass fraction in the range of W_{POPC} 0.27-0.31 for 1 to 2.5 % w/w POPC + GDX and $W_{\text{POPC}} = 0.45-0.54$ for 0.25 and 0.5 % w/w POPC + GDX. As above, this discontinuity marked by a significant increase in turbidity identifies the phase boundary.

A similar data set, but this time employing digested phospholipid plus oleic acid, to represent digested biliary lipid, is presented in Figure 3.5b. A similar profile was evident, but in this case the solubilisation properties were markedly different and the solubilisation capacity for digested

phospholipid was significantly higher, especially at higher lipid concentrations. $W_{\text{LPC+OA}} = 0.49\text{--}0.55$ for all total concentrations of GDX + (equimolar LPC+OA) from 0.25 to 2.5% w/w.

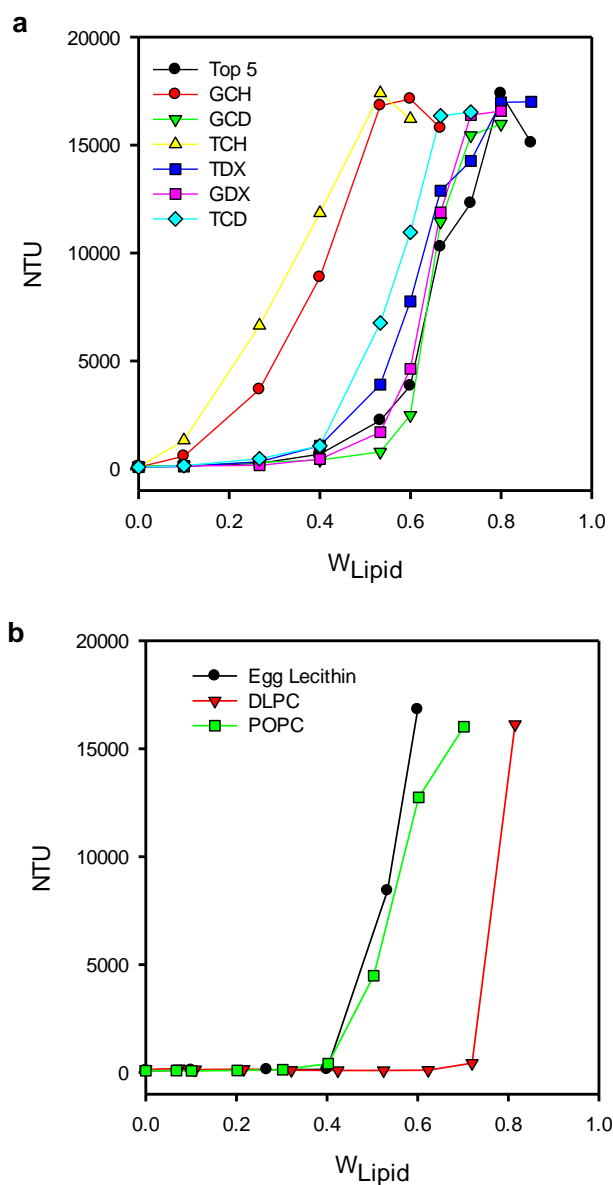


Figure 3.4. Solubilisation of phospholipids by bile salts examined using nephelometry. Measurements were made at a constant total concentration of bile salt plus phospholipid of 1 % w/w. The X-axis shows the mass fraction of POPC, (as a fraction of bile salt plus phospholipid content). (a) A comparison of the ability of six different bile salts (GCH, GDC, TCH, TDX, GDX and TDC) to maintain the phospholipid POPC in micellar phase (low turbidity). A mixture of the five most common bile salts present in human bile in the appropriate physiological molar ratio is also compared (Top 5). (b) Comparison of the ability of GDX to solubilise the phospholipids POPC, DLPC and egg lecithin.

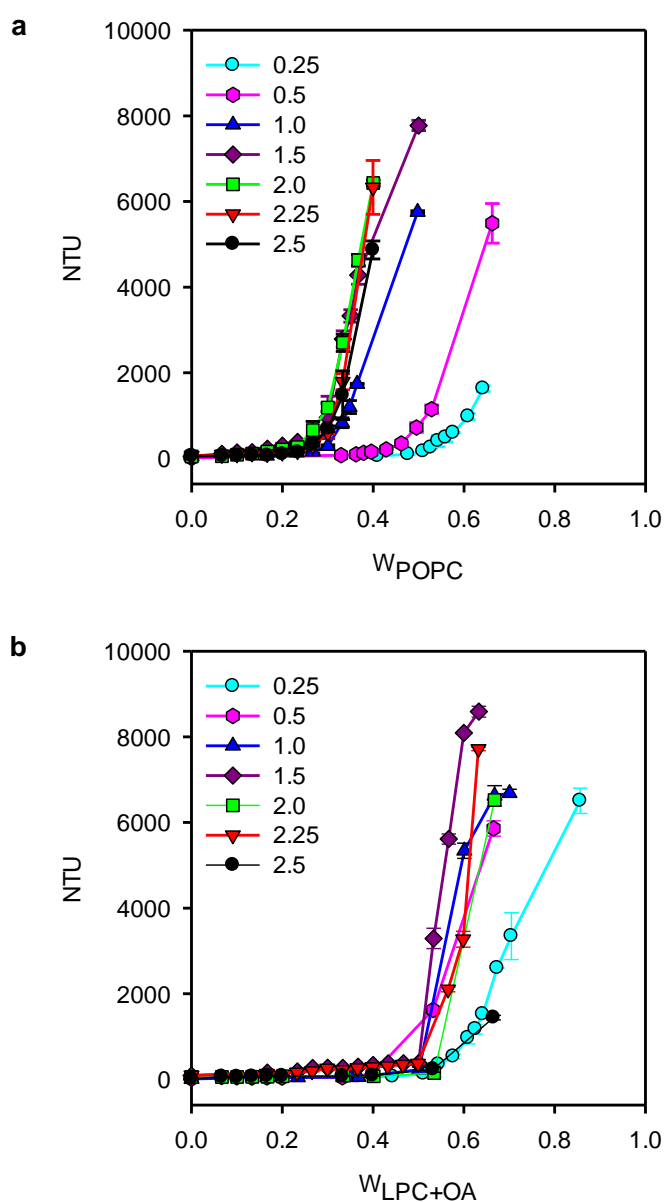


Figure 3.5. Turbidity of ternary systems as a function of phospholipid mass fraction showing the solubilisation of (a) POPC and (b) digested POPC (LPC+OA) by GDX.

3.4.3 Particle Size Measurement of GDX/POPC and GDX/(LPC+OA) Mixtures

Further evidence of the existence of a phase boundary between micellar and (micellar plus vesicular) phases of the ternary systems was obtained by particle sizing. Figure 3.6 presents dynamic light scattering (DLS) results, for 1.5 and 2.5 % w/w total concentrations of GDX/POPC and GDX/(LPC+OA). At low W_{Lipid} for both undigested and digested lipids the particle size data indicated the hydrodynamic diameter of the mixed micelles; as shown in Tables 1 and 2. For mass fractions of lipid in the range $W_{\text{POPC}} = 0.0 - 3.0$ and $W_{\text{LPC+OA}} = 0.0 - 0.4$, the particle size was found to be 3-12 nm in diameter, increasing gradually with W_{Lipid} . At higher values of W_{Lipid} a second population of particles in the range 300-700 nm was evident, indicating that the size distribution had become biphasic, and that vesicles were now present. The emergence of large particles occurred in the range of $W_{\text{POPC}} = 0.30 - 0.35$ and $0.29 - 0.30$ at total concentrations of 1.5 and 2.5 % w/w , respectively. The average polydispersity index (PDI) of the measurements is in the range of 0.18 – 0.37, shown in Table 1 and 2 for individual measurement. To avoid artificially calculated diameter due to the presence of two or more particle population, all the results with polydispersity index of greater than 0.5 were discarded and the experiment was repeated until the moderate PDI value was obtained to all measurements. The average diameters of the particles formed were reproducible with a moderate polydispersity index (PID < 0.5). However, as the samples have more than one molecule which forms a population of more than one particle size, it is impossible to get a very low polydispersity index. Moreover, the correlation function of the samples was carefully monitored during measurement to check whether the fluctuations of the correlation function were uniform. The same significant increase in particle size was observed for the digested POPC in the range of $W_{\text{LPC+OA}} = 0.45-0.55$ for both 1.5 and 2.5% w/w total concentrations of LPC+OA/GDX. This estimate of the phase boundary was in agreement with the estimate obtained by nephelometry. The presence of the large error bars found in the case of the particle size of the vesicles was due to the mixtures being formed by simple agitation. More vigorous agitation or sonication would result in a more reproducible particle size. However, we did not attempt to homogenise the mixtures, or attach any significance to the vesicle diameter. The focus

of the work was to identify the point at which vesicles appear, rather than draw any conclusions from the absolute particle size.

Table 3.1 Summary of the result of particle size (hydrodynamic diameter, D_h) measurement of 1.5% w/w total concentration of lipid and bile salt.

W_{POPC}	Particle Size, nm (Average D_h)		Avg. PDI	W_{LPC+OA}	Particle Size, nm (Average D_h)		Avg. PDI
	Micelle	Vesicle			Micelle	Vesicle	
0.000	4.8	NA	0.18	0.233	5.1	NA	0.25
0.166	4.9	NA	0.23	0.333	6.0	NA	0.24
0.233	6.9	NA	0.33	0.366	5.0	NA	0.37
0.266	7.4	NA	0.30	0.400	5.1	NA	0.28
0.333	7.4	322.0	0.28	0.466	5.7	511.7	0.18
0.366	9.3	287.0	0.22	0.500	5.7	427.4	0.27
0.400	10.3	549.9	0.20	0.533	6.8	365.1	0.33
0.433	12.0	592.3	0.18	0.566	8.5	556.0	0.28

Table 3.2 Summary of the result of particle size (hydrodynamic diameter, D_h) measurement of 2.5% w/w total concentration of lipid and bile salt.

W_{POPC}	Particle Size, nm (Average D_h)		Avg. PDI	W_{LPC+OA}	Particle Size, nm (Average D_h)		Avg. PDI
	Micelle	Vesicle			Micelle	Vesicle	
0.000	3.0	NA	0.18	0.232	4.3	NA	0.21
0.199	4.0	NA	0.35	0.265	4.1	NA	0.22
0.232	4.6	NA	0.36	0.298	4.0	NA	0.23
0.265	4.8	NA	0.35	0.332	4.8	NA	0.19
0.282	5.5	409.3	0.35	0.432	4.9	526.1	0.16
0.298	5.6	725.7	0.32	0.465	6.6	617.1	0.22
0.315	4.7	404.6	0.28	0.498	7.1	583.9	0.26

To allow comparison with the turbidity results, the turbidity data at 1.5 and 2.5 % w/w total lipid concentration is included in Figure 3.6. The appearance of significantly larger particles corresponds to the discontinuity in turbidity, giving confidence that our estimate of the phase boundary from turbidity data is justified. The DLS experiments determined that the undigested

POPC and digested POPC (see Figure 3.6 a/c and b/d) transition from micellar to vesicular at $W_{\text{POPC}}=0.3$ and $W_{\text{LPC+OA}}=0.5$ respectively. Therefore, the undigested phospholipid is less easily solubilised by the bile salt than the digested phospholipid, and a lower W_{POPC} is required to induce the appearance of vesicles.

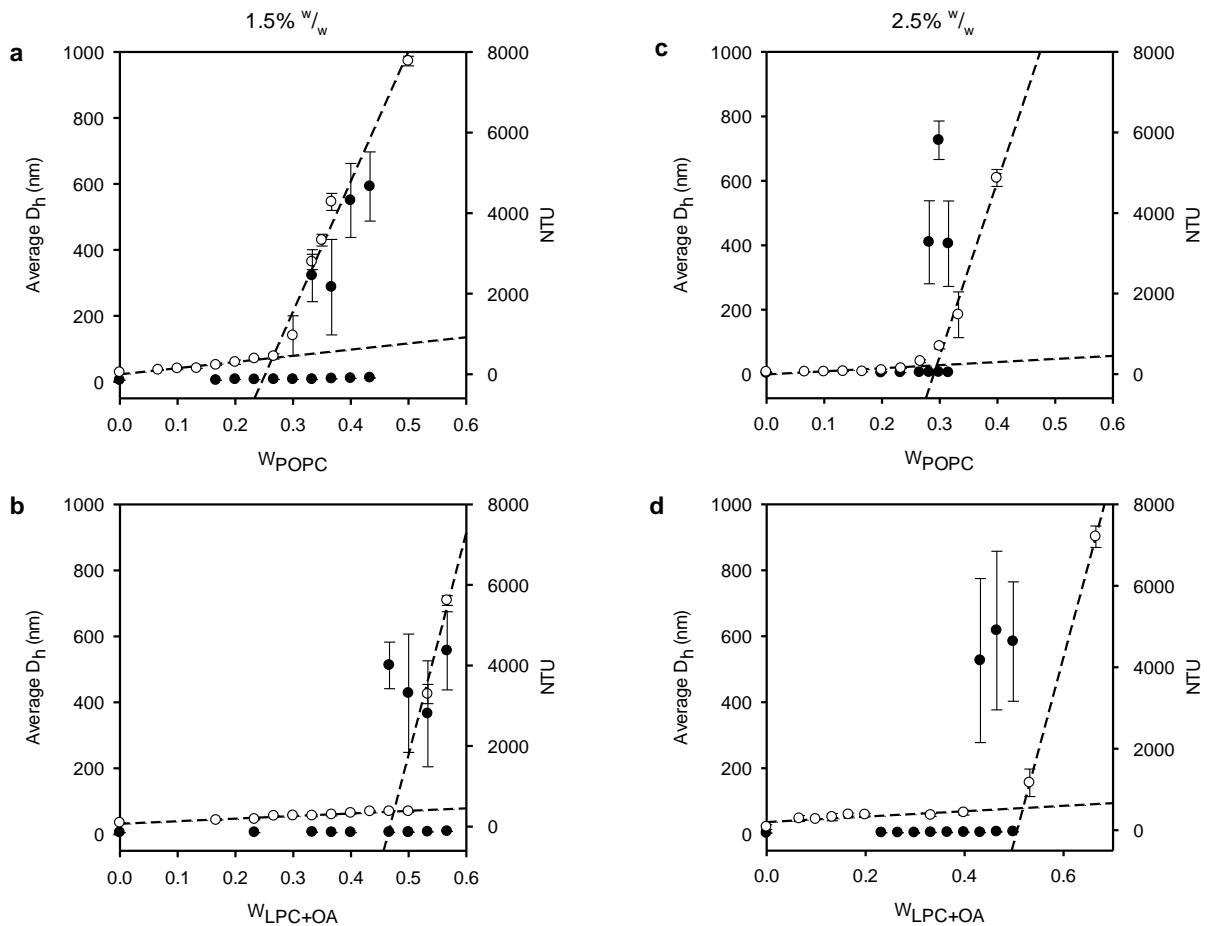


Figure 3.6. Particle size measurement by DLS versus weight fraction of lipid for mixtures of POPC or LPC+OA with GDX/water (Left axis ●) and corresponding turbidity measurements from nephelometry (Right axis, ○) (a) 1.5 % w/w POPC/GDX, (b) 1.5 % w/w LPC+OA/GDX, (c) 2.5 % w/w POPC/GDX and (d) LPC+OA/GDX 2.5 % w/w . The dashed lines represent best fit of the micellar and vesicular components of the turbidity data.

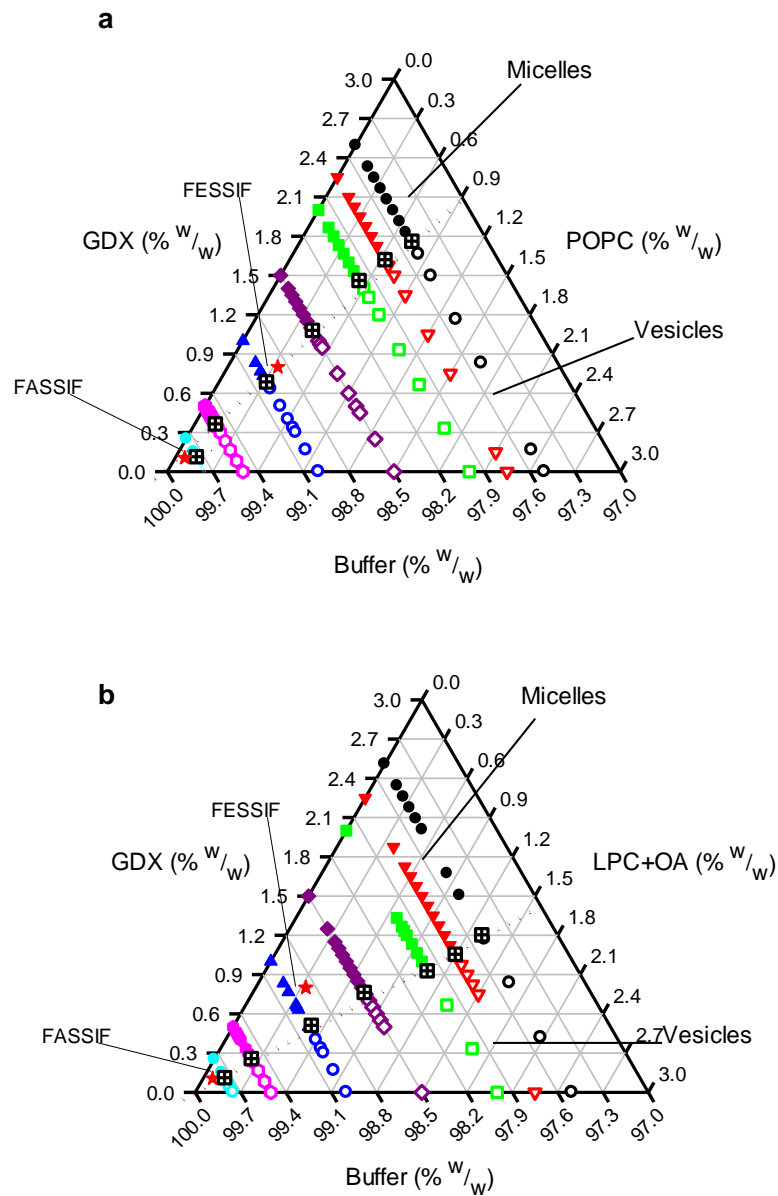


Figure 3.7. Ternary phase diagrams showing the phase behaviour at each composition investigated and the phase boundaries, (a) POPC/GDX/water, (b) LPC+OA/GDX/water. Filled symbols represent composition comprising micelles only and open symbols represent compositions where vesicles are present, with or without mixed micelles. Symbol colour and shape match with the turbidity curves shown in Figure 3.5. Crossed squares mark the phase boundaries calculated from turbidity curves using regression analysis. The dotted line indicates the predicted phase boundary of the system. The upper right and bottom left stars (★), indicated by the labels, represent the compositions of Fed State Simulated Intestinal Fluid (FeSSIF)* and Fasted State Simulated Intestinal Fluid (FaSSIF)^{*109} respectively. (*Note: FeSSIF and FaSSIF media contains NaTCH, whereas NaGDX is used in the diagram.)

3.5 DISCUSSION

Despite the importance of the association structures formed by bile components and digestion products, there is a limited literature on how lipid delivery systems, which often include digestible lipids and surfactants, are incorporated into mixed micelles and vesicles. It has been reported that vesicles can have a higher solubilisation capacity for PWSD than mixed micelles. Thus one would expect that the transitions between micellar and vesicular phases would have a significant effect on bioavailability, and that the influence of the delivery system on which phases are present in the intestine could be an important determinant of intestinal drug absorption^{33b}. It follows that it may be possible to optimize the design of lipid-based delivery systems to provide favorable association structures, depending on the preference of the drug for micelles or vesicles^{35d}.

The complexity of the gut contents during digestion of different types of food would make it difficult to predict the precise nature of the gut contents, or indeed the influence that the excipients present in the delivery system might have on this complex milieu. However, it is important to note that the bioavailability of PWSD administered with or after food is often higher than the fasted state. It is the bioavailability of the drug administered to a fasted state which is of primary interest to formulators of lipid-based delivery systems (LBDDS) since this represents a more challenging absorption environment for PWSD. The main objective of LBDDS is to achieve equivalent bioavailability in the fasted state, when the delivery system may have a critical role in the outcome, and the association structures in the intestine are more likely to be predictable. Hence, we have embarked on a series of studies to improve the understanding of these association structures, and here we report on the structures formed by bile components before and after phospholipid digestion.

Figure 3.1 indicates that digestion of phospholipids after secretion into the duodenum will be rapid and suggests that the properties of mixed micelles of digested bile are of more significance than bile salt/phospholipid micelles. We show in this paper that the phase behaviour changes

significantly after digestion. This is likely to be of physiological significance and may be important in relation to drug solubilisation.

The investigation of lipids-bile salt-water system in this study shows where the phase boundary lies, beyond which the lipids exists at least partly in vesicular form. As W_{Lipid} increases towards unity, a second phase boundary would be expected, beyond which all of the GDX is incorporated in vesicular structures. The absolute sizes of the larger particles, which we suggest are multilamellar liposomes, cannot be adequately determined using DLS. We used DLS simply to identify the point at which large particles can be detected. DLS allowed the phase boundary to be identified adequately but if an accurate estimate of the size of the vesicles had been required, it would have been necessary to use an alternative sizing technique, such as laser Fraunhofer diffraction. We were unable to identify that phase boundary in the current study, though this is not of direct interest since the molar ratios present in the intestine are likely to lie closer to the former phase boundary. The early studies of Small *et. al.* indicated, in studies of lecithin-bile salt-water and lecithin-bile salt-cholesterol in aqueous media, that isotropic micellar solutions are formed at lower concentration of lecithin in the presence of a mixture of bile salts and in the presence of only sodium cholate. Increasing the lecithin concentration in both cases resulted in a mixture of a paracrystalline phase dispersed as myelin forms and mixed micelles^{17h, 17i}. In a study of temperature and concentration dependent lecithin-water systems conducted by Luzzati *et. al.* mostly the lamellar phase was observed for the systems at temperature lower than the melting temperature of lecithin, whereas crystalline phase was observed for the dry lecithin system^{17g}. Shipley *et. al.* indicated in their study of the interaction of cholesterol esters with phospholipids that hydrated dimyristoyl lecithin forms a lamellar liquid-crystalline phase at temperatures beyond 23°C. Our studies of GDX and POPC or digested POPC are consistent with the above studies, and provide more detail of the phase behaviour of dilute systems. POPC is below its melting temperature under the experimental conditions described here and therefore would be expected to form lamellar liquid crystalline. All the turbidity measurements were taken at 37°C and the all

the systems reached equilibrium within 10 min after mixing. As the solvent was water, there was no significant evaporation during the stabilisation period. Moreover, in our study we focused on the properties of biliary lipids at physiological concentration, temperature and pH. The comparison made in this study is between POPC, which has two hydrocarbon chains (in the 1, 2 positions), and LPC which has a single hydrocarbon chain (in the 1 position) in combination with oleic acid. From the chemical structure of these compounds it is expected that they will form different phases when they interact with water and bile salt. POPC which has a tendency to form a bilayer in aqueous environment due to its double hydrocarbon chain can resist the solubilisation effect of bile salt micelles more than LPC. Hence, POPC forms a vesicular or lamellar phase in the presence of bile salts at relatively lower concentrations of POPC. Bile salts interact with the phosphate head group of POPC but their solubilisation capacity is limited by the preference of POPC to form a flatter surface than LPC+OA. In the case of LPC and OA, the presence of two separate alkane chains introduces significant flexibility, allowing the compounds to form a more curved interface. As a result micellar structures are formed at significantly lower proportions of bile salt compared to POPC. Higher concentrations of LPC and oleic acid, with corresponding lower concentration of bile salt, are required to form vesicular phases. This phenomenon was also observed in our molecular dynamics simulations¹¹⁹.

As indicated on the phase diagrams in Figure 3.7, the key finding of this study is that there is a significant shift in the phase boundary towards higher W_{Lipid} after digestion of the phospholipid, indicating the increased ability of the bile salt to solubilise these digested lipid species. This trend occurred at all concentrations studied, representative of the range of bile concentrations in the intestine. This observation implies that as bile leaves the gall bladder and enters the intestine, its rapid digestion induces a phase transition from lamellar into micellar form, which may facilitate more rapid solubilisation of lipid digestion products, from the surface of droplets of dietary fat. A more rapid and potent solubilizing system is useful for the role of bile in the intestine but could be potentially damaging to the epithelial cell membranes of the gall bladder. Thus we hypothesise

that sequestration of bile salts in vesicular form by phospholipids is protective and necessary for storage in the gall bladder, but more effective solubilisation capacity is released by immediate digestion after secretion into the intestine. Future work in this field now needs to focus on the association structures that form once digested bile makes contact with LBDDS, before and after their digestion. This will be evaluated in our investigation of similar systems at atomistic details using molecular dynamics simulation methods.

3.6 CONCLUSIONS

In this study, it has been shown that the environment of the small intestine varies depending on the phospholipid and bile salt concentrations. Additionally, there is a clear distinction between undigested and digested phospholipids in the transition of colloidal phases from micelles to vesicles. The phase behaviour of bile salt and undigested and digested phospholipids conducted here provides an improved understanding of the environment of the small intestine in relation to the absorption of PWSDs. Future studies will be conducted to assess the impact of bile dilution as well as the presence of exogenous lipid digestion products in the absorption process of PWSD candidates.

3.7 ACKNOWLEDGMENT

Funding support from Australian Research Council (ARC) Linkage Grant awarded to Monash University in collaboration with Capsugel is greatly acknowledged. W.A.B also would like to thank Orlagh Feeney for conducting the digestion experiment of phosphatidylcholine.

Declaration for Thesis Chapter 4

Declaration by candidate

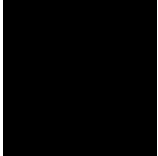

In the case of Chapter 4, the nature and extent of my contribution to the work was the following:

Nature of contribution	Extent of contribution
Planning and executing computer simulation work, data evaluation and drafting and revision of manuscript	65%

The following co-authors contributed to the work. If co-authors are students at Monash University, the extent of their contribution in percentage terms must be stated:

Name	Nature of contribution	Extent of contribution
D. K. Chalmers*	Project supervisor, data and manuscript review	NA
C. W. Pouton	Project supervisor, data and manuscript review	NA
C. J. H. Porter	Project co-supervisor, data and manuscript review	NA
D. B. Warren	Supervision of computer simulation works and manuscript review	NA
S. J. Heady	Performing the NMR spectroscopy	NA
H. Benameur	External supervision and manuscript review	NA

The undersigned hereby certify that the above declaration correctly reflects the nature and extent of the candidate's and co-authors' contributions to this work*.

Candidate's Signature		Date: 12/06/2015
Main Supervisor's Signature		Date: 12/06/2015

"A computer will do what you tell it to do, but that may be much different from what you had in mind."

Joseph Weizenbaum

CHAPTER FOUR

THE PHASE BEHAVIOUR OF MODEL INTESTINAL FLUIDS STUDIED USING MOLECULAR DYNAMICS SIMULATIONS; THE IMPACT OF LIPID DIGESTION

*Woldeamanuel A. Birru³, Dallas B. Warren³, Stephen J. Headey¹, Hassan Benameur⁴,
Christopher J. H. Porter³, Colin W. Pouton^{2,3} and David K. Chalmers¹*

¹Medicinal Chemistry, Monash Institute of Pharmaceutical Sciences*

²Drug Discovery Biology, Monash Institute of Pharmaceutical Sciences

³Drug Delivery, Disposition and Dynamics, Monash Institute of Pharmaceutical Sciences

⁴Capsugel Research & Development, Pharmaceutical Sciences, Strasbourg France.

*Monash Institute of Pharmaceutical Sciences, Monash University (Parkville Campus), 381
Royal Parade, Parkville, Victoria 3052, Australia

4 THE PHASE BEHAVIOUR OF MODEL INTESTINAL FLUIDS STUDIED USING MOLECULAR DYNAMICS SIMULATIONS; THE IMPACT OF LIPID DIGESTION

4.1. ABSTRACT

Molecular dynamics (MD) simulation is a powerful method for investigating phase behaviour at a molecular level. In this study we have used MD to model the phase behaviour of bile within the GI tract, before and after digestion of the bile phospholipid by pancreatic and gastric lipases. Bile is represented by a model system composed of POPC, sodium glycodeoxycholate (GDX) and water. Digested bile is modelled by a 1:1 mixture of oleic acid and 1-palmitoyl-2-hydroxy-sn-glycerol-3-phosphocoline (LPC), GDX and water. The phases formed by the undigested and digested POPC are compared and the intermolecular interaction of the lipids and bile salt investigated. The possible arrangements of the bile salt and the lipids are also predicted. Furthermore, the effect of different ionization states of oleic acid, the digested product of POPC, on the phase formation is also observed. There is a generally good agreement between MD simulation results and the experimental results although some discrepancy were found in the predicted and experimental positions of the phase boundary between micelle and lamellar phases in the POPC/GDX/water system. This illustrates that the MD approach is critical to the understanding of the study of phase behaviour of different molecules especially lipids and fatty acids. MD simulation also plays a vital role in driving the improvement of the absorption and bioavailability of poorly water-soluble drug candidates.

4.2. INTRODUCTION

Oral administration is the preferred method for the delivery of drugs into systemic circulation. However, for a significant number of drug compounds, poor solubility of the active agent in the gastrointestinal tract (GIT) results in low or variable uptake into the circulation and

correspondingly poor drug efficacy. In many cases, the bioavailability of poorly water soluble drugs (PWSDs) can be improved by careful formulation using solubilizing excipients. Lipid-based drug formulations are an important example of this approach.¹²⁰ Lipid formulations range from simple solutions of drug in oil to complex colloidal systems comprising drug, oils, water, surfactants and co-solvents.¹²¹ They have been shown to effectively enhance the oral bioavailability of poorly water-soluble drugs,¹²¹⁻¹²² yet the implementation of lipid-based formulations has so far been limited⁹ due, in part, to a lack of basic quantitative knowledge and understanding of drug trafficking between the lipid formulation, digested lipid components within the small intestine, and the epithelial boundary where absorption occurs. One approach to improving our understanding of these processes is to develop model systems that reproduce the key features of the intestinal environment using a relatively small number of pure molecular components. The interactions of drugs within such systems can be more easily studied within the laboratory environment and the study of the simplified system can be closely coupled to the use of computational models to develop our understanding of the key physicochemical processes that control drug absorption.

Oral drugs are absorbed into the bloodstream through the stomach and intestine. The large surface area and longer drug residence times within the intestine means that intestinal absorption accounts for the bulk of the uptake of most drugs and particularly for PWSDs. The gastric fluids within the intestine contain water, bile salts and lipids derived from bile, electrolytes and protein (mucins, enzymes, etc). Food and food digestion products are also present following a meal. The lipid phases present within the intestine play an important role in solubilizing PWSDs and it is important to understand the nature of the lipid phases produced by phospholipid/bile salt mixtures and how these phases change under the various conditions present in the GIT.

One of the key processes within the GIT is the digestion of phospholipids, and other compounds containing ester groups, by gastric and pancreatic lipases. Phosphatidylcholines are quickly hydrolysed to lysophosphatidylcholine and free fatty acids by phospholipase A2 (Figure 4.1).¹²³ We have recently shown, using *in vitro* model systems, that the digestion process significantly

alters the phase behaviour of systems of bile salt/phospholipid and bile salt/digested phospholipid.¹²⁴ Notably, the formation of mixed micelles rather than lamellar phases occurs much more easily once the phospholipid is digested. The digestion of the endogenous phospholipids that are secreted in bile is therefore expected to affect the phases present within the GIT.

The formation of the mixed micelles of bile salts and phospholipid and their transition to vesicles/lamellae with increasing concentration of lipids was observed about 40 years ago in an experimental study performed by Small *et al.*^{17h} Historically, a number of experimentally-derived simple models have been proposed to describe the nature of bile salt/phospholipid mixed micelles (see for example models by Small¹²⁵, Mazer *et al.*¹²⁶, Ulmius *et al.*¹²⁷ and Nichols and Ozarowski⁶¹). These models generally imply that bile salt/phospholipid micelles are quite ordered in nature with the molecules of bile salt and phospholipid arranged in clearly distinct locations within the micelle and, that a single description is appropriate over a range of bile salt/phospholipid micelles ratios and concentrations. These models are simplifications in that they do not describe how the micelles change in size with variation in phospholipid and bile salt concentrations and also do not describe the dynamic nature of micelles. A more complex model for phospholipid/bile salt micelles was proposed by Marrink and Mark,¹²⁸ who used molecular dynamics simulations to model single micelles of bile/phospholipid mixtures. In this early MD study, the micelles were of fixed size but nevertheless, the simulations revealed that rather than being well-ordered, the micelles are irregular in structure and dynamic and that the phospholipid and bile salts are not strongly localized within the micelle.

In this study, we have used a series of more than 40 MD simulations to explore the behaviour of ternary systems of water, bile salt and phospholipid in the micelle and vesicle regions of the phase diagram and also investigated the changes that result from hydrolysis of the phospholipid into molecules of lysophosphocholine and fatty acid. The methodology used in this work is based on our previous studies, which show that the use of multiple MD simulations can be used effectively to understand the lipid structures that form in aqueous solution.^{26c, 40, 129} The computational models in this work are designed to complement the experimental model systems that we have

developed using pure molecular components¹²⁴ in order to establish a close relationship between our theoretical and experimental studies. The influence of pH on phase behaviour is also investigated. Additionally, we investigate the molecular diffusion coefficients of the associated particles formed by undigested and digested phospholipids by using NMR. The information derived from this work will ultimately assist the development of lipid-based drug formulations.

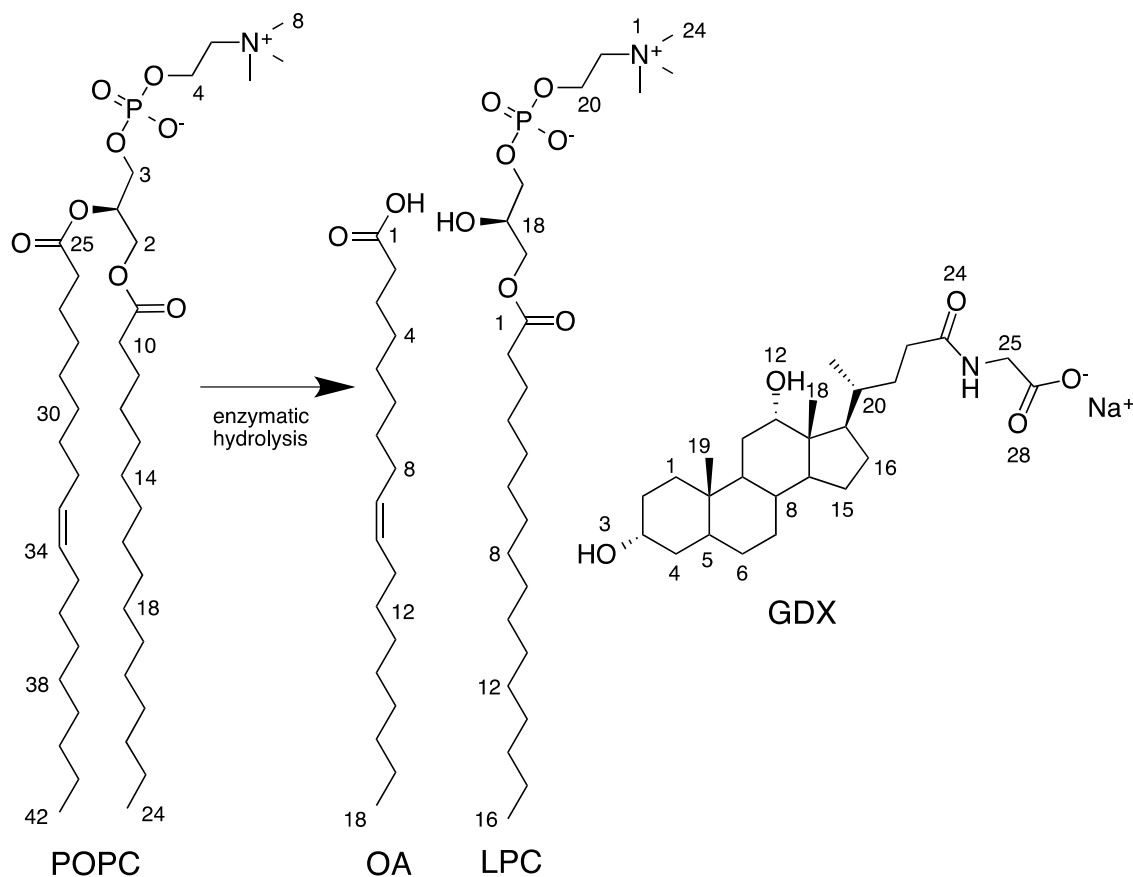


Figure 4.1. Structures of 1-palmitoyl-2-oleoyl-*sn*-glycerol-3-phosphocholine (POPC), 1-palmitoyl-2-hydroxy-*sn*-glycerol-3-phosphocoline (LPC), oleic acid (OA), which are used as models for phospholipid and hydrolysed phospholipid in this work, and glycodeoxycholic acid, sodium salt (GDX) which is used as a representative bile salt. The numbering system used in this paper is shown.

4.3. MATERIALS AND METHODS

4.3.1 NMR Methods

The phospholipids 1-palmitoyl-2-oleoyl-sn-glycerol-3-phosphocholine (POPC) and 1-palmitoyl-2-hydroxy-sn-glycerol-3-phosphocoline (LPC) were obtained from Avanti Polar Lipids, Inc. in powder form. Glycodeoxycholic acid, sodium salt (GDX) was obtained from Calbiochem, oleic acid (OA) (> 99% pure) was obtained from Sigma-Aldrich. Deuterium oxide (D₂O, 99%) was obtained from Cambridge Isotope Laboratories Inc. Sodium hydroxide, sodium phosphate monohydrate and sodium chloride were analytical grade.

The blank fasted state simulated intestinal fluid¹³⁰ buffer (FaSSIF) was based on the composition of FaSSIF buffer, minus the phospholipid and bile salt and is composed of: 0.00348 g of NaOH and 0.03954 g of NaH₂PO₄·H₂O and 0.06186 g of NaCl in a 10 ml of purified water. The pH was adjusted to 6.5 ± 0.02 using 1 M NaOH and 1 M HCl as required.

Phospholipid solutions were prepared using the evaporated film method; 0.0375 g of lipid (POPC or LPC+OA) was dissolved in 5 ml of methanol in a round bottom flask. The methanol was removed using a rotary evaporator and placed under high vacuum for 1 hour to ensure that all the methanol was evaporated. The resulting lipid film was dispersed in 1.5 g of the deuterium oxide aqueous phase blank FaSSIF buffer, generating a 2.5% w/w solution. The aqueous solutions of 2.5% w/w GDX were prepared by dissolution of 0.0875 g of GDX in 3.5 g of blank FaSSIF buffer made using D₂O. Seven different proportions of undigested and digested phospholipids with bile salt were prepared as shown in Table 4.1. These representative mixtures are taken from the phase transition curve identified by using turbidity and particle size measurement experiments conducted by Birru *et. al.*¹²⁴.

Table 4.1. Mass fractions (*W*) of GDX, POPC and LPC+OA used in the NMR diffusion experiments

Sample	W_{GDX}	W_{POPC}	Sample	W_{GDX}	$W_{\text{LPC+OA}}$
1	1	0	8	1	0
2	0.866	0.133	9	0.867	0.133
3	0.799	0.200	10	0.667	0.332
4	0.733	0.266	11	0.601	0.398
5	0.667	0.333	12	0.468	0.531
6	0.599	0.400	13	0.335	0.665
7	0.460	0.533	14	0.167	0.832

Diffusion ordered spectroscopy (DOSY) spectra were acquired on a Bruker AVANCE 600 MHz NMR spectrometer using a pseudo 2D version of a stimulated echo sequence with a 100 ms longitudinal echo gradient delay and bipolar gradient pulses of 1.5 ms.¹³¹ Each pseudo 2D spectrum consisted of 12 1D spectra where the gradient strength was varied linearly from 5 to 95%. Spectra were processed using Topspin 1.3.

4.3.2 Molecular Dynamics Simulations

Molecular dynamics simulations were performed using GROMACS version 4.5.4¹³² Calculations were performed using the Victorian Life Sciences Computation Initiative (VLSCI) Linux cluster comprised of 1088 Intel Nehalem compute cores running at 2.66GHz connected using InfiniBand. The GROMOS 53a6 united atom force field⁴⁷ was used to represent POPC, GDX, LPC and OA. This force field is parameterized to reproduce free energies of solvation in water and cyclohexane and has been used extensively to model proteins, micelles and membranes. The cis double bond in oleic acid was modelled using dihedral parameters developed by Barchar *et al.*^{17a, 133} Water was modelled using rigid SPC water and constrained using SETTLE.¹³⁴ The remaining solute bonds were constrained by the LINCS algorithm.⁷⁹ Periodic boundary conditions were employed. A cut-off distance of 0.9 nm was used for short range electrostatic interactions and van der Waals

interactions and the particle-mesh Ewald (PME) method¹³⁵ was used for long range electrostatic interactions. Temperature coupling used the velocity rescale algorithm¹³⁶ with a reference temperature of 310 K. Production runs used isotropic Parrinello-Rahman¹³⁷ pressure coupling algorithms with a reference pressure of 1 bar and a compressibility of $4.5 \times 10^{-5} \text{ bar}^{-1}$.

Simulations utilized a 15 nm cubic periodic cell which, for these systems, provides an appropriate trade-off between periodic cell artefacts and CPU time. Starting model structures were built using the Silico⁴⁵ script *random_box*. The required numbers of solute and water molecules were randomly positioned in the simulation cell, giving systems ranging from 150,000 to 300,000 atoms, see Table 4.2 for details. MD simulations were established using: (1) A steepest descents minimization of 500 steps to remove bad van der Waals contacts between atoms. (2) A constant volume simulation of 5,000 steps with a time step of 2 fs. (3) A constant pressure simulation of 10,000 steps using Berendsen isotropic pressure coupling with a coupling time constant of 0.1 ps and time step of 2 fs. (4) A simulation of 50,000 steps using a time step of 2 fs, Parrinello-Rahman pressure coupling, a pressure coupling time constant of 2.0 ps, and v-rescale temperature coupling with a 0.1 ps temperature coupling time constant. Each production simulation was run for 200 ns with a time step of 5 fs, a pressure reference of 1 bar using Parrinello-Rahman pressure coupling with time constant of 2 ps, v-rescale temperature coupling with a reference temperature of 310 K corresponding to the experimentally determined phase diagram by our group and temperature coupling time constant of 0.1 ps. The temperature coupling was applied by separating the system into two groups (water and non-water) that maintain the reference temperature correctly to the reference of the heat bath.

Molecular aggregation was analysed using the Silico⁴⁵ script *find_aggregate*, which combines molecules into aggregates by comparing distances between carbon atoms. Two molecules are considered to be part of the same aggregate if they have carbon atoms separated by a distance of less than 0.4 nm. Visualization of the simulation trajectories was performed using VMD¹³⁸ and images for publication were produced using PyMol.¹³⁹ Radial distribution functions (RDFs) were

calculated with the GROMACS program `g_rdf` with a bin width of 0.004 nm run on the last 10 ns of the production run. Spatial distributions function (SDF) which describe the three dimensional probability of finding a particle around a given reference were calculated with `g_sdf` distributed with GROMACS 4.0.7 using a bin width of 0.09 nm and a cell size 8×8×8 nm. The `g_sdf` tool requires three reference atoms in a molecule.

4.4. RESULTS AND DISCUSSION

In this study we have used molecular simulation to better understand the phase behaviour of the ternary POPC/GDX/water system and the physicochemical changes that occur following enzymatic hydrolysis of the POPC component to give LPC+OA/GDX/water. These systems model intestinal fluid before and after digestion by lipases. We have recently performed a complementary experimental study¹²⁴ where we investigated micelle and vesicle formation in dilute mixtures of bile salt with phospholipid or with hydrolysed phospholipid. The position of the micelle-vesicle phase boundary was determined using dynamic light scattering and nephelometry, revealing that lamellar phases (e.g. vesicles) form more readily with phospholipid present than with the digestion product. Mixed micelles of digested bile have a higher capacity for solubilisation of lipids and fat digestion products and can be expected to have a different capacity to solubilize lipophilic drugs.

4.4.1 The Effects of Phospholipid Digestion

To investigate the molecular factors controlling the formation of micelles or lamellar phases in intact and digested bile, we simulated two phase systems; the ternary POPC/GDX/water system (i.e. bile salt plus phospholipid) and the ternary LPC+OA/GDX/water system with LPC and OA maintained at a 1:1 mass ratio, which would be expected from lipid digestion. In this first set of simulations the oleic acid molecule was modelled as being fully protonated (OA). The effect of changing the ionization state of the oleic acid is considered further below. Each simulation was performed for a total of 200 ns and, as we have previously observed for other molecular

species,^{26c, 40, 129} the lipid systems rapidly and spontaneously form colloidal aggregates. From the initial random configuration, aggregates start to form within 10 ns. After 50 ns the aggregates become quite stable and are in equilibrium throughout the remaining 150 ns of simulation. A plot showing this is available in Appendix 3, Figure 9.3.1.

Table 4.2 records the molecular composition of the simulations performed and the nature of the colloidal aggregates present at the last 10 ns of the simulation. In both the digested and undigested model systems, the total number of aggregates and mean size of the aggregates formed in the simulations was calculated using *find_aggregate*. This program identifies hydrophobic aggregates of molecules (e.g. micelles or vesicles/lamellae) in a given periodic system. It is important to note that, in many of the simulations, the sizes of the molecular aggregates formed was limited by the number of molecules present in the simulated system and the simulation results should be interpreted with care when only a small number of aggregates are present at the end of the simulation. For example, simulations **7** and **11** both produce single micelle-like aggregates that, on closer inspection, have a lamellar structure, that is, the 'micelle' resembles a small section of bilayer with the hydrocarbon tails of the phospholipids aligned in separate leaflets. In these simulations, globular aggregates have formed because there are insufficient molecules present to form a complete bilayer. This is confirmed by inspection of simulations **16** and **17** that respectively contain the same proportions of bile salt and phospholipid as simulations **7** and **8** but at higher concentrations. Simulation **16** formed a disordered lamellar system and **17** formed a well-ordered bilayer, indicating that these phases would also form in the more dilute systems if a larger system were to be studied. In Table 4.2 we have annotated the cases where we expect the apparent phase produced by the simulation does not reflect the thermodynamically stable phase. These annotations are made where a micelle-like structure is observed, but only a small number of aggregates are present (often only a single aggregate), or the observed aggregates have a large range of sizes.

Table 4.2. Simulations modelling the ternary POPC/GDX/water and LPC+OA/GDX/water phase systems.

NO. SERIES		NO. OF MOLECULES				COMPOSITION (% W/W)			MEDIAN AGGREGATE SIZE / NUM. AGGREGATES ^a	STRUCTURE IN FINAL STATE
		POPC	LPC/OA	GDX	Water	POPC	LPC/OA	GDX		
1	A/E	-	-	236	105570	-	-	5.2	20/12	Micelles
2	B/F	-	-	466	100238	-	-	9.7	29/15	Prolate micelles
3	C/G	-	-	575	88118	-	-	15.0	56/10	Prolate micelles
4	D/H			982	88118			22.5	47/3	Wormy micelles
5	A	64	-	118	105806	1.6	-	3.0	19/8	Micelles
6	A	88	-	81	105806	2.2	-	2.0	45/4 ^b	Micelles
7	A	118	-	24	105806	3.0	-	0.6	142/1 ^b	Lamellar
8	A	135	-	-	105806	3.4	-	-	135/1 ^b	Lamellar secondary micelle
9	B	125	-	233	100518	3.0	-	6.0	40/8	Micelles
10	B	172	-	165	100073	4.0	-	4.0	63/5	Micelles
11	B	236	-	47	100191	6.0	-	1.0	283/1 ^b	Lamellar
12	B	263	-	-	100238	7.0	-	-	263/1 ^b	Lamellar
13	C	175	-	400	89937	5.0	-	10.0	95/6	Spherical and wormy micelles
14	C	285	-	290	89211	7.5	-	7.5	286/2	Wormy micelles
15	C	375	-	233	89937	9.0	-	6.0	607/1 ^b	Disordered lamellar
16	C	476	-	95	89843	12.4	-	2.4	571/1 ^b	Disordered lamellar
17	C	567	-	-	89100	15.0	-	-	567/1 ^b	Lamellar
18	D	111		699	89937	3.0		17.0	44/5	Wormy micelles
19	D	260		466	89211	6.7		11.5	190/3 ^b	Wormy micelles
20	E	-	31/31	118	105806	-	1.0	3.0	21/8	Micelles
21	E	-	43/43	81	105806	-	1.7	2.0	26/5	Micelles
22	E	-	58/58	24	105806	-	3.0	0.6	70/2 ^b	Micelles ^c
23	E	-	65/65	-	105806	-	3.0	-	130/1 ^b	Oblate micelle ^c
24	F	-	61/61	233	100518	-	2.4	6.0	50/8	Spherical micelles
25	F	-	84/84	165	100073	-	3.6	4.0	56/6	Oblate micelles
26	F	-	115/115	47	100191	-	5.0	1.0	139/2 ^b	Oblate micelles ^c
27	F	-	128/128	-	100238	-	5.0	-	256/1 ^b	Oblate micelle ^c
28	H		183/183	233	89937		7.6	6.0	86/6	Oblate micelles
29	H		232/232	95	89843		9.9	2.5	279/2 ^b	Oblate micelles
30	H		250/250		89100		11.0	-	500/1 ^b	Vesicle-like lamellar
31	G	-	175/175	400	100500	-	6.0	9.0	122/6	Wormy micelles
32	G	-	285/285	290	110900	-	9.0	6.0	429/2	Wormy micelles
33	G	-	375/375	233	130000	-	11.0	4.0	982/1	Wormy micelles
34	G	-	476/476	95	130000	-	13.0	2.0	1047/1	Disordered lamellar
35	G	-	567/567	-	140500	-	15.0	-	1134/1 ^b	Lamellar
36	H	-	127/127	699	89937		5.0	17.0	282/4	Wormy micelles
37	H	-	169/169		89211		7.0	12.0	121/7	Wormy micelles

^aAggregate numbers and median values exclude any isolated molecules. ^bA small number of aggregates are observed. The median value will not be a reliable estimate of the true aggregate size. ^cThe observed structure is expected to be affected by the number of molecules present in the modelled system.

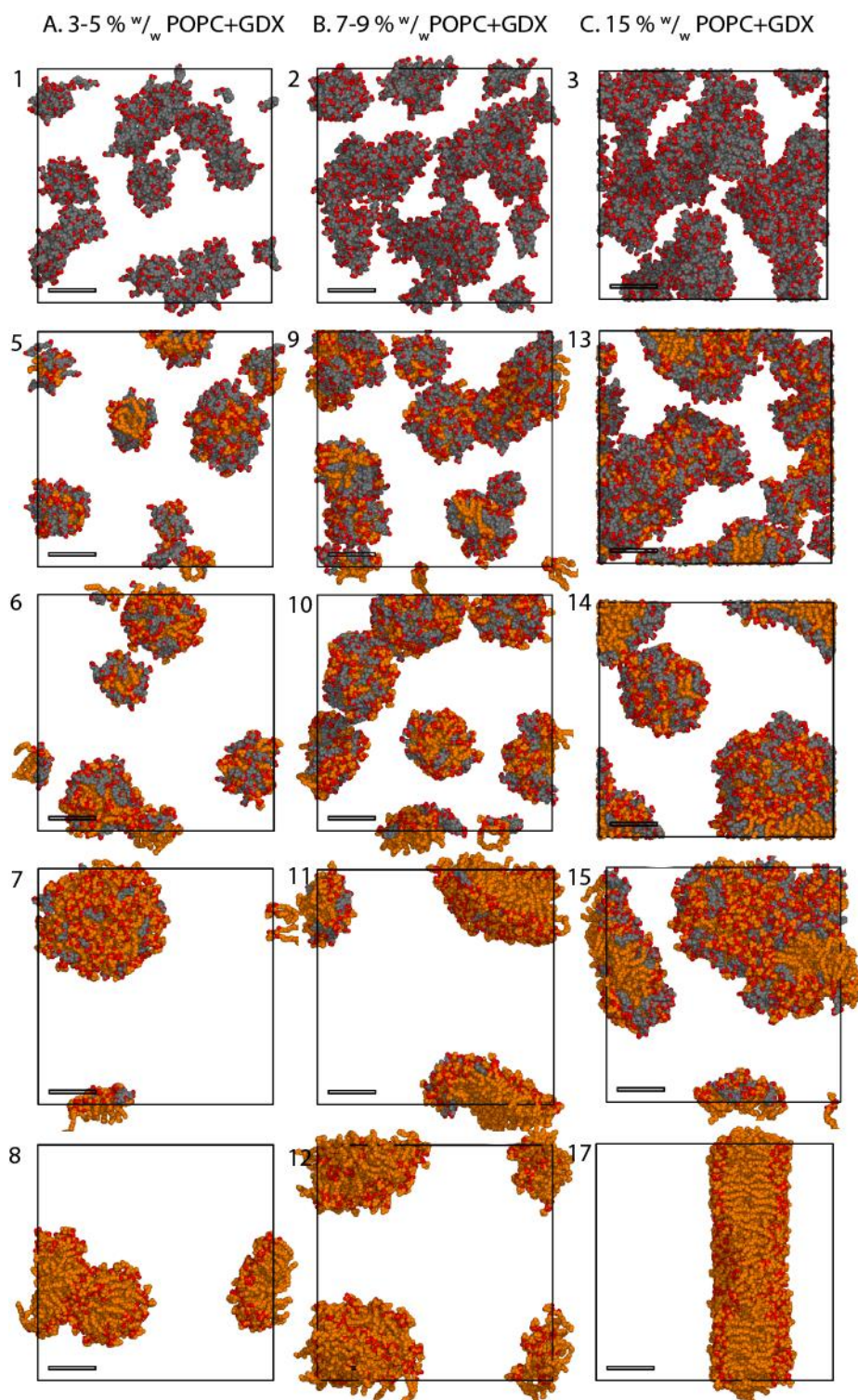


Figure 4.2. Final structures from the phospholipid/bile salt simulations (POPC/GDX/water) showing the progression from dynamic GDX micelles (e.g. simulation 1), through mixed micelles (e.g. 6) to large aggregates (e.g. 17) and finally to distinct lamellar phase (17). The simulation numbering is described in Table 4.2. Atom colouring; GDX is grey, POPC is orange and oxygen atoms are red. Boxes indicate the periodic cell. The scale bar is 3.0 nm. Water molecules are not shown.

Figure 4.2 shows a selection of final structures obtained from the GDX/POPC/water simulations. The simulations were performed in four series (A-D) which traverse the phase diagram from high GDX concentration to high POPC concentrations and contain successively greater lipid content. The simulations in set C maintain a constant amount total lipid (POPC+GDX) of 15% by mass. Simulations **1-4** are the starting points for each series and consist only of GDX in water. These simulations clearly display the non-classical surfactant behaviour of bile-salt micelles; the micelles are generally irregular in shape and not strongly organized, changing dynamically through the course of the simulation as observed previously^{26c}. As the GDX concentration is increased in simulations **1** to **4**, the micelles progress from being roughly spherical with free GDX present (simulation **1**) through elongated or prolate micelles (**2**), to extended wormy micelles (**4**). Simulations **5, 9, 13** and **19** contain GDX and POPC in the ratio of 2:1 by mass and form mixed micelles structured with the hydrophobic POPC tails in the interior and the GDX located on the surface. Simulations **5** and **9**, having lower total lipid content, form discrete, roughly spherical micelles while simulation **13** with more lipid present, forms a mix of wormy micelles and spherical micelles. Simulations **6, 10** and **14** contain equal masses of POPC and GDX. These simulations also form spherical micelles at lower total lipid concentrations which and wormy micelles as the lipid content is increased. Simulations **7, 11** and **15** contain more POPC than GDX and, rather than forming discrete micelles, form single aggregates with evidence of lamellar structure. This suggests that mixtures of POPC and GDX in these ratios would be expected to form large lamellar structures such as vesicles or phase separated systems. The final group of simulations, **8, 12** and **17**, are POPC/water systems. When the lipid content is low, these simulations produce single apparent micelles with a lamellar structure. When the lipid content is higher, a bilayer forms that spans the simulation cell. Again, these simulations indicate the formation of lamellar phases.

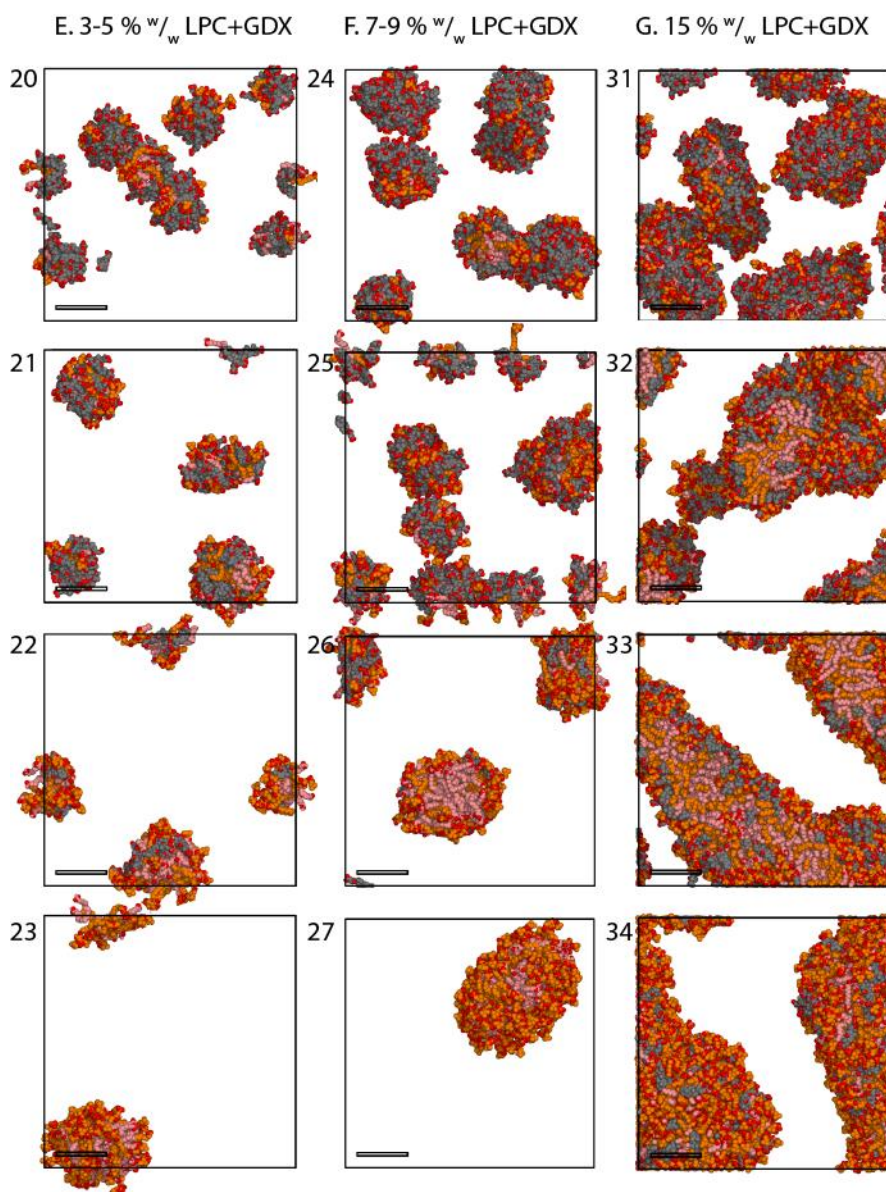


Figure 4.3. Final structures of the simulations of the hydrolysed phospholipid/bile salt system (LPC+OA/GDX/water) showing progression from discrete micelles at high ratios of bile salt/lipid ratios to single, large aggregates as the bile salt concentration is reduced. Simulation numbering is described in Table 4.2. Atom colouring; GDX is grey, LPC is orange, OA is pink and oxygen atoms are red. The box indicates the periodic cell. The scale bars are 3.0 nm. Water molecules are not shown.

Figure 4.3 shows the final structures produced by simulations of bile salt and digested phospholipid composed of equimolar amount of LPC and OA. These simulations were also performed in four series (D-G) with series F maintaining constant total lipid content. The structures produced by simulations with high ratios of GDX to LPC+OA and a total lipid content below about 12.5 % (simulations **20**, **21**, **24**, **25** and **28**) produce discrete mixed micelles with the OA in the core surrounded by LPC and with GDX on the exterior. These micelles became progressively more oblate as the proportion of LPC+OA increased. As the total lipid content increased (simulations **31**, **32**, **36** and **37**) the micelles became elongated and form extended wormy micelles. At higher ratios of LPC+OA to GDX (simulations **22**, **26**, **29**, **33** and **34**) only one or two large oblate aggregates formed, often with a lamellar structure. This suggests that these ratios would be expected to form lamellar structures or a phase separated system. The simulations containing only LPC+OA and water (**23**, **27**, **30** and **35**) produced clearly lamellar systems with simulation **30** producing a vesicle-like structure which is expected to be an artefact resulting from the limited size of the simulation. Simulation **35**, which contained a larger amount of LPC+OA produced a simple bilayer sheet.

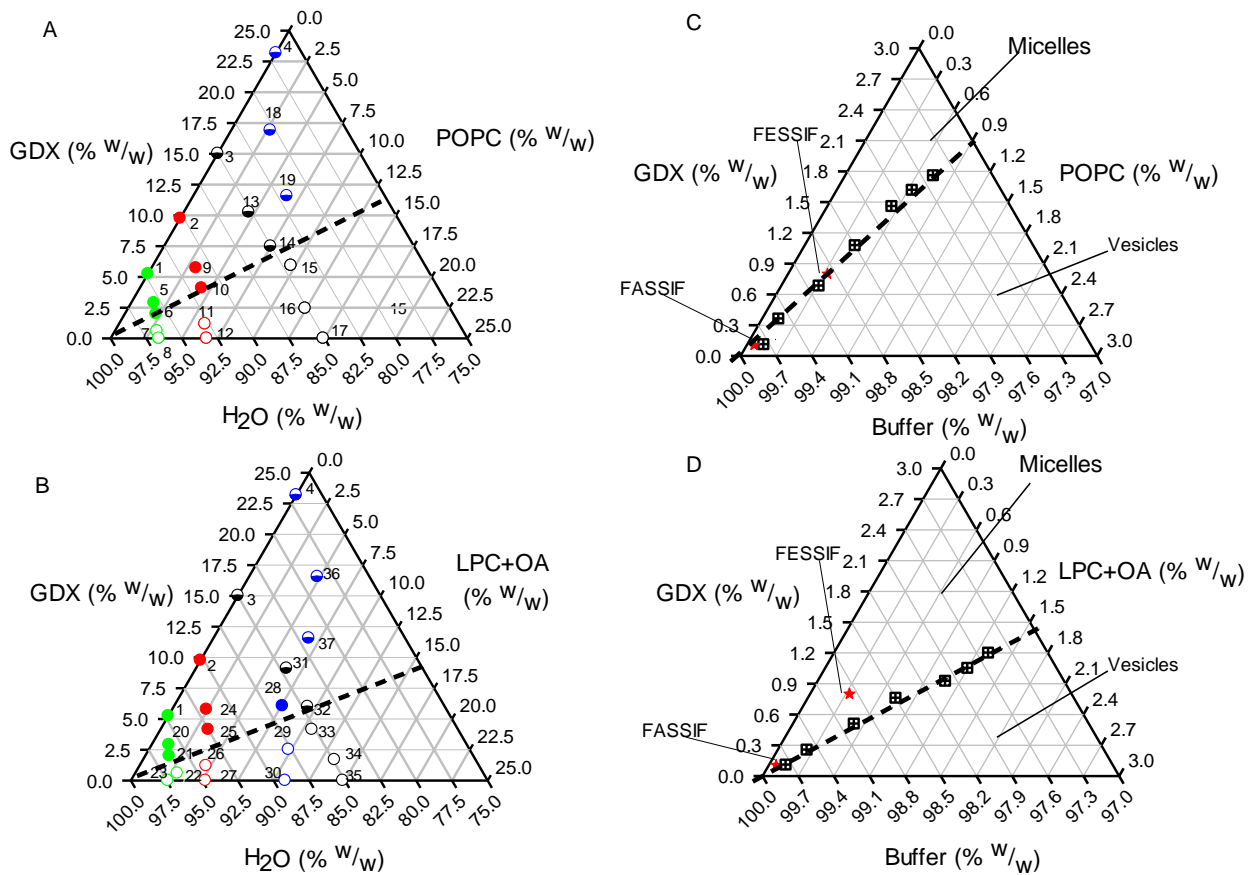


Figure 4.4. Predicted and experimental ternary phase diagrams for GDX with digested and undigested phospholipid. (A) Predicted diagrams for POPC/GDX/water and (B) LPC+OA/GDX/water. Filled circles represent micelles. Half-filled circles denote extended, wormy micelles. Open circles denote simulations predicted to form lamellar or phase separated systems. Points are coloured by simulation series. (C) Experimental phase boundaries between micelle and vesicle phases for the GDX/POPC/water and (D) for LPC+OA/GDX/water taken from reference ¹²⁴. The upper right and bottom left stars (★), indicated by the labels, represent the compositions of Fed StateSimulated Intestinal Fluid (FeSSIF)* and Fasted StateSimulated Intestinal Fluid FaSSIF*¹⁰⁹ respectively. Note that the predicted phase diagrams cover a much larger concentration range than the experimental study.

Figures 4.4A and B show phase diagrams derived from inspection of the final simulation structures, these are compared to the experimentally measured phase diagrams¹²⁴ for similar systems in Figures 4.4C and D. In Figures 4A and B, the different colloidal structures formed; spherical micelles, extended micelles and lamellar aggregates were plotted using different symbols. In both phase diagrams, three regions are present. When the total lipid concentration was below about 12.5% and the ratio of bile salt to phospholipid was high, spherical or prolate micelles were formed. A region of extended micelles was present where the total lipid concentration was above 12.5%. The third region occurred when the ratio of bile salt to phospholipid was lower and larger aggregates with a lamellar structure formed. As discussed above, in this region the nature of the structure that formed (oblate micelle, vesicle-like structure or lamellar sheet) was constrained by the limited size of the simulated system and indicated the formation of lamellar structures such as vesicles or phase separated systems. The phase diagrams for the digested and undigested systems are very similar with only a small shift in the position of the micelle/lamellar phase boundary between the undigested and digested systems.

For comparison with the modelled systems, Figures 4.4C and D show the experimentally determined boundaries for the transition from mixed micelles to vesicles in systems composed of GDX/POPC/water and GDX/LPC+OA/water in a system buffered at pH 6.5 which we determined previously by nephelometry and dynamic light scattering. In contrast to the model studies, these phase diagrams showed a clear difference between the undigested and digested systems, with vesicles forming more readily in the presence of POPC and micelle formation being favoured upon digestion to LPC+OA although it should be noted that the total lipid concentrations differ quite substantially, with the maximum experimental lipid concentration being 2.5% w/w and the minimum modelled concentration being approximately 2.5 % w/w.

The comparison of experimental and calculated values using simulation methods is an important way to validate whether simulations can reproduce experimental data. Unfortunately, there is a big limitation in the validation process of the experimental data. The first limitation is lack of

accurate description of complex real life experiments into molecular models. The more complex the molecular model becomes, the more it is exposed to error. Another limitation is the difference in solute concentration between the experimental and the simulated systems. The simulation system is carried out at approximately ten times higher concentration than the experimental system. This was necessary to reduce the amount of water in the simulated systems, which makes the calculations practical. Using the exact experimental concentration in the modelling work would be wasteful of computational time, as it will be simulating a very large box of water molecules containing a very small number of surfactant molecules. On the other hand, it would not be possible to conduct the experimental work using the exact concentration of the modelling work because the system would be too concentrated.

4.4.2 The Impact of Fatty Acid Ionisation on Mixed Micelle Formation

One of the digestion products of the phospholipid is oleic acid. In the aqueous environment, the physical properties of oleic acid, or fatty acids in general, are influenced by the ionization state of the carboxylic group which, in isolation, has a pK_a around 4.8.¹⁴⁰ But since medium and long-chain fatty acid fatty acids have a tendency to form self-assembled structures in an aqueous environment their apparent pK_a (pK_a^{app}) is raised due to the high negative surface charge of the aggregates which lowers the H^+ activity and increases the pH of the solution.¹⁴¹ A range of pK_a^{app} values for oleic acid are reported in the literature (6-8.5).^{19a, 141-142} It is believed that fatty acids in the fully protonated state form oil droplets, in the partially ionized state form crystalline and liquid-crystalline phases and, when fully ionized, form micelles.^{27d, 27e, 140}

Table 4.3. Simulations modelling the ternary LPC+50%OA+50%OLAT/GDX/water and LPC+100%OLAT/GDX/water phase systems.

NO.	SERIES	NO. OF MOLECULES					COMPOSITION (% W/W)		MEDIAN AGGREGATE SIZE / NUM. AGGREGATES ^a	STRUCTURE IN FINAL STATE
		LPC	OA	OLAT	GDX	Water	LPC/ (OA+OLAT)	GDX		
38	I	62	31	31	233	100518	2.5	5.6	30/10	Micelles
39	I	84	42	42	165	100073	3.4	4.0	51/7	Micelles
40	I	116	58	58	47	100191	4.8	1.2	63//4 ^b	Oblate micelles
41	I	128	64	64	-	100238	5.3	0.0	128/2 ^b	Oblate micelles
42	J	61	-	61	233	89937	2.7	6.2	22/13	Micelles
43	J	84	-	84	165	89211	3.8	4.5	36/7	Micelles
44	J	115	-	115	47	89937	5.3	1.3	19/6 ^b	Micelles
45	J	128	-	128	-	89843	5.9	0.0	46/5 ^b	Micelles

^aAggregate numbers and median values exclude any isolated molecules. ^bA small number of aggregates are observed. The median value will not be a reliable estimate of true aggregate size. ^cThe observed structure is expected to be affected by the number of molecules present in the modelled system.

Standard molecular dynamics simulations cannot model proton transfer. Simulations generally use predetermined protonation states based on pK_a values for titratable functional groups such as carboxylic acids or amines. While methods for constant pH molecular dynamics simulations in explicit solvent are under active development (see for example Morrow *et al.*¹⁴³), high-performance constant pH MD methods are not yet available, so to gain an understanding of the structural changes that can be expected from changes in the environmental pH, we performed additional MD simulations with oleic acid present as 50:50 mixture of protonated and deprotonated forms (simulations **38-41**) and also in the completely deprotonated form (**42-45**). In all simulations the GDX was treated as being completely ionised with a sodium counter ion.

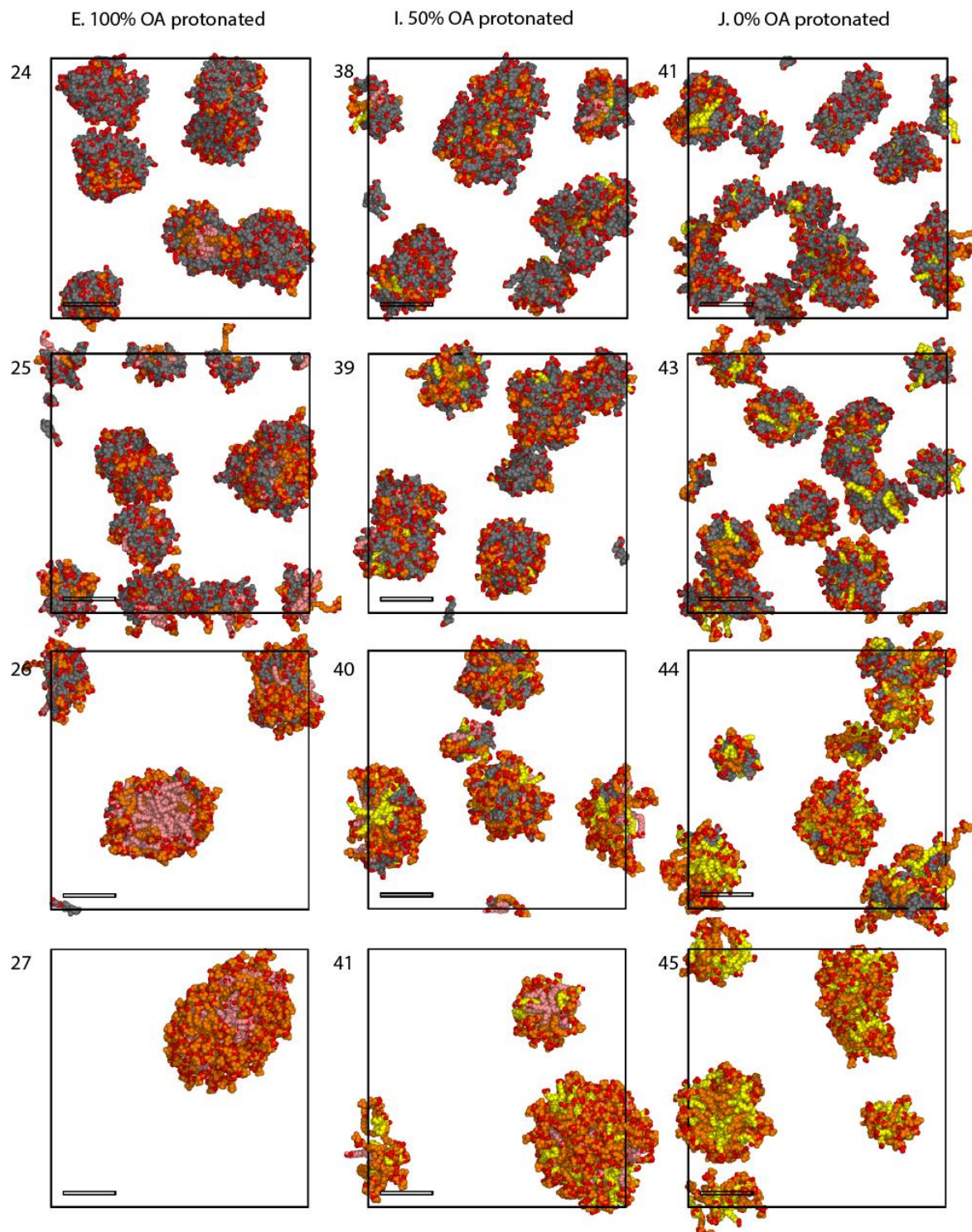


Figure 4.5. Final frames of simulations of the LPC+OA/GDX/water ternary system showing a formation of smaller aggregates due to the repulsion effect of negatively charged oleate molecules. Simulation numbering is described in Table 4.2. Atom colouring; GDX is grey, LPC is orange, oleic acid (OA) is pink, oleate (OLAT) is yellow and oxygen atoms are red. The box indicates the periodic boundary. Scale length 3.0 nm. Water molecules are not shown.

As is evident in Figure 4.5, increasing ionisation of the oleic acid substantially reduces the size of the micelles formed due to the electrostatic repulsion of the ionized head groups and increased interaction with water. These effects of ionisation are also clearly evident in the radial distribution functions (RDFs) shown in Figure 4.6. When the oleic acid is protonated (OA), there is a large peak in the RDF at 0.3 nm indicating a significant hydrogen bonding interaction between the head groups (Figure 4.6a). In contrast, when oleic acid is deprotonated (OLAT), the strong electrostatic repulsion between the head groups prevents close association of the head groups. The RDF results in Figure 4.6a also show that the interaction between the hydroxyl oxygen atoms at two different ionization states are significantly different. On the other hand, oleate oxygen atoms interact with water oxygen atoms more strongly than the protonated oleic acid shown in Figure 4.6b.

Although it is not possible to calculate the pK_a value of the assembly of the fatty acids, we observed major structural differences between the protonated and deprotonated systems which agree with experimental studies of the ionization and phase behaviour of fatty acids in water. Cistola *et. al.* investigated medium-chain (10- and 12-carbon) and long-chain (18-carbon) fatty acids in water as a function of the ionization state of the carboxyl group. They observed at pH 7 lamellar and aqueous phases, between pH 7 and 9, a two-phase region containing a lamellar fatty acid soap in an aqueous phase, at pH 9, a three-phase region containing a lamellar fatty acid-soap, micellar, and aqueous phases; and at pH values above 9, a two-phase region containing micellar and aqueous phases¹⁴¹. Salentinig *et. al.* studied self-assembled structures formed by oleic acid in water and observed that aggregate formation is strongly pH dependent observing transformations from microemulsions through micellar cubosomes, hexosomes and bicontinuous cubosomes to vesicles as a function of increasing pH.^{19a}

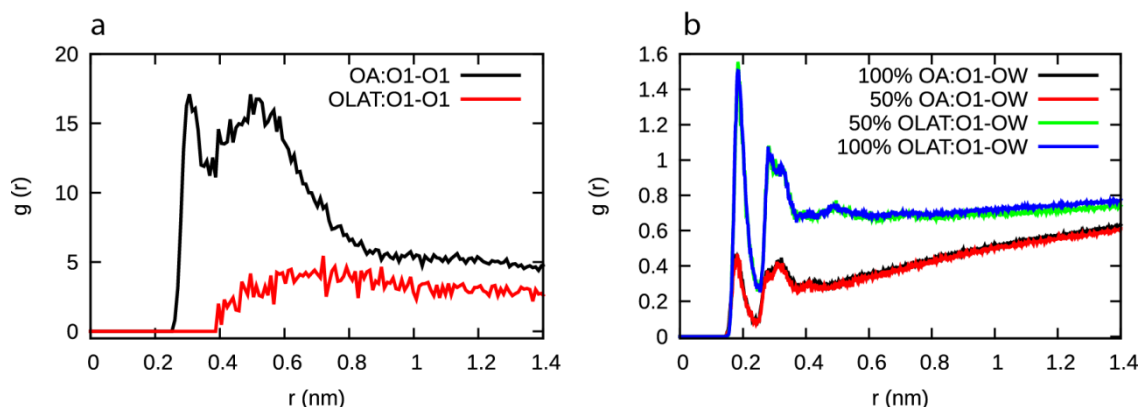


Figure 4.6. Radial distribution functions, $g(r)$, for mixtures of GDX with oleic acid in the protonated form (OA) and deprotonated form (OLAT). (a) Self interaction of the carboxylic acid oxygen atom O1 in OA and OLAT. (b) Interaction of oxygen O1 with the water oxygen atom (OW) in simulations containing 100% OA molecules, 50% OA and OLAT and 100% OLAT.

4.4.3 The Interaction of Bile Salt with Digested and Undigested Lipids

In this section we investigate the interaction of GDX with digested and undigested lipids. Atom spatial distributions functions (SDFs), the three dimensional equivalent of radial distribution functions, were calculated for the interaction of phospholipid molecules with GDX and with LPC+OA. Figure 4.7 shows the spatial distribution functions of water (OW) and terminal carbon atoms for lipids (POPC:C42, C24, LPC:C16 and OA:C18), around the GDX molecule using C3, C7 and C12 as reference atoms. Additionally, we calculated the spatial distribution function of lipids with the hydrophobic head of POPC and LPC (atoms N and P). The probability values used to generate the iso-surfaces are reported in Appendix 3, Table 9.3.1. The SDFs show that the interaction of GDX with digested and undigested lipids are very similar. The high probability iso-surfaces for the water and lipid carbon atoms clearly highlight the hydrophobic and hydrophilic faces of the steroid skeleton. The glycine carboxylate group is also makes a strong interaction with water. The SDFs show that the hydrophilic face of the steroid is associated with the phospholipid quaternary nitrogen and phosphate groups.

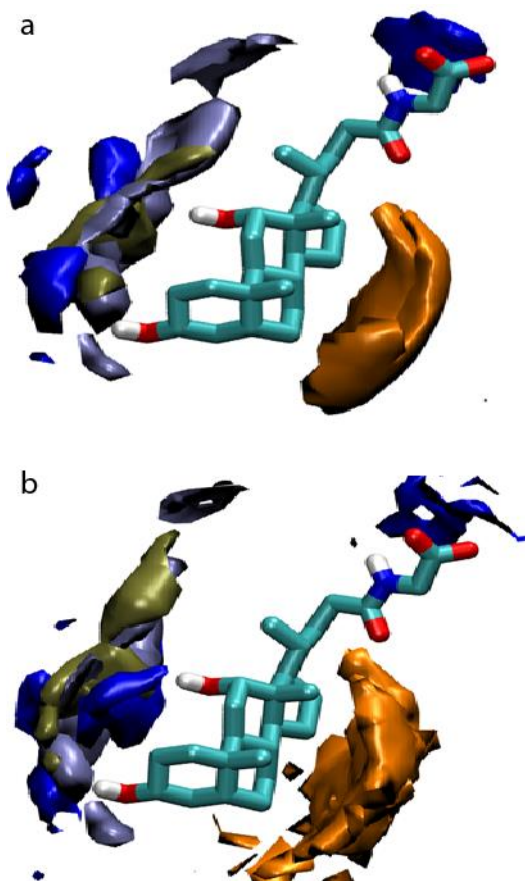


Figure 4.7. Spatial distribution functions for the interaction of POPC and LPC with GDX. (a) POPC/GDX/H₂O: water-OW (light blue), POPC: P (tan), POPC: N (dark blue) and POPC carbon atoms C24 and C42 (orange) around GDX in the POPC/GDX/H₂O mixture. (b) LPC+OA/GDX/H₂O: water-OW (light blue), LPC: P (tan), LPC: N (dark blue) and LPC carbon atoms C16 and OA C18 (orange) around GDX in the POPC/GDX/H₂O mixture. The cut-offs used to generate the surfaces are listed in Appendix 3, Table 9.3.1.

Representative examples of the interactions between POPC and GDX are shown in Figure 4.8. It is clear that the hydrophilic parts of POPC mostly interact with the hydrophilic chain of GDX (glycine part) and with the hydroxyl groups present on the steroid. The hydrocarbon part of the steroid backbone of GDX preferentially interacts with the hydrocarbon chain of POPC. What we observed from the final frames the last 10 ns of the simulation is that in the case of micelle formation, GDX molecules tend to locate on the surface of the micelle by interacting with the hydrocarbon chain of POPC exposing the OH group of the steroid to surrounding water molecules

and allowing the glycine part to interact with the hydrophilic head of POPC, shown in Figure 4.8a. This was also observed in other similar MD studies.^{26c, 58, 60} When bilayer-like structures were formed, the GDX molecules tended to arrange themselves parallel to lipids as is evident in Figures 4.8b and 8c. There is also an interaction between the GDX hydroxyl groups with the head group of the POPC shown in Figure 4.8d.

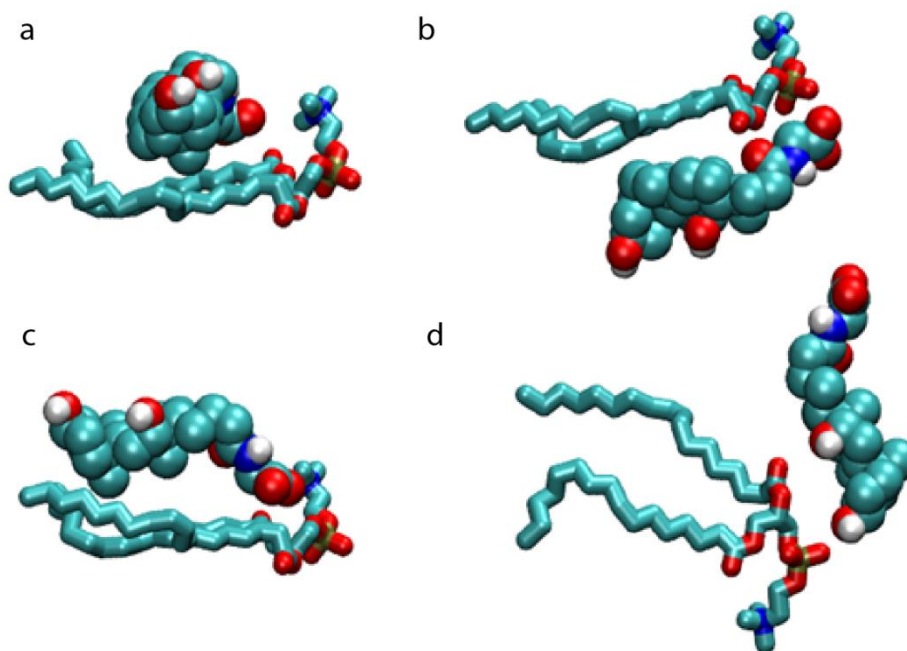


Figure 4.8. Typical relative arrangements of POPC and GDX molecules taken from simulations of the POPC/GDX/H₂O system. Atom colouring: cyan carbon; red oxygen; white polar hydrogen blue nitrogen and tan phosphorous.

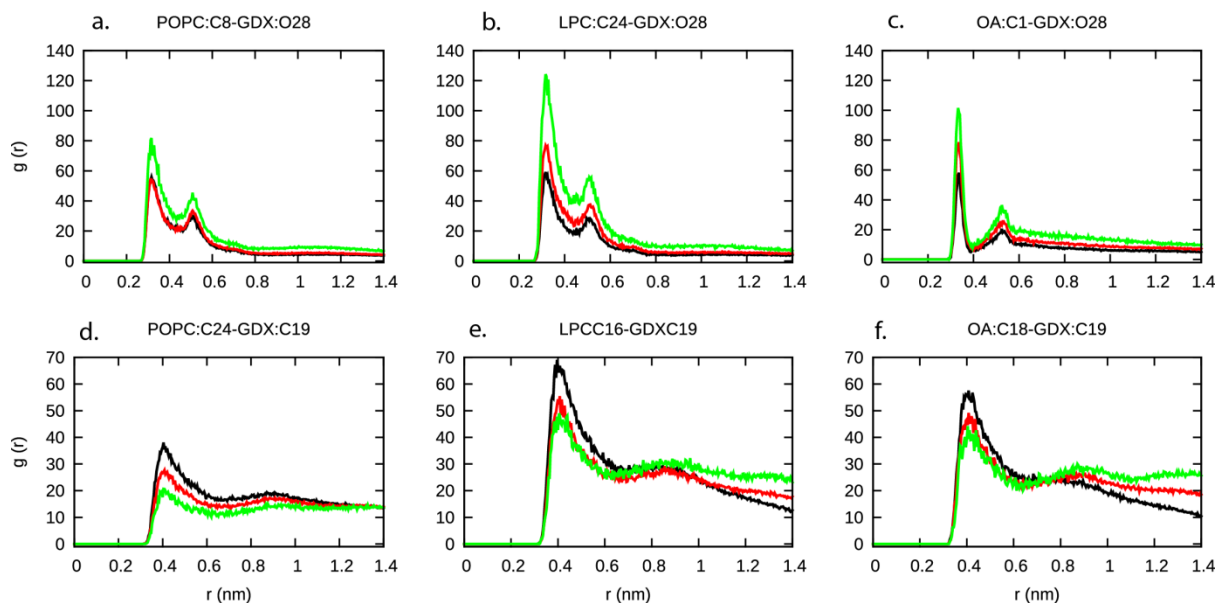


Figure 4.9. Radial distribution functions for the POPC/GDX/water and LPC+OA/GDX/water systems. (a-c) Interactions of O28 atoms of GDX with hydrophilic head atoms of POPC, LPC and OA. (d-f) Interactions of C19 atoms of GDX with hydrophobic terminal atoms of POPC, LPC and OA. Line colouring for % w/w lipids concentration 1.6 (black), 2.2 (red) and 3.0 (green).

Figure 4.9 shows RDF plots for key atom pairs (C8-O28, C24-O28, C1-C28 and C24-C19, C16-C19, C18-C19) show that the interaction between the head groups of POPC and LPC with the glycine moiety of GDX is significantly stronger than with the hydrophobic tails of the lipids. It is demonstrated in Figure 4.9 that atom O28 of GDX interacts with C8 more strongly than the rest of the head part of POPC at a closer distance of 0.4 nm. This interaction becomes stronger as the concentration of POPC increases. This indicates the interaction changes upon the phase change from micelle to bilayer. This change also occurred for LPC and OA as shown in Figure 4.7. In the case of carbon atom C20, which is the glycine tail of GDX, it exhibited a very similar interaction to O28 of GDX with the hydrophobic tail of POPC but it exhibits different interaction profile with the hydrophilic head. Atoms O28 showed preferential interaction with C8 of POPC whereas atoms C20 interacted with all of the carbon atoms on the hydrophilic head part of POPC in a similar manner. This fact indicates that the O28 atoms mostly protrude into the water surface

and interact with water and the top part of the hydrophilic region of the lipid. For C20, since it is closer to the steroid part of GDX it most likely to be found interacting with lipids rather than water in both undigested and digested lipid simulations. The RDFs for the carbon atoms C20 of GDX with POPC as well as LPC+OA atoms are quite similar showing only a very small difference with POPC. Detailed RDF plots are available in Appendix 3, Figure 9.3.2 – 9.3.5.

For the interaction of the steroid region of GDX we calculated RDFs by choosing atoms from various positions. For the carbon atoms C1, C2, C6, C7, C15, C16, C18, and C19, for oxygen atoms O3, and O12 were chosen. Atoms C1, C2, C6, C7, C15 and C16 of GDX exhibited very similar interactions with the head group of POPC, specifically with atoms C1, C2, C3 and C4. But C1, C2, C6, C7, C15 and C16 of GDX showed significantly less interaction with atom C8 of POPC. RDF plots are available in Appendix 3 Figure 9.3.6 for atoms C1, C6 and C16 of GDX with the head group of POPC. Comparing the interaction of these same atoms of GDX with digested POPC again showed similar behaviour by interacting with atom C18 of LPC and atom C1 of OA more strongly in a range of 0.4-0.6 nm distance; plots are available in appendix 3, Figure 9.3.7. Considering the interactions of these GDX atoms with the hydrophobic tails, it was observed that the interaction decreased when going down to the terminal carbon atoms of POPC and LPC+OA.

In the case of atoms C19 and C18 of GDX, no interaction was observed with the hydrophilic part of POPC as it was observed with the other carbon atoms present within the steroid region; the RDF plot is shown on Figure 4.9 for only C19 atoms of GDX. These two atoms show preferential interaction with the hydrophilic tails of POPC. Interestingly, C18 and C19 show a high interaction with the terminal carbon atoms (C24, C42 for POPC, C16 and C18 for LPC and OA respectively). RDF plots are available in Appendix 3, Figure 9.3.8 and 9.3.9. This fact is very obvious when there is low concentration of lipids in the system. This indicates that in micelles, GDX interacts with the hydrophobic part of lipids facing the two carbon atoms (C18 and C19), which are perpendicular to the steroid plane. At higher concentration of lipid these interactions significantly

decline, indicating that the terminal carbon atoms of lipids are mostly interacting with each other as vesicular or lamellar-like structure are formed.

The interactions of the hydroxyl oxygen atoms O3 and O12 of GDX with the hydrophilic and hydrophobic regions of lipids was also investigated. They showed other interesting interactions with the hydrophilic head with high affinity in both POPC and LPC+OA simulations. (RDF plots for POPC available in Appendix 3, Figure 9.3.10 and 9.3.11). Again, both oxygen atoms do not interact with the tails of the lipids, especially with the terminal carbon atoms. The interaction declines when it goes from C10 and C25 (positions closer to the hydrophilic head), toward C24 and C42 (terminal carbon atoms) on both chains.

The per-molecule solvent accessible surface area (SASA) is a useful way to investigate the interplay between the bile salt and phospholipid system components. Figure 4.10 plots the SASA as a function of phospholipid content for series A, B and C of the POPC/GDX/water system and for series E, F and G of the POPC/LPC+OA/water system. All systems show similar behaviour, with the SASA of GDX having a minimum value of 3-4 nm² when no phospholipid is present which steadily increases as the fraction of digested or undigested phospholipid is increased. The greater exposure of the GDX is driven by the stronger hydrophobic association of POPC and of LPC+OA, and the SASA of the POPC and LPC+OA correspondingly decreases as the phospholipid content increases. The POPC SASA drops to about 4 nm² as the phospholipid becomes lamellar and the LPC and OA molecules reach minimum values of about 5 and 3 nm² respectively.

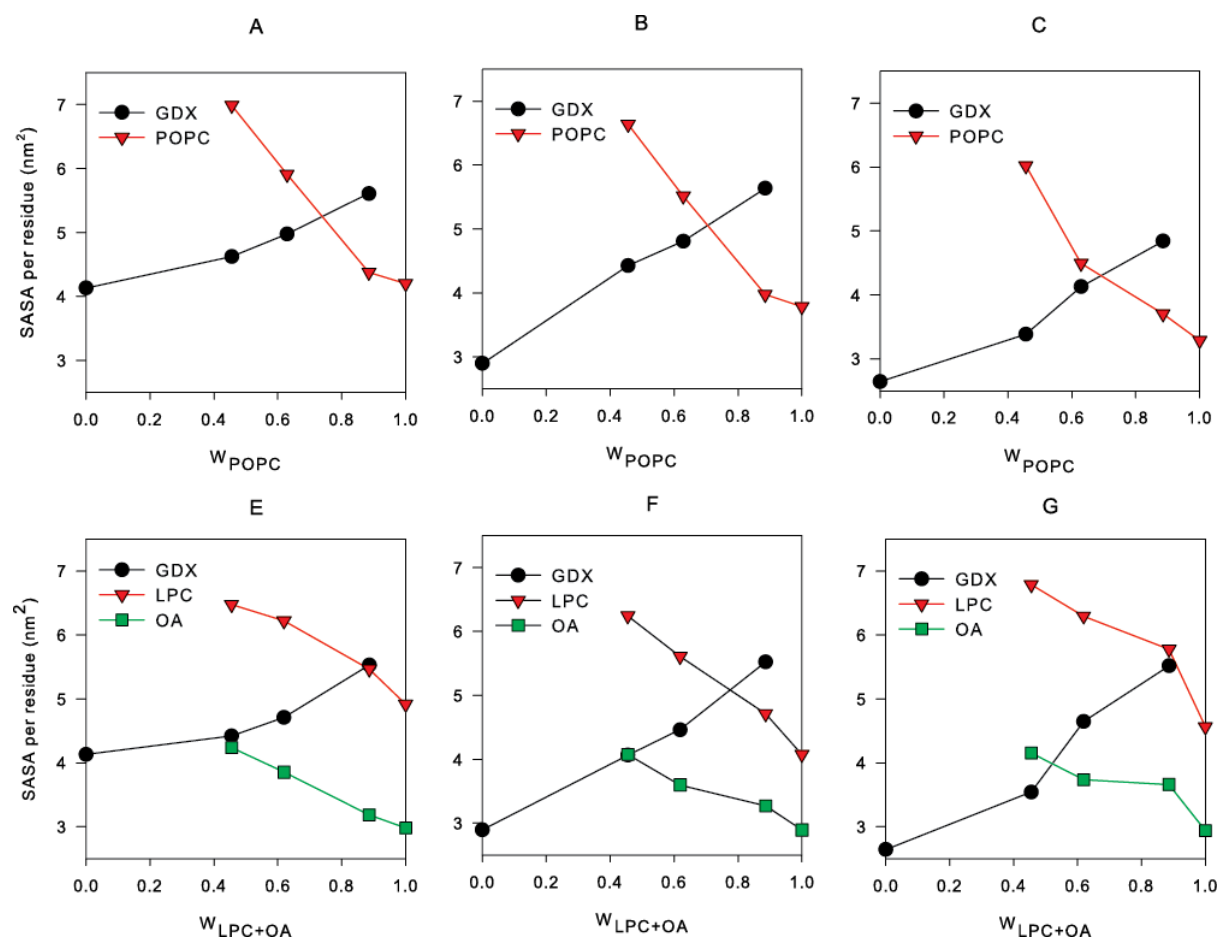


Figure 4.10. Per-residue solvent accessible surface areas of GDX and the digested and undigested phospholipid plotted as a fraction of total phospholipid in the system.

4.4.4 Micelle Diffusion

NMR is a powerful experimental method for the study of diffusion coefficients of within complex mixtures. Using the published ^1H NMR chemical shift assignments of GDX¹⁴⁴ we selected three protons (H5, H15 and H25, refer to Figure 4.1) from different sites of GDX molecule and determined their diffusion coefficient using a DOSY experiment. Plots of the experimental diffusion coefficient of the bile salt (GDX) against POPC and LPC+OA mass fraction are shown in Figures 4.11a and b respectively. The 2D DOSY spectra are provided in Appendix 3, Figure 9.3.12 and 9.3.13. The spectra show the diffusion of the mixtures on the y-axis and the chemical shift of the protons on the GDX molecules on the x-axis. On the DOSY spectrum of POPC, Appendix 3, Figure 9.3.12, the purple spectrum represents $W_{\text{POPC}} = 0$ ($W_{\text{GDX}} = 1$), red represents $W_{\text{POPC}} = 0.133$, blue represents $W_{\text{POPC}} = 0.200$, cyan represents $W_{\text{POPC}} = 0.266$, pink and light blue spectra are under the cyan spectra represents $W_{\text{POPC}} = 0.333$ and $W_{\text{POPC}} = 0.400$ respectively and green represents $W_{\text{POPC}} = 0.533$. As it is indicated on the plots, the diffusion of the GDX slows with increasing phospholipid concentration and increasing micelle size. The POPC/GDX coefficients are plotted up to a POPC mass fraction of 0.533. Above this ratio, the sample became appreciably cloudy as the lipid precipitated from the aqueous phase. Similarly, the LPC+OA sample precipitated above a mass fraction of 0.7. The DOSY spectrum of LPC+OA, Appendix 3, Figure 9.3.13, the red spectrum represents $W_{\text{LPC+OA}} = 0$ ($W_{\text{GDX}} = 1$), blue represents $W_{\text{LPC+OA}} = 0.133$, purple represents $W_{\text{LPC+OA}} = 0.322$, pink represents $W_{\text{POPC}} = 0.398$, green spectra represents $W_{\text{POPC}} = 0.531$ and another purple at the top represents $W_{\text{POPC}} = 0.665$. Comparison between the GDX/POPC and GDX/LPC+OA systems showed that the diffusion of the undigested micelles slows more rapidly with increased phospholipid content than the digested case. Figures 4.11b and c shows diffusion coefficients calculated from MD simulation. The diffusion coefficients are calculated for the last 10 ns of the simulation using `g_msd` which uses the Einstein relation. The diffusion coefficient is determined by linear regression of mean square displacement. The results from simulation agree qualitatively with experiment; the overall diffusion rates are slightly

higher than measured experimentally but show very similar changes with increasing phospholipid concentration. The variances in calculation were very small and do not appear on the figures.

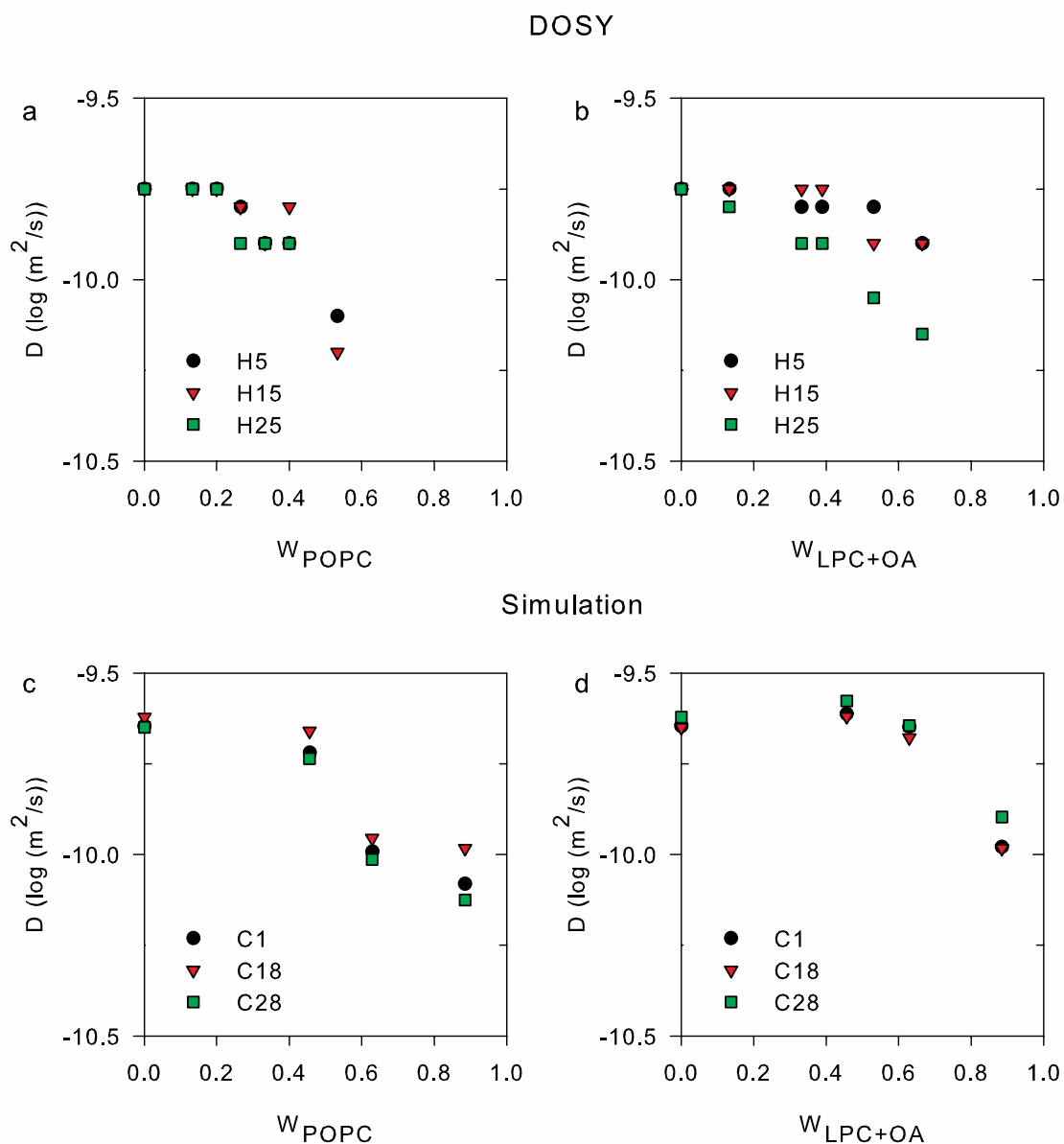


Figure 4.11. Diffusion coefficients of GDX within GDX/POPC/water and GDX/LPC+OA/water mixtures determined from DOSY NMR experiment and MD simulation. Experimental results are (a) POPC/GDX/D₂O and (b) LPC+OA/GDX/D₂O. Simulation data taken from (c) simulation series A and (d) simulation series E, (series A and E are closer in concentration to the experiment). The X-axis represents the mass of phospholipid/(mass phospholipid+GDX).

4.5. CONCLUSIONS

In this study we have performed an extensive molecular dynamics study, modelling the phase behaviour of the ternary POPC/GDX/water and LPC+OA/GDX/water systems. These simulations were able to predict, at a qualitative level, the experimentally observed phase behaviour of these systems conducted by our group¹²⁴. This study gives us a molecular level understanding of the interactions between phospholipids and bile salts. Understanding of the behaviour of the GI tract at different conditions, especially understanding of the effect of digestion of POPC, will give us an opportunity to predict the phase changes that might occur when formulation excipients are present within the GI tract. Depending on the effects that the formulation excipients generate, we can optimize our choice of species of lipid formulation to bring the desired phase behaviour in the GI tract particularly in the small intestine. This knowledge will allow us to improve the solubility and absorption of poorly water soluble drug candidates by selecting the right excipients.

4.6. ACKNOWLEDGEMENT

Funding support from Australian Research Council (ARC) Linkage Grant LP120100600 awarded to Monash University in collaboration with Capsugel is greatly acknowledged. We would also like to thank the Victorian Life Sciences Computation Initiative (VLSCI) for technical support and Merit Allocation Scheme grants of CPU time and systems support.

Declaration for Thesis Chapter 5

Declaration by candidate

In the case of Chapter 5, the nature and extent of my contribution to the work was the following:

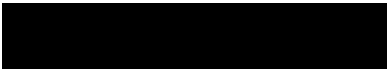
Nature of contribution	Extent of contribution
Planning and executing experimental and computer simulation work, data evaluation and drafting and revision of manuscript	70%

The following co-authors contributed to the work. If co-authors are students at Monash University, the extent of their contribution in percentage terms must be stated:

Name	Nature of contribution	Extent of contribution
C. W. Pouton*	Project supervisor, data and manuscript review	NA
D. K. Chalmers	Project supervisor, data and manuscript review	NA
C. J. H. Porter	Project co-supervisor, data and manuscript review	NA
D. B. Warren	Supervision of experimental and computer simulation works and manuscript review	NA
S. Han	Supervision of analytical work with LC-MS	NA
H. Benameur	External supervision and manuscript review	NA

The undersigned hereby certify that the above declaration correctly reflects the nature and extent of the candidate's and co-authors' contributions to this work*.

**Candidate's
Signature**

		Date: 12/06/2015
Main Supervisor's Signature		Date: 12/06/2015

“A pure heart won’t get us out of conflict and controversy. It may well be the very thing that gets us into it.”

John Hagee

CHAPTER FIVE

MODELLING THE PHASE BEHAVIOUR AND DRUG SOLUBILISATION CAPACITY OF A TYPE I LIPID-BASED DRUG FORMULATION AFTER DIGESTION IN THE INTESTINE: AN EXPERIMENTAL AND MOLECULAR DYNAMICS STUDY

Woldeamanuel A. Birru³, Dallas B. Warren³, Sifei Han³, Hassan Benameur⁴, Christopher J. H. Porter³, Colin W. Pouton^{2,3} and David K. Chalmers¹

¹Medicinal Chemistry, Monash Institute of Pharmaceutical Sciences*

²Drug Discovery Biology, Monash Institute of Pharmaceutical Sciences

³Drug Delivery, Disposition and Dynamics, Monash Institute of Pharmaceutical Sciences

⁴Capsugel Research & Development, Pharmaceutical Sciences, Strasbourg France.

*Monash Institute of Pharmaceutical Sciences, Monash University (Parkville Campus), 381 Royal Parade, Parkville, Victoria 3052, Australia

5 MODELLING THE PHASE BEHAVIOUR AND DRUG SOLUBILISATION CAPACITY OF A TYPE I LIPID-BASED DRUG FORMULATION AFTER DIGESTION IN THE INTESTINE: AN EXPERIMENTAL AND MOLECULAR DYNAMICS STUDY

5.1 ABSTRACT

Administering poorly water-soluble drugs in a formulation containing lipids is one way of improving the bioavailability of poorly water-soluble drug candidates. During administration of lipids such as tri or di glycerides, digestion generates free fatty acids and monoglycerides that can be solubilised by biliary components. This leads to an increase in the solubilisation of co-administered poorly water soluble drugs in the small intestine due to the formation of colloidal phases including vesicles and mixed micelles offering a high surface area for drug distribution to and from the aqueous phase.

In this study we investigate phase behaviour of a model gastrointestinal microenvironment consisting of digested bile, digested triglyceride and water using nephelometry, dynamic light scattering and polarizing light microscopy. We compare these experimental studies to molecular dynamics (MD) simulations of these systems. We also extend this work to investigate the capacity of this lipidic microenvironment to solubilise the poorly water-soluble drug danazol using LC-MS and molecular dynamics simulation techniques. The results show how the formulation lipids alter the environment of the gastrointestinal tract and improve the solubility of danazol. The MD simulations can reproduce the experimental results suggesting that MD could be used as a tool to predict the fate of drugs after digestion of lipid-based formulations in the intestine.

5.2 INTRODUCTION

Lipid based drug delivery systems (LBDDS) are classified into five distinct groups (Type I, II, IIIA, IIIB and IV) on the basis of the formulation composition and properties^{2, 4b}. The principal components of Type I formulations are triglycerides or mixed glycerides² and they are the most lipophilic formulations out of the five types. These formulations form coarse emulsions on dispersion in aqueous fluids and when they enter the small intestine, the ester groups of the triglyceride are quickly hydrolyzed by pancreatic lipases promoting the dispersion of the lipid phase into micelles and vesicles. In contrast, Type II, IIIA/B and Type IV formulations are self-emulsifying systems often produce nanosized emulsions and micelles in the GI tract. For these systems, digestion is not essential for dispersion^{4b}, though if they contain a significant mass of oil (Type II, IIA) they are likely to be affected by digestion.

Using experimental studies and MD simulations, we have shown that digestion of formulation components significantly alters the microstructure of the lipid components within the GI fluid¹²⁴. Therefore, assessment of phase behaviour of the GI tract and its impact on the solubility of poorly water-soluble drug candidates during the presence of the digestion products of Type I and II formulation is necessary for a complete understanding of formulation performance.

The lipidic microenvironment of the GI tract can be studied using a variety of experimental techniques which provide information about the nature of the colloidal particles present; however, detailed understanding is hindered by the large number of different molecular species present, the complexity of the phase behaviour and the limited resolution of the experimental methods. We have previously established that the MD simulations are a powerful method for obtaining atomic level information about the phase behaviour of colloidal species and used in conjunction with appropriate model experimental systems, can greatly improve our understanding of the consequences of the mixing of lipids and amphiphilic molecules within the GI tract^{40, 64}. MD can also be utilized to study the partitioning of PWSDs within the lipidic microenvironment and the fate

of PWSD that occur on dispersion and digestion of the PWSD in the GI tract⁶⁴. It can also reveal any changes in microstructure caused by the drug.

In this study we model the effect of adding a simple Type I formulation, with and without the PWSD danazol (Figure 5.1) into the lipid environment of the upper GI tract. A type I triglyceride formulation is assumed to be converted by digestion into a 1:2 molar mixture of glyceryl monooleate and oleic acid. We use both experimental and MD techniques to evaluate the phase changes that occur within the digested triglyceride, phospholipid and bile salt mixture, which models the small intestinal contents in the fasted state. The structures of the molecules are used throughout the study are shown in Figure. 5.1. Using the same mixture of materials, we modeled the impact of adding digested triglyceride to the intestinal contents on the solubility of danazol using both experimental and MD methods. This is the first study of quaternary phase behaviour using a model system of digested lipid, digested triglyceride, bile salt and water using both experimental and MD techniques.

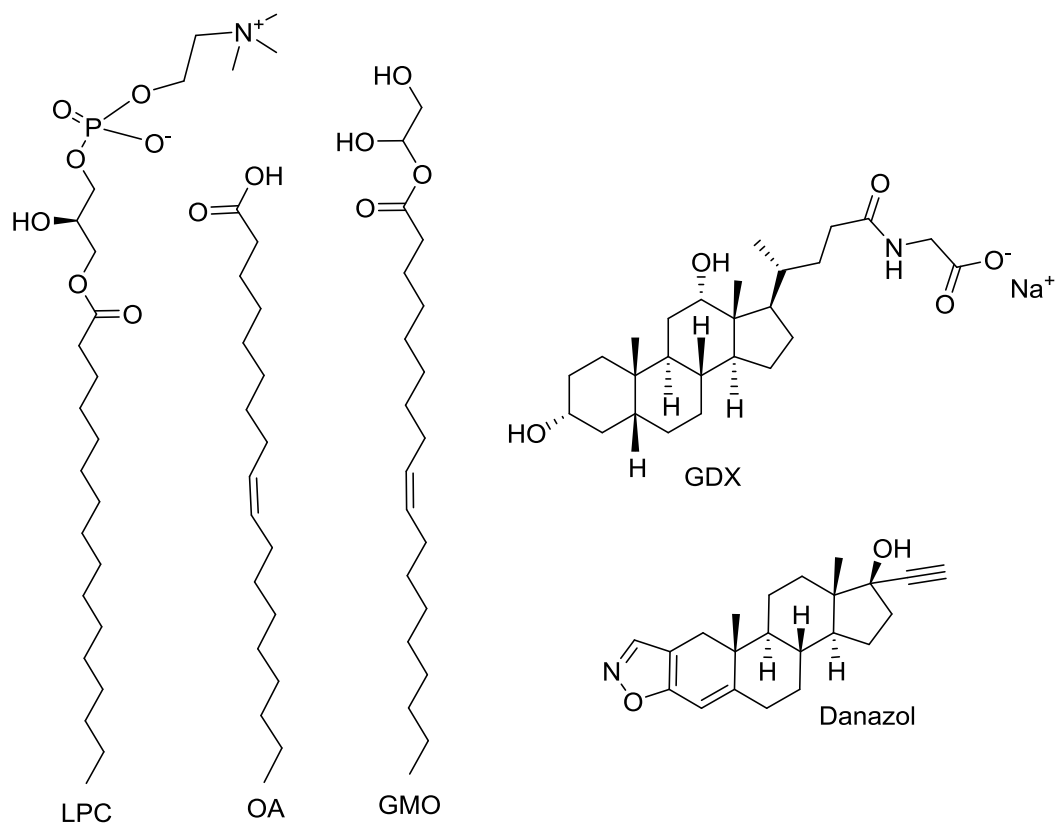


Figure 5.1. Structures of 1-palmitoyl-2-hydroxy-sn-glycerol-3-phosphocoline (LPC), oleic acid (OA), glycerol 1-mono-oleate (GMO), glycodeoxycholic acid, sodium salt (GDX) and danazol.

5.3 MATERIALS AND METHODS

5.3.1 Materials

The digested phospholipid, 1-palmitoyl-2-hydroxy-sn-glycerol-3-phosphocoline (LPC) was obtained from Avanti Polar Lipids, Inc. in powder form. Glycodeoxycholic acid, sodium salt (GDX) was obtained from Calbiochem, oleic acid (OA) (> 99% pure) and glycerol 1-mono-oleate (GMO) were obtained from Sigma-Aldrich. Danazol (17 β -hydroxy-2,4,17 α -pregnadien-20-yn[2,3-d]isoxazole) was obtained from Sterling Pharmaceuticals Pty Ltd. (Sydney, Australia). Sodium hydroxide (pellets), sodium phosphate monohydrate and sodium chloride were analytical grade. All water used was obtained from a Milli-Q water purification system (Millipore). Methanol and chloroform used in this work were HPLC grade from Merck (Melbourne, Australia).

5.3.2 Fasted Simulated Intestinal Fluids Buffer

Fasted state simulated intestinal fluid buffer (FaSSIF buffer) was based on the published composition of complete FaSSIF¹⁰⁹, minus the phospholipid and bile salt components and thus was composed of: 0.174 g of NaOH, and 1.977 g of NaH₂PO₄·H₂O and 3.093 g of NaCl in a 500 ml of purified water. The pH was adjusted to 6.50 \pm 0.02 using 1 M NaOH and 1 M HCl as required.

5.3.3 Preparation of Lipid Stock Solutions

Lipid solutions were prepared using the evaporated film method; 0.200 g of lipid (LPC+OA) was dissolved in 10 ml of methanol and the methanol evaporated within a round bottom flask using a rotary evaporator. The resulting lipid film was then dispersed in 7.00g of the aqueous phase blank buffer, generating a 2.5% w/w stock solution. This stock solution was diluted and vortex-mixed for 5 minutes to prepare 0.47 % w/w solutions as required.

5.3.4 Preparation of Mixture of Bile Salt and Digested Triglyceride

The aqueous stock solutions of 2.5% w/w GDX was prepared by dissolution of 0.200 g of GDX into 7.800 g of blank buffer. In this stock solution 0.150 g of GMO and 0.238 g of OA were dissolved to give 6.0 % w/w mixture of GMO+OA+GDX solution. This stock was again diluted to give 4.54, 3.65, 3.04, 2.42, 1.81, 1.81, 1.53, 1.30, 1.06, 0.76, 0.48, 0.42, 0.37, 0.24, 0.12, 0.02 % w/w d TGL solutions as required.

5.3.5 Turbidity

The required volume of the digested lipid and the mixture of digested triglyceride and bile salt stock solutions were pipetted as required, and mixed *in situ* within the individual wells of a 96 microwell plate with the plate then introduced into the nephelometer. The delay between mixing of the solution and the first turbidity measurement was recorded (approximately 9 to 10 minutes). Turbidity measurements of each plate were repeated every 10 minutes until the signal reached a stable value. All measurements were performed at 37 °C and the average of 3 data sets was taken for each solution.

The turbidity of the mixtures, measured in nephelometry turbidity unit (NTU), was monitored using a NEPHLOstar Galaxy (BMG Labtechnologies, Germany) microplate nephelometer, which measured the turbidity as a function of back scattered light, (not light absorption). The nephelometer program settings used were: gain = 70, cycle time = 30 s, measurement time per well = 0.30 s, positioning delay = 0.5 s. The backscattered laser light ($\lambda = 635$ nm) was monitored at an angle of 80 °. 96-microwell plates, made from polystyrene, with flat-bottomed wells (NUNC, Thermo Scientific, USA) were used.

The turbidity curve for quaternary mixture was plotted as signal versus mass fraction of digested triglyceride (dTGL). The phase boundary between micelles and vesicles phases was subsequently located as the point of intersection of lines fitted to the two adjoining regions of the turbidity curve. An example of the turbidity curve is shown in previous studies, indicating how the phase boundary was identified¹²⁴.

5.3.6 Dynamic Light Scattering

A Malvern Zetasizer Nano ZS ZEN3600 (Worcestershire, UK) was used to measure the hydrodynamic diameter of particles. Measurements were conducted at 37 °C using low-volume disposable sizing cuvettes (cell type ZEN0112, Sarstedt, Germany). The backscattered laser light ($\lambda = 633\text{nm}$) was monitored at measurement angle of 173°. The viscosity of the dispersant (water) was used as sample viscosity. The equipment was calibrated using 60 nm \pm 2.7 nm and 220 \pm 6nm diameter nanosphere size standards of polystyrene polymer latex (supplied by Duke scientific corporation, USA) in water. The polydispersity index (PDI) for the standards were < 0.2 .

The required volume of the digested lipid, bile salt and digested triglyceride stock solutions were pipetted as required, and mixed *in situ* within the individual cuvette and then introduced into the nanosizer. Solutions were prepared in the region of the phase boundary where previously identified using turbidity measurement. Measurement was carried out one day after sample preparation and the average of 6 data sets was taken for each solution.

Particle size can be determined by measuring the random changes in the intensity of light scattered from a mixture or solution¹¹¹. Using the refractive index of lipid the instrument generates the distribution of volume and numbers of particle sizes from the intensity distribution. In this study, since interested in determining the phase boundary where the first vesicles are formed, we use the intensity distribution to analyse our data. The reason the intensity distribution is preferred is that at the phase boundary the volume or number of vesicles within the mixture is negligible compared to the volume or number of micellar particles. Hence, there will be no visible peak for the volume or number distribution of the vesicular particles at the point at which the vesicles just appear in the solution.

5.3.7 LC-MS assays

The LCMS 2010 system (Shimadzu, Japan) which included an LC-20AD binary pump, a SIL-20AC refrigerated autosampler, a mobile phase vacuum degassing unit (DGU-20A₅) and a temperature-controlled column compartment (CTO-20A), coupled with a singlequadrupole mass

spectrometer (Shimadzu LCMS 2010) equipped with an electrospray ionization source. The autosampler was maintained at 15 °C and the column at 40 °C. A Phenomenex Gemini C6-phenyl column (50 × 2.0 mm, 3 µm) was used to allow separation. Samples were eluted via gradient elution at a flow rate of 300 µL/min. The mobile phases consisted of a mixture of solvent A (95% v/v Milli-Q water:5% v/v MeOH) and solvent B (5% v/v Milli-Q water:95% v/v MeOH) both containing 1 mM ammonium formate and 0.1% formic acid. The initial percentage of solvent B was 60%. The proportion of solvent B was linearly increased to 100% over 3 min and was held at 100% for 4 min. After 13 min, the gradient was returned to 60% solvent B within 1 min until the end of the 13 min run time to achieve re-equilibration. Under the above-mentioned conditions, the retention times of danazol were m/z 4.1 and m/z 315.10 for the internal standard, progesterone. The MS conditions were as follows: drying gas flow, 10 L/min; nebulizing gas flow, 1.5 L/min; CDL 250 °C, heat block 200 °C; interface voltage, 4.5 kV; and detector voltage, 1.5 kV. Selected-ion monitoring was accomplished at m/z 338.10 for danazol, and m/z 315.10 for the internal standard, progesterone. The chromatographic data were acquired and analyzed using the LabSolution software package, 5.31.277 (Shimadzu).

The sample injection volume was 10 µl. Standard solution of danazol (1.0–40.0 ng/ml) was prepared by dilution of a concentrated 1 mg/ml stock solution with acetonitrile. Linearity across the working concentrations the drug was confirmed during each LC-MS assay using standard measures of regression. The LC-MS assay for danazol was validated by replicate ($n = 5$) analyses of quality control samples at low (1 ng/ml), medium (10.0 ng/ml) and high (40.0 ng/ml) concentrations and was found to be accurate to within $\pm 10\%$ of target and precise to within 10% CV.

5.3.8 Microscopy

Micrographs were recorded using Zeiss Axiolab Emicroscope equipped with HFS 91 hot stage with TP 93 temperature programmer (Linkam, Surrey, UK) and Zeiss MC-80 35 mm camera (Zeiss, Oberkochen, Germany).

5.3.9 Molecular Dynamics Simulation

MD simulations were performed using GROMACS version 4.6⁴³. Calculations were performed using the Victorian Life Sciences Computation Initiative (VLSCI) the RHEL 6 operating system, a variety of Linux, comprised of 1120 Intel Sandy Bridge compute cores running at 2.7 GHz. Parallel scaling of sample simulations (20,000 steps) were performed to determine the optimum conditions to operate the simulations to achieve an efficient use of CPU time. For the 15 nm box length simulations, the optimum utilization was determined to be 32 CPUs. The GROMOSs 53A6 united atom force field⁴⁷ was used to represent GDX, LPC, GMO and OA. This force field is parameterized to reproduce free energies of solvation in water and cyclohexane and has been used extensively to model proteins, micelles and membranes. The cis double bond in oleic acid was modeled using dihedral parameters developed by Barchar *et. al.*^{17a, 133}. Water was modeled using rigid SPC water and constrained using SETTLE¹³⁴. The remaining solute bonds were constrained by the LINCS algorithm⁷⁹. Isotropic periodic boundary conditions were also employed. A cut-off distance of 0.9 nm for both electrostatic and van der Waals interactions and the particle-mesh Ewald (PME) method¹⁴⁵ was used for long range electrostatic interactions. Temperature coupling used the velocity rescale algorithm¹⁴⁶ with a reference temperature of 310 K. production run used Parrinello-Rahman¹⁴⁷ pressure coupling algorithms with a reference pressure of 1 bar and a compressibility of $4.5 \times 10^{-5} \text{ bar}^{-1}$.

The starting model was built using the Silico script⁴⁵ random_box. The required number of LPC+OA, dTGL (GMO+2OA), GDX and water molecules were added randomly positioned in the simulation cell giving simulation size in the range of 200,000 to 300,000 atoms. The following series of simulations was performed for each system:

1. A steepest descent minimization of 500 steps to remove bad van der Waals contacts between atoms,
2. A constant volume simulation of 5,000 steps with a time step of 2 fs,
3. A constant pressure simulation of 10,000 steps using Berendsen isotropic pressure coupling with a coupling time constant of 0.1 with time step of 2 fs,
4. A pre-production simulation of 50,000 steps and a time step 2 fs using Parrinello-Rahman pressure coupling using a pressure coupling time constant of 0.1 ps and v-rescale temperature coupling using a 0.1 ps coupling constant.
5. A production simulation run of 200 ns with time step of 5 fs was used, along with a pressure reference of 1 bar and pressure coupling time constant of 2 ps, v-rescale temperature coupling with a time constant of 0.1 ps and a reference temperature of 310 K corresponding to the experimentally determined phase diagram done in this study.

Molecular aggregation was analyzed using the *Silico* script⁴⁵ *find_aggregate*, which combines molecules into aggregates by comparing distances between carbon atoms. Two molecules are considered to be part of the same aggregate if they have carbon atoms separated by a distance of less than 0.4 nm. Visualization of the simulation trajectories was performed using VMD¹³⁸ and images for publication were produced using PyMol¹³⁹ Diffusion coefficients were calculated using the GROMACS program *g_msdf*⁴³.

5.4 RESULTS

5.4.1. Experimental Studies

The first part of this work aims to understand the effect digested triglyceride has upon the phase behaviour of digested lipid and bile salt using a simplified model system. This builds on our previous work which investigated of the phase behaviour of undigested and digested phospholipids and bile¹²⁴. The system used in the present study is composed of a lysophospholipid, oleic acid, bile salt and digested triglyceride (dTGL) - a 1:2 mole ratio of glycerol 1-mono-oleate and fatty acid. Figure 5.2 shows the range of mixtures investigated in the present

study on a quaternary phase diagram. The phase formation was initially measured using nephelometry (turbidity measurements), a high-throughput¹¹² method that can readily be performed in 96-well plates and can easily distinguish between micellar and vesicle/lamellar phases. The nephelometry results were then cross-validated using dynamic light scattering (DLS) measurements. We also investigated the samples using crosspolarizing light microscopy to observe the formation of liquid crystalline phases at high concentration of digested triglyceride. After analysing the phase formation we investigated the solubility of danazol using as model PWSD drug in selected mixtures of these systems using liquid chromatography and mass spectroscopy (LC-MS) method. These mixtures contained different concentrations of digested triglyceride and selected from both micellar and vesicular regions of the phase.

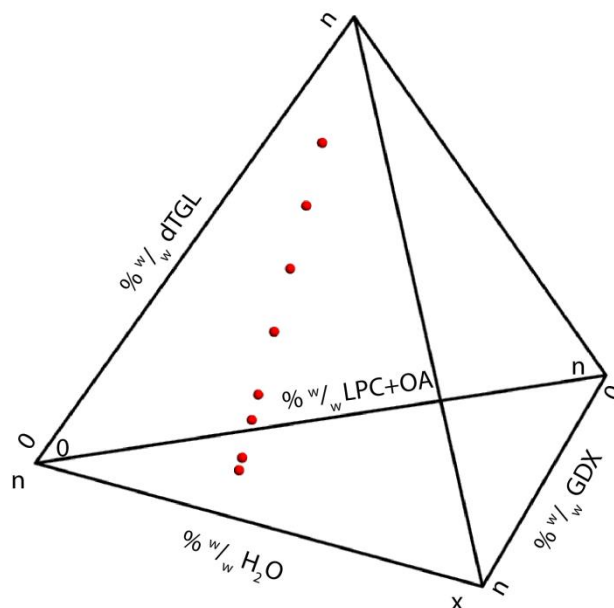


Figure 5.2. Quaternary phase diagrams showing the composition investigated (•) experimentally and through MD simulation. The total lipid concentration of the MD simulations was greater than the experimental studies and the value of n on each the LPC+OA, dTGL and GDX axes is 7 % w/w for the experimental investigations and 50 % for the MD simulation. The value of x on the water axis is 93 for the experiment and 50% w/w for the MD simulations. The proportion of lipid materials in the experimental and MD simulations were equivalent. The overall concentration used in the experimental work reflected what would be expected in the intestine. A higher concentration of lipids was necessary for MD simulations to ensure that computing time was used economically.

5.4.2. Turbidity Measurement of LPC+OA/GDX/dTGL/H₂O

In this study we were interested in observing the phase change that occurs when digested triglycerides are introduced to the digested phospholipids and bile salt. This will help us in understanding the change in phase behaviour that occurs when glyceride-based lipid formulations reach the upper GI tract. In a related study, we have investigated the phase behaviour of mixtures of digested and undigested bile. As an extension of the later study, in this experiment we determined the phase boundary between micellar and vesicular phases of the quaternary system of digested POPC (LPC+OA), GDX, digested TGL (GMO+OA) and water within the region of physiologically relevant concentrations.

The initial aggregation of digested phospholipids and fatty acid causes a strong backscattering of the laser light and consequent rapid increase in the turbidity detected. Figure 5.3a presents the turbidity for these systems as a function of digested glyceride mass fraction. It is clearly demonstrated in the plot that the significant increase in turbidity occurs with increased digested glyceride fraction in the range of W_{GMO} 0.4-0.45. This discontinuity and significant increase in turbidity indicate the phase boundary between micelles and vesicles/lamella.

5.4.2.1 Particle Size Measurement of LPC+OA/GDX/dTGL/H₂O

Particle size measurement was also utilized to identify the boundary between micellar and vesicular/lamellar phases of the quaternary system of LPC+OA, GDX, dTGL and water at different proportion of digested lipids, digested triglyceride and bile salt. Figure 5.3b presents the results of dynamic light scattering experiments. To produce each mixture the mass fraction of dTGL was varied and the particle diameter was determined. The plot clearly validates the significant increase in particle size that occurs with increased dTGL mass fraction in the range of $W_{\text{dTGL}} = 0.40$ -0.45. The particle size of the micelles, mass fraction of dTGL in the range of $W_{\text{dTGL}} = 0.0$ -0.4 was found to be in the range of 7-80 nm in diameter and for vesicles that form at high lipid content the particle size was higher (diameter in the range 80-600nm). The average polydispersity index (PDI) of the measurements were in the range of 0.13 – 0.39. To avoid artificially calculated diameter artefacts due to the presence of two or more particle population, all the results with polydispersity index of greater than 0.5 were discarded and the experiment was repeated until a moderate PDI value was achieved for all measurements. The average diameters of the particles formed were reproducible with a moderate polydispersity index ($\text{PID} < 0.5$). However, as the samples have more than one molecule which forms a population of more than one particle size, it was not possible to achieve a low polydispersity index. Moreover, the correlation function of the samples was carefully monitored during measurement to check whether the fluctuations of the correlation function were uniform. The presence of the large error bars found in the case of the particle size of the vesicles is due to the mixtures being formed by simple agitation. More vigorous agitation or

signification would result in a more reproducible particle size. However, such treatment would be of questionable comparison to what occurs within the gastro intestinal tract. Additionally, what is ultimate interest here is that appearance of the vesicles rather than an accurate measure of their particle size.

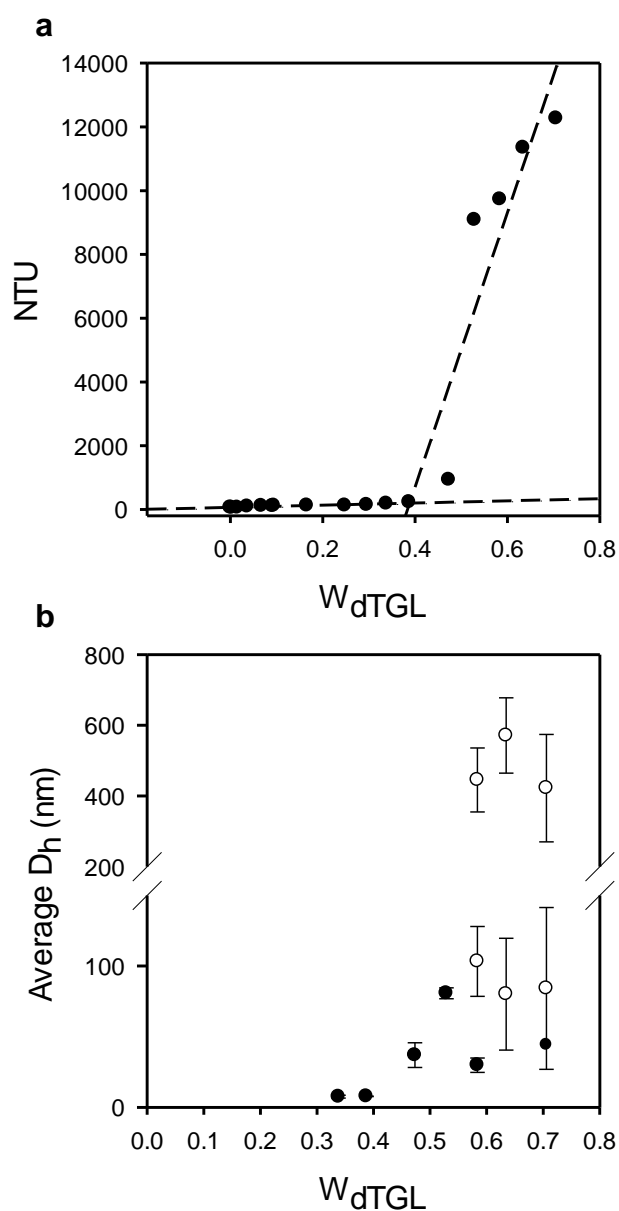


Figure 5.3. The effects of adding digested triglyceride (dTGL) to a mixture of bile salt and digested phospholipid. X-axis shows the total mass fraction of dTGL (as a fraction of bile salt, lipid and triglyceride) where $x=0$ indicates the absence of dTGL and $x=0.8$ indicates the highest concentration of dTGL in the mixture. (a) Turbidity measurements by nephelometry, with increased turbidity showing the formulation of vesicle/lamellar phases (b) Corresponding particle size measurement of the system by DLS. (●) and (○) represent micelles and vesicles respectively.

Samples of LPC+OA/GDX/dTGL/H₂O mixtures with higher concentrations of dTGL were assessed under the light microscope with and without cross polarizing filters. The samples were transferred onto microscope slides to identify the possible formation of liquid crystalline phases. Slides were viewed by cross polarizing light microscope. Birefringent lamellar liquid crystal regions were identified by characteristic textures of oily lines and their distinguished pink and blue colours which are shown in Figure 5.4a, b and c.

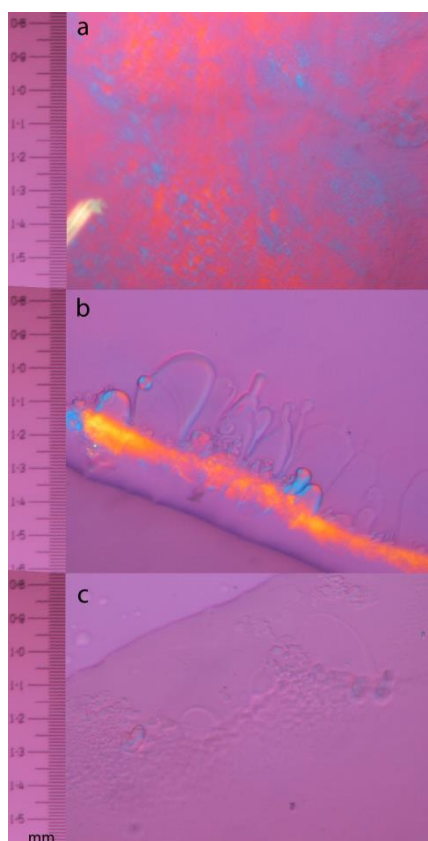


Figure 5.4. Representative cross-polarized light micrographs (magnification 20 X) of the brightly birefringent oily lines and their distinguished pink and blue colours of the lamellar liquid crystal phases observed (a) $W_{dTGL}=0.70$ and (b) 0.63 respectively, and (c) the nonbirefringent mixture in the micellar region (magnification 20 X) $W_{dTGL}=0.33$.

5.4.2.2 Danazol Equilibrium Solubility

The equilibrium solubility of danazol within bile salt/digested phospholipid/digested glyceride system was evaluated using an HPLC assay. Danazol solubility values in bile salt/phospholipid

($W_{\text{dTGL}} = 0$) and in the presence of increasing amount of dTGL are presented in Figure 5.5. It was not surprising that the solubility of danazol is lowest in the mixtures of digested POPC alone and highest in the presence of digested triglyceride.

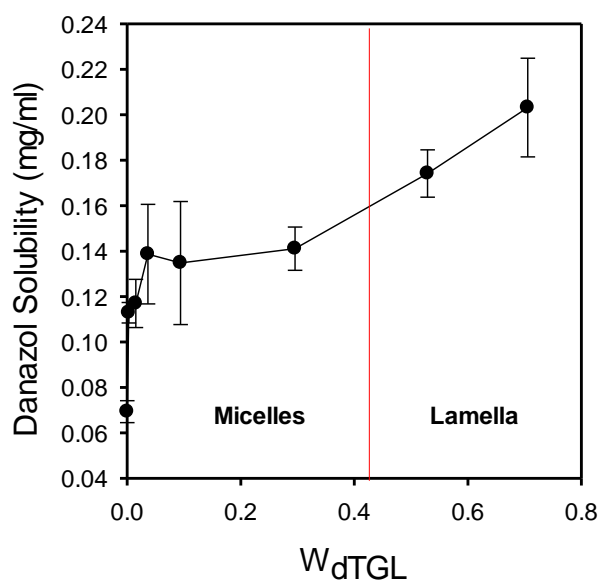


Figure 5.5. Danazol solubility as a function of increasing concentration of digested triglyceride in the mixture of LPC+OA/GDX/dTGL/H₂O. X-axis shows the total mass fraction of dTGL (as a fraction of bile salt, lipid and triglyceride) where $x=0$ indicates the absence of dTGL and $x=0.8$ indicates the highest concentration of dTGL in the mixture.

5.4.3. Modelling Studies

The second part of this work used molecular dynamics simulations to investigate the molecular interactions that regulate the formation of different phases in the LPC+OA/GDX/dTGL/H₂O system. We simulated the quaternary LPC+OA/GDX/dTGL/H₂O system at concentrations ranging from 0 to 40 % w/w total digested triglyceride. In addition, we have simulated the dispersion and dynamics of danazol at concentrations ranging from 2.5 to 20 mg/ml. It is estimated that the ‘concentration’ of lipid formulation within the GI tract is likely to be less than 1 % w/w , assuming that a 1 g lipid formulation capsule disperse into 250 cm³ gastrointestinal content⁶⁴. Hence, in our MD work to avoid unnecessary CPU time on simulating interaction of water molecules we choose a higher concentration of digested lipid and bile salt concentration of 5 % w/w and minimum

digested triglyceride concentration of 3 % ^w/_w, keeping the lipid material in proportion to the mixture used in the laboratory based experiments.

5.4.3.1. Simulation of the phase of Quaternary System of LPC+OA/GDX/dTGL/H₂O

We investigated the phase behaviour of quaternary LPC+OA/GDX/dTGL/H₂O system by running several independent simulations using varying amounts of LPC, OA, GMO, GDX and water, listed in Table 5.1. The final frames of selected simulations are shown in Figure 5.6 with the LPC, OA, GMO and GDX molecules coloured differently to distinguish them. In these simulations a progression from simple micelles to secondary then cylindrical micelles and a transition to lamellar and hexagonal phases was observed. The molecular compositions of each simulation and the nature of the colloidal aggregates present at the end of the simulation are recorded in Table 5.1. The total number of aggregates and mean size of the aggregates formed in the simulations were calculated using the *find_aggregate* program which identifies hydrophobic aggregates of molecules (e.g. micelles or vesicles/lamellae) in a given periodic system. It is important to note that, in many of the simulations, the sizes of the molecular aggregates formed is limited by the number of molecules present in the simulated system and the simulation results should be interpreted with care when only a small number of aggregates are present at the end of the simulation.

Table 5.1. Simulations of the quaternary /LPC+OA/GDX/dTGL/H₂O phase systems.

SIM. No.	No. of Molecules						Composition				Median agg. size/Num.	Structure in final state
	GMO	OA (GMO)	LPC	OA (LPC)	GDX	Water	GMO	LPC	OA	GDX		
1	-	-	37	37	149	107070	-	0.9	0.5	3.6	23/10 ^b	Micelles and isolated molecules
2	66	132	36	36	144	103858	1.2	0.9	2.3	3.5	36/7 ^b	Oblate micelles
3	110	220	35	35	141	101717	1.9	0.9	3.6	3.4	138/4 ^b	Spherical micelles
4	176	352	34	34	137	98505	3.1	0.8	5.4	3.3	181/4	Spherical micelles
5	220	441	33	33	134	96363	3.9	0.8	6.6	2.2	167/3	One Lamellar and two oblate micelles
6	286	573	32	32	129	93151	5.0	0.8	8.4	3.1	700/2	
7	330	660	32	32	126	91010	5.8	0.8	9.6	3.0	802/2	Lamellar micelle
8	396	793	30	30	122	87797	7.0	0.7	11.5	2.9	1625/1	Cylindrical micelles
9	440	880	30	30	119	85656	7.7	0.7	12.7	2.9	2009/1	Cylindrical micelle
10	550	1101	28	28	112	80303	9.7	0.7	15.7	2.7	2126/1	Lamella
11	660	1321	26	26	104	74949	11.6	0.6	18.8	2.5	2445/1	Hexagonal
12	881	1541	22	22	89	64242	15.5	0.5	24.8	2.1	3800/1	Hexagonal

^aAggregate numbers and median values exclude any isolated molecules. ^bA small number of aggregates are observed. The median value will not be a reliable estimate of true aggregate size.

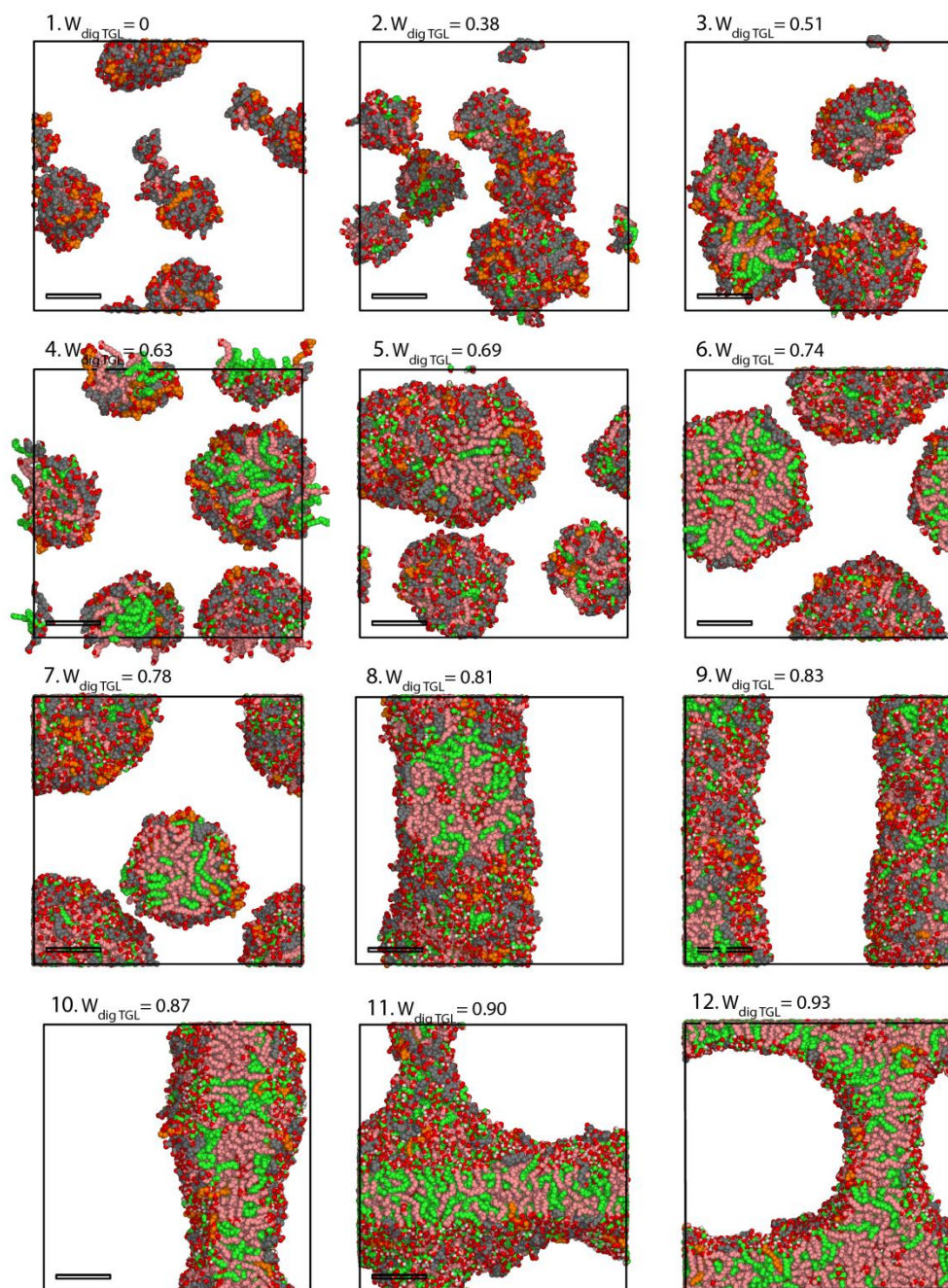


Figure 5.6. Final frames from simulations of the LPC+OA/GDX/dTGL/H₂O quaternary system showing a progression from simple micelles through mixed and cylindrical micelle to hexagonal structure then emulsion at higher concentration of GMO. Simulation numbering is described in Table 5.1. Atom colouring; GDX is grey, LPC is orange, OA is pink, GMO green and oxygen atoms are red. The box indicates the periodic boundary. Scale length 3.0 nm. Water atoms have been omitted.

To understand the changes occurring within the system we calculated the self-diffusion coefficient of water and OA, LPC, GDX and GMO molecules. This analysis provides us useful information where the phase change occurs when there is a sharp change in the molecular mobility of the molecules. The bigger the aggregate the slower their molecular mobility will be. Analysis of all the lipids, bile salt and water self-diffusion coefficient shows that the slow self-diffusion coefficients in the quaternary system of LPC+OA/GDX/dTGL/H₂O as a function of increasing concentration of digested glyceride are shown in Figure. 5.7a and b. The diffusion coefficient of all the component decreases rapidly when the mass fraction of digested triglyceride reached 0.6, coinciding with the phase transition from smaller spherical micelle to lamellar shaped secondary micelles. The diffusion decreased even more rapidly beyond 0.7 mass fraction of digested triglyceride, coinciding with the phase transition from large lamellar shape secondary micelles to cylindrical micelle, to lamella phase and then to hexagonal phase. The self-diffusion coefficient of water decreases sharply as the amount of bulk water in the system decreased. When the mass fraction of digested glyceride reached 0.8 the phase became more hexagonal that attributed to the water molecules bound to lipid head groups as shown in Figure 5.7b.

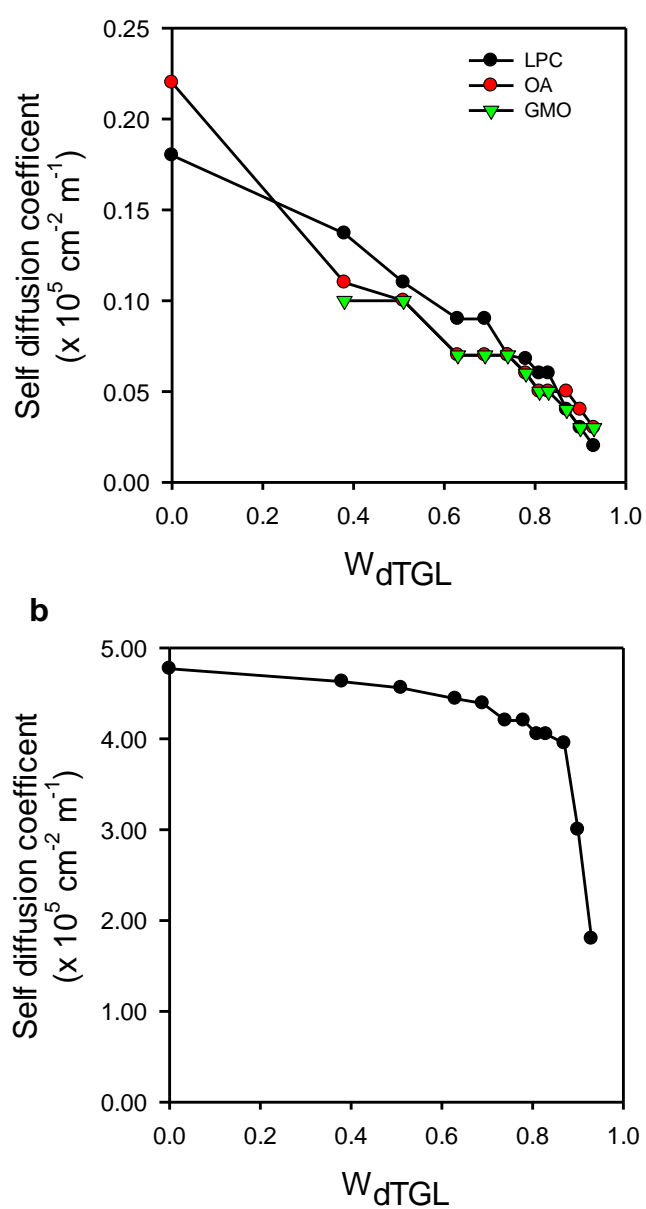


Figure. 5.7 Calculated self-diffusion coefficients of the components of (a) LPC+OA/GDX/dTGL/H₂O. (b) Water.

5.4.3.2. Simulation of the dispersion and dynamics of Danazol in the Quaternary System of LPC+OA/GDX/dTGL/H₂O

To examine the behaviour of drugs within the Type I formulation, we performed a set of 30, 200 ns MD simulations by taking five of the previously studied LPC+OA/GDX/dTGL/H₂O mixtures of the model system and adding danazol as model PWSD in 6 different conditions, 2.5, 5.0, 7.5, 10.0, 15.0 and 20.0 mg/ml of danazol, which corresponds to 15, 30, 45, 60, 96 and 120 danazol molecules respectively. Danazol has a logP value of 4.5 and a water solubility of 1.0 µg/ml, and therefore is a highly lipophilic compound and exhibits very low aqueous solubility¹⁴⁸. It has been widely studied as a model drug in different lipid-based drug formulations studies^{35a, 149}. The higher danazol concentrations were considered to investigate the significant drug-drug interactions that can occur at higher loadings. In each case, the simulation was started from a random starting configuration as described in Methods section.

To investigate the dispersion of drug molecules and their dynamic behaviour within the quaternary system, we analysed the localization of drug molecules within the mixture, aggregation of drug and the drug diffusion properties. Figures 5.8 a and b show the locations of the drug molecules at the completion of each 200 ns simulation within 12 selected quaternary simulations. Figures showing the final frames of all 30 simulations are included in Appendix 4. To highlight the danazol molecules they are coloured yellow and are also shown as a separate image below the picture of the complete mixture. The final simulation of frames clearly show that the danazol molecules preferentially reside within the hydrophobic (alkane-chain) region of the quaternary system at all concentrations.

Table 5.2. Aggregation profile of danazol in the quaternary phase systems of LPC+OA/GDX/dTGL/H₂O.

Sim. No	Parent Sim. No	W _{dTGL}	DANAZOL (gm/ml)	NO. OF DANAZOL Mol.	MEDIAN AGG. SIZE	NUM. OF AGG.	MAX AGG. SIZE
13	1	0	2.5	15	2	2	2
14	1	0	5	30	2	4	7
15	1	0	7.5	45	2	7	6
16	1	0	10	60	2	9	9
17	1	0	15	90	4	13	11
18	1	0	20	120	4	13	24
19	2	0.38	2.5	15	3	1	3
20	2	0.38	5	30	2	3	4
21	2	0.38	7.5	45	2	3	4
22	2	0.38	10	60	2	10	6
23	2	0.38	15	90	2	11	9
24	2	0.38	20	120	2	22	11
25	5	0.69	2.5	15	3	4	2
26	5	0.69	5	30	2	8	4
27	5	0.69	7.5	45	3	7	4
28	5	0.69	10	60	2	8	6
29	5	0.69	15	90	3	16	7
30	5	0.69	20	120	3	31	10
31	8	0.81	2.5	15	2	2	2
32	8	0.81	5	30	2	4	3
33	8	0.81	7.5	45	2	8	4
34	8	0.81	10	60	2	8	6
34	8	0.81	15	90	3	16	7
36	8	0.81	20	120	3	31	10
37	10	0.87	2.5	15	3	2	2
38	10	0.87	5	30	2	3	2
39	10	0.87	7.5	45	2	11	2
40	10	0.87	10	60	2	14	3
41	10	0.87	15	90	2	14	4
42	10	0.87	20	120	2	24	7

^aAggregate numbers and median values exclude any isolated molecules.

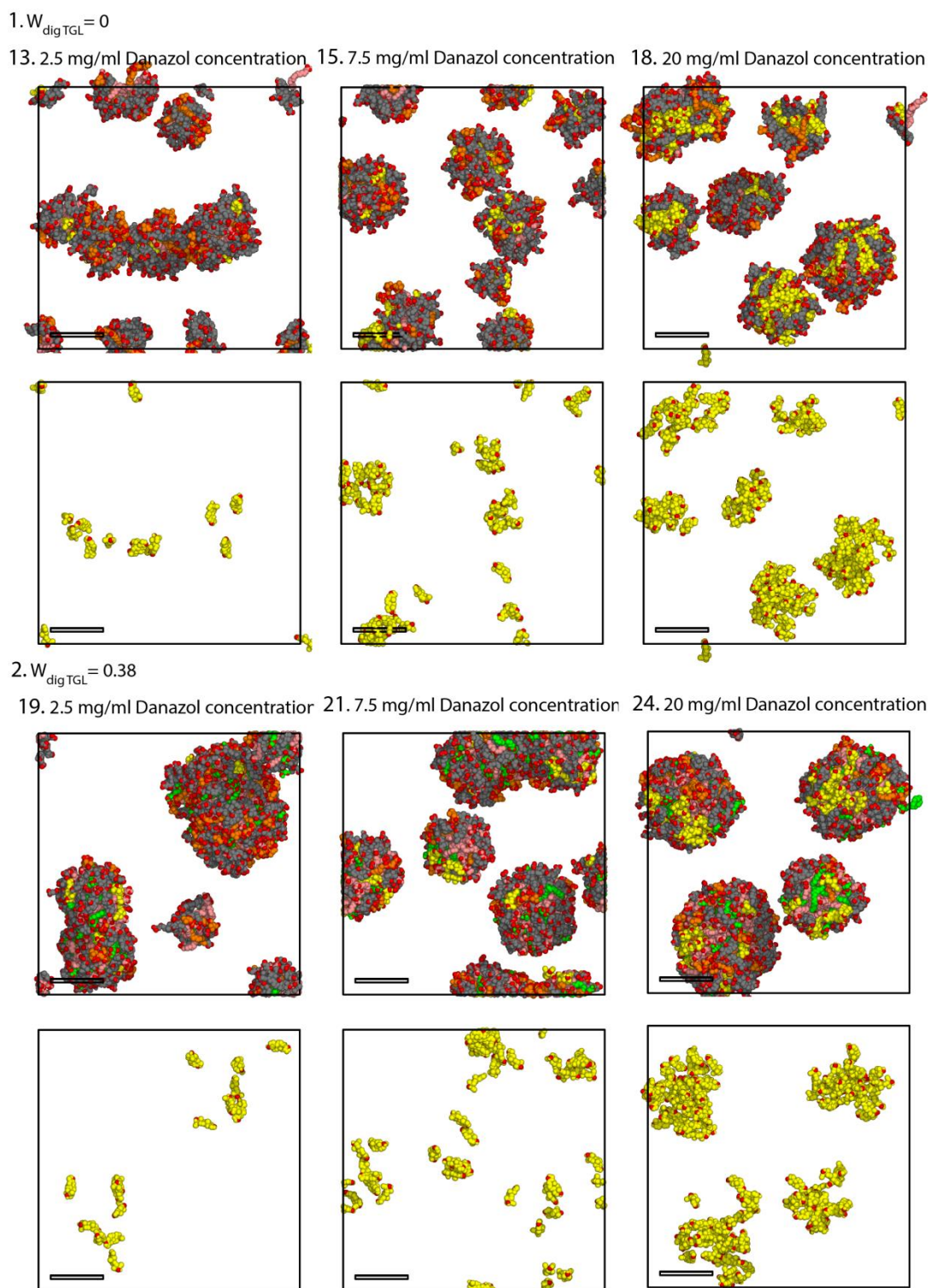
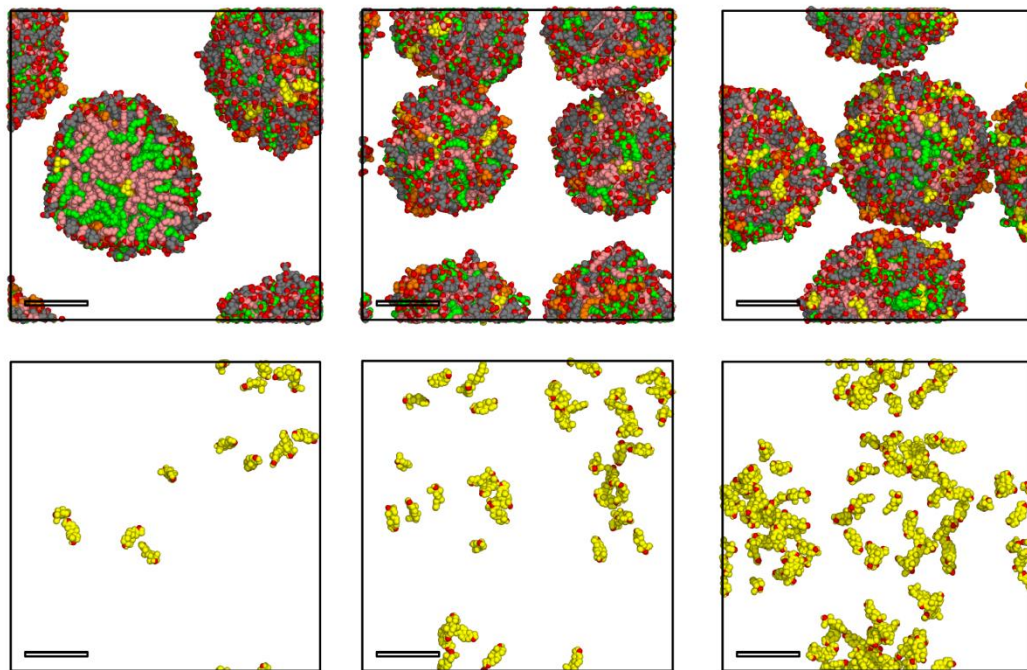


Figure 5.8a. Localization of drugs within the final frames of selected simulation, with changing danazol concentration. Danazol coloured yellow. Molecule colouring is as described in Figure 5.6 and simulation numbering is described in Table 5.2.

5. $W_{\text{dig TGL}} = 0.69$

25. 2.5 mg/ml Danazol concentration 27. 7.5 mg/ml Danazol concentration 30. 20 mg/ml Danazol concentration



10. $W_{\text{dig TGL}} = 0.87$

37. 2.5 mg/ml Danazol concentration 39. 7.5 mg/ml Danazol concentration 42. 20 mg/ml Danazol concentration

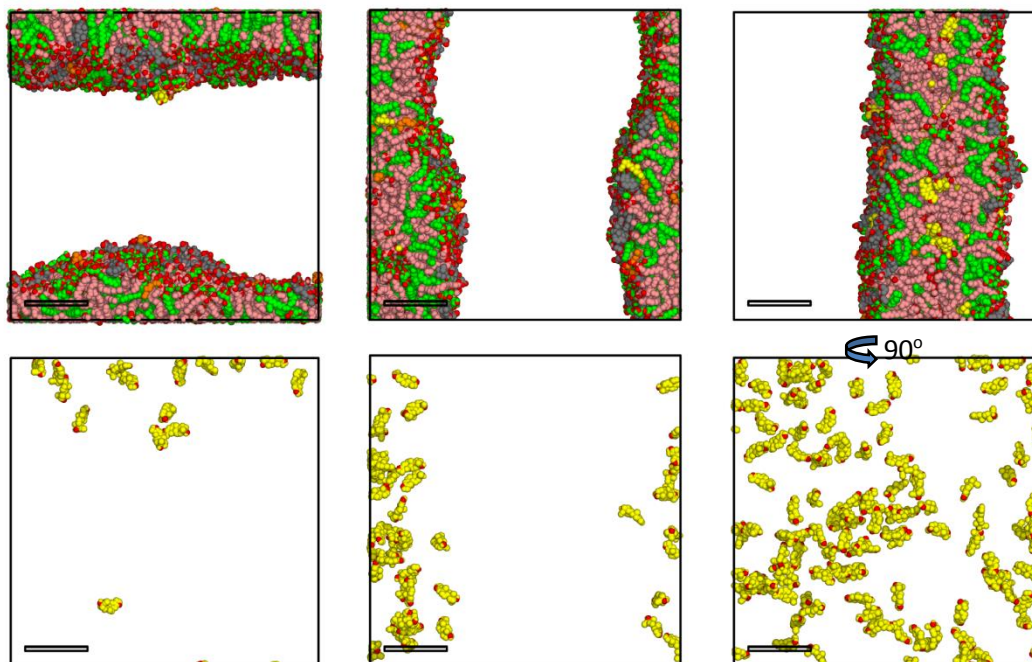


Figure 5.8b. Localization of drugs within the final frames of selected simulation, with changing danazol concentration. Danazol coloured yellow. Molecule colouring is as described in Figure 5.6 and simulation numbering is described in Table 5.2.

The self-diffusion coefficient of danazol molecules in each mixture was also evaluated, shown in Figure 5.9a. As a hydrophobic compound danazol molecules are more localized in the lipid phase and exhibit maximum molecular mobility in the micelle phase where there is fastest mobility of the lipids themselves (see Figure. 5.7a) followed by a sharp drop in mobility upon formation of the lipid lamellar and hexagonal phases again where there is slowest mobility of the lipids themselves. To evaluate the drug-drug interaction within the system we calculated the maximum aggregate size of danazol within each system; these are shown in Figure 5.9b. This analysis indicates that when the concentration of danazol increases the drug-drug interaction increases, as the maximum aggregate size indicates that the maximum number of molecules exist in one aggregate.

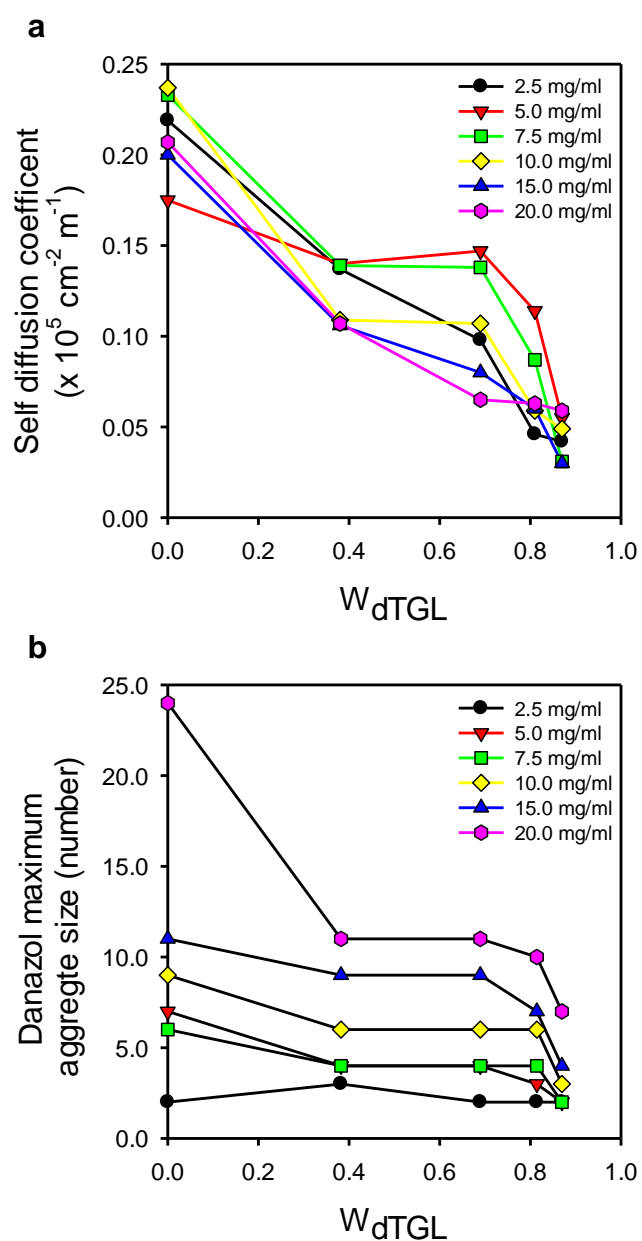


Figure 5.9. (a) Calculated self-diffusion coefficient and (b) predicts maximum aggregate size of danazol within LPC+OA/GDX/dTGL/ H_2O mixture with changing concentration of danazol and increasing the mass fraction of digested triglyceride.

5.5 DISCUSSION

It is known that the bioavailability of PWSD can be improved by coadministration with lipids, which can increase drug absorption by enhancing solubilisation and dissolution^{28a}. However, the understanding of the interaction of lipid-based formulations with gastrointestinal fluids and endogenous biliary lipids has been hindered by a lack of predictive formulation assessment studies. The phases that are formed between lipid-based formulations and gastrointestinal fluids and endogenous biliary lipids have been described as a simple range of colloidal intestinal phases^{17c, 150}, although the nature of the phases formed have not been understood at the molecular level. It is desirable to understand the issues associated with performance of lipid-based formulations in terms of their impact on the phase behaviour of the gastrointestinal fluids. In particular, we seek to understand the solubilisation capacity of different phases formed on digestion for poorly water-soluble drugs, and the impact that this has on whether or not the drug is maintained in solution, and whether the drug might precipitate during the digestion and dispersion process. The ability of a lipid-based formulation to maintain drug in a solubilized state and to inhibit drug precipitation is highly dependent on the nature of the formulation excipients included, and this is further complicated by the realization that the properties of the excipients can change significantly during dispersion and digestion in the GI tract^{17d, 35a, 150-151}.

This work is the first study to investigate the association structures formed after digested bile makes contact with a digested LBDDS. As the concentration of the digested triglyceride increased, the phase behaviour changed from a mixed micellar structure to a more complicated mixture of vesicular/lamellar and hexagonal structures. Additionally, this study showed that the solubilisation behaviour of lipophilic drugs on digestion of simple triglyceride lipid formulations is a function of the concentration of the digested triglyceride, which dictates the nature of the colloidal phases produced on digestion of the formulation lipids, and their ability to solubilize drug.

As indicated by the turbidity measurements shown in Figure 5.3a, the DLS study in Figure 5.3b, as well as the cross polarizing light microscope images in Figure 5.4, the main finding of this study

is that as the mass fraction of digested triglyceride increases in the system there is a phase transition from smaller spherical micelles to larger vesicular/multilamellar structures. The MD trend in results also clearly correlated well with these experimental studies. The entire system spontaneously organized into micellar structures at no or low digested triglyceride concentrations. At higher triglyceride concentrations, phase separation occurred as shown in Figure 5.6 in order of increasing digested triglyceride concentration. These structures are consistent with our previous results which were obtained using only biliary lipids (undigested and/or digested POPC, bile salt, oleic acid and water)¹²⁴. In the MD simulations we noted that more complex hexagonal structures formed with higher concentration of digested glyceride.

The investigation of the solubility of the PWSD danazol showed that with increasing digested triglyceride concentration the solubility increased as indicated in Figure 5.5. This is in agreement with published data¹⁵². In other studies it has been suggested that digestion of formulation lipids may lead to a loss of solubilisation capacity of the formulation and a decrease in bioavailability^{151b, 151c, 152a, 153}. In our previous study, we observed that after digestion of biliary lipids, the solubilisation capacity of bile salt for lipids increased. Hence, higher lipid concentration was required to form larger vesicular colloidal structures¹²⁴. However, in this current study we did not compare the solubilisation capacity between undigested and digested triglyceride alone. Instead we added in model digestion products, which model dietary triglycerides or a Type I lipid-based formulation. We clearly observed that higher digested lipid concentration in the GI tract can lead to a more solubilisation capacity of PWSD. This was also supported by MD simulations. We correlated the simulation and experimental data in Figure 5.10 showing that with higher dose of danazol we see more aggregation (which may represent crystallisation) of danazol in the system containing lower concentrations of digested glyceride. This was also supported by the LC-MS study which showed that when more digested triglyceride was present, a larger mass of danazol was solubilised.

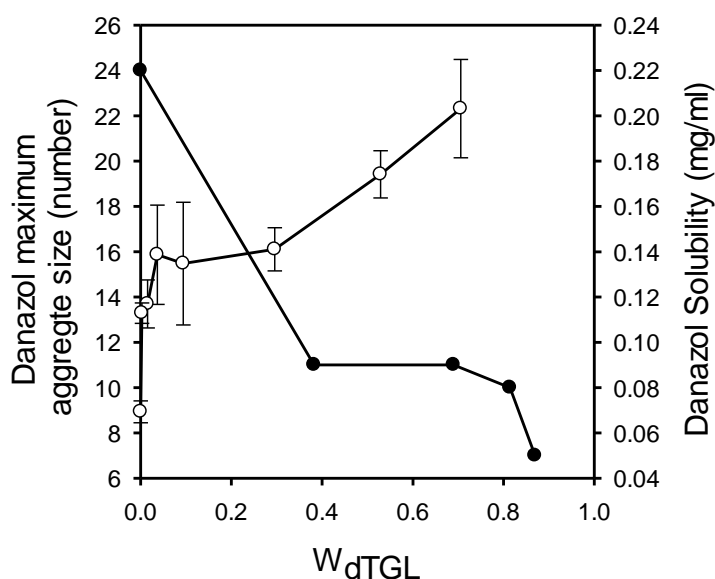


Figure 5.10. Comparison of maximum aggregate size of danazol molecules using MD simulations (●, left axis) and the corresponding solubility measurements from LC-MS (○, right axis) as a function of digested triglyceride.

The use of MD models for this study provides important information about the localization of the lipophilic drugs within the mixture of the formulation-lipid and the GI fluids, and is indicative of dynamic processes, such as aggregation that will result in poor solubilisation properties, as shown in Figures 5.8a and b. Data files detailing localization of danazol within the final frames of all simulation are available in the Appendix 9.4. In this work we have used the 53A6 lipid force field which has been updated in subsequent work¹⁵⁴. Although the newer lipid parameters influence the observed properties of lipid bilayers, we do not believe that the lipid force field will radically influence the phase behaviours of these kinds of mixtures as we are dealing with larger interaction profile of lipids rather than a specific interaction of atoms in the lipid-lipid interactions. This study provides a foundation for the *in silico* design of lipid formulations, to further the understanding of the behaviour of a wider range of drugs in different lipid formulations and their fate after they are released into the GI lumen.

5.6 CONCLUSION

The digestion of formulation excipients and their phase formation in the environment of the GI tract is an important process to improve the dissolution and absorption of poorly water-soluble drugs. However, these processes are currently poorly understood. This study has explored in detail the impact of digested triglyceride on the phase behaviour of the GI tract particularly in the presence of digested phospholipid and bile salt mixture using both experimental and MD simulation techniques. Additionally, it has explored the impact of digested triglyceride on the solubility of poorly water-soluble drug candidates using danazol as a model drug. The results suggest that knowledge of the impact of formulation excipients on the phase behaviour of the GI tract and drug solubility may give us a better understanding of the performance of lipid-based formulations and help us to optimize the concentration of different excipients in lipid-formulation. The positive correlation between *in vivo* and *in silico* results gives us confidence to use MD simulations to model more complex events that occur on dispersion and digestion of the formulation in the GI tract and explore them at an atomistic level of detail. Moreover, this study suggested that MD can be used as a prediction tool to model the fate of poorly water-soluble drugs in the GI lumen after they are released from the capsule in the stomach.

5.7 ACKNOWLEDGMENT

Funding support from Australian Research Council (ARC) Linkage Grant awarded to Monash University in collaboration with Capsugel is greatly acknowledged. We would like to thank the Victorian Life Science Computation Initiative (VLSCI) for technical support and Merit Allocation Scheme grants of CPU time and system support.

"Honour for those who never forsake the truth even when things seem dark and grim, who try over and over again, who are never discouraged by insult, humiliation and even defeat."

Nelson Mandela

CHAPTER SIX

SUMMARY

6 SUMMARY

The primary objective of this thesis was to explore the benefit of atomistic molecular dynamics (MD) simulation to gain insight into the behaviour of lipid-based drug delivery systems (LBDDS). This study had two significant objectives. The first was to improve the limitations of currently available force fields, particularly for LBDDS that include non-ionic surfactants. The second objective was to investigate the impact of digestion of biliary lipids and the role of digestion products on the phase behaviour of the contents of the gastrointestinal (GI) tract. It was also of interest to evaluate the solubilisation capacity of these colloidal structures for poorly water-soluble drugs (PWSD), using laboratory experimental techniques and MD simulations.

The objective of research on LBDDS since the 1980's has been to understand the relationship between their composition and their ability to self-emulsify, and to link these properties to their performance *in vivo* and drug bioavailability. Previous work has focussed on the bulk properties of the formulations with limited ability to probe the microstructure of the formulations. The research presented here, however, opens a novel approach to understanding the internal structure of LBDDS, and the interaction of LBDDS with GI fluids at atomistic level. A more detailed understanding of these interaction patterns will give us a better understanding of formulation performance and therefore improved ability to predict performance from *in vitro* and *in silico* studies of the formulation.

In the past, a few simulation studies have been carried out using bile salts and mixed bile salt-lecithin systems but studies on lipid formulations date back less than five years. The first study to model the formation of mixed micelle in human bile was done by Marrink and Mark⁵⁹ using phospholipids (PC), bile salts (BS) and cholesterol (CH). These authors were able to show that mixed micelles were globular in nature and they described time-dependent changes in the structure of the micells as they approached equilibrium. Warren *et. al.*^{55, 64} also studied the aggregation behaviour of bile salts, showing that aggregation number could be adequately

modelled by MD simulations, and later published what is probably the first study on glyceride lipid formulations with propylene glycol and water. In their recent work Warren *et. al* investigated the phase behaviour of type I glyceride formulations and investigated the distribution and location of different PWSDs as water was added to the formulation. This study indicated that MD simulations can predict whether or not drugs are likely to partition into the aqueous phase as a lipid formulation is dispersed in an aqueous medium. King *et. al.*⁴⁰ used MD simulation to explore the phase behaviour study of the ternary sodium laurate/sodium oleate/water system. The phase behaviour of this system has been well-documented and served as a good model to ask whether MD simulation could predict phase behaviour across a wide variety of mixture compositions. The work was successful with this simple ternary system, and it suggested that MD has the potential to predict phase behaviour in more complex systems. We gain fundamental understanding from these studies on how MD can be used to probe the internal structure of LBDDS and the interaction of LBDDS with GI fluids at atomistic level, though at present there have been no attempts to model the complexity that results from digestion of a LBDDS in the presence of bile. Some of the limitations of MD simulation were also explored in this thesis.

MD simulation is well advanced in modelling protein structures. However, the force fields incorporated in most of MD simulation packages are not optimised for molecules that are not intensively used in the modelling study of protein structures. Hence, the first part of this project (Chapter 2), dealt with the validation and parameterisation of the force field with a view to improving its applicability to MD simulations of LBDDS. This proved to be a difficult problem and emphasised that more work will need to be done in the future on parameterisation. Any given force field involves the estimation of a large number of parameters, and the values of these parameters have to be carefully selected so that their accuracy should reflect the reliability of the force field. Parameterisation can be carried out in one of two ways; either by reproducing properties calculated using a higher level theoretical approach, or by an iterative approach based on reproducing known experimental properties using the given force field^{47, 155}. The parametrisation study in this project was an attempt to modify the GROMOS 53A6 united atom

force field. This force field is part of the GROMACS MD simulation package, which was used for the rest of the MD simulation studies. This force field is a good choice for biomolecular systems containing proteins, DNA, sugars, and lipids but proved to have limitations for modelling of polyethoxylated materials and typical heterocyclic drugs. We identified the octanol/water logP as an experimental value that is often available for drugs and related small molecules. This property is not usually used for parameterisation but is particularly appropriate for phase behaviour studies, which are heavily influenced by partitioning phenomena. By choosing a series of well-known simple compounds we reasoned that we could use experimental values of logP to improve parameterisation of the force field for our use with drugs and LBDDSs. The first set of simulations used partitioning coefficient (logP) values and other thermodynamics properties (density, heat of vaporization etc.) using a homologous series of number of alkanols. Using the original GROMOS 53A6 force field, the accuracy of the results of the calculated logP values and other thermodynamics properties of the alcohols was evaluated by comparing MDS estimations with experimental data. The results obtained suggested clearly that GROMOS 53A6 could not accurately reproduce the experimental logP results and indicated that modification would be necessary to improve its accuracy. In some cases the MD estimate of logP was several orders of magnitude away from the experimental value. In summary, iterative procedure was explored and improved the MD estimates for alkanols, though it was not possible to obtain precise, correct estimates and logP was typically at best 5 - 10 fold higher than the experimental value.

This study also explored logP of ethoxy compounds, which were of high significance given their importance in relation to non-ionic surfactants. The parametrisation procedures were intensive studies that required significant computational power. Particularly, the logP calculation required the use of relative free energy calculations in water and octanol, which are computationally expensive. But, the continued increase in computational power and the accuracy of methods to calculate relative free energies allowed us to proceed with this parametrization procedure. As well as the charge modification on the ether oxygen, modification of the dihedral bond for polyethylene glycols (PEG) was performed during this study. We gave a great deal of attention to the

modification of PEG, as in addition to being used in LBDDS, these materials are used in foods, cosmetics, and are widely used to stabilize, immobilize, or modify the physical properties of biological molecules¹⁵⁶. A well optimised force field will be beneficiary not only for the study of LBDDS but also in many other areas of research but as yet this appears to be some way off for PEGylated materials.

The second part of this study (Chapter 3 and 4), used the GROMOS53A6 force field to explore the role of bile components in the GI lumen. Specifically, the experiments were designed to model the influence of digestion of lecithins on the phase behaviour of bile. The results of this study suggested that there is a significant difference between the digested and undigested bile systems which may be physiologically relevant, and may have evolved as a mechanism to change the solubilisation capacity of bile after secretion into the duodenum. Experimental studies of phase behaviour were carried out in parallel with the MD studies. In the case of digested biliary lipids, a higher molar ratio of lipid to bile salt was required to cause a transition to the vesicular phase. This tells us that the mixed micelles formed by the digested bile components can incorporate more lipid molecules; hence they might be expected to have a different solubilisation capacity to solubilize digested dietary triglycerides or PWSD. MD simulations revealed clear differences in the morphology of the digested mixed micelles and undigested micelles, indicating that MD simulations had valuable predictive potential.

One potential pitfall of the method used was the need to use higher concentrations of lipids for the MD studies. The experimental study was conducted at physiological concentrations, but simulating the system at the same concentration would have been inefficient. Much of the computing time would have been used to simulate interactions of water molecules, with only a very small number of biliary lipid molecules. To avoid this inefficiency we chose a higher concentration of biliary lipids. This approach is reasonable because the phase boundary between the [micelle] and [micelle + vesicle] phases occurred at a constant weight fraction of the components at both concentrations.

The use of MD analysis allowed the lipid and bile salt intermolecular interaction to be investigated in detail, allowing the prediction of likely arrangements of the bile salt and lipids; information which cannot be obtained using any spectroscopic methods. The results of the MD study suggested that MD modelling can provide a better insight to the understanding of the study of self-assembly behaviour of different molecules that are involved in LBDDS.

The final part of this thesis (Chapter 5) dealt with more detailed evaluation of the impact of digestion products derived from the formulation lipids on the GI fluids, particularly on the digested biliary lipids using both experimental and MD simulation. This was an attempt to begin the exploration of the complex contents of the GI lumen after administration of a LBDDS. The work focused on the molecules that might be present after dosing a simple oily LBDDS to a fasted GI tract. Whilst this may seem to be a simplification due to lack of food, it is more important to understand the fasted state than the fed state. Generally, PWSD are more bioavailable when administered with food, so the more important issue is to understand what happens when a formulation is administered in the absence of food. The digestive process is stimulated by the presence of even a small mass of lipid, so digestion of the LBDDS is expected to occur quite quickly in the intestine, and the phases formed could have a profound influence on the fate of the drug. In this study, we were keen to initiate studies which included components of the formulation so that we can begin to anticipate the phases that are formed in the intestine. The simplified model system that was developed in the previous chapters (Chapter 3 and 4) focussed on bile, and was used to design the experimental and modelling procedures. The main objective of this last part of the study (Chapter 5) was to understand the effect of digested triglyceride on the phase behaviour of digested lipid and bile salt. Triglycerides represent the simplest form of LBDDS (a Type I) formulation, which does not contain any surfactant. In Chapter 5 the structures formed between digested triglycerides and digested bile was investigated. Furthermore, the solubilisation capacity of these mixtures on PWSD candidate danazol was investigated using LC-MS as well as MD simulation. The results suggested that digestion of formulation excipients could alter the phase

behaviour of the GI tract and might give rise to structures that have different solubilisation capacity for PWSD. This initial study using both experimental and modelling techniques suggested how modelling tools could potentially be used to optimize the concentration of different excipients in lipid-formulation, though the present study highlighted the current limitations of this approach.

The first and most significant limitation was the lack of accuracy in including pH effects in the MD simulations. In many biological processes, particularly in the GI tract, change in pH is a driving force of phase formation and it brings a significant impact in the performance of formulation excipients in the solubilisation capacity of PWSD. All our MD simulations were performed with fixed protonation states. Although, there is a method known as constant pH molecular dynamics (CpHMD), which has been recently developed, there are several drawbacks to this method, which do not allow us to use it in the current study. Some of the drawbacks are; less accurate in conformational dynamics; the mismatch of implicit and explicit solvent, as explicit ions are neglected; its slow pK_a convergence (10 ns for most residues); and its complicated treatment of electrostatic interactions mainly the long-range electrostatics¹⁵⁷. Additionally, it has only been tested on very small scale simulations. Hence, it is not sufficiently reliable at this stage to use on large scale calculations such as those used in this PhD project.

The second significant limitation of this PhD project was the lack of availability of variety of validated and reliable force fields to be used without an intensive modification for all the excipients of the formulations. In this study, a great deal of time was invested to modify currently available force fields to use them in modelling of formulations which have excipients other than lipids. Although, the current modified version of GROMOS 53A6 united atom force field resulted in an improvement in calculated logP values of certain number of PEG molecules, there is still much room for improvement before it can be used with confidence for simulating the self-assembly process of non-ionic surfactants. Additionally, as all force fields aim at an accurate representation of specific aspects of a physical system, a careful selection, modification and validation process of currently available force fields is necessary to simulate the localization and dynamic processes

of the lipophilic drugs more accurately within the mixture of the formulations and within the GI fluids.

Finally, the PhD project identified a fundamental opportunity to continue this work in the future, particularly in the development of more robust and more descriptive analysis tools of the MD simulation results. The current analysis tools are very limited and mainly adapted from traditionally available MD analysis tools that were developed to analyse protein structures and some are in-house software. Although, there is continued increase in computational power, it is noted that there are a limited number of studies conducted using MD simulation in the area of LBDDS. It would be very useful if continued efforts will be made in the development of more improved force fields, various types of analysis tools, and more accurate and easy to use constant pH molecular dynamics (CpHMD) techniques to simulate and gaining detailed insights of very complex systems.

"It always seems impossible until it's done."

Nelson Mandela

CHAPTER SEVEN

EPILOGUE

7 EPILOGUE

My personal motivation of the present work was the development of an “*in-silico* formulation tool” as a new approach to predict the performance of lipid-based formulations by using molecular modelling method. I admit that this will not happen in a single PhD project. Still, I learned a lot about current approaches to the problem and, probably even more important, about the restrictions we have to live within this area. While there is a continual increment of computational power and efficient parallelisation on MD software, there are still significant shortcomings, resulting partly from the way force fields validated and partly from the underlying lack of experimental results in the validation process. While I frankly hope that one day a well optimised and easy to modify force field that describe all parameters of any molecule efficiently will be developed that ‘comprehends’ which structural or non-structural changes influence changes in biological processes. I also recognized that this goal is far from being achieved today and requires a great deal of effort.

8 REFERENCES

1. Pouton, C. W.; Porter, C. J. H., Formulation of lipid-based delivery system for oral administration: Materials, methods and strategies. *Advanced Drug Delivery Reviews* **2007**, 625-637.
2. Pouton, C. W., Lipid formulations for oral administration of drugs: non-emulsifying, self-emulsifying and 'self-microemulsifying' drug delivery systems. *Eur J Pharm Sci* **2000**, 11, S93-S98.
3. Tieleman, D. P.; Marrink, S. J.; Berendsen, H. J. C., A computer perspective of membranes: molecular dynamics studies of lipid bilayer systems. *Bba-Rev Biomembranes* **1997**, 1331 (3), 235-270.
4. (a) MacGregor, K. J.; Embleton, J. K.; Lacy, J. E.; Perry, E. A.; Solomon, L. J.; Seager, H.; Pouton, C. W., Influence of lipolysis on drug absorption from the gastrointestinal tract. *Advanced Drug Delivery Reviews* **1997**, 25 (1), 33-46; (b) Pouton, C. W., Formulation of poorly water-soluble drugs for oral administration: Physicochemical and physiological issues and the lipid formulation classification system. *Eur J Pharm Sci* **2006**, 29 (3-4), 278-287.
5. Porter, C. J. H.; Pouton, C. W.; Cuine, J. F.; Charman, W. N., Enhancing intestinal drug solubilisation using lipid-based delivery systems. *Advanced Drug Delivery Reviews* **2008**, 60 (6), 673-691.
6. Porter, C. J.; Trevaskis, N. L.; Charman, W. N., Lipids and lipid-based formulations: optimizing the oral delivery of lipophilic drugs. *Nat Rev Drug Discov* **2007**, 6 (3), 231-48.
7. Rabinow, B. E., Nanosuspensions in drug delivery. *Nat Rev Drug Discov* **2004**, 3 (9), 785-796.
8. Hauss, D. J., Oral Lipid-Based Formulations, Enhancing the Bioavailability of Poorly Water-Soluble Drugs. . *Informa Healthcare USA, New York* **2007**.
9. Porter, C. J.; Charman, W. N., In vitro assessment of oral lipid based formulations. *Adv Drug Deliv Rev* **2001**, 50 Suppl 1, S127-47.
10. Pouton, C. W., Self-Emulsifying Drug Delivery Systems - Assessment of the Efficiency of Emulsification. *Int J Pharmaceut* **1985**, 27 (2-3), 335-348.
11. Wakerly, M. G.; Pouton, C. W.; Meakin, B. J.; Morton, F. S., Self-Emulsification of Vegetable Oil-Nonionic Surfactant Mixtures - a Proposed Mechanism of Action. *Acs Symposium Series* **1986**, 311, 242-255.
12. Pouton, C. W., Formulation of self-emulsifying drug delivery systems. *Advanced Drug Delivery Reviews* **1997**, 25 (1), 47-58.

13. (a) Uddin, M. H.; Rodriguez, C.; Watanabe, K.; Lopez-Quintela, A.; Kato, T.; Furukawa, H.; Harashima, A.; Kunieda, H., Phase behavior and formation of reverse cubic phase based emulsion in water/poly(oxyethylene) poly(dimethylsiloxane) surfactants/silicone oil systems. *Langmuir* **2001**, *17* (17), 5169-5175; (b) Fendler, J. H., Membrane Mimetic Chemistry. *Wiley, New York* **1982**.
14. Lindfield, W. M., Anionic Surfactants. *Marcel Dekker, New York* **1976**.
15. Mckenzie, D. A., Non-Ionic Surfactants. *J Am Oil Chem Soc* **1978**, *55* (1), 93-97.
16. Jungerman, E., Cationic Surfactants. *Marcel Dekker, New York* **1970**.
17. (a) Bachar, M.; Brunelle, P.; Tieleman, D. P.; Rauk, A., Molecular dynamics simulation of a polyunsaturated lipid bilayer susceptible to lipid peroxidation. *J Phys Chem B* **2004**, *108* (22), 7170-7179; (b) Chernomordik, L. V.; Zimmerberg, J., Bending Membranes to the Task - Structural Intermediates in Bilayer Fusion. *Curr Opin Struc Biol* **1995**, *5* (4), 541-547; (c) Staggars, J. E.; Hernell, O.; Stafford, R. J.; Carey, M. C., Physical-chemical behavior of dietary and biliary lipids during intestinal digestion and absorption. 1. Phase behavior and aggregation states of model lipid systems patterned after aqueous duodenal contents of healthy adult human beings. *Biochemistry* **1990**, *29* (8), 2028-40; (d) Hernell, O.; Staggars, J. E.; Carey, M. C., Physical-chemical behavior of dietary and biliary lipids during intestinal digestion and absorption. 2. Phase analysis and aggregation states of luminal lipids during duodenal fat digestion in healthy adult human beings. *Biochemistry* **1990**, *29* (8), 2041-56; (e) Mazer, N. A.; Benedek, G. B.; Carey, M. C., Quasielastic light-scattering studies of aqueous biliary lipid systems. Mixed micelle formation in bile salt-lecithin solutions. *Biochemistry* **1980**, *19* (4), 601-15; (f) Tardieu, A.; Luzzati, V.; Reman, F. C., Structure and Polymorphism of Hydrocarbon Chains of Lipids - Study of Lecithin-Water Phases. *Journal of molecular biology* **1973**, *75* (4), 711-8; (g) Tardieu, A.; Luzzati, V., Structure and polymorphism of the hydrocarbon chains of lipids: a study of lecithin-water phases. *J Mol Biol* **1973**, *75* (4), 711-33; (h) Small, D. M.; Bourges, M. C.; Dervichian, D. G., The biophysics of lipidic associations. I. The ternary systems: lecithin-bile salt-water. *Biochim Biophys Acta* **1966**, *125* (3), 563-80; (i) Small, D. M.; Bourges, M.; Dervichian, D. G., Ternary and quaternary aqueous systems containing bile salt, lecithin, and cholesterol. *Nature* **1966**, *211* (5051), 816-8.
18. Kossena, G. A.; Charman, W. N.; Boyd, B. J.; Porter, C. J., A novel cubic phase of medium chain lipid origin for the delivery of poorly water soluble drugs. *J Control Release* **2004**, *99* (2), 217-29.
19. (a) Salentinig, S.; Sagalowicz, L.; Glatter, O., Self-Assembled Structures and pK(a) Value of Oleic Acid in Systems of Biological Relevance. *Langmuir* **2010**, *26* (14), 11670-11679; (b) Cistola, D. P.; Hamilton, J. A.; Jackson, D.; Small, D. M., Ionization and phase behavior of fatty acids in water: application of the Gibbs phase rule. *Biochemistry* **1988**, *27* (Copyright (C) 2011 U.S. National Library of Medicine.), 1881-8.
20. Saad, A. L. G.; El-Kholy, S. A.; Barakat, Y., Relaxation behavior and dipole moment of some nonionics. Part 1. CMC and thermodynamics of ethoxylated oleic acid in nonaqueous medium. *Z. Phys. Chem. (Munich)* **1998**, *203* (Copyright (C) 2011 American Chemical Society (ACS). All Rights Reserved.), 73-85.

21. (a) Kunieda, H.; Uddin, M. H.; Horii, M.; Furukawa, H.; Harashima, A., Effect of hydrophilic- and hydrophobic-chain lengths on the phase behavior of A-B-type silicone surfactants in water. *J Phys Chem B* **2001**, 105 (23), 5419-5426; (b) Kunieda, H.; Kabir, H.; Aramaki, K.; Shigeta, K., Phase behavior of mixed polyoxyethylene-type nonionic surfactants in water. *J Mol Liq* **2001**, 90 (1-3), 157-166.
22. Silverthorn, D. G., *Human Physiology*. sixth ed.; Pearson Education, Inc., 2013.
23. Williams, H. D.; Trevaskis, N. L.; Yeap, Y. Y.; Anby, M. U.; Pouton, C. W.; Porter, C. J. H., Lipid-Based Formulations and Drug Supersaturation: Harnessing the Unique Benefits of the Lipid Digestion/Absorption Pathway. *Pharmaceut Res* **2013**, 30 (12), 2976-2992.
24. Persson, E. M.; Nilsson, R. G.; Hansson, G. I.; Lofgren, L. J.; Liback, F.; Knutson, L.; Abrahamsson, B.; Lennernas, H., A clinical single-pass perfusion investigation of the dynamic in vivo secretory response to a dietary meal in human proximal small intestine. *Pharmaceut Res* **2006**, 23 (4), 742-751.
25. Maldonado-Valderrama, J. W., P.; Macierzanka, A.; Mackie, A., The role of bile salts in digestion. *Adv Colloid Interface Sci* **2011**, 165 (1), 36-46.
26. (a) Gallo-Torres, H. E., Obligatory role of bile for the intestinal absorption of vitamin E. *Lipids* **1970**, 5 (4), 379-84; (b) Dowling, R. H.; Mack, E.; Small, D. M., Biliary lipid secretion and bile composition after acute and chronic interruption of the enterohepatic circulation in the Rhesus monkey. IV. Primate biliary physiology. *J Clin Invest* **1971**, 50 (9), 1917-26; (c) Warren, D. B.; Chalmers, D. K.; Hutchison, K.; Dang, W. B.; Pouton, C. W., Molecular dynamics simulations of spontaneous bile salt aggregation. *Colloid Surface A* **2006**, 280 (1-3), 182-193.
27. (a) Fini, A.; Roda, A., Chemical-Properties of Bile-Acids .4. Acidity Constants of Glycine-Conjugated Bile-Acids. *J Lipid Res* **1987**, 28 (7), 755-759; (b) Hofmann, A. F.; Roda, A., Physicochemical Properties of Bile-Acids and Their Relationship to Biological Properties - an Overview of the Problem. *J Lipid Res* **1984**, 25 (13), 1477-1489; (c) Carey, M. C., Bile-Acids and Bile-Salts - Ionization and Solubility Properties. *Hepatology* **1984**, 4 (5), S66-S71; (d) Small, D. M.; Cabral, D. J.; Cistola, D. P.; Parks, J. S.; Hamilton, J. A., The ionization behavior of fatty acids and bile acids in micelles and membranes. *Hepatology* **1984**, 4 (5 Suppl), 77S-79S; (e) Cabral, D. J.; Hamilton, J. A.; Small, D. M., The Ionization Behavior of Bile-Acids in Different Aqueous Environments. *J Lipid Res* **1986**, 27 (3), 334-343.
28. (a) Humberstone, A. J.; Charman, W. N., Lipid-based vehicles for the oral delivery of poorly water soluble drugs. *Advanced Drug Delivery Reviews* **1997**, 25 (1), 103-128; (b) Bakala N'Goma J-C.; Amara, S. D., K.; Jannin, V. and Carrière, F., Understanding the lipid-digestion processes in the GI tract before designing lipid-based drug-delivery systems. *Therapeutic delivery* **2012**, 3 (1), 105-124.
29. (a) Hoffman, N. E., Relationship between Uptake in-Vitro of Oleic Acid and Micellar Solubilization. *Biochimica Et Biophysica Acta* **1970**, 196 (2), 193-&; (b) Borgstrom, B., On the Mechanism of the Intestinal Fat Absorption .4. Metabolism of Lipids. *Acta Physiol Scand* **1952**, 25 (4), 291-314.

30. Mohsin, K., Design of Lipid-Based Formulations for Oral Administration of Poorly Water-Soluble Drug Fenofibrate: Effects of Digestion. *Aaps Pharmscitech* **2012**, 13 (2), 637-646.
31. (a) Farr, H. W., Fluid and Electrolyte Balance - with Special Reference to the Gastrointestinal Tract. *Am J Nurs* **1954**, 54 (7), 826-831; (b) Hoffman, N. E.; Simmonds, W. J.; Morgan, R. G. H., Effect of Micellar Solubilization on Mucosal Metabolism of Absorbed Glyceryl-1-Monoether. *Aust J Exp Biol Med* **1972**, 50 (Dec), 803-812; (c) Simmonds, W. J., Role of Micellar Solubilization in Lipid Absorption. *Aust J Exp Biol Med* **1972**, 50 (Aug), 403-&.
32. Williams, H. D.; Trevaskis, N. L.; Charman, S. A.; Shanker, R. M.; Charman, W. N.; Pouton, C. W.; Porter, C. J. H., Strategies to Address Low Drug Solubility in Discovery and Development. *Pharmacol Rev* **2013**, 65 (1), 315-499.
33. (a) Yeap, Y. Y.; Trevaskis, N. L.; Porter, C. J. H., Lipid Absorption Triggers Drug Supersaturation at the Intestinal Unstirred Water Layer and Promotes Drug Absorption from Mixed Micelles. *Pharmaceut Res* **2013**, 30 (12), 3045-3058; (b) Yeap, Y. Y.; Trevaskis, N. L.; Quach, T.; Tso, P.; Charman, W. N.; Porter, C. J. H., Intestinal Bile Secretion Promotes Drug Absorption from Lipid Colloidal Phases via Induction of Supersaturation. *Mol Pharmaceut* **2013**, 10 (5), 1874-1889.
34. (a) Kleberg, K.; Jacobsen, J.; Mullertz, A., Characterising the behaviour of poorly water soluble drugs in the intestine: application of biorelevant media for solubility, dissolution and transport studies. *J Pharm Pharmacol* **2010**, 62 (11), 1656-1668; (b) Kleberg, K.; Jacobsen, F.; Fatouros, D. G.; Mullertz, A., Biorelevant Media Simulating Fed State Intestinal Fluids: Colloid Phase Characterization and Impact on Solubilization Capacity. *J Pharm Sci-Us* **2010**, 99 (8), 3522-3532.
35. (a) Anby, M. U.; Williams, H. D.; McIntosh, M.; Benameur, H.; Edwards, G. A.; Pouton, C. W.; Porter, C. J. H., Lipid Digestion as a Trigger for Supersaturation: Evaluation of the Impact of Supersaturation Stabilization on the in Vitro and in Vivo Performance of Self-Emulsifying Drug Delivery Systems. *Mol Pharmaceut* **2012**, 9 (7), 2063-2079; (b) Williams, H. D.; Sassene, P.; Kleberg, K.; Calderone, M.; Igonin, A.; Jule, E.; Vertommen, J.; Blundell, R.; Benameur, H.; Mullertz, A.; Pouton, C. W.; Porter, C. J. H.; Consortium, L., Toward the Establishment of Standardized In Vitro Tests for Lipid-Based Formulations, Part 3: Understanding Supersaturation Versus Precipitation Potential During the In Vitro Digestion of Type I, II, IIIA, IIIB and IV Lipid-Based Formulations. *Pharmaceut Res* **2013**, 30 (12), 3059-3076; (c) Williams, H. D.; Sassene, P.; Kleberg, K.; Bakala-N'Goma, J. C.; Calderone, M.; Jannin, V.; Igonin, A.; Partheil, A.; Marchaud, D.; Jule, E.; Vertommen, J.; Maio, M.; Blundell, R.; Benameur, H.; Carriere, F.; Mullertz, A.; Porter, C. J. H.; Pouton, C. W., Toward the establishment of standardized in vitro tests for lipid-based formulations, part 1: Method parameterization and comparison of in vitro digestion profiles across a range of representative formulations. *J Pharm Sci-Us* **2012**, 101 (9), 3360-3380; (d) Yeap, Y. Y.; Trevaskis, N. L.; Porter, C. J. H., The Potential for Drug Supersaturation during Intestinal Processing of Lipid-Based Formulations May Be Enhanced for Basic Drugs. *Mol Pharmaceut* **2013**, 10 (7), 2601-2615.

36. Berne, B. J.; Pecora, R., *Light Scattering, With Applications to Chemistry, Biology and Physics. Dover Publications Inc.* **2003**.
37. Johnson, C. S., Diffusion ordered nuclear magnetic resonance spectroscopy: principles and applications. *Prog Nucl Mag Res Sp* **1999**, 34 (3-4), 203-256.
38. Leach, A., *Molecular Modeling: Principle and applications*. Second ed.; Prentice-Hall: 2001.
39. Parrinello, M.; Rahman, A., Polymorphic Transitions in Single-Crystals - a New Molecular-Dynamics Method. *J Appl Phys* **1981**, 52 (12), 7182-7190.
40. King, D. T.; Warren, D. B.; Pouton, C. W.; Chalmers, D. K., Using Molecular Dynamics to Study Liquid Phase Behavior: Simulations of the Ternary Sodium Laurate/Sodium Oleate/Water System. *Langmuir* **2011**, 27 (18), 11381-11393.
41. Shvab, I.; Sadus, R. J., Intermolecular potentials and the accurate prediction of the thermodynamic properties of water. *Journal of Chemical Physics* **2013**, 139 (19).
42. Vega, C.; Abascal, J. L., Simulating water with rigid non-polarizable models: a general perspective. *Phys Chem Chem Phys* **2011**, 13 (44), 19663-88.
43. Spoel, D. v. d.; Lindahl, E.; Hess, B.; van Buuren, A. R.; Apol, E.; Meulenhoff, P. J.; Tieleman, D. P.; Sijbers, A. L. T. M.; Feenstra, K. A.; Drunen, R. v.; Berendsen, H. J. C., *Gromacs User Manual version 4.5*, www.gromacs.org 2005.
44. Lindahl, E.; Hess, B.; van der Spoel, D., GROMACS 3.0: a package for molecular simulation and trajectory analysis. *J Mol Model* **2001**, 7 (8), 306-317.
45. Chalmers, D. K.; Roberts, B. P., *Silico: A Perl Molecular Toolkit*. <http://silico.sourceforge.net> **2010**.
46. (a) Horta, B. H., B. A. C.; Fuchs, P. F. J.; van Gunsteren, W. F.; Hunenberger, P. H., New Interaction Parameters for Oxygen Compounds in the GROMOS Force Field: Improved Pure-Liquid and Solvation Properties for Alcohols, Ethers, Aldehydes, Ketones, Carboxylic Acids, and Esters. *Journal of Chemical Theory and Computation* **2011**, 7 (4), 1016-1031; (b) Hess, B.; van der Vegt, N. F. A., Hydration thermodynamic properties of amino acid analogues: A systematic comparison of biomolecular force fields and water models. *J Phys Chem B* **2006**, 110 (35), 17616-17626.
47. Oostenbrink, C.; Villa, A.; Mark, A. E.; Van Gunsteren, W. F., A biomolecular force field based on the free enthalpy of hydration and solvation: The GROMOS force-field parameter sets 53A5 and 53A6. *J Comput Chem* **2004**, 25 (13), 1656-1676.
48. Wendoloski, J. J.; Kimatian, S. J.; Schutt, C. E.; Salemme, F. R., Molecular-Dynamics Simulation of a Phospholipid Micelle. *Science* **1989**, 243 (4891), 636-638.
49. Wymore, T.; Gao, X. F.; Wong, T. C., Molecular dynamics simulation of the structure and dynamics of a dodecylphosphocholine micelle in aqueous solution. *J Mol Struct* **1999**, 485, 195-210.

50. Tieleman, D. P.; van der Spoel, D.; Berendsen, H. J. C., Molecular dynamics simulations of dodecylphosphocholine micelles at three different aggregate sizes: Micellar structure and chain relaxation. *J Phys Chem B* **2000**, *104* (27), 6380-6388.
51. Marrink, S. J.; Tieleman, D. P.; Mark, A. E., Molecular dynamics simulation of the kinetics of spontaneous micelle formation. *J Phys Chem B* **2000**, *104* (51), 12165-12173.
52. Marrink, S. J.; Lindahl, E.; Edholm, O.; Mark, A. E., Simulation of the spontaneous aggregation of phospholipids into bilayers. *J Am Chem Soc* **2001**, *123* (35), 8638-8639.
53. Marrink, S. J.; Tieleman, D. P., Molecular dynamics simulation of a lipid diamond cubic phase. *J Am Chem Soc* **2001**, *123* (49), 12383-12391.
54. Knecht, V.; Mark, A. E.; Marrink, S. J., Phase behavior of a phospholipid/fatty acid/water mixture studied in atomic detail. *J Am Chem Soc* **2006**, *128* (6), 2030-2034.
55. Warren, D. B.; Chalmers, D. K.; Pouton, C. W., Structure and dynamics of glyceride lipid formulations, with propylene glycol and water. *Mol Pharmaceut* **2009**, *6* (2), 604-14.
56. Janosi, L.; Gorfe, A. A., Simulating POPC and POPC/POPG Bilayers: Conserved Packing and Altered Surface Reactivity. *Journal of Chemical Theory and Computation* **2010**, *6* (10), 3267-3273.
57. (a) Carey, M. C.; Small, D. M., Micelle Formation by Bile-Salts - Physical-Chemical and Thermodynamic Considerations. *Arch Intern Med* **1972**, *130* (4), 506; (b) Kawamura, H.; Murata, Y.; Yamaguchi, T.; Igimi, H.; Tanaka, M.; Sugihara, G.; Kratochvil, J. P., Spin-Label Studies of Bile-Salt Micelles. *J Phys Chem-Us* **1989**, *93* (8), 3321-3326; (c) Giglio, E.; Loreti, S.; Pavel, N. V., Exafs - a New Approach to the Structure of Micellar Aggregates. *J Phys Chem-Us* **1988**, *92* (10), 2858-2862.
58. Turner, D. C.; Yin, F. C.; Kindt, J. T.; Zhang, H. L., Molecular Dynamics Simulations of Glycocholate-Oleic Acid Mixed Micelle Assembly. *Langmuir* **2010**, *26* (7), 4687-4692.
59. Marrink, S. J.; Mark, A. E., Molecular dynamics simulations of mixed micelles modeling human bile. *Biochemistry* **2002**, *41* (17), 5375-5382.
60. Sayyed-Ahmad, A.; Lichtenberger, L. M.; Gorfe, A. A., Structure and Dynamics of Cholic Acid and Dodecylphosphocholine-Cholic Acid Aggregates. *Langmuir* **2010**, *26* (16), 13407-13414.
61. Nichols, J. W.; Ozarowski, J., Sizing of lecithin-bile salt mixed micelles by size-exclusion high-performance liquid chromatography. *Biochemistry* **1990**, *29* (19), 4600-6.
62. Prakash, P.; Sayyed-Ahmad, A.; Zhou, Y.; Volk, D. E.; Gorenstein, D. G.; Dial, E.; Lichtenberger, L. M.; Gorfe, A. A., Aggregation behavior of ibuprofen, cholic acid and dodecylphosphocholine micelles. *Bba-Biomembranes* **2012**, *1818* (12), 3040-3047.
63. Watanabe, K.; Ferrario, M.; Klein, M. L., Molecular-Dynamics Study of a Sodium Octanoate Micelle in Aqueous-Solution. *J Phys Chem-Us* **1988**, *92* (3), 819-821.

64. Warren, D. B.; King, D.; Benameur, H.; Pouton, C. W.; Chalmers, D. K., Glyceride Lipid Formulations: Molecular Dynamics Modeling of Phase Behavior During Dispersion and Molecular Interactions Between Drugs and Excipients. *Pharm Res* **2013**.
65. Chandrasekhar, I.; Oostenbrink, C.; van Gunsteren, W. F., Simulating the physiological phase of hydrated DPPC bilayers: The ester moiety. *Soft Mater* **2004**, 2 (1), 27-45.
66. (a) Garrido, N. M.; Queimada, A. J.; Jorge, M.; Macedo, E. A.; Economou, I. G., 1-Octanol/Water Partition Coefficients of n-Alkanes from Molecular Simulations of Absolute Solvation Free Energies. *Journal of Chemical Theory and Computation* **2009**, 5 (9), 2436-2446; (b) Sangster, J., Octanol-Water Partition-Coefficients of Simple Organic-Compounds. *J Phys Chem Ref Data* **1989**, 18 (3), 1111-1229.
67. Christ, C. D.; Mark, A. E.; van Gunsteren, W. F., Feature Article Basic Ingredients of Free Energy Calculations: A Review. *J Comput Chem* **2010**, 31 (8), 1569-1582.
68. Jorgensen, W. L.; Briggs, J. M.; Contreras, M. L., Relative partition coefficients for organic solutes from fluid simulations. *The Journal of Physical Chemistry* **1990**, 94 (4), 1683-1686.
69. Christophe C., P. A., Free Energy Calculations - Theory and Applications in Chemistry and Biology. *Springer, Berlin Germany* **2007**.
70. Spoel, D. v. d.; Lindahl, E.; Hess, B.; van Buuren, A. R.; Apol, E.; Meulenhoff, P. J.; Tieleman, D. P.; Sijbers, A. L. T. M.; Feenstra, K. A.; Drunen, R. v.; Berendsen, H. J. C., *Gromacs User Manual version 4.0* www.gromacs.org. 2005.
71. Bennett, C. H., Efficient estimation of free energy differences from Monte Carlo data. *Journal of Computational Physics* **1976**, 22 (2), 245-268.
72. van Gunsteren, W. F. B., H. J. C. , Leap-frog Algorithm for Stochastic Dynamics. *Mol Simulat* **1988**, 1 (3), 173-185.
73. Mobley, D. L.; Bayly, C. I.; Cooper, M. D.; Shirts, M. R.; Dill, K. A., Small molecule hydration free energies in explicit solvent: An extensive test of fixed-charge atomistic simulations. *Journal of Chemical Theory Computation* **2009**, 5 (2), 350-358.
74. (a) Oliveira, C. A., Guimaraes C. R. W., Alencastro R. B. , Molecular Dynamics Study on Liquid 1-Octanol. Part 2. Water-Saturated 1-Octanol Solution. *International Journal of Quantum Chemistry* **2002**, 90, 786-791; (b) Marcus, Y., Structural Aspects of Water in 1-Octanol. *J Solution Chem* **1989**, 19.
75. Maestro, version 9.0. 2009.
76. Berendsen, H. J. C.; Postma, J. P. M.; van Gunsteren, W. F.; Hermans, J.; Pullman, B., Interaction models for water in relation to protein hydration. In *Intermolecular forces*, Pullman, B., Ed. D. Reidel Publishing Company: Dordrecht: 1981; pp 331-342.
77. Liu, D. C. N., J. , On the Limited Memory BFGS Method for Large Scale Optimazation. *Mathematical Programming* **1989**, 45 (3), 503-528.

78. Shirts, M. R.; Pitera, J. W.; Swope, W. C.; Pande, V. S., Extremely precise free energy calculations of amino acid side chain analogs: Comparison of common molecular mechanics force fields for proteins. *Journal of Chemical Physics* **2003**, 119 (11), 5740-5761.
79. Hess, B.; Bekker, H.; Berendsen, H. J. C.; Fraaije, J. G. E. M., LINCS: A linear constraint solver for molecular simulations. *J Comput Chem* **1997**, 18 (12), 1463-1472.
80. (a) Van der Spoel, D.; Lindahl, E.; Hess, B.; Groenhof, G.; Mark, A. E.; Berendsen, H. J. C., GROMACS: Fast, flexible, and free. *J Comput Chem* **2005**, 26 (16), 1701-1718; (b) Berendsen, H. J. C.; Vanderspoel, D.; Vandrunen, R., Gromacs - a Message-Passing Parallel Molecular-Dynamics Implementation. *Comput Phys Commun* **1995**, 91 (1-3), 43-56; (c) Bekker, H.; Berendsen, H. J. C.; Dijkstra, E. J.; Achterop, S.; Vondrumen, R.; Vanderspoel, D.; Sijbers, A.; Keegstra, H.; Reitsma, B.; Renardus, M. K. R., Gromacs - a Parallel Computer for Molecular-Dynamics Simulations. *Physics Computing '92* **1993**, 252-256.
81. van der Spoel, D.; Lindahl, E.; Hess, B.; van Buuren, A. R.; Apol, E.; Meulenhoff, P. J.; Tieleman, D. P.; Sijbers, A. L. T. M.; Feenstra, K. A.; van Drunen, R.; Berendsen, H. J. C., *GROMACS User Manual version 4.5.4*. 2010.
82. Anderson, P. M.; Wilson, M. R., Developing a force field for simulation of poly(ethylene oxide) based upon ab initio calculations of 1,2-dimethoxyethane. *Mol Phys* **2005**, 103 (1), 89-97.
83. Xue, Y.; O'Mara, M. L.; Surawski, P. P.; Trau, M.; Mark, A. E., Effect of poly(ethylene glycol) (PEG) spacers on the conformational properties of small peptides: a molecular dynamics study. *Langmuir* **2011**, 27 (1), 296-303.
84. (a) Begum, R.; Matsuura, H., Conformational properties of short poly(oxyethylene) chains in water studied by IR spectroscopy. *J Chem Soc Faraday T* **1997**, 93 (21), 3839-3848; (b) Matsuura, H.; Sagawa, T., Anomalous Conformational Behavior of Short Poly(Oxyethylene) Chains in Water - an Ft-Ir Spectroscopic Study. *J Mol Liq* **1995**, 65-6, 313-316; (c) Masatoki, S.; Takamura, M.; Matsuura, H.; Kamogawa, K.; Kitagawa, T., Raman-Spectroscopic Observations of Anomalous Conformational Behavior of Short Poly(Oxyethylene) Chains in Water. *Chem Lett* **1995**, (11), 991-992.
85. Garrido, N. M.; Queimada, A. n. J.; Jorge, M.; Macedo, E. n. A.; Economou, I. G., 1-Octanol/Water Partition Coefficients of n-Alkanes from Molecular Simulations of Absolute Solvation Free Energies. *J Chem Theory Comput* **2009**, 5 (9), 2436-2446.
86. (a) Shirts, M. R.; Pande, V. S., Comparison of efficiency and bias of free energies computed by exponential averaging, the Bennett acceptance ratio, and thermodynamic integration. *J Chem Phys* **2005**, 122 (14), 44107-44107; (b) de Ruiter, A.; Boresch, S.; Oostenbrink, C., Comparison of thermodynamic integration and Bennett acceptance ratio for calculating relative protein-ligand binding free energies. *J Comput Chem* **2013**, 34 (12), 1024-1034.
87. Lide, D. R., Editor, CRC handbook of chemistry and physics. *CRC Press*. **2009**.

88. Hansch, C.; Leo, A.; Hoekman, D. H.; Heller, S. R., *Exploring QSAR: Hydrophobic, Electronic, and Steric Constants*. American Chemical Society: 1995; Vol. 2.
89. Michielan, L.; Bacilieri, M.; Kaseda, C.; Moro, S., Prediction of the aqueous solvation free energy of organic compounds by using autocorrelation of molecular electrostatic potential surface properties combined with response surface analysis. *Bioorgan Med Chem* **2008**, 16 (10), 5733-5742.
90. Shirts, M. R.; Pande, V. S., Solvation free energies of amino acid side chain analogs for common molecular mechanics water models. *Journal of Chemical Physics* **2005**, 122 (13).
91. Shivakumar, D.; Williams, J.; Wu, Y. J.; Damm, W.; Shelley, J.; Sherman, W., Prediction of Absolute Solvation Free Energies using Molecular Dynamics Free Energy Perturbation and the OPLS Force Field. *Journal of Chemical Theory and Computation* **2010**, 6 (5), 1509-1519.
92. Horta, B. A. C.; Fuchs, P. F. J.; van Gunsteren, W. F.; Hünenberger, P. H., New Interaction Parameters for Oxygen Compounds in the GROMOS Force Field: Improved Pure-Liquid and Solvation Properties for Alcohols, Ethers, Aldehydes, Ketones, Carboxylic Acids, and Esters. *J Chem Theory Comput* **2011**, 7 (4), 1016–1031.
93. CRC Handbook of Chemistry and Physics. 91st (Internet Version 2011) ed.; Haynes, W. M., Ed. CRC Press/Taylor and Francis: Boca Raton, Florida, 2010. <http://www.hbcpnetbase.com>.
94. Månsson, M.; Sellers, P.; Stridh, G.; Sunner, S., Enthalpies of vaporization of some 1-substituted n-alkanes. *The Journal of Chemical Thermodynamics* **1977**, 9 (1), 91-97.
95. Meylan, W. M.; Howard, P. H., Atom/fragment contribution method for estimating octanol–water partition coefficients. *Journal of Pharmaceutical Sciences* **1995**, 84 (1), 83-92.
96. Leahy, D. E., Intrinsic molecular volume as a measure of the cavity term in linear solvation energy relationships: Octanol-water partition coefficients and aqueous solubilities. *Journal of Pharmaceutical Sciences* **1986**, 75 (7), 629-636.
97. Sangster, J., Octanol-Water Partition Coefficients of Simple Organic Compounds. *J Phys Chem Ref Data* **1989**, 18 (3), 1111-1229.
98. Hansch, C. L. A., *Substituent constants for correlation analysis in chemistry and biology*. Wiley: New York, 1979.
99. Inc., A. C. D., ACD/Labs Percepta Predictors. Toronto, ON, Canada, 2012; Vol. version 12.
100. Ishihama, Y.; Oda, Y.; Uchikawa, K.; Asakawa, N., Evaluation of Solute Hydrophobicity by Microemulsion Electrokinetic Chromatography. *Analytical Chemistry* **1995**, 67 (9), 1588-1595.

101. (a) Klimovich, P. V.; Mobley, D. L., Predicting hydration free energies using all-atom molecular dynamics simulations and multiple starting conformations. *J Comput Aid Mol Des* **2010**, *24* (4), 307-316; (b) Jorge, M.; Garrido, N. M.; Queimada, A. J.; Economou, I. G.; Macedo, E. A., Effect of the Integration Method on the Accuracy and Computational Efficiency of Free Energy Calculations Using Thermodynamic Integration. *Journal of Chemical Theory and Computation* **2010**, *6* (4), 1018-1027; (c) Garrido, N. M.; Queimada, A. J.; Jorge, M.; Economou, I. G.; Macedo, E. A., Molecular simulation of absolute hydration Gibbs energies of polar compounds. *Fluid Phase Equilibr* **2010**, *296* (2), 110-115; (d) Conrad Shyu, F. M. Y., Accurate Estimation of Solvation Free Energy Using Polynomial Fitting Techniques *Wiley Periodicals, Inc.* **2010**; (e) Winger, M.; de Vries, A. H.; van Gunsteren, W. F., Force-field dependence of the conformational properties of α,ω -dimethoxypolyethylene glycol. *Mol Phys* **2009**, *107* (13), 1313-1321; (f) Shivakumar, D.; Deng, Y. Q.; Roux, B., Computations of Absolute Solvation Free Energies of Small Molecules Using Explicit and Implicit Solvent Model. *Journal of Chemical Theory and Computation* **2009**, *5* (4), 919-930.
102. (a) Rao, B. G.; Singh, U. C., A free energy perturbation study of solvation in methanol and dimethyl sulfoxide. *J. Am. Chem. Soc.* **1990**, *112* (Copyright (C) 2011 American Chemical Society (ACS). All Rights Reserved.), 3803-11; (b) Jorgensen, W. L.; Briggs, J. M.; Contreras, M. L., Relative partition coefficients for organic solutes from fluid simulations. *J. Phys. Chem.* **1990**, *94* (Copyright (C) 2011 American Chemical Society (ACS). All Rights Reserved.), 1683-6.
103. Aubert, B.; *et al*, Observation of $B(+)\rightarrow\text{phiphiK}(+)$ and evidence for $B(0)\rightarrow\text{phiphiK}(0)$ below $\eta(c)$ threshold. *Phys Rev Lett* **2006**, *97* (26), 261803.
104. (a) Persson, E. M.; Gustafsson, A. S.; Carlsson, A. S.; Nilsson, R. G.; Knutson, L.; Forsell, P.; Hanisch, G.; Lennernas, H.; Abrahamsson, B., The effects of food on the dissolution of poorly soluble drugs in human and in model small intestinal fluids. *Pharmaceut Res* **2005**, *22* (12), 2141-2151; (b) Ogata, H.; Aoyagi, N.; Kaniwa, N.; Ejima, A., Effect of food on bioavailability of metronidazole from sugar-coated tablets having different dissolution rates in subjects with low gastric acidity. *International journal of clinical pharmacology, therapy, and toxicology* **1986**, *24* (6), 279-82; (c) Arumi, P.; Chauhan, K.; Charman, W. N., Accommodation and acuity under night-driving illumination levels. *Ophthalmic Physiol Opt* **1997**, *17* (4), 291-9; (d) Mattson, F. H.; Volpenhein, R. A., The Digestion and Absorption of Triglycerides. *The Journal of biological chemistry* **1964**, *239*, 2772-7; (e) Bisgaier, C. L.; Glickman, R. M., Intestinal synthesis, secretion, and transport of lipoproteins. *Annu Rev Physiol* **1983**, *45*, 625-36.
105. Van Speybroeck, M.; Williams, H. D.; Nguyen, T. H.; Anby, M. U.; Porter, C. J. H.; Augustijns, P., Incomplete Desorption of Liquid Excipients Reduces the in Vitro and in Vivo Performance of Self-Emulsifying Drug Delivery Systems Solidified by Adsorption onto an Inorganic Mesoporous Carrier. *Mol Pharmaceut* **2012**, *9* (9), 2750-2760.
106. Williams, H. D.; Sassene, P.; Kleberg, K.; Bakala-N'Goma, J. C.; Calderone, M.; Jannin, V.; Igonin, A.; Partheil, A.; Marchaud, D.; Jule, E.; Vertommen, J.; Maio, M.; Blundell, R.; Benameur, H.; Carriere, F.; Mullertz, A.; Porter, C. J.; Pouton, C. W., Toward the establishment of standardized in vitro tests for lipid-based formulations, part 1:

method parameterization and comparison of in vitro digestion profiles across a range of representative formulations. *J Pharm Sci* **2012**, 101 (9), 3360-80.

107. Bunge, A.; Muller, P.; Stockl, M.; Herrmann, A.; Huster, D., Characterization of the ternary mixture of sphingomyelin, POPC, and cholesterol: Support for an inhomogeneous lipid distribution at high temperatures. *Biophysical Journal* **2008**, 94 (7), 2680-2690.

108. Mazer, N. A.; Carey, M. C., Quasi-Elastic Light-Scattering-Studies of Aqueous Biliary Lipid Systems - Cholesterol Solubilization and Precipitation in Model Bile Solutions. *Biochemistry* **1983**, 22 (2), 426-442.

109. Marques, M., Dissolution Media Simulating Fasted and Fed States. *Dissolut Technol* **2004**, 18 (3), 16.

110. Warren, D. B.; Anby, M. U.; Hawley, A.; Boyd, B. J., Real Time Evolution of Liquid Crystalline Nanostructure during the Digestion of Formulation Lipids Using Synchrotron Small-Angle X-ray Scattering. *Langmuir* **2011**, 27 (15), 9528-9534.

111. (a) Chu, B.; Liu, T. B., Characterization of nanoparticles by scattering techniques. *J Nanopart Res* **2000**, 2 (1), 29-41; (b) Pecora, R., Dynamic light scattering measurement of nanometer particles in liquids. *J Nanopart Res* **2000**, 2 (2), 123-131.

112. Hoelke, B.; Gieringer, S.; Arlt, M.; Saal, C., Comparison of nephelometric, UV-spectroscopic, and HPLC methods for high-throughput determination of aqueous drug solubility in microtiter plates. *Anal Chem* **2009**, 81 (8), 3165-72.

113. Mijajlovic, M.; Wright, D.; Zivkovic, V.; Bi, J. X.; Biggs, M. J., Microfluidic hydrodynamic focusing based synthesis of POPC liposomes for model biological systems. *Colloid Surface B* **2013**, 104, 276-281.

114. (a) Booker, M. L.; Lamorte, W. W.; Ahrendt, S. A.; Lillemoe, K. D.; Pitt, H. A., Distribution of Phosphatidylcholine Molecular-Species between Mixed Micelles and Phospholipidcholesterol Vesicles in Human Gallbladder Bile - Dependence on Acyl Chain-Length and Unsaturation. *J Lipid Res* **1992**, 33 (10), 1485-1492; (b) Redinger, R. N.; Small, D. M., Bile Composition, Bile-Salt Metabolism and Gallstones. *Arch Intern Med* **1972**, 130 (4), 618-&.

115. Donovan, J. M.; Jackson, A. A.; Carey, M. C., Molecular species composition of inter-mixed micellar/vesicular bile salt concentrations in model bile: dependence upon hydrophilic-hydrophobic balance. *J Lipid Res* **1993**, 34 (7), 1131-40.

116. (a) Palacios, L. E.; Wang, T., Extraction of egg-yolk lecithin. *J Am Oil Chem Soc* **2005**, 82 (8), 565-569; (b) Palacios, L. E.; Wang, T., Egg-yolk lipid fractionation and lecithin characterization. *J Am Oil Chem Soc* **2005**, 82 (8), 571-578.

117. (a) Voelker, D. R., Lipid assembly into cell membranes. *N Comp Bioc* **2008**, 441-484; (b) van Meer, G.; Voelker, D. R.; Feigenson, G. W., Membrane lipids: where they are and how they behave. *Nat Rev Mol Cell Bio* **2008**, 9 (2), 112-124.

118. Williams, H. D.; Anby, M. U.; Sassene, P.; Kleberg, K.; Bakala-N'Goma, J. C.; Calderone, M.; Jannin, V.; Igonin, A.; Partheil, A.; Marchaud, D.; Jule, E.; Vertommen, J.; Maio, M.; Blundell, R.; Benameur, H.; Carriere, F.; Mullertz, A.; Pouton, C. W.; Porter, C. J. H., Toward the Establishment of Standardized in Vitro Tests for Lipid-Based Formulations. 2. The Effect of Bile Salt Concentration and Drug Loading on the Performance of Type I, II, IIIA, IIIB, and IV Formulations during in Vitro Digestion. *Mol Pharmaceut* **2012**, 9 (11), 3286-3300.
119. Birru, W. A.; Warren, D. B.; Heady, J. S.; Benameur, H.; Porter, C. J. H.; Pouton, C. W.; Chalmers, D. K., The phase behavior of model intestinal fluids studied using molecular dynamics simulations and NMR; the impact of lipid digestion. *Unpublished results* **2014**.
120. Pouton, C. W.; Porter, C. J. H., Formulation of lipid-based delivery system for oral administration: Materials, methods and strategies. *Adv Drug Deliv Rev.* **2007**, 625-637.
121. Williams, H. D.; Sassene, P.; Kleberg, K.; Bakala-N'Goma, J. C.; Calderone, M.; Jannin, V.; Igonin, A.; Partheil, A.; Marchaud, D.; Jule, E.; Vertommen, J.; Maio, M.; Blundell, R.; Benameur, H.; Carriere, F.; Mullertz, A.; Porter, C. J. H.; Pouton, C. W., Toward the establishment of standardized in vitro tests for lipid-based formulations, part 1: Method parameterization and comparison of in vitro digestion profiles across a range of representative formulations. *J Pharm Sci-Us* **2012**, 101 (9), 3360-3380.
122. Williams, H. D.; Sassene, P.; Kleberg, K.; Calderone, M.; Igonin, A.; Jule, E.; Vertommen, J.; Blundell, R.; Benameur, H.; Mullertz, A.; Pouton, C. W.; Porter, C. J.; Consortium, L., Toward the establishment of standardized in vitro tests for lipid-based formulations, part 3: understanding supersaturation versus precipitation potential during the in vitro digestion of type I, II, IIIA, IIIB and IV lipid-based formulations. *Pharmaceutical research* **2013**, 30 (12), 3059-76.
123. Whitcomb, D. C.; Lowe, M. E., Human Pancreatic Digestive Enzymes. *Dig Dis Sci* **2007**, 52, 1–17.
124. Birru, W. A.; Warren, D. B.; Williams, H. D.; Benameur, H.; Porter, C. J. H.; Chalmers, D. K.; Pouton, C. W., Digestion of phospholipids after secretion of bile into the duodenum changes the phase behaviour of bile components. *Submitted* **2014**.
125. Small, D. M., *Gastroenterology* **1967**, 52 (3), 607-610.
126. Mazer, N. A.; Benedek, G. B.; Carey, M. C., Quasielastic light-scattering studies of aqueous biliary lipid systems. Mixed micelle formation in bile salt-lecithin solutions. *Biochemistry* **1980**.
127. Ulmius, J.; Lindblom, G.; Wennerstrom, H.; Johansson, L. B.; Fontell, K.; Soderman, O.; Arvidson, G., Molecular organization in the liquid--crystalline phases of lecithin--sodium cholate-water systems studied by nuclear magnetic resonance. *Biochemistry* **1982**, 21 (7), 1553-60.
128. Marrink, S. J.; Mark, A. E., Molecular Dynamics Simulations of Mixed Micelles Modeling Human Bile. *Biochemistry* **2002**, 41, 5375–5382.

129. Warren, D. B.; Chalmers, D. K.; Pouton, C. W., Structure and dynamics of glyceride lipid formulations, with propylene glycol and water. *Mol Pharm* **2009**, 6 (2), 604-14.
130. Marques, M. R. C.; Loebenberg, R.; Almukainzi, M., Simulated Biological Fluids with Possible Application in Dissolution Testing. *Dissolut Technol* **2011**, 18 (3), 15-28.
131. Wu, D. H.; Chen, A. D.; Johnson, C. S., Advances in diffusion ordered NMR spectroscopy. *Bull Magn Reson* **1995**, 17 (1-4), 21-26.
132. Pronk, S.; Pall, S.; Schulz, R.; Larsson, P.; Bjelkmar, P.; Apostolov, R.; Shirts, M. R.; Smith, J. C.; Kasson, P. M.; van der Spoel, D.; Hess, B.; Lindahl, E., GROMACS 4.5: a high-throughput and highly parallel open source molecular simulation toolkit. *Bioinformatics* **2013**, 29 (7), 845-54.
133. Martinez-Seara, H.; Rog, T.; Karttunen, M.; Reigada, R.; Vattulainen, I., Influence of cis double-bond parametrization on lipid membrane properties: how seemingly insignificant details in force-field change even qualitative trends. *J Chem Phys* **2008**, 129 (10), 105103.
134. Miyamoto, S.; Kollman, P. A., Settle - an Analytical Version of the Shake and Rattle Algorithm for Rigid Water Models. *J Comput Chem* **1992**, 13 (8), 952-962.
135. Darden, T.; York, D.; Pedersen, L., Particle Mesh Ewald - an N.Log(N) Method for Ewald Sums in Large Systems. *The Journal of chemical physics* **1993**, 98 (12), 10089-10092.
136. Bussi, G.; Donadio, D.; Parrinello, M., Canonical sampling through velocity rescaling. *The Journal of chemical physics* **2007**, 126 (1).
137. Berendsen, H. J. C. P., J. P. M.; Vangunsteren, W. F.; Dinola, A.; Haak, J. R., Molecular Dynamics with Coupling to an External Bath. *The Journal of chemical physics* **1984**, 81 (8), 3684-3690.
138. Humphrey, W.; Dalke, A.; Schulten, K., VMD: Visual molecular dynamics. *J Mol Graphics* **1996**, 14 (1), 33-8.
139. *The PyMOL Molecular Graphics System, 1.5; Schrödinger, LLC.*
140. Cistola, D. P.; Atkinson, D.; Hamilton, J. A.; Small, D. M., Phase-Behavior and Bilayer Properties of Fatty-Acids - Hydrated 1-1 Acid Soaps. *Biochemistry* **1986**, 25 (10), 2804-2812.
141. Cistola, D. P.; Hamilton, J. A.; Jackson, D.; Small, D. M., Ionization and Phase-Behavior of Fatty-Acids in Water - Application of the Gibbs Phase Rule. *Biochemistry* **1988**, 27 (6), 1881-1888.
142. Kanicky, J. R.; Shah, D. O., Effect of Premicellar Aggregation on the pKa of Fatty Acid Soap Solutions. *Langmuir* **2003**, 19 (Copyright (C) 2011 American Chemical Society (ACS). All Rights Reserved.), 2034-2038.

143. Morrow, B. H.; Koenig, P. H.; Shen, J. K., Self-Assembly and Bilayer-Micelle Transition of Fatty Acids Studied by Replica-Exchange Constant pH Molecular Dynamics. *Langmuir* **2013**, 29, 14823–14830.
144. (a) Ijare, O. B.; Somashekar, B. S.; Gowda, G. A.; Sharma, A.; Kapoor, V. K.; Khetrpal, C. L., Quantification of glycine and taurine conjugated bile acids in human bile using ^1H NMR spectroscopy. *Magn Reson Med* **2005**, 53 (6), 1441-6; (b) Ijare, O. B.; Somashekar, B. S.; Jadegoud, Y.; Nagana Gowda, G. A., ^1H and ^{13}C NMR characterization and stereochemical assignments of bile acids in aqueous media. *Lipids* **2005**, 40 (10), 1031-41.
145. Darden, T.; York, D.; Pedersen, L., Particle Mesh Ewald - an $N\log(N)$ Method for Ewald Sums in Large Systems. *Journal of Chemical Physics* **1993**, 98 (12), 10089-10092.
146. Bussi, G.; Donadio, D.; Parrinello, M., Canonical sampling through velocity rescaling. *Journal of Chemical Physics* **2007**, 126 (1).
147. Berendsen, H. J. C. P., J. P. M.; Vangunsteren, W. F.; Dinola, A.; Haak, J. R., Molecular Dynamics with Coupling to an External Bath. *Journal of Chemical Physics* **1984**, 81 (8), 3684-3690.
148. Bakatselou, V.; Oppenheim, R. C.; Dressman, J. B., Solubilization and Wetting Effects of Bile-Salts on the Dissolution of Steroids. *Pharmaceut Res* **1991**, 8 (12), 1461-1469.
149. (a) Clarysse, S.; Brouwers, J.; Tack, J.; Annaert, P.; Augustijns, P., Intestinal drug solubility estimation based on simulated intestinal fluids: Comparison with solubility in human intestinal fluids. *Eur J Pharm Sci* **2011**, 43 (4), 260-269; (b) Bevernage, J.; Forier, T.; Brouwers, J.; Tack, J.; Annaert, P.; Augustijns, P., Excipient-Mediated Supersaturation Stabilization in Human Intestinal Fluids. *Mol Pharmaceut* **2011**, 8 (2), 564-570.
150. Armand, M.; Borel, P.; Dubois, C.; Senft, M.; Peyrot, J.; Salducci, J.; Lafont, H.; Lairon, D., Physicochemical Properties of Emulsions and Lipolysis of Dietary-Fat in the Human Stomach. *Gastroenterology* **1993**, 104 (4), A608-A608.
151. (a) Kaukonen, A. M.; Boyd, B. J.; Charman, W. N.; Porter, C. J. H., Drug solubilization behavior during in vitro digestion of suspension formulations of poorly water-soluble drugs in triglyceride lipids. *Pharmaceut Res* **2004**, 21 (2), 254-260; (b) Kaukonen, A. M.; Boyd, B. J.; Porter, C. J. H.; Charman, W. N., Drug solubilization behavior during in vitro digestion of simple triglyceride lipid solution formulations. *Pharmaceut Res* **2004**, 21 (2), 245-253; (c) Porter, C. J. H.; Kaukonen, A. M.; Boyd, B. J.; Edwards, G. A.; Charman, W. N., Susceptibility to lipase-mediated digestion reduces the oral bioavailability of danazol after administration as a medium-chain lipid-based microemulsion formulation. *Pharmaceut Res* **2004**, 21 (8), 1405-1412; (d) Porter, C. J. H.; Kaukonen, A. M.; Taillardat-Bertschinger, A.; Boyd, B. J.; O'Connor, J. M.; Edwards, G. A.; Charman, W. N., Use of in vitro lipid digestion data to explain the in vivo performance of triglyceride-based oral lipid formulations of poorly water-soluble drugs: Studies with halofantrine. *J Pharm Sci-U.S.* **2004**, 93 (5), 1110-1121.

152. (a) Kossena, G. A.; Charman, W. N.; Boyd, B. J.; Dunstan, D. E.; Porter, C. J., Probing drug solubilization patterns in the gastrointestinal tract after administration of lipid-based delivery systems: a phase diagram approach. *J Pharm Sci-Us* **2004**, 93 (2), 332-48; (b) Kossena, G. A.; Boyd, B. J.; Porter, C. J.; Charman, W. N., Separation and characterization of the colloidal phases produced on digestion of common formulation lipids and assessment of their impact on the apparent solubility of selected poorly water-soluble drugs. *J Pharm Sci-Us* **2003**, 92 (3), 634-48.
153. (a) Cuine, J. F.; McEvoy, C. L.; Charman, W. N.; Pouton, C. W.; Edwards, G. A.; Benameur, H.; Porter, C. J. H., Evaluation of the impact of surfactant digestion on the bioavailability of danazol after oral administration of lipidic self-emulsifying formulations to dogs. *J Pharm Sci-Us* **2008**, 97 (2), 995-1012; (b) Cuine, J. F.; Charman, W. N.; Pouton, C. W.; Edwards, G. A.; Porter, C. J. H., Increasing the proportional content of surfactant (Cremophor EL) relative to lipid in self-emulsifying lipid-based formulations of danazol reduces oral bioavailability in beagle dogs. *Pharmaceut Res* **2007**, 24 (4), 748-757.
154. Poger, D.; Van Gunsteren, W. F.; Mark, A. E., A new force field for simulating phosphatidylcholine bilayers. *J Comput Chem* **2010**, 31 (6), 1117-25.
155. (a) Hagler, A. T.; Ewig, C. S., On the Use of Quantum Energy Surfaces in the Derivation of Molecular-Force Fields. *Comput Phys Commun* **1994**, 84 (1-3), 131-155; (b) Mackerell, A. D.; Bashford, D.; Bellott, M.; Dunbrack, R. L.; Evanseck, J. D.; Field, M. J.; Fischer, S.; Gao, J.; Guo, H.; Ha, S.; Joseph-McCarthy, D.; Kuchnir, L.; Kuczera, K.; Lau, F. T. K.; Mattos, C.; Michnick, S.; Ngo, T.; Nguyen, D. T.; Prodhom, B.; Reiher, W. E.; Roux, B.; Schlenkrich, M.; Smith, J. C.; Stote, R.; Straub, J.; Watanabe, M.; Wiorkiewicz-Kuczera, J.; Yin, D.; Karplus, M., All-atom empirical potential for molecular modeling and dynamics studies of proteins. *J Phys Chem B* **1998**, 102 (18), 3586-3616.
156. (a) Nolan, J. P.; Lauer, S.; Prossnitz, E. R.; Sklar, L. A., Flow cytometry: a versatile tool for all phases of drug discovery. *Drug Discov Today* **1999**, 4 (4), 173-180; (b) Miller, C. R.; Vogel, R.; Surawski, P. P. T.; Corrie, S. R.; Ruhmann, A.; Trau, M., Biomolecular screening with novel organosilica microspheres. *Chem Commun* **2005**, (38), 4783-4785.
157. Chen, W.; Morrow, D. H.; Shi, C.; Shen, J. K., Recent development and application of constant pH molecular dynamics. *Mol Simulat* **2014**.

APPENDICES

9 APPENDICES

9.1 APPENDIX 1

Supporting information for Chapter 2

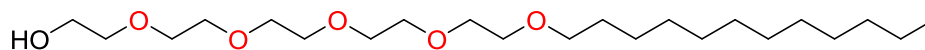
Table 9.1.1 Charge variation vs. $\log P$ values for Octanol

No.	CHARGE			Calculated $\log P$
	H	CH ₂	O	
CH-001	0.420	0.290	-0.710	4.40
CH-002	0.370	0.280	-0.650	4.03
CH-003	0.365	0.285	-0.650	4.09
CH-004	0.361	0.289	-0.650	3.77
CH-005	0.350	0.300	-0.650	3.90
CH-006	0.340	0.310	-0.650	4.05
CH-007	0.407	0.156	-0.563	4.64

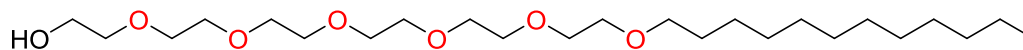
RED: GROMOS 53A6

GREEN: GRMOS 53A6_{oxy} (Horta *et. al.*)

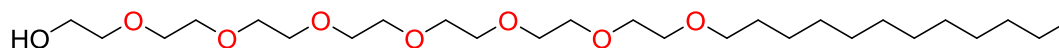
BLUE: GROMOS 53A6_{PEG} (this work)



pentaethylene glycol monododecyl ether (C12E5)



hexethylene glycol monododecyl ether (C12E6)



heptethylene glycol monododecyl ether C12E7)

Figure 9.1.1 Structures of selected PEG molecules

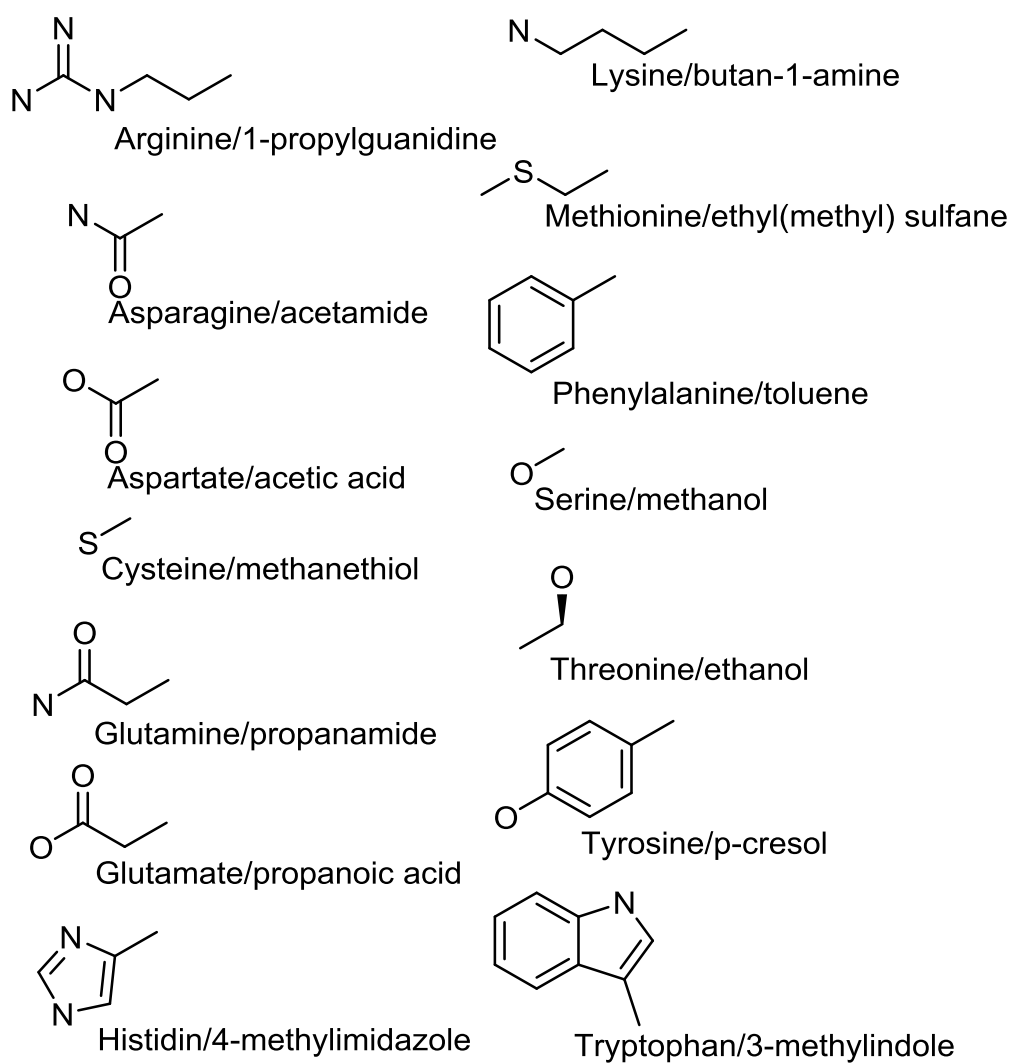


Figure 9.1.2 Structures of amino acid analogues

9.2 APPENDIX 2

Supporting information for Chapter 3

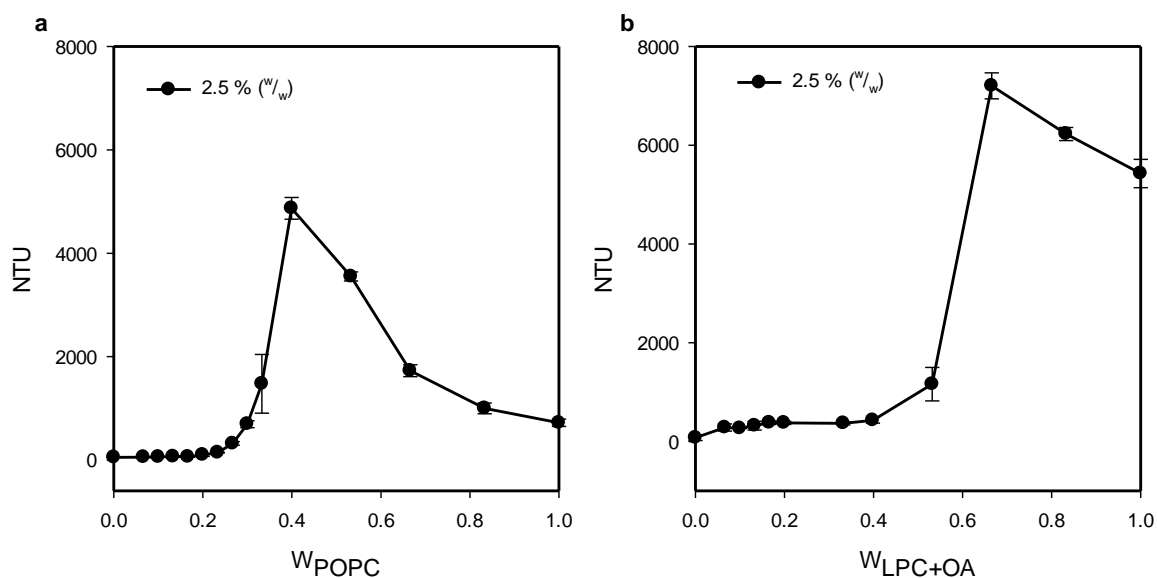


Figure 9.2.1 Complete solubilisation plot of POPC and digested POPC (LPC+OA) by GDX at varying total lipid concentrations 2.5 % w/w. See Figure 3 for description of X-axis. (a) Turbidity of POPC/GDX mixtures. (b) Turbidity of LPC+OA/GDX mixtures.

Table 9.2.1 Predicted phase boundary from regression analysis

% w/w	Mass Fraction	
	POPC	LPC+OA
0.25	0.54 [†]	0.55 [†]
0.5	0.45 [†]	0.49 [†]
1.0	0.31 [†]	0.49 [†]
1.5	0.27 [*]	0.53 [†]
2.0	0.27 [*]	0.54 [†]
2.25	0.28 [*]	0.49 [†]
2.5	0.29 [†]	0.52 [†]

^aThese fractions represent the phase boundaries calculated from turbidity curves using regression analysis. †The average of 3 data sets was taken for each solution in turbidity measurement. *The average of 2 data sets was taken for each solution in turbidity measurement.

9.3 APPENDIX 3

Supporting information for Chapter 4

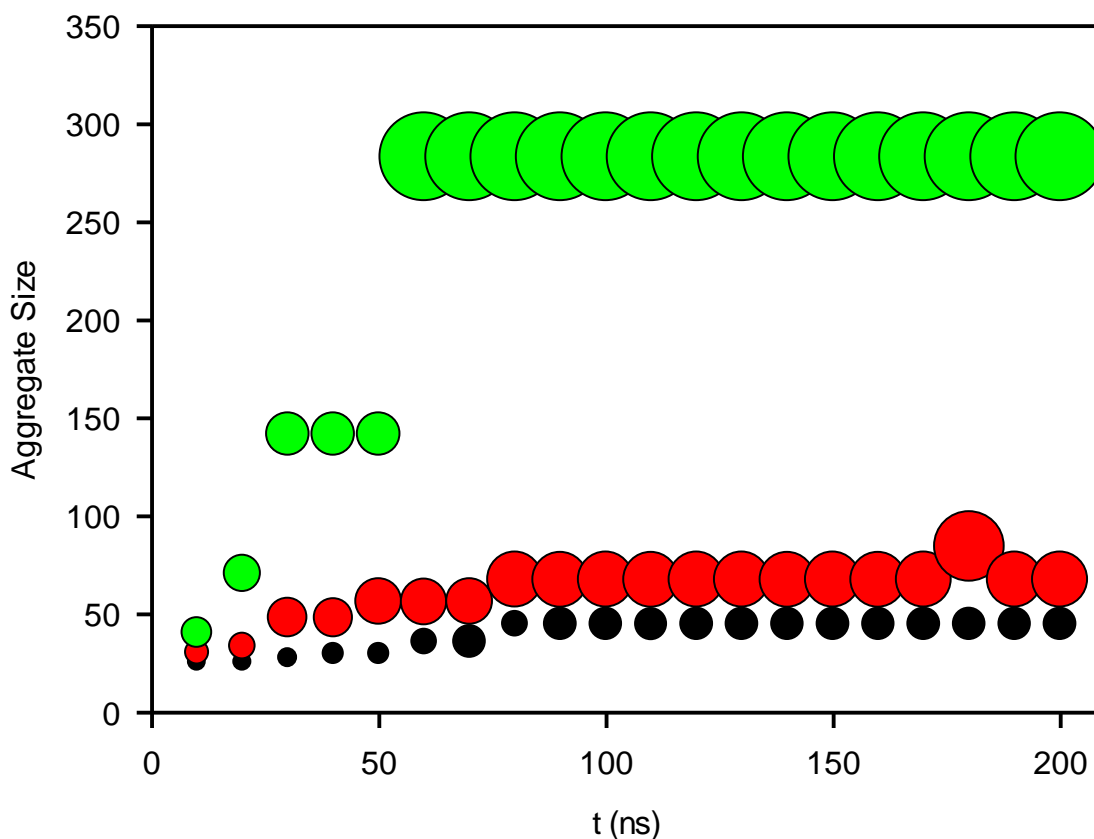


Figure 9.3.1 Progress of aggregation over the whole 200ns simulation time for simulation number 9 (black), 10 (red) and 11 (green). Simulation numbering is described in Table 4.2. The number of aggregated are calculated at every 10ns simulation.

Table 9.3.1 Spatial distribution probabilities of the lipid atoms and water used for generating probability surfaces around the GDX molecule in Figures 13.

Molecules	Spatial distribution probability						
	[C42]	[C24]	[N]	[P]	[C16]	[C18]	[OW]
POPC	57.18	57.79	35.64	40.04	-	-	-
LPC	-	-	47.64	72.78	134.19	-	-
OA	-	-	-	-	-	125.78	-
Water	-	-	-	-	-	-	28.24

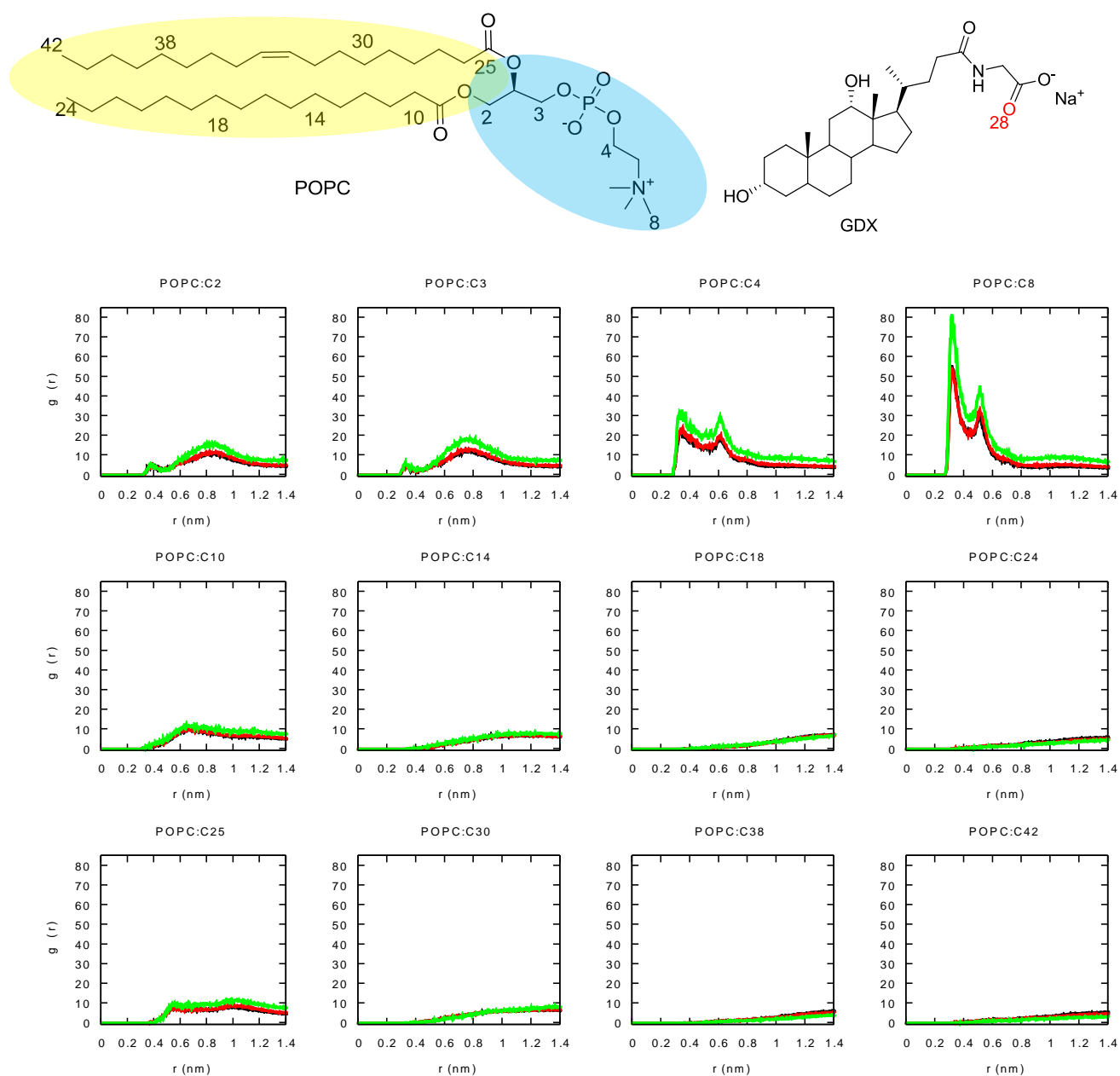


Figure 9.3.2 Radial distribution functions, $g(r)$, for ternary mixtures of POPC/GDX/water. Interactions of O28 atom of GDX with different atoms of POPC. Line coloring for % w/w POPC concentration 2 (black), 3 (red) and 4 (green).

a

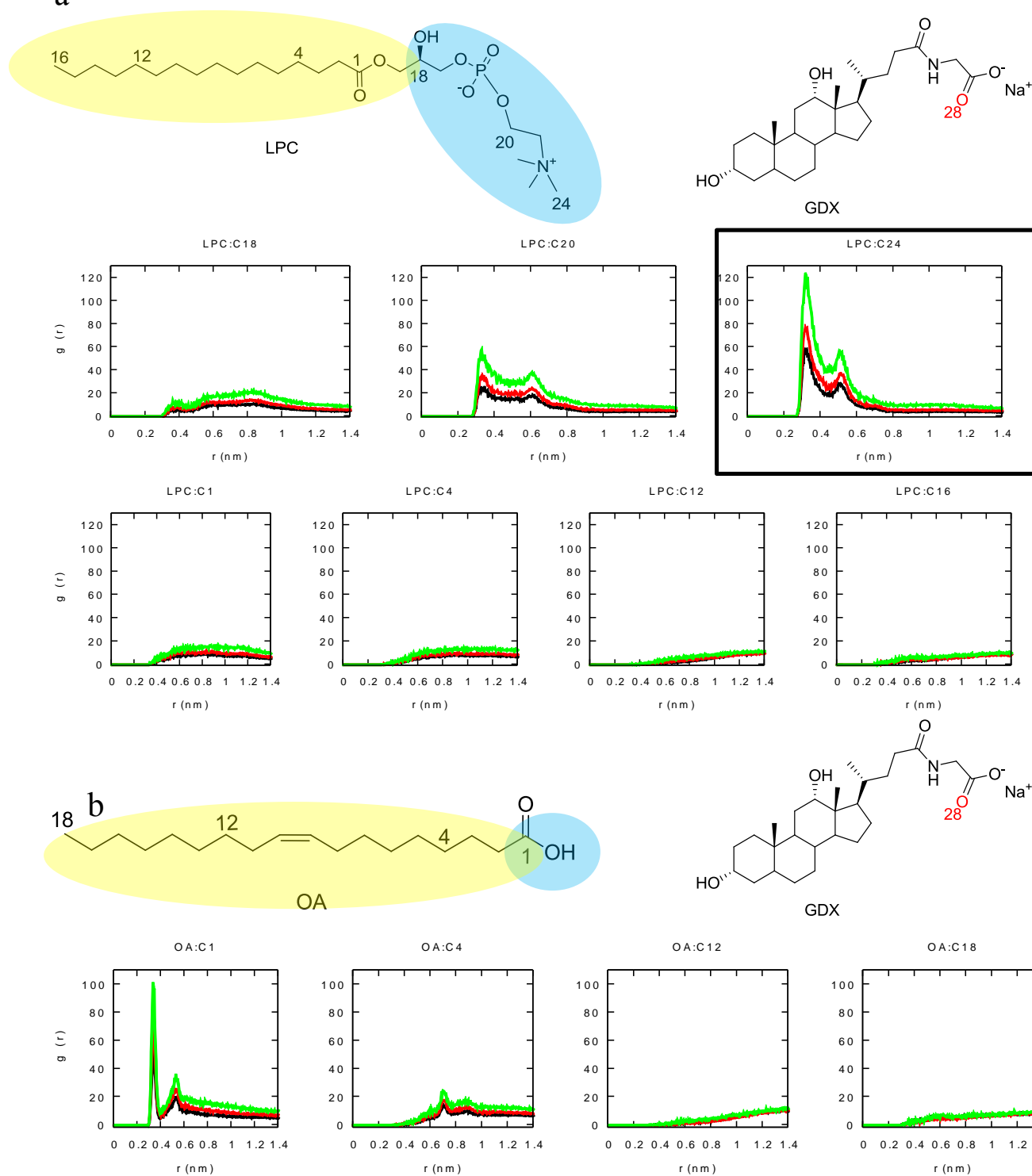


Figure 9.3.3 Radial distribution functions, $g(r)$, for ternary mixtures of LPC+OA/GDX/water. (a) Interaction of O28 atom of GDX with different atoms of LPC, (b) with different atoms of OA. Line coloring for % w/w POPC concentration 2 (black), 3 (red) and 4 (green).

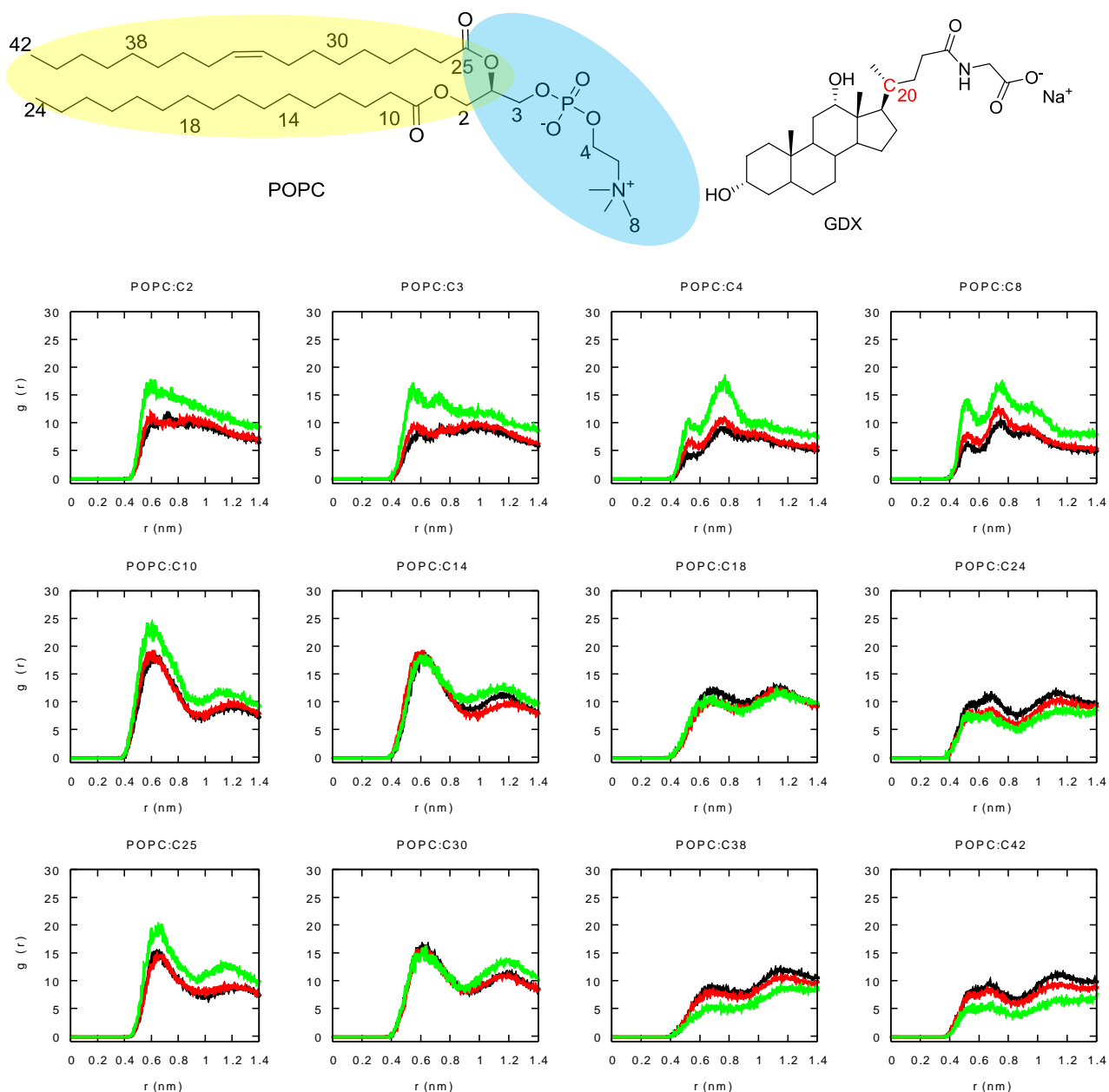


Figure 9.3.4 Radial distribution functions, $g(r)$, for ternary mixtures of POPC/GDX/water. Interaction of C20 atom of GDX with different atoms of POPC. Line coloring for % w/w POPC concentration 2 (black), 3 (red) and 4 (green).

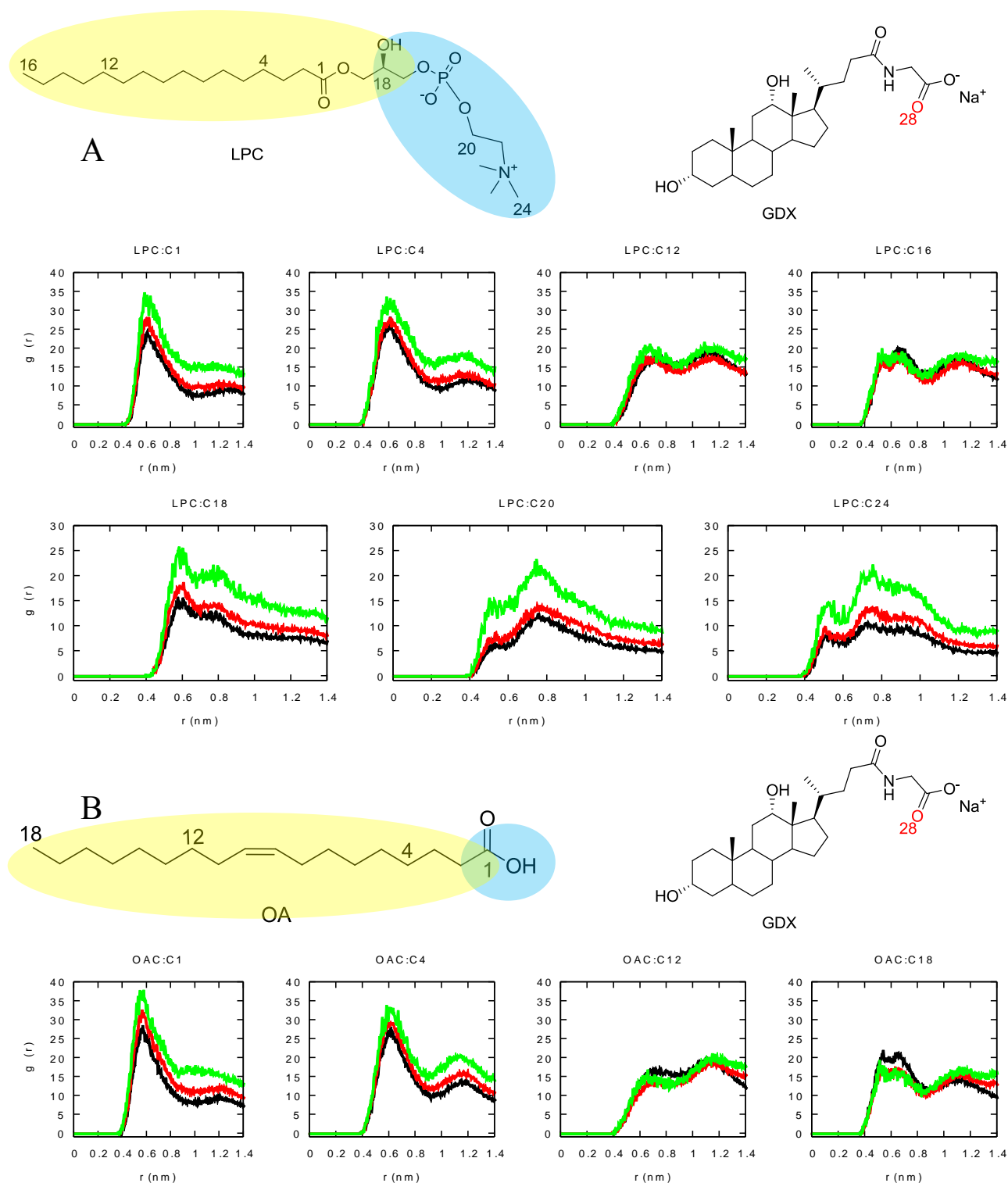


Figure 9.3.5 Radial distribution functions, $g(r)$, for ternary mixtures of LPC+OA/GDX/water. Interaction of C20 atom of GDX with different atoms of (A) LPC, (B) OA. Increasing LPC+OA concentration 2 (black), 3 (red) and 4 (green) % w/w.

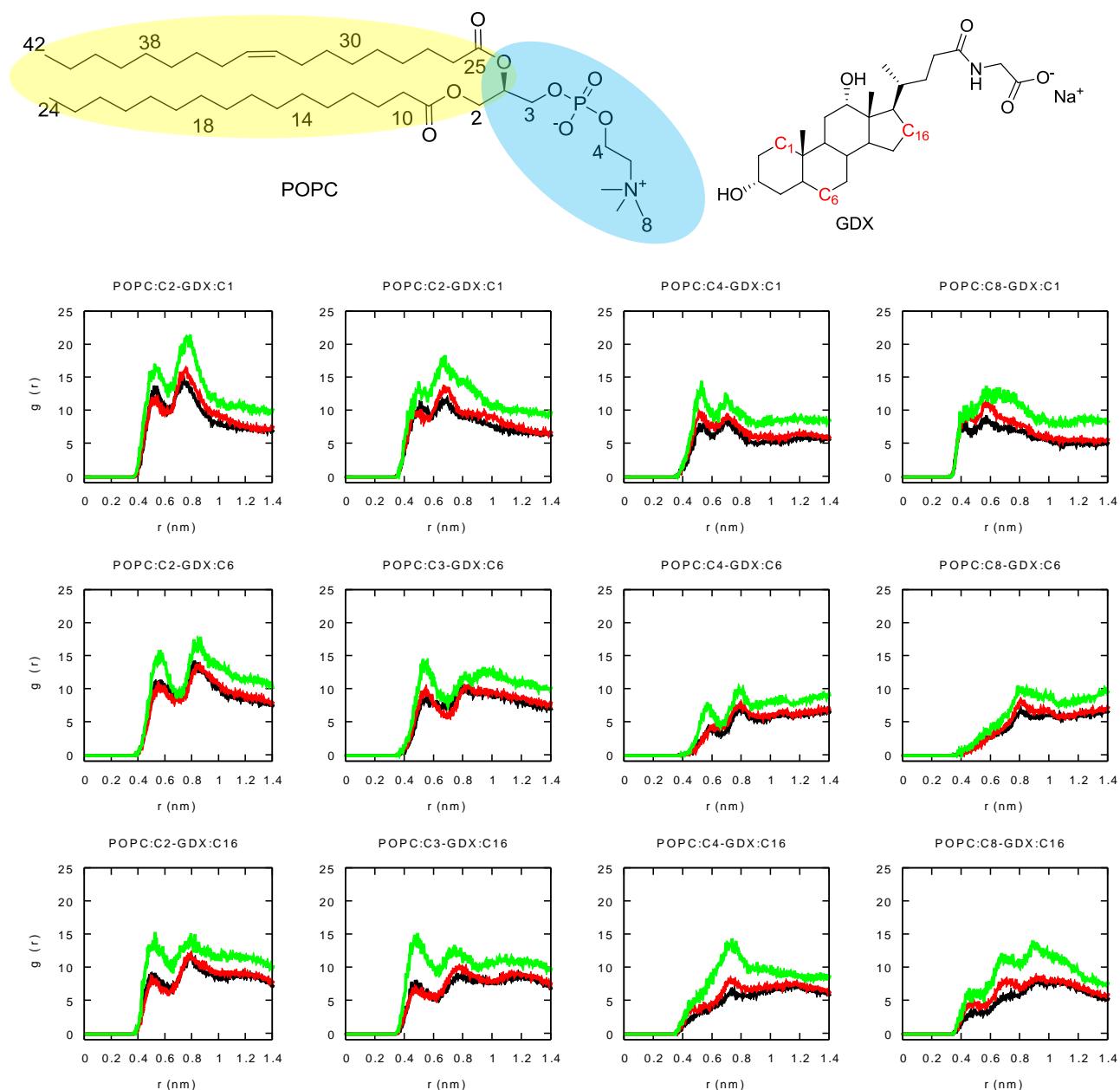


Figure 9.3.6 Radial distribution functions, $g(r)$, for ternary mixtures of POPC/GDX/water. Interactions of atoms C1, C6 and C16 of GDX with C2, C3, C4 and C8 atoms of POPC. Line coloring for % w/w POPC concentration 2 (black), 3 (red) and 4 (green).

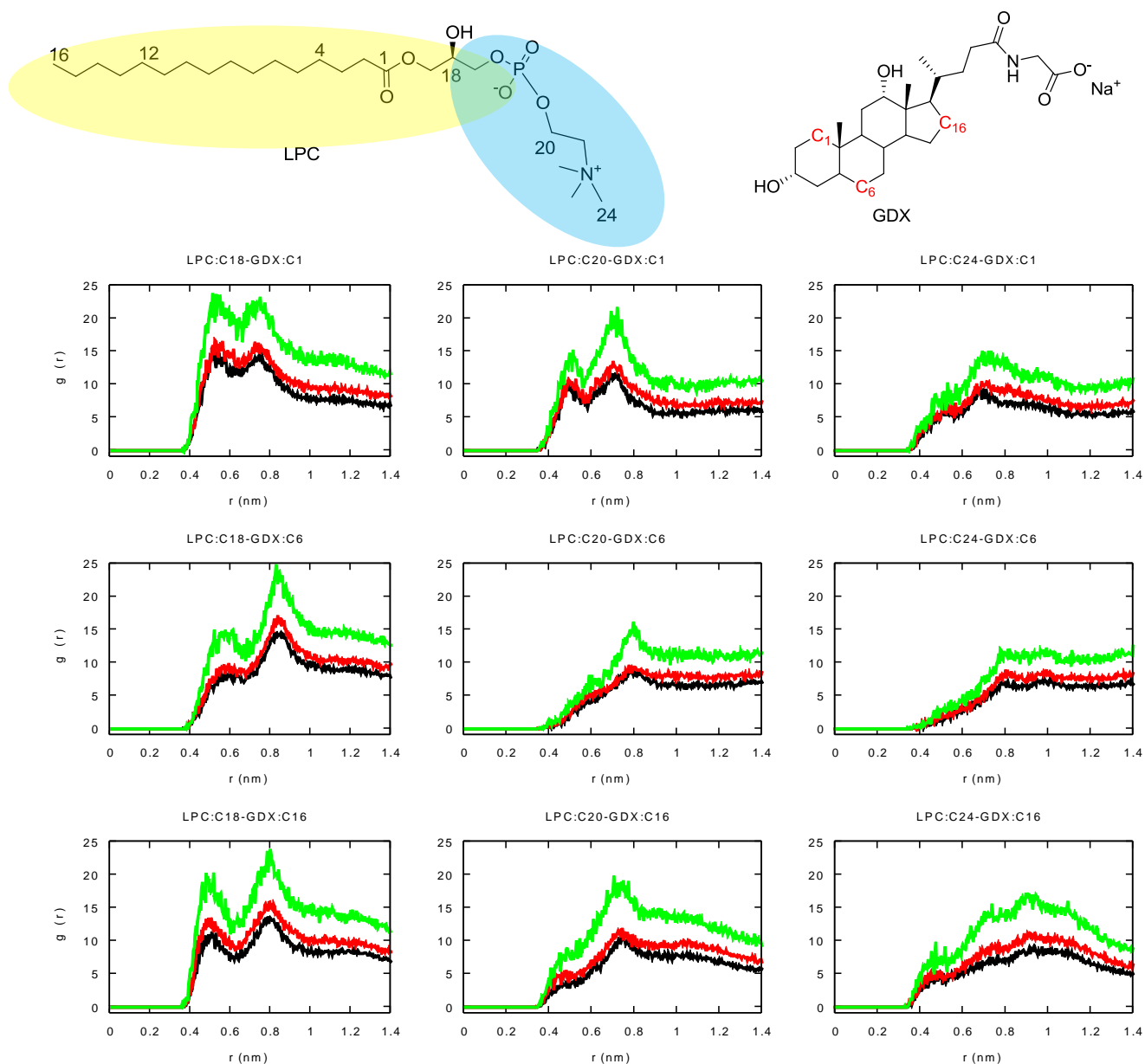


Figure 9.3.7 Radial distribution functions, $g(r)$, for ternary mixtures of LPC+OA/GDX/water. Interactions of atoms C1, C6 and C16 of GDX with C18, C20, and C24 of LPC. Increasing lipid concentration 2 (black), 3 (red) and 4 (green) % w/w

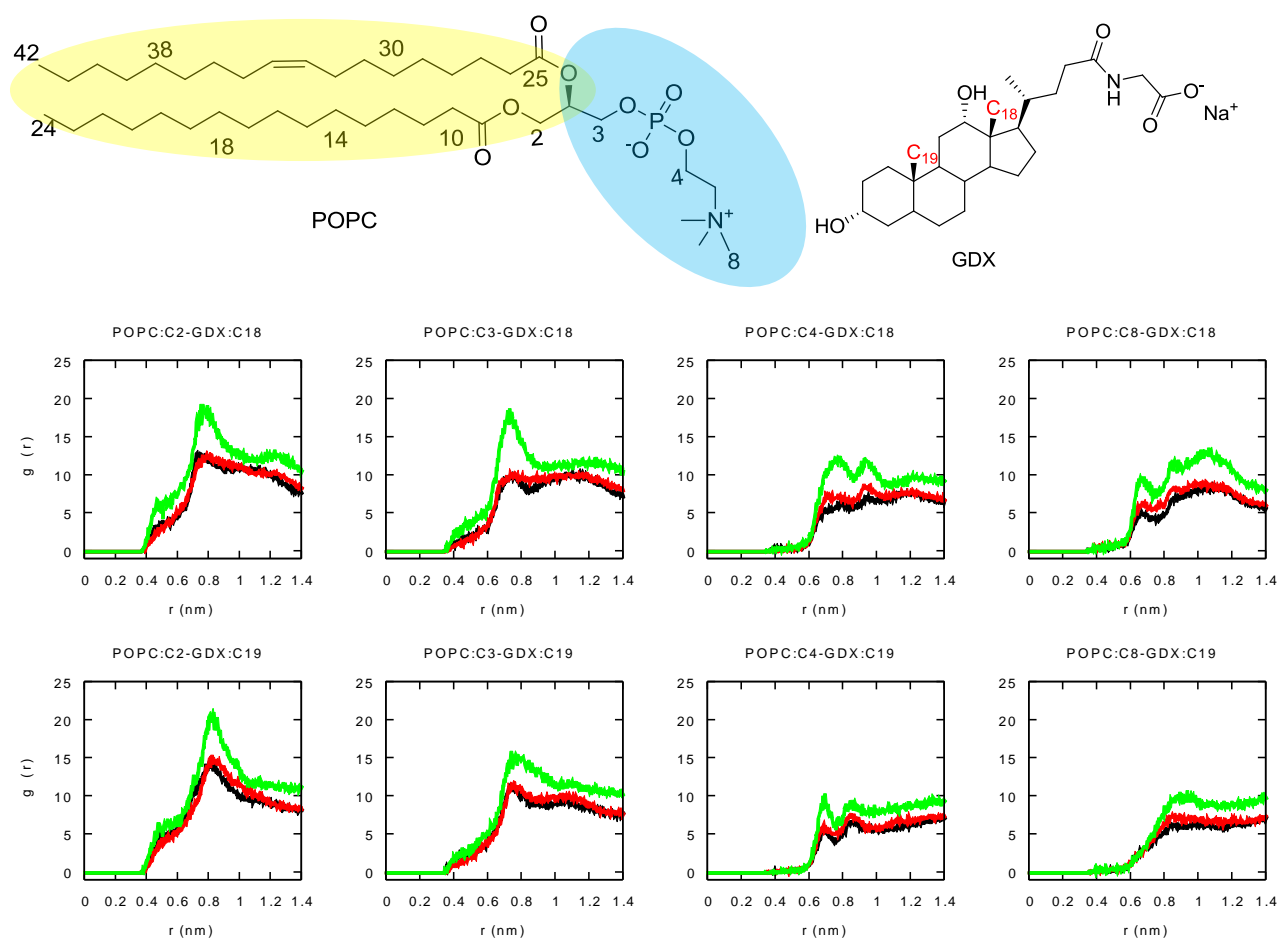


Figure 9.3.8 Radial distribution functions, $g(r)$, for ternary mixtures of POPC/GDX/water. Interaction of atoms C18 and C19 of GDX with C2, C3, C4 and C8 atoms of POPC. Line coloring for % w/w POPC concentration 2 (black), 3 (red) and 4 (green).

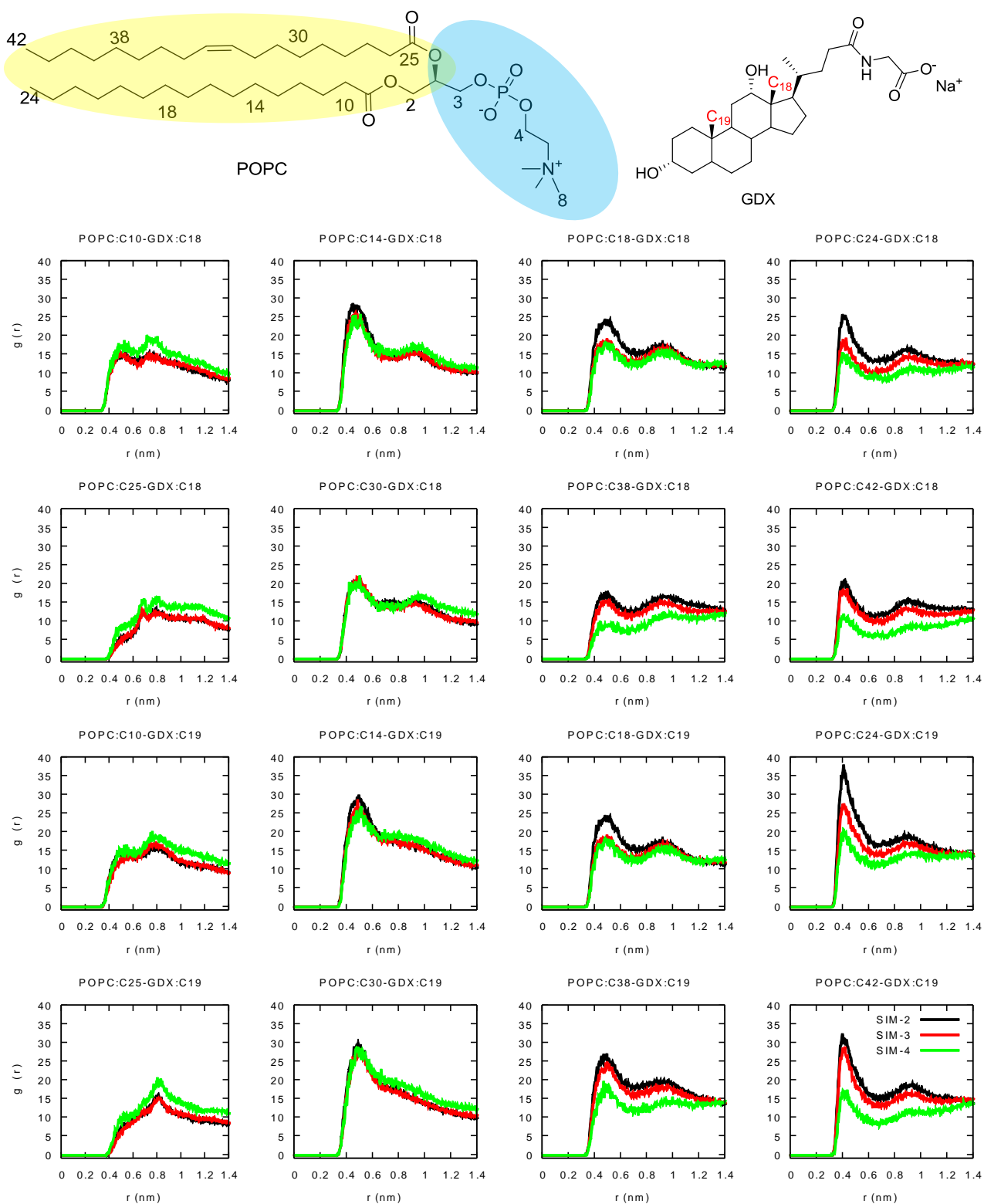


Figure 9.3.9 Radial distribution functions, $g(r)$, for ternary mixtures of POPC/GDX/water. Interaction of atoms C18 and C19 of GDX with hydrophobic tail of POPC. Line coloring for % w/w POPC concentration 2 (black), 3 (red) and 4 (green).

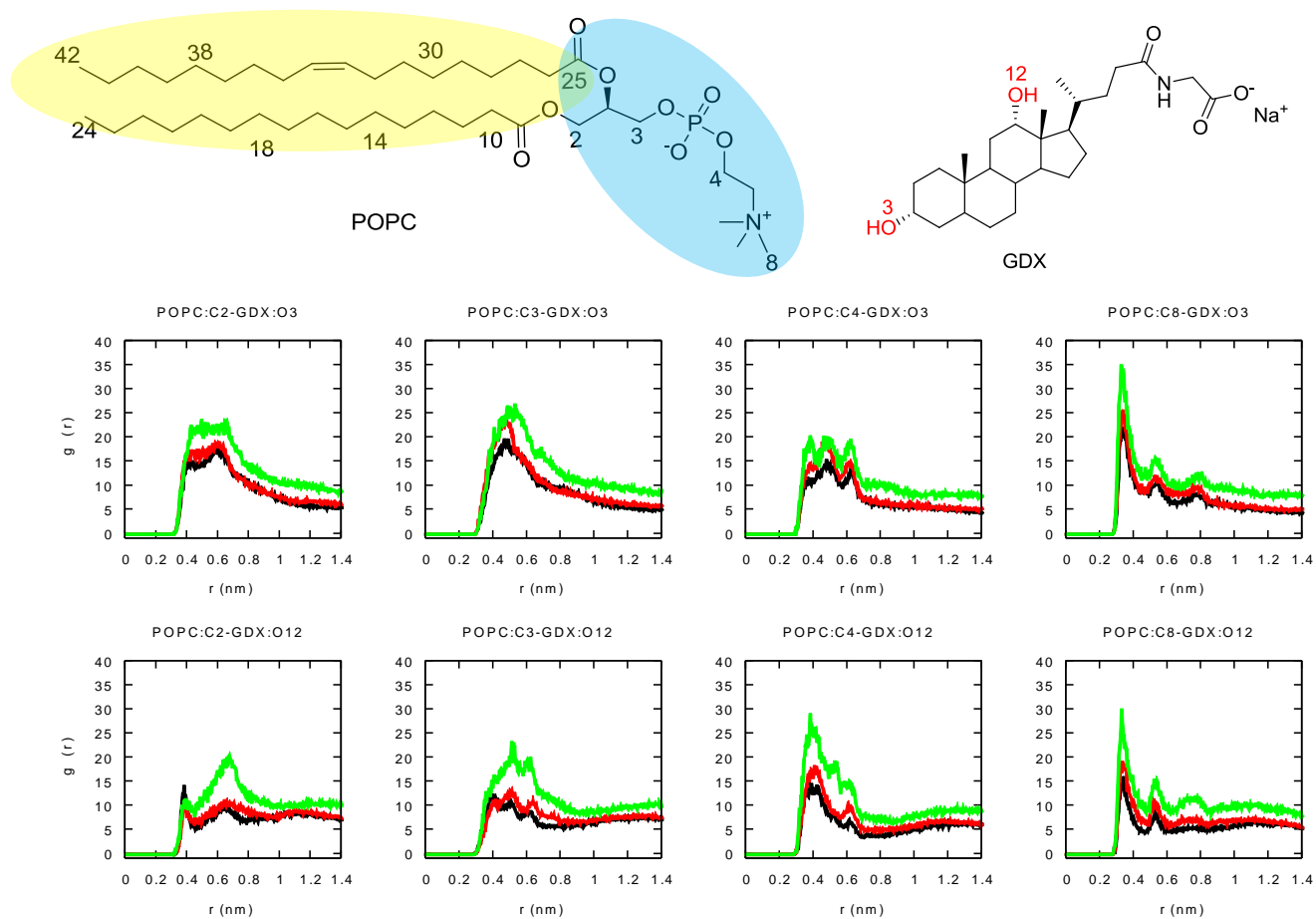


Figure 9.3.10 Radial distribution functions, $g(r)$, for ternary mixtures of POPC/GDX/water. Interaction of atoms O3 and O12 of GDX with hydrophilic head of POPC. Line coloring for % w/w POPC concentration 2 (black), 3 (red) and 4 (green).

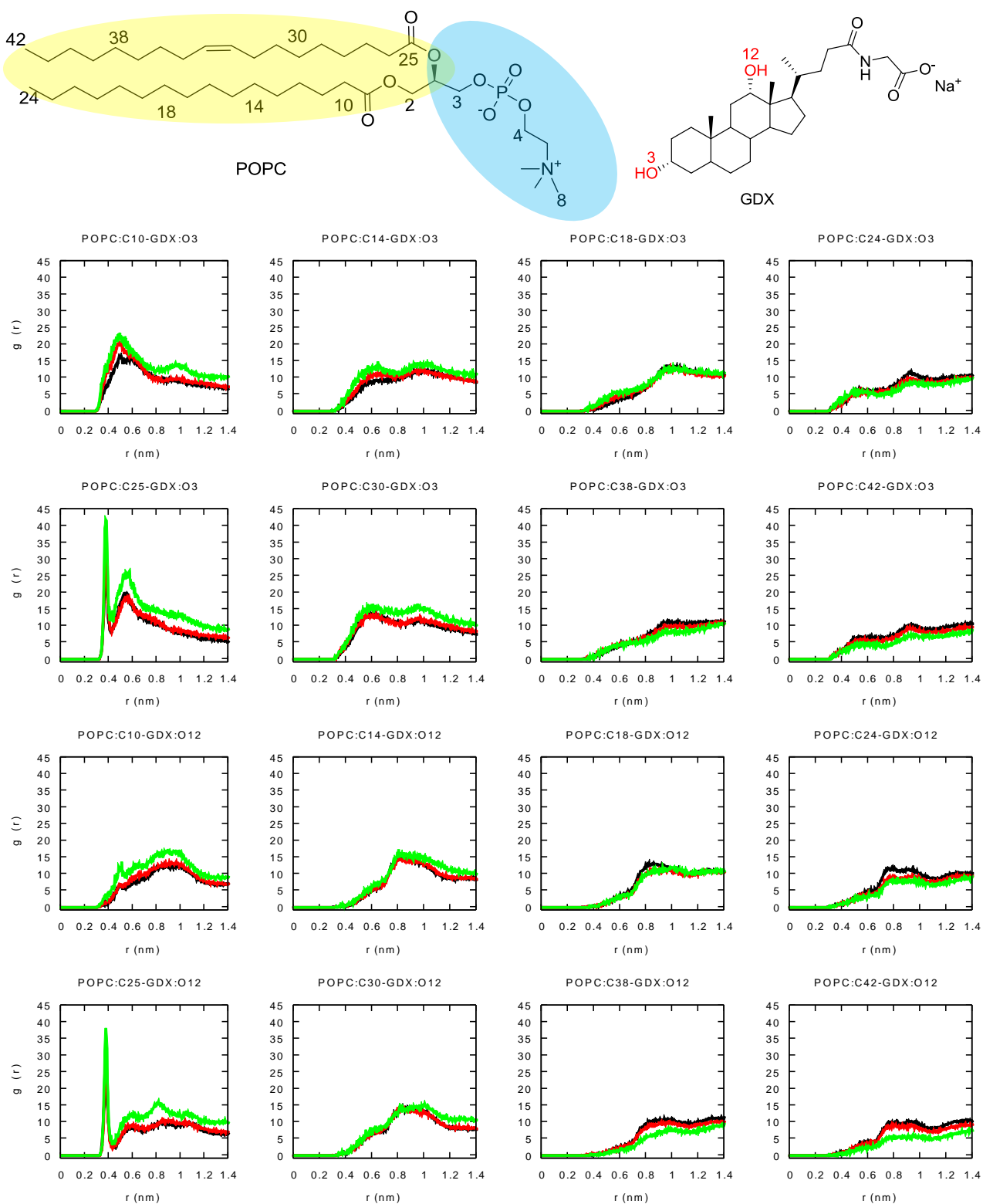


Figure 9.3.11 Radial distribution functions, $g(r)$, for ternary mixtures of POPC/GDX/water. Interaction of atoms O3 and O12 of GDX with hydrophobic tail of POPC. Line coloring for % w/w POPC concentration 2 (black), 3 (red) and 4 (green).

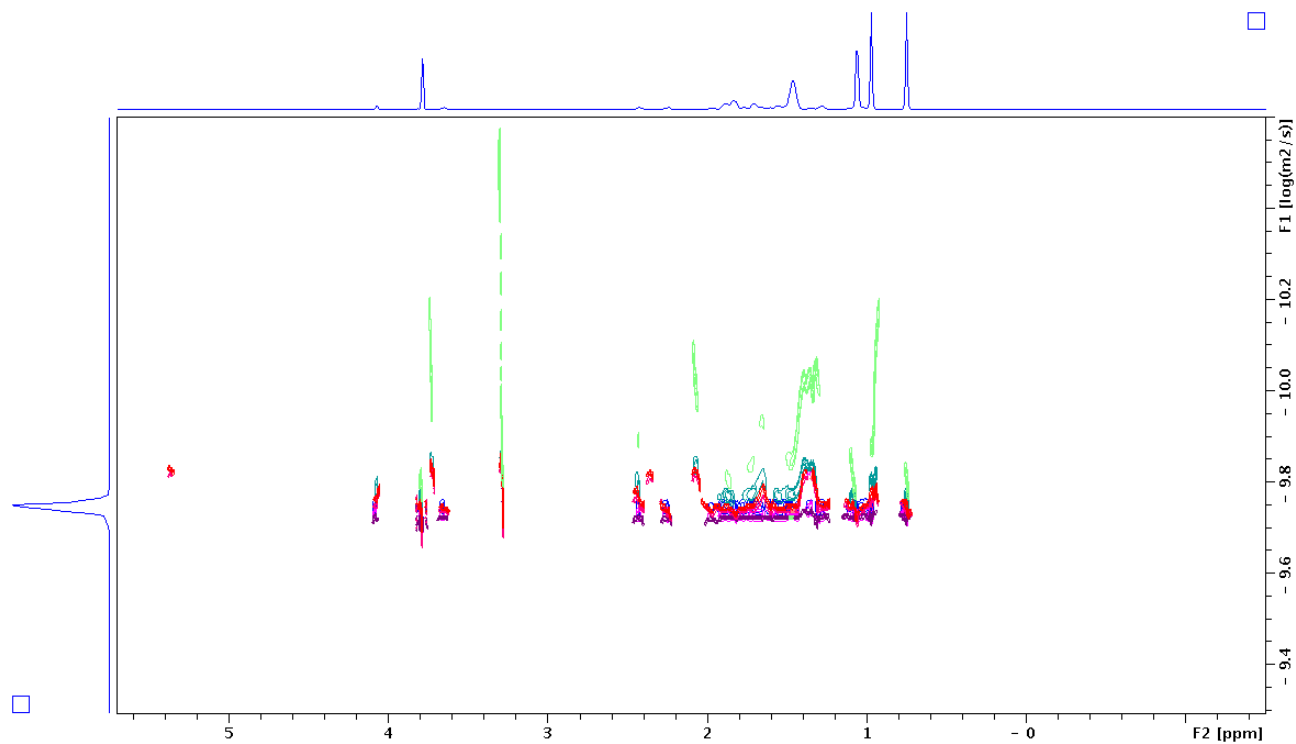


Figure 9.3.12 DOSY-NMR result of POPC/GDX mixture at different mass fractions of POPC and GDX

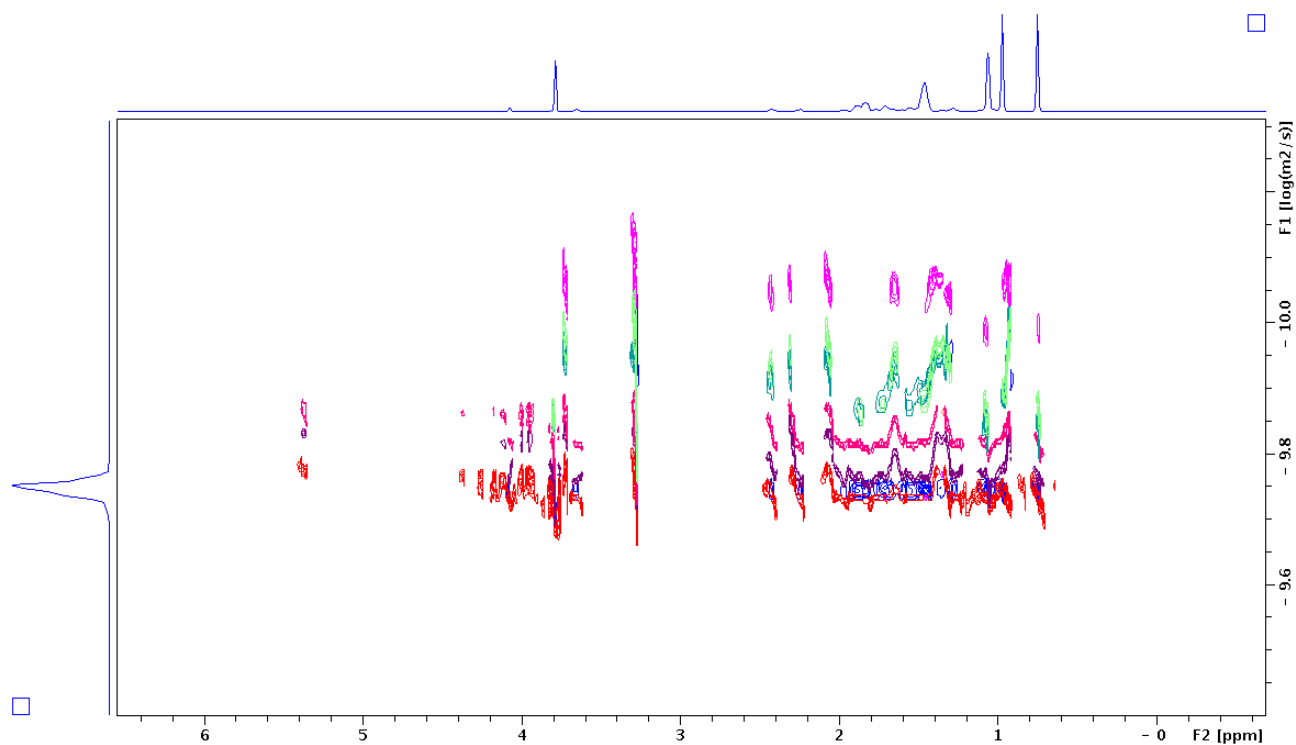


Figure 9.3.13 DOSY-NMR result of LPC+OA/GDX mixture at different mass fractions of LPC+OA and GDX

9.4 APPENDIX 4

Supporting information for Chapter 5

$$1. W_{\text{dig TGL}} = 0$$

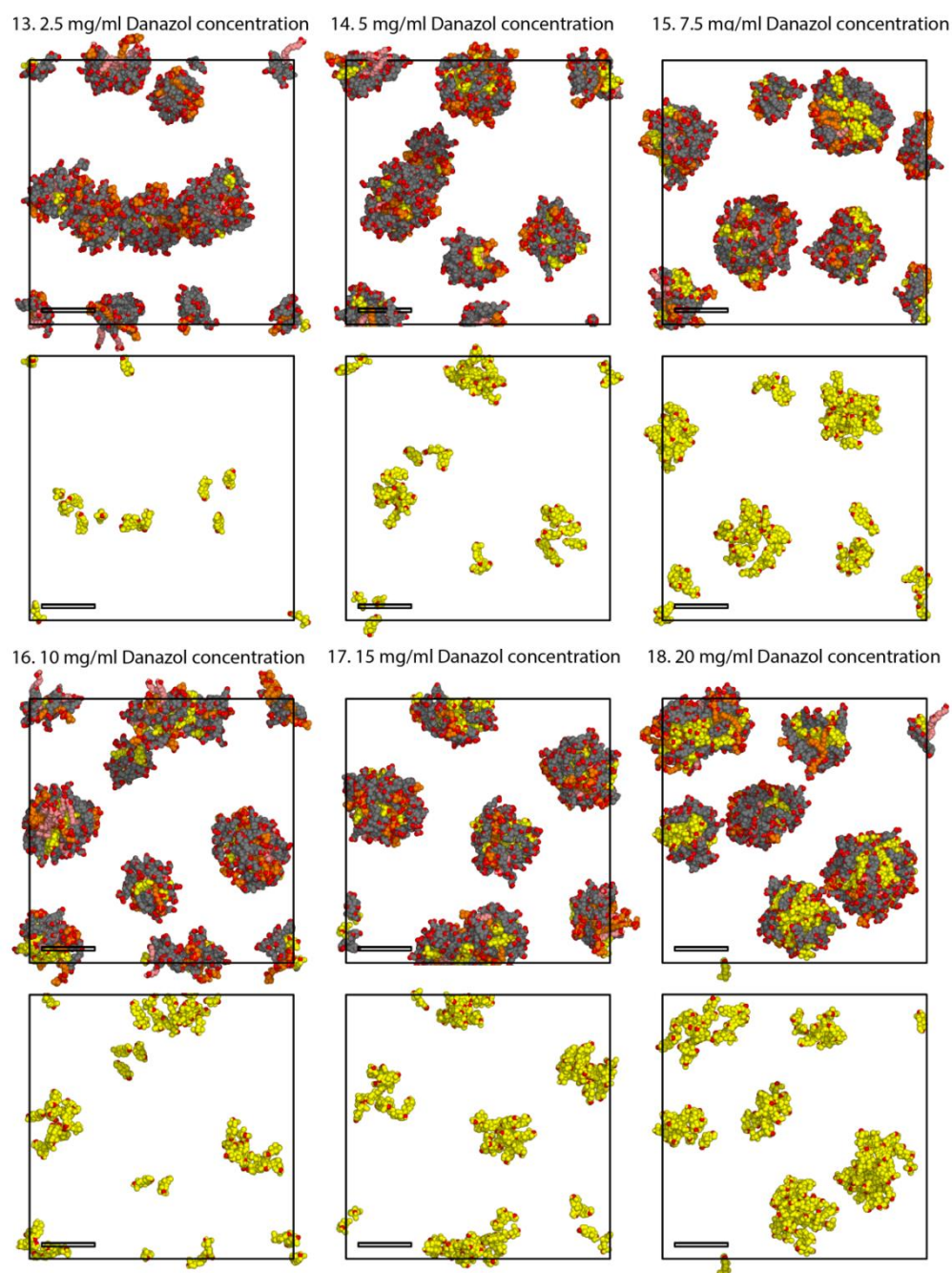
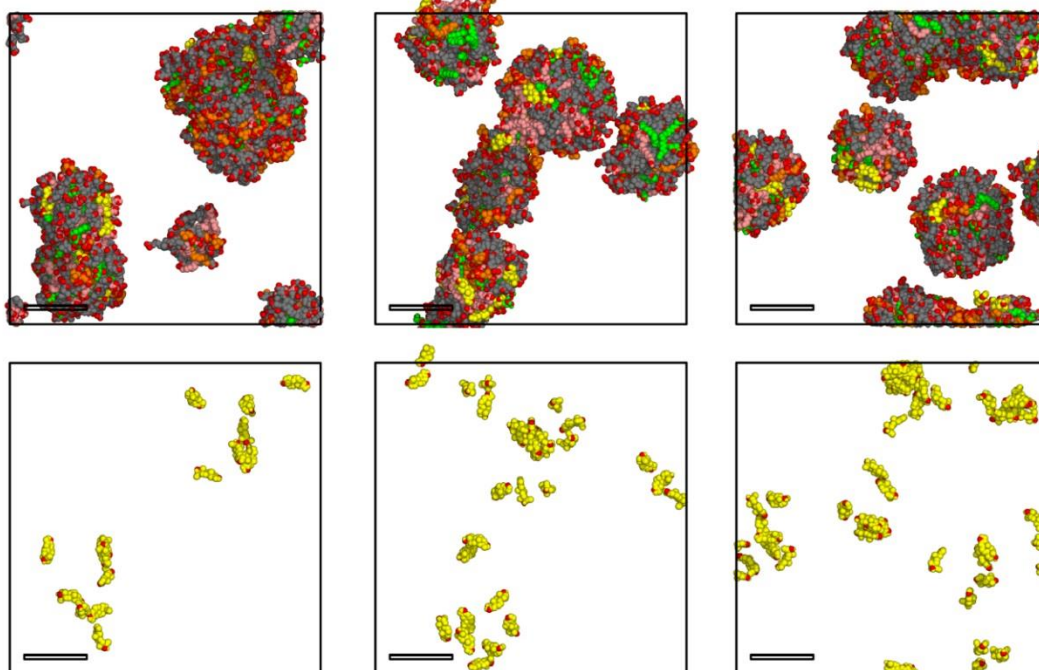


Figure 9.4.1 Localization of drugs within the final frames of selected simulation, with changing danazol concentration. Danazol coloured yellow. Molecule colouring is as described in Figure 5.6 and simulation numbering is described in Table 5.2.

$$2. W_{\text{dig TGL}} = 0.38$$

19. 2.5 mg/ml Danazol concentration 20. 5 mg/ml Danazol concentration 21. 7.5 mg/ml Danazol concentration



22. 10 mg/ml Danazol concentration 23. 15 mg/ml Danazol concentration 24. 20 mg/ml Danazol concentration

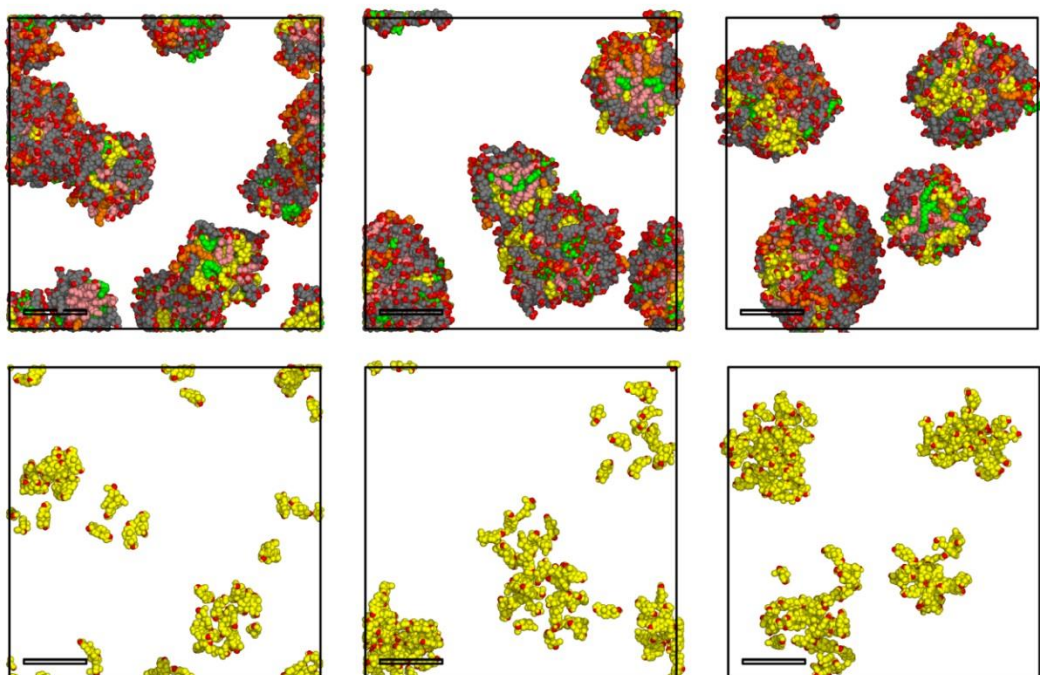
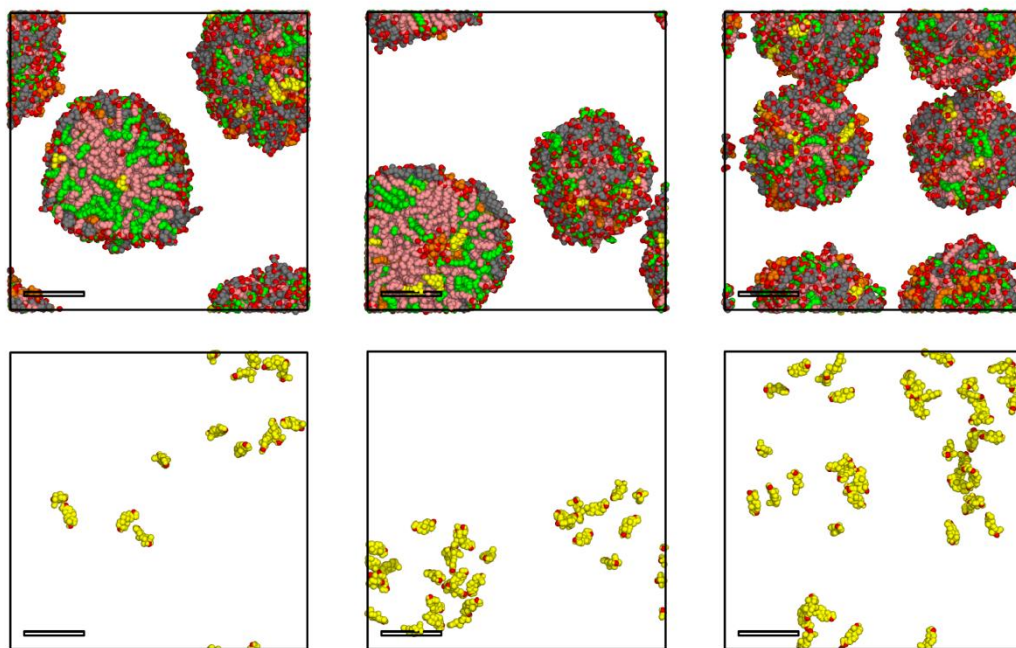


Figure 9.4.2 Localization of drugs within the final frames of selected simulation, with changing danazol concentration. Danazol coloured yellow. Molecule colouring is as described in Figure 5.6 and simulation numbering is described in Table 5.2.

5. $W_{\text{dig TGL}} = 0.69$

25. 2.5 mg/ml Danazol concentration 26. 5 mg/ml Danazol concentration 27. 7.5 mg/ml Danazol concentration



28. 10 mg/ml Danazol concentration 29. 15 mg/ml Danazol concentration 30. 20 mg/ml Danazol concentration

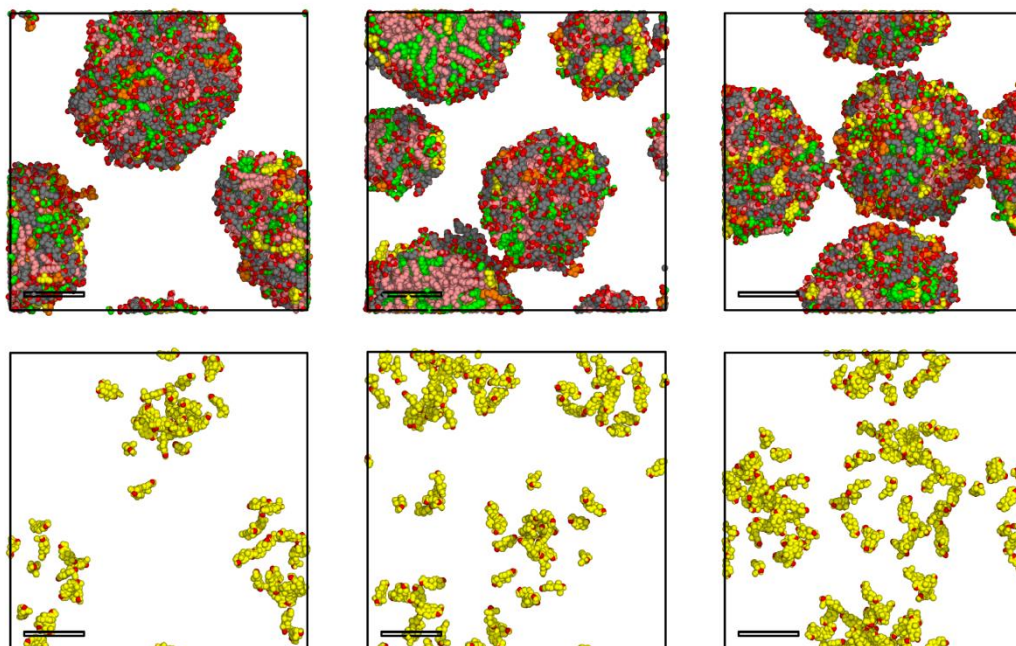


Figure 9.4.3 Localization of drugs within the final frames of selected simulation, with changing danazol concentration. Danazol coloured yellow. Molecule colouring is as described in Figure 5.6 and simulation numbering is described in Table 5.2.

$$8. W_{\text{dig TGL}} = 0.81$$

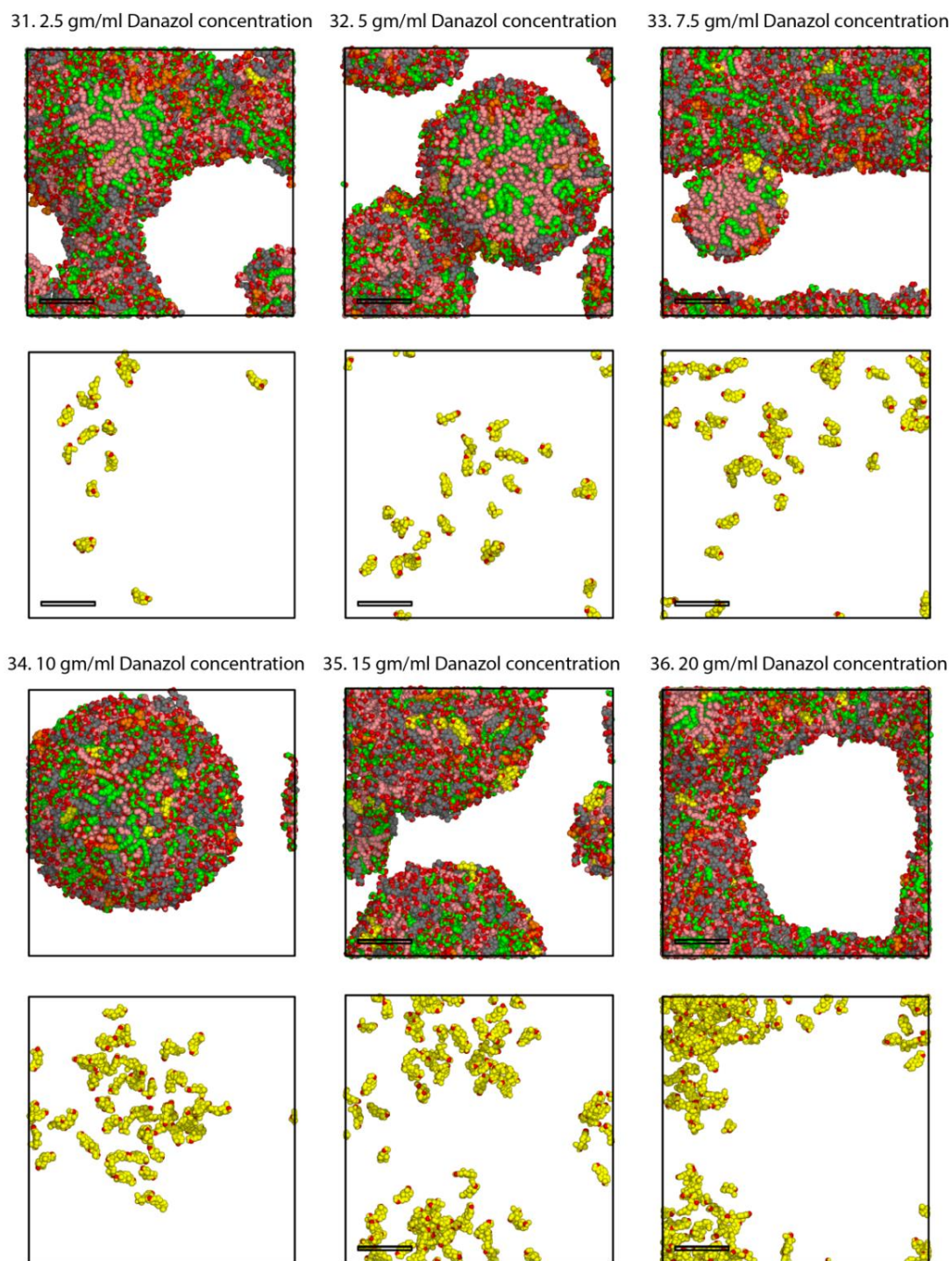
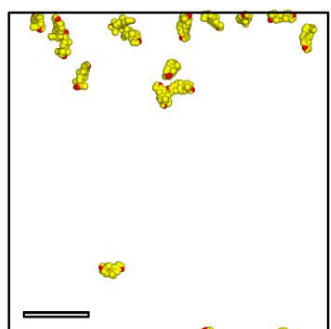
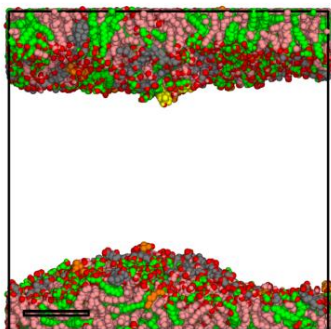


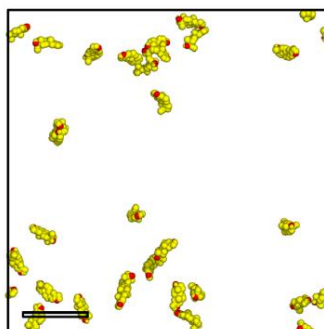
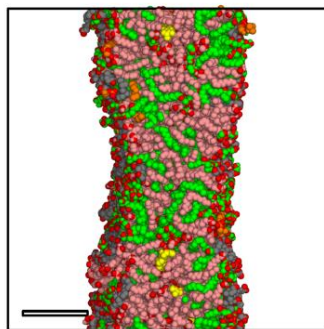
Figure 9.4.4 Localization of drugs within the final frames of selected simulation, with changing danazol concentration. Danazol coloured yellow. Molecule colouring is as described in Figure 5.6 and simulation numbering is described in Table 5.2.

10. $W_{\text{digTGL}} = 0.87$

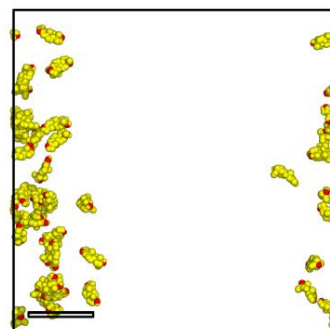
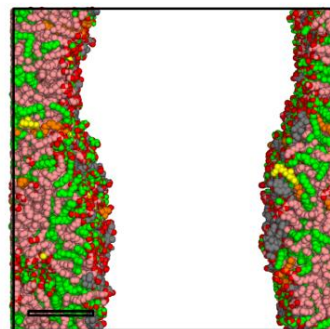
37. 2.5 mg/ml Danazol concentration



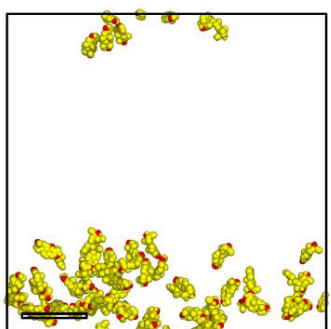
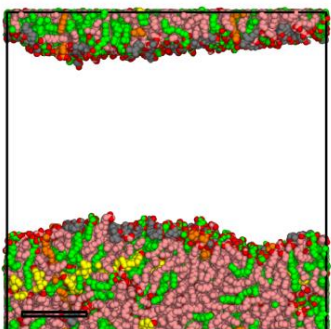
38. 5 mg/ml Danazol concentration



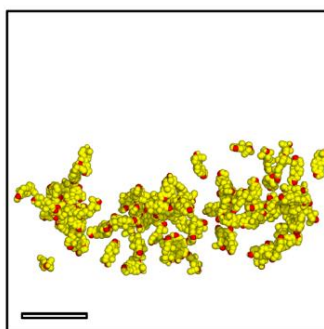
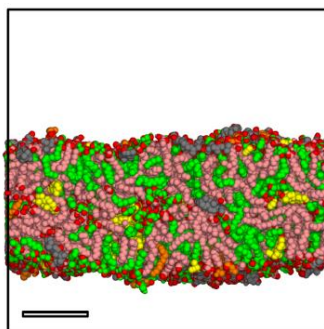
39. 7.5 mg/ml Danazol concentration



40. 10 mg/ml Danazol concentration



41. 15 mg/ml Danazol concentration



42. 20 mg/ml Danazol concentration

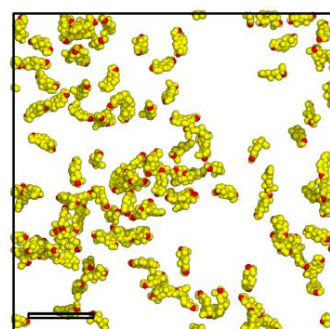
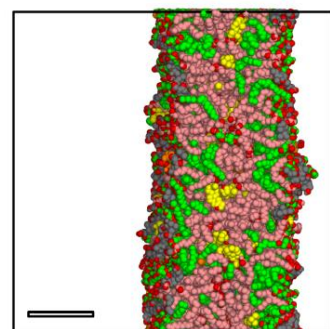


Figure 9.4.5 Localization of drugs within the final frames of selected simulation, with changing danazol concentration. Danazol coloured yellow. Molecule colouring is as described in Figure 5.6 and simulation numbering is described in Table 5.2.

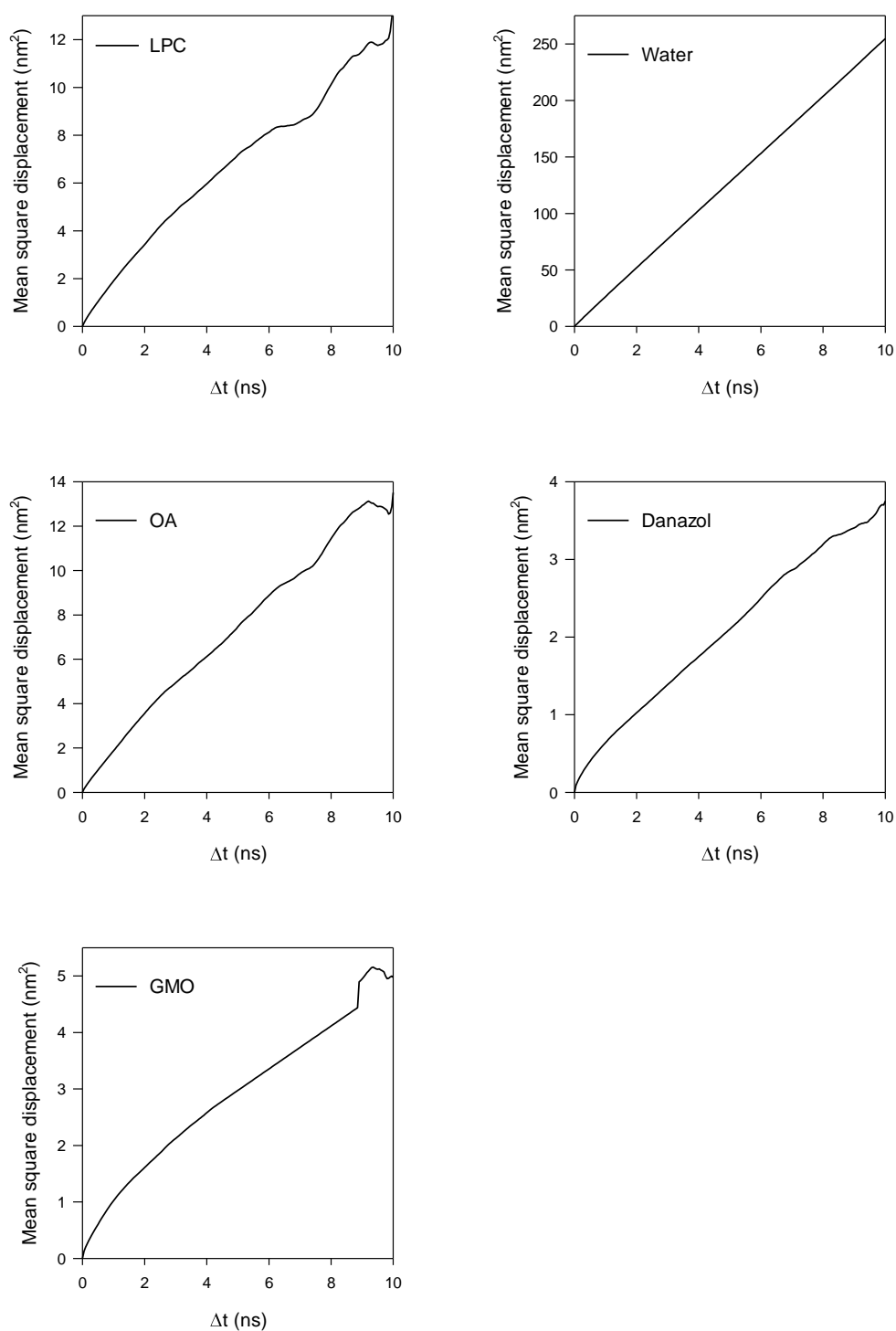


Figure 9.4.6 Mean square displacement of LPC, OA, GMO, water and danazol molecules with in the last 10ns time frame, in the quaternary system of LPC+OA/GDX/dig TGL/water.

9.5 APPENDIX 5

Topologies of compounds used in the phase behaviour study

Topology for 1-palmitoyl-2-oleoyl-sn-glycerol-3-phosphocholine (POPC)

[moleculetype]

; Name

POP 3

[atoms]

; nr	type	resnr	residue	atom	cgnr	charge	mass	typeB	chargeB	massB
1	OA	1	POP	O3	1	-0.7	15.9994		; qtot -0.7	
2	P	1	POP	P1	1	1.7	30.9738		; qtot 1	
3	OM	1	POP	O4	1	-0.8	15.9994		; qtot 0.2	
4	OM	1	POP	O5	1	-0.8	15.9994		; qtot -0.6	
5	OA	1	POP	O6	1	-0.8	15.9994		; qtot -1.4	
6	CH2	1	POP	C4	1	0.4	14.027		; qtot -1	
7	CH2	1	POP	C3	2	0.4	14.027		; qtot -0.6	
8	CH1	1	POP	C2	2	0.3	13.019		; qtot -0.3	
9	OA	1	POP	O2	2	-0.7	15.9994		; qtot -1	
10	CH0	1	POP	C25	2	0.7	12.011		; qtot -0.3	
11	O	1	POP	O25	2	-0.7	15.9994		; qtot -1	
12	CH2	1	POP	C26	3	0	14.027		; qtot -1	
13	CH2	1	POP	C27	4	0	14.027		; qtot -1	
14	CH2	1	POP	C28	5	0	14.027		; qtot -1	
15	CH2	1	POP	C29	6	0	14.027		; qtot -1	
16	CH2	1	POP	C30	7	0	14.027		; qtot -1	
17	CH2	1	POP	C31	8	0	14.027		; qtot -1	
18	CH2	1	POP	C32	9	0	14.027		; qtot -1	
19	CH1	1	POP	C33	10	0	13.019		; qtot -1	
20	CH1	1	POP	C34	11	0	13.019		; qtot -1	
21	CH2	1	POP	C35	12	0	14.027		; qtot -1	
22	CH2	1	POP	C36	13	0	14.027		; qtot -1	
23	CH2	1	POP	C37	14	0	14.027		; qtot -1	

24	CH2	1	POP	C38	15	0	14.027 ; qtot -1
25	CH2	1	POP	C39	16	0	14.027 ; qtot -1
26	CH2	1	POP	C40	17	0	14.027 ; qtot -1
27	CH2	1	POP	C41	18	0	14.027 ; qtot -1
28	CH3	1	POP	C42	19	0	15.035 ; qtot -1
29	CH2	1	POP	C1	20	0.5	14.027 ; qtot -0.5
30	OA	1	POP	O1	20	-0.7	15.9994 ; qtot -1.2
31	CH0	1	POP	C9	20	0.8	12.011 ; qtot -0.4
32	O	1	POP	O9	20	-0.6	15.9994 ; qtot -1
33	CH2	1	POP	C10	21	0	14.027 ; qtot -1
34	CH2	1	POP	C11	22	0	14.027 ; qtot -1
35	CH2	1	POP	C12	23	0	14.027 ; qtot -1
36	CH2	1	POP	C13	24	0	14.027 ; qtot -1
37	CH2	1	POP	C14	25	0	14.027 ; qtot -1
38	CH2	1	POP	C15	26	0	14.027 ; qtot -1
39	CH2	1	POP	C16	27	0	14.027 ; qtot -1
40	CH2	1	POP	C17	28	0	14.027 ; qtot -1
41	CH2	1	POP	C18	29	0	14.027 ; qtot -1
42	CH2	1	POP	C19	30	0	14.027 ; qtot -1
43	CH2	1	POP	C20	31	0	14.027 ; qtot -1
44	CH2	1	POP	C21	32	0	14.027 ; qtot -1
45	CH2	1	POP	C22	33	0	14.027 ; qtot -1
46	CH2	1	POP	C23	34	0	14.027 ; qtot -1
47	CH3	1	POP	C24	35	0	15.035 ; qtot -1
48	CH2	1	POP	C5	36	0.3	14.027 ; qtot -0.7
49	NL	1	POP	N5	36	-0.5	14.0067 ; qtot -1.2
50	CH3	1	POP	C8	36	0.4	15.035 ; qtot -0.8
51	CH3	1	POP	C7	36	0.4	15.035 ; qtot -0.4
52	CH3	1	POP	C6	36	0.4	15.035 ; qtot 0

[bonds]

; ai	aj	funct	c0	c1	c2	c3
1	2	2	gb_28			
1	7	2	gb_18			
2	3	2	gb_24			
2	4	2	gb_24			
2	5	2	gb_28			
5	6	2	gb_18			
6	48	2	gb_27			
7	8	2	gb_27			
8	9	2	gb_18			
8	29	2	gb_27			
9	10	2	gb_18			
10	11	2	gb_5			
10	12	2	gb_27			
12	13	2	gb_27			
13	14	2	gb_27			
14	15	2	gb_27			
15	16	2	gb_27			
16	17	2	gb_27			
17	18	2	gb_27			
18	19	2	gb_27			
19	20	2	gb_10			
20	21	2	gb_27			
21	22	2	gb_27			
22	23	2	gb_27			
23	24	2	gb_27			
24	25	2	gb_27			
25	26	2	gb_27			
26	27	2	gb_27			
27	28	2	gb_27			

```

29 30 2 gb_18
30 31 2 gb_18
31 32 2 gb_5
31 33 2 gb_27
33 34 2 gb_27
34 35 2 gb_27
35 36 2 gb_27
36 37 2 gb_27
37 38 2 gb_27
38 39 2 gb_27
39 40 2 gb_27
40 41 2 gb_27
41 42 2 gb_27
42 43 2 gb_27
43 44 2 gb_27
44 45 2 gb_27
45 46 2 gb_27
46 47 2 gb_27
48 49 2 gb_21
49 50 2 gb_21
49 51 2 gb_21
49 52 2 gb_21

```

[pairs]

```

; ai  aj funct      c0      c1      c2      c3
  1   6   1
  1   9   1
  1  29   1
  2   8   1
  2  48   1
  3   6   1
  3   7   1

```

```

4  6  1
4  7  1
5  7  1
6  50 1
6  51 1
6  52 1
7  10 1
7  30 1
8  11 1
8  12 1
8  31 1
9  13 1
9  30 1
10 29 1
11 13 1
17 20 1
18 21 1
19 22 1
29 32 1
29 33 1
30 34 1
32 34 1

```

[angles]

```

; ai  aj  ak  funct      c0      c1      c2      c3
2   1   7   2   ga_26
1   2   3   2   ga_14
1   2   4   2   ga_14
1   2   5   2   ga_5
3   2   4   2   ga_29
3   2   5   2   ga_14
4   2   5   2   ga_14

```

2	5	6	2	ga_26
5	6	48	2	ga_13
1	7	8	2	ga_13
7	8	9	2	ga_13
7	8	29	2	ga_13
9	8	29	2	ga_13
8	9	10	2	ga_12
9	10	11	2	ga_33
9	10	12	2	ga_19
11	10	12	2	ga_30
10	12	13	2	ga_15
12	13	14	2	ga_13
13	14	15	2	ga_13
14	15	16	2	ga_13
15	16	17	2	ga_13
16	17	18	2	ga_13
17	18	19	2	ga_13
18	19	20	2	ga_27
19	20	21	2	ga_27
20	21	22	2	ga_13
21	22	23	2	ga_13
22	23	24	2	ga_13
23	24	25	2	ga_13
24	25	26	2	ga_13
25	26	27	2	ga_13
26	27	28	2	ga_13
8	29	30	2	ga_13
29	30	31	2	ga_12
30	31	32	2	ga_33
30	31	33	2	ga_19
32	31	33	2	ga_30

```

31 33 34 2 ga_15
33 34 35 2 ga_13
34 35 36 2 ga_13
35 36 37 2 ga_13
36 37 38 2 ga_13
37 38 39 2 ga_13
38 39 40 2 ga_13
39 40 41 2 ga_13
40 41 42 2 ga_13
41 42 43 2 ga_13
42 43 44 2 ga_13
43 44 45 2 ga_13
44 45 46 2 ga_13
45 46 47 2 ga_13
6 48 49 2 ga_15
48 49 50 2 ga_11
48 49 51 2 ga_11
48 49 52 2 ga_11
50 49 51 2 ga_24
50 49 52 2 ga_24
51 49 52 2 ga_24
[ dihedrals ]
; ai aj ak al funct c0 c1 c2 c3 c4 c5
7 1 2 5 1 gd_19
2 1 7 8 1 gd_30
1 2 5 6 1 gd_19
2 5 6 48 1 gd_30
5 6 48 49 1 gd_4
1 7 8 9 1 gd_1
7 8 9 10 1 gd_30
7 8 29 30 1 gd_1

```

8	9	10	11	1	gd_23
9	10	12	13	1	gd_40
10	12	13	14	1	gd_34
12	13	14	15	1	gd_34
13	14	15	16	1	gd_34
14	15	16	17	1	gd_34
15	16	17	18	1	gd_34
16	17	18	19	1	gd_34
17	18	19	20	1	gd_34
19	20	21	22	1	gd_34
20	21	22	23	1	gd_34
21	22	23	24	1	gd_34
22	23	24	25	1	gd_34
23	24	25	26	1	gd_34
24	25	26	27	1	gd_34
25	26	27	28	1	gd_34
8	29	30	31	1	gd_30
29	30	31	32	1	gd_23
30	31	33	34	1	gd_40
31	33	34	35	1	gd_34
33	34	35	36	1	gd_34
34	35	36	37	1	gd_34
35	36	37	38	1	gd_34
36	37	38	39	1	gd_34
37	38	39	40	1	gd_34
38	39	40	41	1	gd_34
39	40	41	42	1	gd_34
40	41	42	43	1	gd_34
41	42	43	44	1	gd_34
42	43	44	45	1	gd_34
43	44	45	46	1	gd_34

```

44 45 46 47 1 gd_34
6 48 49 50 1 gd_41
[ dihedrals ]
; ai aj ak al funct c0 c1 c2 c3
7 29 9 8 2 gi_2
10 12 9 11 2 gi_1
18 19 20 21 2 gi_1
31 33 30 32 2 gi_1

```

Topology for Glycodeoxycholic acid (GDX)

[moleculetype]

; Name

GDX 3

[atoms]

; nr	type	resnr	residue	atom	cgmr	charge	mass	typeB	chargeB	massB
1	CH3	1	GDX	C18	1	0	15.035		; qtot 0	
2	CH0	1	GDX	C13	2	0	12.011		; qtot 0	
3	CH1	1	GDX	C12	3	0.15	13.019		; qtot 0.15	
4	OA	1	GDX	O12	3	-0.548	12.9754		; qtot -0.398	
5	H	1	GDX	H12	3	0.398	1.008		; qtot 0	
6	CH2	1	GDX	C11	4	0	14.027		; qtot 0	
7	CH1	1	GDX	C9	5	0	13.019		; qtot 0	
8	CH0	1	GDX	C10	6	0	12.011		; qtot 0	
9	CH3	1	GDX	C19	7	0	15.035		; qtot 0	
10	CH2	1	GDX	C1	8	0	14.027		; qtot 0	
11	CH2	1	GDX	C2	9	0	14.027		; qtot 0	
12	CH1	1	GDX	C3	10	0.15	13.019		; qtot 0.15	
13	OA	1	GDX	O3	10	-0.548	12.9754		; qtot -0.398	
14	H	1	GDX	H3	10	0.398	1.008		; qtot 0	
15	CH2	1	GDX	C4	11	0	14.027		; qtot 0	
16	CH1	1	GDX	C5	12	0	13.019		; qtot 0	

17	CH2	1	GDX	C6	13	0	14.027	; qtot 0
18	CH1	1	GDX	C7	14	0	13.019	; qtot 0
19	CH1	1	GDX	C8	15	0	13.019	; qtot 0
20	CH1	1	GDX	C14	16	0	13.019	; qtot 0
21	CH2	1	GDX	C15	17	0	14.027	; qtot 0
22	CH2	1	GDX	C16	18	0	14.027	; qtot 0
23	CH1	1	GDX	C17	19	0	13.019	; qtot 0
24	CH1	1	GDX	C20	20	0	13.019	; qtot 0
25	CH3	1	GDX	C21	21	0	15.035	; qtot 0
26	CH2	1	GDX	C22	22	0	14.027	; qtot 0
27	CH2	1	GDX	C23	23	0	14.027	; qtot 0
28	C	1	GDX	C24	24	0.38	12.011	; qtot 0.38
29	O	1	GDX	O24	24	-0.38	15.9994	; qtot 0
30	N	1	GDX	N25	25	-0.28	10.9827	; qtot -0.28
31	H	1	GDX	H25	25	0.28	4.032	; qtot 0
32	CH2	1	GDX	C26	26	0	14.027	; qtot 0
33	C	1	GDX	C27	27	0.27	12.011	; qtot 0.27
34	OM	1	GDX	O28	27	-0.635	15.9994	; qtot -0.365
35	OM	1	GDX	O29	27	-0.635	15.9994	; qtot -1

[bonds]

; ai	aj	funct	c0	c1	c2	c3
1	2	2	gb_27			
2	3	2	gb_27			
2	20	2	gb_27			
2	23	2	gb_27			
3	4	2	gb_18			
3	6	2	gb_27			
4	5	2	gb_1			
6	7	2	gb_27			
7	8	2	gb_27			
7	19	2	gb_27			

8	9	2	gb_27
8	10	2	gb_27
8	16	2	gb_27
10	11	2	gb_27
11	12	2	gb_27
12	13	2	gb_18
12	15	2	gb_27
13	14	2	gb_1
15	16	2	gb_27
16	17	2	gb_27
17	18	2	gb_27
18	19	2	gb_27
19	20	2	gb_27
20	21	2	gb_27
21	22	2	gb_27
22	23	2	gb_27
23	24	2	gb_27
24	25	2	gb_27
24	26	2	gb_27
26	27	2	gb_27
27	28	2	gb_27
28	29	2	gb_5
28	30	2	gb_11
30	31	2	gb_2
30	32	2	gb_11
32	33	2	gb_27
33	34	2	gb_5
33	35	2	gb_5

[pairs]

; ai	aj	funct	c0	c1	c2	c3
1	4	1				
1	6	1				
1	19	1				
1	21	1				
1	22	1				
1	24	1				
2	5	1				
2	7	1				
2	18	1				
2	25	1				
2	26	1				
3	8	1				
3	19	1				
3	21	1				
3	22	1				
3	24	1				
4	7	1				
4	20	1				
4	23	1				
5	6	1				
6	9	1				
6	10	1				
6	16	1				
6	18	1				
6	20	1				
6	23	1				
7	11	1				
7	15	1				
7	17	1				

7	21	1
8	12	1
8	18	1
8	20	1
9	11	1
9	15	1
9	17	1
9	19	1
10	13	1
10	15	1
10	17	1
10	19	1
11	14	1
11	16	1
12	17	1
13	16	1
14	15	1
15	18	1
16	19	1
17	20	1
18	21	1
19	22	1
19	23	1
20	24	1
21	24	1
22	25	1
22	26	1
23	27	1
25	27	1
26	29	1
26	30	1

27 31 1

27 32 1

28 33 1

29 31 1

29 32 1

30 34 1

30 35 1

31 33 1

[angles]

	ai	aj	ak	funct	c0	c1	c2	c3
--	----	----	----	-------	----	----	----	----

1	2	3	2	ga_13				
---	---	---	---	-------	--	--	--	--

1	2	20	2	ga_13				
---	---	----	---	-------	--	--	--	--

1	2	23	2	ga_13				
---	---	----	---	-------	--	--	--	--

3	2	20	2	ga_13				
---	---	----	---	-------	--	--	--	--

3	2	23	2	ga_13				
---	---	----	---	-------	--	--	--	--

20	2	23	2	ga_13				
----	---	----	---	-------	--	--	--	--

2	3	4	2	ga_13				
---	---	---	---	-------	--	--	--	--

2	3	6	2	ga_15				
---	---	---	---	-------	--	--	--	--

4	3	6	2	ga_13				
---	---	---	---	-------	--	--	--	--

3	4	5	2	ga_12				
---	---	---	---	-------	--	--	--	--

3	6	7	2	ga_15				
---	---	---	---	-------	--	--	--	--

6	7	8	2	ga_15				
---	---	---	---	-------	--	--	--	--

6	7	19	2	ga_15				
---	---	----	---	-------	--	--	--	--

8	7	19	2	ga_15				
---	---	----	---	-------	--	--	--	--

7	8	9	2	ga_13				
---	---	---	---	-------	--	--	--	--

7	8	10	2	ga_13				
---	---	----	---	-------	--	--	--	--

7	8	16	2	ga_13				
---	---	----	---	-------	--	--	--	--

9	8	10	2	ga_13				
---	---	----	---	-------	--	--	--	--

9	8	16	2	ga_13				
---	---	----	---	-------	--	--	--	--

10	8	16	2	ga_13				
----	---	----	---	-------	--	--	--	--

8	10	11	2	ga_15				
---	----	----	---	-------	--	--	--	--

10	11	12	2	ga_15
11	12	13	2	ga_13
11	12	15	2	ga_13
13	12	15	2	ga_13
12	13	14	2	ga_12
12	15	16	2	ga_15
8	16	15	2	ga_15
8	16	17	2	ga_15
15	16	17	2	ga_13
16	17	18	2	ga_15
17	18	19	2	ga_13
7	19	18	2	ga_15
7	19	20	2	ga_15
18	19	20	2	ga_15
2	20	19	2	ga_15
2	20	21	2	ga_15
19	20	21	2	ga_15
20	21	22	2	ga_15
21	22	23	2	ga_15
2	23	22	2	ga_15
2	23	24	2	ga_15
22	23	24	2	ga_15
23	24	25	2	ga_15
23	24	26	2	ga_15
25	24	26	2	ga_15
24	26	27	2	ga_15
26	27	28	2	ga_15
27	28	29	2	ga_22
27	28	30	2	ga_19
29	28	30	2	ga_33
28	30	31	2	ga_32

28 30 32 2 ga_31

31 30 32 2 ga_18

30 32 33 2 ga_13

32 33 34 2 ga_22

32 33 35 2 ga_22

34 33 35 2 ga_38

[dihedrals]

; ai	aj	ak	al	funct	c0	c1	c2	c3	c4	c5
1	2	3	4	1	gd_1					
1	2	20	19	1	gd_1					
1	2	23	22	1	gd_1					
6	3	4	5	1	gd_30					
2	3	6	7	1	gd_1					
3	6	7	8	1	gd_1					
6	7	8	9	1	gd_1					
6	7	19	18	1	gd_1					
7	8	10	11	1	gd_1					
7	8	16	15	1	gd_1					
8	10	11	12	1	gd_1					
10	11	12	13	1	gd_1					
11	12	13	14	1	gd_30					
11	12	15	16	1	gd_30					
12	15	16	8	1	gd_1					
8	16	17	18	1	gd_1					
16	17	18	19	1	gd_1					
17	18	19	7	1	gd_1					
7	19	20	2	1	gd_1					
2	20	21	22	1	gd_1					
20	21	22	23	1	gd_1					
21	22	23	2	1	gd_1					
2	23	24	25	1	gd_1					

```

23 24 26 27 1 gd_1
24 26 27 28 1 gd_1
26 27 28 29 1 gd_40
27 28 30 32 1 gd_39
28 30 32 33 1 gd_39
30 32 33 34 1 gd_40
[ dihedrals ]
; ai aj ak al funct c0 c1 c2 c3
2 1 3 20 2 gi_2
3 2 6 4 2 gi_2
7 6 8 19 2 gi_2
8 7 10 9 2 gi_2
12 11 15 13 2 gi_2
15 17 8 16 2 gi_2
18 20 7 19 2 gi_2
20 2 19 21 2 gi_2
23 2 22 24 2 gi_2
24 23 25 26 2 gi_2
28 27 30 29 2 gi_1
30 28 32 31 2 gi_1
33 32 34 35 2 gi_1

```

Topology for 1-palmitoyl-2-hydroxy-sn-glycerol-3-phosphocoline (LPC)

[moleculetype]

; Name

Lysed_OPC 3

[atoms]

```

; nr type resnr residue atom cgnr charge mass typeB chargeB massB
1 CH3 1 POP C16 1 0 15.035 ; qtot -1
2 CH2 1 POP C15 2 0 14.027 ; qtot -1
3 CH2 1 POP C14 3 0 14.027 ; qtot -1

```

4	CH2	1	POP	C13	4	0	14.027	; qtot -1
5	CH2	1	POP	C12	5	0	14.027	; qtot -1
6	CH2	1	POP	C11	6	0	14.027	; qtot -1
7	CH2	1	POP	C10	7	0	14.027	; qtot -1
8	CH2	1	POP	C9	8	0	14.027	; qtot -1
9	CH2	1	POP	C8	9	0	14.027	; qtot -1
10	CH2	1	POP	C7	10	0	14.027	; qtot -1
11	CH2	1	POP	C6	11	0	14.027	; qtot -1
12	CH2	1	POP	C5	12	0	14.027	; qtot -1
13	CH2	1	POP	C4	13	0	14.027	; qtot -1
14	CH2	1	POP	C3	14	0	14.027	; qtot -1
15	CH2	1	POP	C2	15	0	14.027	; qtot -1
16	CH0	1	POP	C1	16	0.8	12.011	; qtot -0.4
17	O	1	POP	O1	16	-0.6	15.9994	; qtot -1
18	OA	1	POP	O2	16	-0.7	15.9994	; qtot -1.2
19	CH2	1	POP	C17	16	0.5	14.027	; qtot -0.5
20	CH1	1	POP	C18	17	0.5	13.019	; qtot -0.3
21	CH2	1	POP	C19	18	0	14.027	; qtot -0.6
22	OA	1	POP	O3	19	-0.8	15.9994	; qtot -0.6
23	P	1	POP	P1	19	1.7	30.9738	; qtot 1
24	OA	1	POP	O4	19	-0.8	15.9994	; qtot 0.2
25	CH2	1	POP	C20	19	0.4	14.027	; qtot -1
26	CH2	1	POP	C21	20	0.3	14.027	; qtot -0.7
27	NL	1	POP	N1	20	-0.5	14.0067	; qtot -1.2
28	OM	1	POP	O5	19	-0.8	15.9994	; qtot -1.4
29	OA	1	POP	O6	17	-0.7	12.9754	; qtot -0.7
30	OM	1	POP	O7	19	-0.7	15.9994	; qtot -0.7
31	CH3	1	POP	C22	20	0.4	15.035	; qtot -0.8
32	CH3	1	POP	C23	20	0.4	15.035	; qtot -0.4
33	CH3	1	POP	C24	20	0.4	15.035	; qtot 0
34	H	1	POP	H1	17	0.2	4.032	; qtot -0.2

[bonds]

; ai	aj	funct	c0	c1	c2	c3
1	2	2	gb_27			
2	3	2	gb_27			
3	4	2	gb_27			
4	5	2	gb_27			
5	6	2	gb_27			
6	7	2	gb_27			
7	8	2	gb_27			
8	9	2	gb_27			
9	10	2	gb_27			
10	11	2	gb_27			
11	12	2	gb_27			
12	13	2	gb_27			
13	14	2	gb_27			
14	15	2	gb_27			
15	16	2	gb_27			
16	17	2	gb_5			
16	18	2	gb_18			
18	19	2	gb_18			
19	20	2	gb_27			
20	21	2	gb_27			
20	29	2	gb_18			
29	34	2	gb_1			
21	22	2	gb_18			
22	23	2	gb_28			
23	24	2	gb_28			
23	28	2	gb_24			
23	30	2	gb_24			
24	25	2	gb_18			
25	26	2	gb_27			

26 27 2 gb_21

27 31 2 gb_21

27 32 2 gb_21

27 33 2 gb_21

[pairs]

	ai	aj	funct	c0	c1	c2	c3
	22	25	1				
	22	26	1				
	22	18	1				
	22	19	1				
	22	29	1				
	23	20	1				
	23	26	1				
	30	21	1				
	30	25	1				
	28	25	1				
	28	21	1				
	24	21	1				
	25	31	1				
	25	32	1				
	25	33	1				
	20	16	1				
	19	34	1				
	21	34	1				
	19	17	1				
	19	15	1				
	18	14	1				
	18	29	1				
	17	14	1				

[angles]

; ai	aj	ak	funct	c0	c1	c2	c3
1	2	3	2	ga_13			
2	3	4	2	ga_13			
3	4	5	2	ga_13			
4	5	6	2	ga_13			
5	6	7	2	ga_13			
6	7	8	2	ga_13			
7	8	9	2	ga_13			
8	9	10	2	ga_13			
9	10	11	2	ga_13			
10	11	12	2	ga_13			
11	12	13	2	ga_13			
12	13	14	2	ga_13			
13	14	15	2	ga_13			
14	15	16	2	ga_13			
15	16	17	2	ga_30			
15	16	18	2	ga_13			
17	16	18	2	ga_33			
16	18	19	2	ga_9			
18	19	20	2	ga_30			
19	20	21	2	ga_13			
19	20	29	2	ga_30			
21	20	29	2	ga_30			
20	29	34	2	ga_12			
20	21	22	2	ga_30			
21	22	23	2	ga_26			
22	23	28	2	ga_14			
22	23	24	2	ga_5			
28	23	24	2	ga_14			
30	23	24	2	ga_14			

```

28 23 30 2 ga_29
22 23 30 2 ga_14
23 24 25 2 ga_26
24 25 26 2 ga_13
25 26 27 2 ga_15
26 27 31 2 ga_11
26 27 32 2 ga_11
26 27 33 2 ga_11
31 27 32 2 ga_24
32 27 33 2 ga_24
31 27 33 2 ga_24

```

[dihedrals]

```

; ai  aj  ak  al funct      c0      c1      c2      c3      c4      c5
  1   2   3   4   1  gd_34
  2   3   4   5   1  gd_34
  3   4   5   6   1  gd_34
  4   5   6   7   1  gd_34
  5   6   7   8   1  gd_34
  6   7   8   9   1  gd_34
  7   8   9  10   1  gd_34
  8   9  10  11   1  gd_34
  9  10  11  12   1  gd_34
 10  11  12  13   1  gd_34
 11  12  13  14   1  gd_34
 12  13  14  15   1  gd_34
 13  14  15  16   1  gd_34
 17  16  15  14   1  gd_34
 17  16  18  19   1  gd_23
 18  19  20  29   1  gd_2
 18  19  20  21   1  gd_1
 19  20  29  34   1  gd_30

```

```

21  20  29  34   1  gd_30
20  21  22  23   1  gd_30
23  24  25  26   1  gd_30
21  22  23  24   1  gd_19
22  23  24  25   1  gd_19
24  25  26  27   1  gd_4
25  26  27  31   1  gd_41
25  26  27  32   1  gd_41
25  26  27  33   1  gd_41

```

[dihedrals]

```

; ai  aj  ak  al funct      c0      c1      c2      c3
16  15  17  18  2  gi_1
20  19  21  29  2  gi_2

```

Topology for Oleic Acid (OA)

[moleculetype]

; Name

OLE 3

[atoms]

; nr	type	resnr	residue	atom	cgnr	charge	mass	typeB	chargeB	massB
1	CH3	1	OLE	C1	1	0	15.035	; qtot 0		
2	CH2	1	OLE	C2	2	0	14.027	; qtot 0		
3	CH2	1	OLE	C3	3	0	14.027	; qtot 0		
4	CH2	1	OLE	C4	4	0	14.027	; qtot 0		
5	CH2	1	OLE	C5	5	0	14.027	; qtot 0		
6	CH2	1	OLE	C6	6	0	14.027	; qtot 0		
7	CH2	1	OLE	C7	7	0	14.027	; qtot 0		
8	CH2	1	OLE	C8	8	0	14.027	; qtot 0		
9	CR1	1	OLE	C9	9	0	13.019	; qtot 0		
10	CR1	1	OLE	C10	10	0	13.019	; qtot 0		
11	CH2	1	OLE	C11	11	0	14.027	; qtot 0		

12	CH2	1	OLE	C12	12	0	14.027 ; qtot 0
13	CH2	1	OLE	C13	13	0	14.027 ; qtot 0
14	CH2	1	OLE	C14	14	0	14.027 ; qtot 0
15	CH2	1	OLE	C15	15	0	14.027 ; qtot 0
16	CH2	1	OLE	C16	16	0	14.027 ; qtot 0
17	CH2	1	OLE	C17	17	0	14.027 ; qtot 0
18	C	1	OLE	C18	18	0.33	12.011 ; qtot 0.33
19	O	1	OLE	O1	18	-0.45	15.9994 ; qtot -0.12
20	OA	1	OLE	O2	18	-0.288	12.9754 ; qtot -0.408
21	H	1	OLE	H1	18	0.408	4.032 ; qtot 0

[bonds]

; ai	aj	funct	c0	c1	c2	c3
1	2	2	gb_27			
2	3	2	gb_27			
3	4	2	gb_27			
4	5	2	gb_27			
5	6	2	gb_27			
6	7	2	gb_27			
7	8	2	gb_27			
8	9	2	gb_27			
9	10	2	gb_10			
10	11	2	gb_27			
11	12	2	gb_27			
12	13	2	gb_27			
13	14	2	gb_27			
14	15	2	gb_26			
15	16	2	gb_26			
16	17	2	gb_26			
17	18	2	gb_26			
18	19	2	gb_5			
18	20	2	gb_13			

```

    20  21   2  gb_1
[ pairs ]
; ai  aj funct      c0      c1      c2      c3
  1   4   1
  2   5   1
  3   6   1
  4   7   1
  5   8   1
  6   9   1
  7  10   1
  8  11   1
  9  12   1
 10  13   1
 11  14   1
 12  15   1
 13  16   1
 14  17   1
 15  18   1
 16  19   1
 16  20   1
 17  21   1
 19  21   1
[ angles ]
; ai  aj  ak funct      c0      c1      c2      c3
  1   2   3   2  ga_15
  2   3   4   2  ga_15
  3   4   5   2  ga_15
  4   5   6   2  ga_15
  5   6   7   2  ga_15
  6   7   8   2  ga_15
  7   8   9   2  ga_15

```

```

8  9  10  2  ga_15
9  10  11  2  ga_15
10 11  12  2  ga_15
11 12  13  2  ga_15
12 13  14  2  ga_15
13 14  15  2  ga_15
14 15  16  2  ga_15
15 16  17  2  ga_15
16 17  18  2  ga_15
17 18  19  2  ga_30
17 18  20  2  ga_19
19 18  20  2  ga_33
18 20  21  2  ga_12

```

[dihedrals]

```

; ai  aj  ak  al funct      c0      c1      c2      c3      c4      c5
1  2  3  4  1  gd_34
2  3  4  5  1  gd_34
3  4  5  6  1  gd_34
4  5  6  7  1  gd_34
5  6  7  8  1  gd_34
6  7  8  9  1  0    3.350  1
6  7  8  9  1  180  1.660  2
6  7  8  9  1  0    7.333  3
7  8  9  10 1  180  7.470  1
7  8  9  10 1  0    3.900  2
7  8  9  10 1  180  1.100  3
7  8  9  10 1  90   -5.685  0
8  9  10  11 1  180  7.470  1
8  9  10  11 1  0    3.900  2
8  9  10  11 1  90   -5.685  0
9  10  11  12 1  0    3.350  1

```

```

9  10  11  12  1  180  1.660  2
9  10  11  12  1  0   7.333  3
10 11  12  13  1  gd_34
11 12  13  14  1  gd_34
12 13  14  15  1  gd_34
13 14  15  16  1  gd_34
14 15  16  17  1  gd_34
15 16  17  18  1  gd_34
16 17  18  20  1  gd_40
17 18  20  21  1  gd_12
[ dihedrals ]
; ai  aj  ak  al      funct      c0      c1      c2      c3
   8   9  10  11      2  gi_1
  17  20  19  18      2  gi_1

```

Topology for glycerol 1-mono-oleate (GMO)

```

[ moleculetype ]
; Name
GMO           3
[ atoms ]
; nr      type resnr residue atom  cgnr  charge  mass typeB  chargeB  massB
   1     CH2    1   GMO    C1    1     0.1   14.027 ; qtot 0.25
   2     OA     1   GMO    O1    1    -0.18  15.9994 ; qtot 0.07
   3     CH1    1   GMO    C2    2     0.15  13.019 ; qtot 0.15
   4     OA     1   GMO    O2    2    -0.548  12.9754 ; qtot -0.398
   5      H     1   GMO    H2    2     0.398   4.032 ; qtot 0
   6     CH2    1   GMO    C3    3     0.15  14.027 ; qtot 0
   7     OA     1   GMO    O3    3    -0.548  12.9754 ; qtot -0.548
   8      H     1   GMO    H3    3     0.398   4.032 ; qtot -0.15
   9      C     1   GMO    C4    1     0.27  12.011 ; qtot 0.34
  10      O     1   GMO    O4    1    -0.19  15.9994 ; qtot 0.15

```

11	CH2	1	GMO	C5	4	0	14.027 ; qtot 0
12	CH2	1	GMO	C6	5	0	14.027 ; qtot 0
13	CH2	1	GMO	C7	6	0	14.027 ; qtot 0
14	CH2	1	GMO	C8	7	0	14.027 ; qtot 0
15	CH2	1	GMO	C9	8	0	14.027 ; qtot 0
16	CH2	1	GMO	C10	9	0	14.027 ; qtot 0
17	CH2	1	GMO	C11	10	0	14.027 ; qtot 0
18	CR1	1	GMO	C12	11	0	13.019 ; qtot 0
19	CR1	1	GMO	C13	12	0	13.019 ; qtot 0
20	CH2	1	GMO	C14	13	0	14.027 ; qtot 0
21	CH2	1	GMO	C15	14	0	14.027 ; qtot 0
22	CH2	1	GMO	C16	15	0	14.027 ; qtot 0
23	CH2	1	GMO	C17	16	0	14.027 ; qtot 0
24	CH2	1	GMO	C18	17	0	14.027 ; qtot 0
25	CH2	1	GMO	C19	18	0	14.027 ; qtot 0
26	CH2	1	GMO	C20	19	0	14.027 ; qtot 0
27	CH3	1	GMO	C21	20	0	15.035 ; qtot 0

[bonds]

; ai	aj	funct	c0	c1	c2	c3
1	2	2	gb_18			
1	3	2	gb_27			
3	4	2	gb_18			
4	5	2	gb_1			
3	6	2	gb_27			
6	7	2	gb_18			
7	8	2	gb_1			
2	9	2	gb_13			
9	10	2	gb_5			
9	11	2	gb_27			
11	12	2	gb_27			
12	13	2	gb_27			

13	14	2	gb_27
14	15	2	gb_27
15	16	2	gb_27
16	17	2	gb_27
17	18	2	gb_27
18	19	2	gb_10
19	20	2	gb_27
20	21	2	gb_27
21	22	2	gb_27
22	23	2	gb_27
23	24	2	gb_27
24	25	2	gb_27
25	26	2	gb_27
26	27	2	gb_27

[pairs]

; ai	aj	funct	c0	c1	c2	c3
1	5	1				
1	7	1				
1	10	1				
1	11	1				
2	4	1				
2	6	1				
2	12	1				
3	9	1				
3	8	1				
4	2	1				
4	7	1				
5	6	1				
15	18	1				
16	19	1				
17	20	1				

```

18 21 1
19 22 1
[ angles ]
; ai aj ak funct c0 c1 c2 c3
1 2 9 2 ga_12
2 1 3 2 ga_13
1 3 4 2 ga_13
1 3 6 2 ga_13
4 3 6 2 ga_13
3 4 5 2 ga_12
3 6 7 2 ga_13
6 7 8 2 ga_12
2 9 10 2 ga_33
2 9 11 2 ga_30
10 9 11 2 ga_19
9 11 12 2 ga_13
11 12 13 2 ga_13
12 13 14 2 ga_13
13 14 15 2 ga_13
14 15 16 2 ga_13
15 16 17 2 ga_13
16 17 18 2 ga_13
17 18 19 2 ga_13
18 19 20 2 ga_13
19 20 21 2 ga_13
20 21 22 2 ga_13
21 22 23 2 ga_13
22 23 24 2 ga_13
23 24 25 2 ga_13
24 25 26 2 ga_13
25 26 27 2 ga_13

```

[dihedrals]

	ai	aj	ak	al	funct	c0	c1	c2	c3	c4	c5
	3	1	2	9	1	gd_23					
	2	1	3	6	1	gd_34					
	1	3	4	5	1	gd_23					
	1	3	6	7	1	gd_34					
	3	6	7	8	1	gd_23					
	1	2	9	11	1	gd_23					
	2	9	11	12	1	gd_40					
	15	16	17	18	1	0	3.350	1			
	15	16	17	18	1	180	1.660	2			
	15	16	17	18	1	0	7.333	3			
	16	17	18	19	1	180	7.470	1			
	16	17	18	19	1	0	3.900	2			
	16	17	18	19	1	180	-1.100	3			
	16	17	18	19	1	90	-5.685	0			
	18	19	20	21	1	180	7.470	1			
	18	19	20	21	1	0	3.900	2			
	18	19	20	21	1	180	-1.100	3			
	18	19	20	21	1	90	-5.685	0			
	19	20	21	22	1	0	3.350	1			
	19	20	21	22	1	180	1.660	2			

[dihedrals]

	ai	aj	ak	al	funct	c0	c1	c2	c3
	6	4	1	3	2	gi_2			
	9	11	2	10	2	gi_1			
	17	18	19	20	2	gi_1			

ether

double bond

[dihedrals]

	ai	aj	ak	al	funct	c0	c1	c2	c3	c4	c5
	9	11	12	13	3	9.2789	12.156	-13.120	-3.0597	26.240	-31.495
	11	12	13	14	3	9.2789	12.156	-13.120	-3.0597	26.240	-31.495

lipids for Berger et al. 1997

12	13	14	15	3	9.2789	12.156	-13.120	-3.0597	26.240	-31.495
13	14	15	16	3	9.2789	12.156	-13.120	-3.0597	26.240	-31.495
14	15	16	17	3	9.2789	12.156	-13.120	-3.0597	26.240	-31.495
20	21	22	23	3	9.2789	12.156	-13.120	-3.0597	26.240	-31.495
21	22	23	24	3	9.2789	12.156	-13.120	-3.0597	26.240	-31.495
22	23	24	25	3	9.2789	12.156	-13.120	-3.0597	26.240	-31.495
23	24	25	26	3	9.2789	12.156	-13.120	-3.0597	26.240	-31.495
24	25	26	27	3	9.2789	12.156	-13.120	-3.0597	26.240	-31.495

Topology for DANAZOL developed by Dr. Dallas B. Warren

[moleculetype]

; Name

DAN 3

[atoms]

; nr	type	resnr	residue	atom	cgmr	charge	mass	typeB	chargeB	massB
1	CH1	1	DAN	C1	1	0.209	13.019	; qtot	0.209	
2	NR	1	DAN	N2	1	-0.279	14.0067	; qtot	-0.07	
3	OA	1	DAN	O3	1	-0.117	15.9994	; qtot	-0.187	
4	CH0	1	DAN	C4	1	0.201	12.011	; qtot	0.014	
5	CH1	1	DAN	C5	2	0	13.019	; qtot	0.014	
6	CH0	1	DAN	C6	3	0	12.011	; qtot	0.014	
7	CH0	1	DAN	C7	4	0	12.011	; qtot	0.014	
8	CH3	1	DAN	C22	5	0	15.035	; qtot	0.014	
9	CH2	1	DAN	C8	6	0	14.027	; qtot	0.014	
10	CH0	1	DAN	C9	7	-0.014	12.011	; qtot	0	
11	CH2	1	DAN	C10	8	0	14.027	; qtot	0	
12	CH2	1	DAN	C11	9	0	14.027	; qtot	0	
13	CH1	1	DAN	C12	10	0	13.019	; qtot	0	
14	CH1	1	DAN	C13	11	0	13.019	; qtot	0	
15	CH1	1	DAN	C14	12	0	13.019	; qtot	0	
16	CH0	1	DAN	C15	13	0	12.011	; qtot	0	
17	CH3	1	DAN	C21	14	0	15.035	; qtot	0	

18	CH2	1	DAN	C16	15	0	14.027 ; qtot 0
19	CH2	1	DAN	C17	16	0	14.027 ; qtot 0
20	CH2	1	DAN	C18	17	0	14.027 ; qtot 0
21	CH2	1	DAN	C19	18	0	14.027 ; qtot 0
22	C	1	DAN	C20	19	0.15	17.320 ; qtot 0.15 mass is +5.309
23	OA	1	DAN	O20	19	-0.548	12.9754 ; qtot -0.398
24	H	1	DAN	H20	19	0.398	4.032 ; qtot 0
25	DUM	1	DAN	C23	20	0	0 ; qtot 0
26	CH1	1	DAN	C24	21	0	19.721 ; qtot 0 mass is +6.702

[bonds]

;	ai	aj	funct	c0	c1	c2	c3
	1	2	2	gb_22			
	1	10	2	gb_27			
	2	3	2	gb_13			
	3	4	2	gb_13			
	4	5	2	gb_27			
	4	10	2	gb_10			
	5	6	2	gb_10			
	6	7	2	gb_27			
	6	11	2	gb_27			
	7	8	2	gb_27			
	7	9	2	gb_27			
	7	14	2	gb_27			
	9	10	2	gb_27			
	11	12	2	gb_27			
	12	13	2	gb_27			
	13	14	2	gb_27			
	13	15	2	gb_27			
	14	19	2	gb_27			
	15	16	2	gb_27			
	15	20	2	gb_27			

```

16 17 2 gb_27
16 18 2 gb_27
16 22 2 gb_27
18 19 2 gb_27
20 21 2 gb_27
21 22 2 gb_27
22 23 2 gb_18
23 24 2 gb_1

```

[pairs]

```

; ai  aj funct      c0      c1      c2      c3
  1   5   1
  1   7   1
  2   5   1
  2   9   1
  3   6   1
  3   9   1
  4   7   1
  4  11   1
  5   8   1
  5   9   1
  5  12   1
  5  14   1
  6  10   1
  6  13   1
  6  19   1
  7  12   1
  7  15   1
  7  18   1
  8  10   1
  8  11   1
  8  13   1

```

8	19	1
9	11	1
9	13	1
9	19	1
10	14	1
11	14	1
11	15	1
12	16	1
12	19	1
12	20	1
13	17	1
13	18	1
13	21	1
13	22	1
14	16	1
14	20	1
15	19	1
15	23	1
16	24	1
16	26	1
17	19	1
17	20	1
17	21	1
17	23	1
18	20	1
18	21	1
18	23	1
19	22	1
20	23	1
21	24	1
21	26	1

```

23 26 1
[ angles ]
; ai  aj  ak funct      c0      c1      c2      c3
 2  1 10  2  ga_15
 1  2  3  2  ga_15
 2  3  4  2  ga_13
 3  4  5  2  ga_39
 3  4 10  2  ga_39
 5  4 10  2  ga_27
 4  5  6  2  ga_13
 5  6  7  2  ga_13
 5  6 11  2  ga_27
 7  6 11  2  ga_27
 6  7  8  2  ga_13
 6  7  9  2  ga_27
 6  7 14  2  ga_27
 8  7  9  2  ga_15
 8  7 14  2  ga_15
 9  7 14  2  ga_15
 7  9 10  2  ga_15
 1 10  4  2  ga_39
 1 10  9  2  ga_39
 4 10  9  2  ga_27
 6 11 12  2  ga_15
11 12 13  2  ga_15
12 13 14  2  ga_15
12 13 15  2  ga_15
14 13 15  2  ga_15
 7 14 13  2  ga_15
 7 14 19  2  ga_13
13 14 19  2  ga_13

```

```

13 15 16 2 ga_13
13 15 20 2 ga_15
16 15 20 2 ga_13
15 16 17 2 ga_13
15 16 18 2 ga_13
15 16 22 2 ga_13
17 16 18 2 ga_13
17 16 22 2 ga_13
18 16 22 2 ga_13
16 18 19 2 ga_13
14 19 18 2 ga_15
15 20 21 2 ga_15
20 21 22 2 ga_15
16 22 21 2 ga_13
16 22 23 2 ga_13
21 22 23 2 ga_13
16 22 26 2 ga_15 ; pdb2gmx failed to generate
21 22 26 2 ga_13 ; pdb2gmx failed to generate
23 22 26 2 ga_13 ; pdb2gmx failed to generate
22 23 24 2 ga_12

```

[dihedrals]

```

; ai  aj  ak  al funct      c0      c1      c2      c3      c4      c5
 2   1  10   9   1  gd_34
 1   2   3   4   1  gd_23
 2   3   4   5   1  gd_23
 3   4   5   6   1  gd_34
 5   6   7   9   1  gd_34
 5   6  11  12   1  gd_34
 6   7   9  10   1  gd_34
 6   7  14  13   1  gd_34
 7   9  10   4   1  gd_34

```

```

6  11  12  13  1  gd_34
11  12  13  14  1  gd_34
12  13  14  7   1  gd_34
12  13  15  20  1  gd_34 ; changed last atom from 16
7   14  19  18  1  gd_34
13  15  16  22  1  gd_34 ; changed last atom from 18
13  15  20  21  1  gd_34
15  16  18  19  1  gd_34
15  16  22  21  1  gd_34
16  18  19  14  1  gd_34
15  20  21  22  1  gd_34
20  21  22  16  1  gd_34
21  22  23  24  1  gd_23 ; changed first atom from 16
[ dihedrals ]
; ai  aj  ak  al funct      c0      c1      c2      c3
1  10  4   3   2  gi_1
3   2   1  10   2  gi_1
4  10   3   5   2  gi_1
4   5   6   7   2  gi_1
6   5   7  11   2  gi_1
9   1   4  10   2  gi_1
13  12  14  15   2  gi_2
14  13  19   7   2  gi_2
15  13  20  16   2  gi_2
[ virtual_sites2 ]
; Site from i j      funct  a
; C23 triple bonded carbon
25  22  26   1   0.558
[ constraints ]
; ai  aj funct  b0
22  26   1   0.274

```